USGS
science for a changing world

Prepared in Cooperation with the Oregon Water Resources Department

Groundwater Resources of the Harney Basin, Southeastern Oregon

Scientific Investigations Report 2021-5103

U.S. Department of the Interior
U.S. Geological Survey

Front cover: Background: Photograph of spring and playa lakebed as seen looking south toward Iron Mountain, Oregon. Photograph taken by Halley J. Schibel, Oregon Water Resources Department, July 27, 2017.

Left: Collecting a stable isotope sample from Nichols Spring (U.S. Geological Survey identifier 434736119370401), Oregon. Photograph taken by Hank Johnson, U.S. Geological Survey, July 17, 2018.

Top right: Double O Cold Spring (U.S. Geological Survey identifier 431649119190800), Oregon, as seen looking southeast and downstream along the outflow channel. Photograph taken by Darrick E. Boschmann, Oregon Water Resources Department, April 19, 2017.

Bottom right: Irrigation well as seen looking northwest to Warm Springs Butte, Harney Basin lowlands, Oregon. Photograph taken by Gerald H. Grondin, Oregon Water Resources Department, October 19, 2017

Back cover: Spring and playa lakebed as seen looking south toward Iron Mountain, Oregon. Photograph taken by Halley J. Schibel, Oregon Water Resources Department, July 27, 2017.

Groundwater Resources of the Harney Basin, Southeastern Oregon

By Stephen B. Gingerich, Henry M. Johnson, Darrick E. Boschmann, Gerald H. Grondin, and C. Amanda Garcia

Prepared in cooperation with the Oregon Water Resources Department

Scientific Investigations Report 2021–5103

U.S. Department of the Interior
U.S. Geological Survey

U.S. Geological Survey, Reston, Virginia: 2022

For more information on the USGS—the Federal source for science about the Earth, its natural and living resources, natural hazards, and the environment—visit https://www.usgs.gov or call 1–888–ASK–USGS.

For an overview of USGS information products, including maps, imagery, and publications, visit https://store.usgs.gov/.

Suggested citation:
Gingerich, S.B., Johnson, H.M., Boschmann, D.E., Grondin, G.H., and Garcia, C.A., 2022, Groundwater resources of the Harney Basin, southeastern Oregon: U.S. Geological Survey Scientific Investigations Report 2021–5103, 118 p., https://doi.org/10.3133/sir20215103.

Associated data releases:
Gingerich, S.B., Johnson, H.M., Boschmann, D.E., Grondin, G.H., and Garcia, C.A., 2021, Contour dataset of the potentiometric surfaces of shallow and deep groundwater-level altitudes in Harney Basin, Oregon, February–March 2018: U.S. Geological Survey data release, https://doi.org/10.5066/P9ZJTZUV.

Gingerich, S.B., Johnson, H.M., Boschmann, D.E., Grondin, G.H., Garcia, C.A., and Schibel, H.J., 2022, Location information, discharge, and water-quality data for selected wells, springs, and streams in the Harney Basin, Oregon: U.S. Geological Survey data release, http://doi.org/10.5066/P9J0FE5M.

ISSN 2328-0328 (online)

Acknowledgments

The authors gratefully acknowledge the Harney Groundwater Study Advisory Committee for their local knowledge, comments, questions, suggestions, and assistance. We also thank the residents of the Harney Basin, particularly those individuals who allowed access to property, wells, and springs for groundwater-level measurements and groundwater samples during the study. The Oregon Department of Environmental Quality provided staff to help collect geochemical samples for the study. Halley Schibel, Jonathan LaMarche, Benjamin Scandella, J.R. Johnson, and Donald Swindlehurst of the Oregon Water Resources Department also helped with fieldwork and table and figure preparation. Nicholas Corson-Dosch, Sean Payne, and Gabriel Gordon of the U.S Geological Survey helped with fieldwork and in the preparation of graphs and figures. The staff of Department of Geology and Mineral Industries provided geologic insight and help with GPS elevation surveys. Staff of the Malheur National Wildlife Refuge, the Bureau of Land Management, and the Forest Service provided access and valuable observations. We appreciate data shared by and discussions with Mike Cummings, Robert Perkins, and Kiri Hargie of Portland State University, and Connie Robbins and her students at Crane Union High School. Additional funding was provided by the U.S. Geological Survey Water Availability and Use Science Program.

Contents

Figures

Tables

Plates

Well- and Spring-Identification System

Wells and springs have three identification systems. Example well: HARN0051319; 433425118561801; 23.00S/32.00E-18CCA01.

Oregon State designation: HARN0051319; county name (HARN for Harney) and unique number within the county.

U.S. Geological Survey identifier: 433425118561801; first six digits are the latitude in degree-minute-seconds, the next seven digits are the longitude, and the last two digits indicate a unique number at that location.

Public Land Survey System designation: 23.00S/32.00E-18CCA01, diagrammed in section, Public Land Survey System.

Site Identification—Public Land Survey System
Willamette Principal Meridian

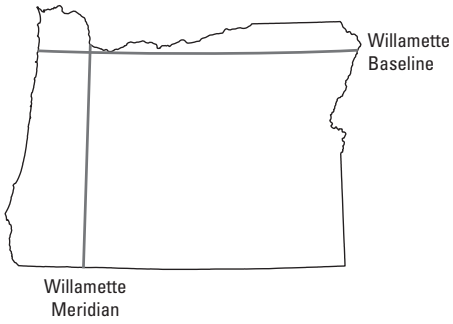

23.00S/32.00E-18CCA01

23.00S	32.00E	18	CCA	01
Township	Range	Section	Quarter-quarter-quarter section	Location sequence

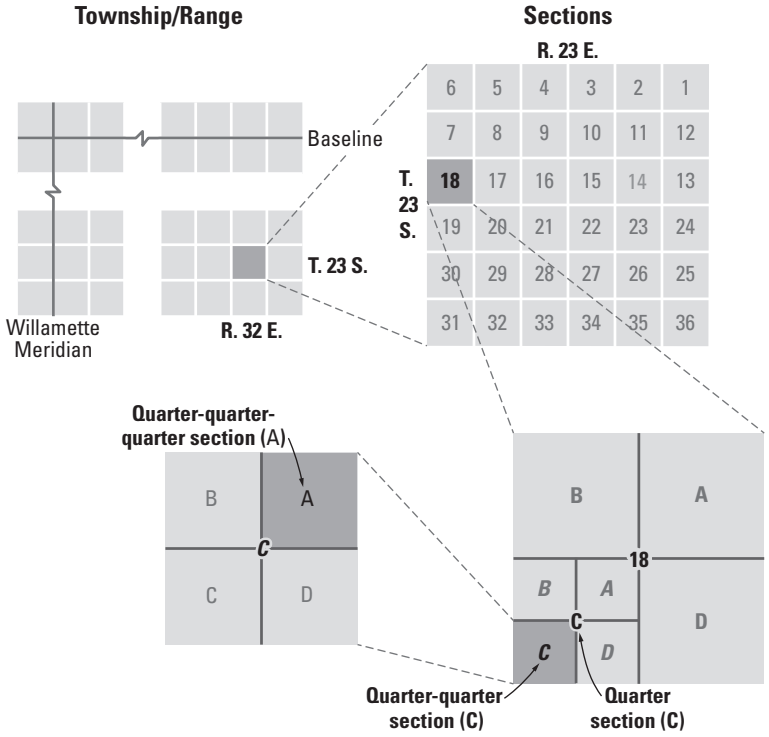

The PLSS system is based on the site's location in the Public Land Survey System. Four quadrants are formed by the intersection of the Willamette base line and principal meridian. The letters N or S locate the township north or south of the base line. The letters E or W locate the range east or west of the principal meridian. The first numeral indicates the township, the second the range, and the third the section in which the well is located. Letters following the section number locate the well within the section. The letters (A-D) are assigned within the section in a counter-clockwise direction beginning with "A" in the northeast quarter of the section. The first letter denotes the quarter section, the second the quarter-quarter section, and the third the quarter-quarter-quarter section. Letters are assigned within each divided subsection in the same manner. Where two or more wells are located within the smallest subdivision, a number indicating the order in which the wells are inventoried follows the letters. For example, well 23.00S/32.00E-18CCA01 is located in the NW 1/4, SW 1/4, SW 1/4, Section 18, T23S, R32E. It is the first inventoried well in that parcel.

Conversion Factors

U.S. customary units to International System of Units

Multiply	By	To obtain
	Length	
inch (in.)	2.54	centimeter (cm)
inch (in.)	25.4	millimeter (mm)
foot (ft)	0.3048	meter (m)
mile (mi)	1.609	kilometer (km)
	Area	
square mile (mi^2)	259.0	hectare (ha)
square mile (mi^2)	2.590	square kilometer (km^2)
	Volume	
acre-foot (acre-ft)	1,233	cubic meter (m^3)
acre-foot (acre-ft)	0.001233	cubic hectometer (hm^3)
	Flow rate	
acre-foot per day (acre-ft/d)	0.01427	cubic meter per second (m^3/s)
acre-foot per year (acre-ft/yr)	1,233	cubic meter per year (m^3/yr)
acre-foot per year (acre-ft/yr)	0.001233	cubic hectometer per year (hm^3/yr)
cubic foot per second (ft^3/s)	0.02832	cubic meter per second (m^3/s)
cubic foot per day (ft^3/d)	0.02832	cubic meter per day (m^3/d)
	Hydraulic conductivity	
foot per day (ft/d)	0.3048	meter per day (m/d)
	Hydraulic gradient	
foot per mile (ft/mi)	0.1894	meter per kilometer (m/km)
	Transmissivity	
foot squared per day (ft^2/d)	0.09290	meter squared per day (m^2/d)
	Application rate	
pound per acre per year ([lb/acre]/yr)	1.121	kilogram per hectare per year ([kg/ha]/yr)

International System of Units to U.S. customary units

Multiply	By	To obtain
	Length	
millimeter (mm)	0.03937	inch (in.)

Temperature in degrees Celsius (°C) may be converted to degrees Fahrenheit (°F) as follows:

$$°F = (1.8 \times °C) + 32.$$

Temperature in degrees Fahrenheit (°F) may be converted to degrees Celsius (°C) as follows:

$$°C = (°F - 32) / 1.8.$$

Datums

Vertical coordinate information is referenced to the North American Vertical Datum of 1988 (NAVD 88).

Horizontal coordinate information is referenced to the North American Datum of 1983 (NAD 83).

Elevation, as used in this report, refers to distance above the vertical datum.

Supplemental Information

Specific conductance is given in microsiemens per centimeter at 25 degrees Celsius (µS/cm at 25 °C).

Abbreviations

BLM	Bureau of Land Management
CRBG	Columbia River Basalt Group
DIC	dissolved inorganic carbon
GMWL	Global Meteoric Water Line
HU	hydrostratigraphic unit
Ma	mega-annum: million years before present
NAD 83	North American Datum of 1983
NAVD 88	North American Vertical Datum of 1988
NGVD 29	National Geodetic Vertical Datum of 1929
NWR	National Wildlife Refuge
OWRD	Oregon Water Resources Department
ppm	parts per million
PRISM	Parameter-Elevation Relationships on Independent Slopes Model
SC	specific conductance
TU	tritium units
USFS	U.S. Forest Service
USFWS	U.S. Fish and Wildlife Service
USGS	U.S. Geological Survey

Groundwater Resources of the Harney Basin, Southeastern Oregon

By Stephen B. Gingerich[1], Henry M. Johnson[1], Darrick E. Boschmann[2], Gerald H. Grondin[2], and C. Amanda Garcia[1]

Abstract

Groundwater development has increased substantially in southeastern Oregon's Harney Basin since 2010, mainly for the purpose of large-scale irrigation. Concurrently, some areas of the basin experienced groundwater-level declines of more than 100 feet, and some shallow wells have gone dry. The Oregon Water Resources Department has limited new groundwater development in the basin until an improved understanding of the groundwater-flow system is available. This report describes the results of a hydrologic investigation undertaken to provide that understanding. The investigation encompasses the groundwater hydrology of the entire 5,240-square-mile Harney Basin.

Most of the precipitation in the Harney Basin falls in the higher-elevation areas of the Blue Mountains and Steens Mountain. Although considerable groundwater recharge occurs in these upland areas, most (83 percent) re-emerges as streams and springs in the uplands. Groundwater recharge in the lowlands is provided through infiltration of surface water flowing onto the lowlands from rivers and streams leaving the uplands and as groundwater flow from the surrounding upland rocks. Water-balance calculations indicate that the rate of groundwater recharge to the Harney Basin lowlands (where most groundwater is withdrawn) averages 173,000 acre-feet per year (acre-ft/yr).

Groundwater in the Harney Basin lowlands mainly discharges through evapotranspiration from groundwater-irrigated (supplied from wells) crops or from natural vegetation drawing groundwater from the shallow water table and capillary fringe. Groundwater discharge in the lowlands is estimated to be about 283,000 acre-ft/yr, which exceeds the estimated groundwater recharge to the lowlands by about 110,000 acre-ft/yr. This imbalance results in removal of groundwater from storage in the aquifer system and is evidenced by the large declines observed in groundwater levels in the areas of greatest groundwater pumpage.

To a large degree, the location and depth of pumpage dictate the timing and distribution of the effects of groundwater use in the Harney Basin. Pumpage is commonly greatest in the areas where higher-permeability geologic units allow for higher well yields. However, many of these higher-permeability units are bounded by lower-permeability units that cannot supply groundwater at a sufficient rate to replenish the areas of greatest pumpage, resulting in groundwater-level declines. Three Harney Basin areas with a combined area exceeding 140 square miles have experienced groundwater-level declines exceeding 40 feet compared to pre-development conditions: near the Weaver Spring/Dog Mountain area, in the northeastern floodplains along Highway 20, and near Crane. Areas of more modest groundwater-level decline (about 10 feet) were identified in the Virginia Valley area and the Silver Creek floodplain north of Riley. Smaller localized areas of groundwater-level depression have also formed around individual wells or groups of wells throughout the Harney Basin lowlands.

Most groundwater being pumped from the Harney Basin lowlands, including all three areas experiencing large groundwater-level declines, was recharged more than 12,000 years ago, near the end of the last glacial period when the climate in the basin was cooler and wetter than today. Geochemical evidence indicates that modern recharge generally circulates to a depth no greater than 100 feet below the floodplains of major rivers and streams in the lowlands. Away from the major river and stream corridors, pre-modern water commonly is found at the water table. Recharge to groundwater and recovery of groundwater levels in the most heavily pumped areas in the Harney Basin lowlands are restricted by the limited spatial extent and depth of modern recharge in the Harney Basin lowlands and the relatively fine-grained deposits underlying most of the lowland areas.

[1]U.S. Geological Survey

[2]Oregon Water Resources Department

Introduction

Southeastern Oregon's Harney Basin has experienced a substantial increase in groundwater development over the last 100 years, with the most rapid increase due to an expansion in crop irrigation during the 1970s and after 2010. The demand for groundwater has increased because little unappropriated surface water is available during the irrigation season (Oregon Water Resources Board, 1967), and the spatial distribution of surface water across the basin is uneven. In 2016, the Oregon Water Resources Department (OWRD) adopted Oregon Administrative Rule 690-512-0020, limiting groundwater development in much of the Harney Basin to only a few uses, due to their determination that groundwater-level declines probably indicated "over appropriation" of groundwater (Oregon Water Resources Department, 2016). As of 2015, more than 287,000 acre-feet (acre-ft) of maximum allowable annual groundwater use had been permitted, exceeding a 1968 estimate of the total annual groundwater recharge for the entire Harney Basin (260,000 acre-ft) (Robison, 1968).

Prior to this investigation, studies of the Harney Basin groundwater-flow system were limited, and the hydrology in many areas was poorly understood. The ability of the groundwater system to sustain existing uses and to accommodate additional development was not well known. Additionally, uncertainty existed regarding the extent to which groundwater development would affect nearby areas and the interconnectedness of the hydrologic system throughout the basin. These concerns led the OWRD to enter into a cooperative agreement with the U.S. Geological Survey (USGS) to conduct a groundwater-availability study of the Harney Basin. The objectives of this study were to (1) develop a quantitative conceptual understanding of the groundwater-flow system of the Harney Basin and (2) develop numerical hydrologic models to test the conceptualization of the groundwater-flow system and accurately simulate its response to historical pumping, current conditions, and future groundwater-withdrawal scenarios. This report summarizes the conceptual framework of the groundwater-flow system in the Harney Basin and provides a foundation for the development of numerical groundwater-flow models to simulate the groundwater-flow system.

Purpose and Scope

This report provides a basin-wide description of the Harney Basin groundwater system including the hydrostratigraphic framework, groundwater flow, and a summary of the hydrologic budget. The groundwater hydrologic budget includes estimates of all groundwater recharge and discharge components in upland and lowland areas and for each of the major stream-drainage basins, providing an understanding of the fate of groundwater from entry to exit. The groundwater budget can help water-resource managers and water users evaluate the outcome of groundwater-management decisions.

Groundwater recharge and discharge were estimated for the period during 1982–2016 (hereinafter referred to as "the study period") from precipitation, streamflow, evapotranspiration (ET), and spring-flow data having various periods of availability. Some of those periods referred to in this report include 1991–2018 for pumpage, 1903–2017 for spring flow, 1900–2016 for long-term precipitation, 1981–2010 for gridded precipitation data, and 1987–2015 for natural evapotranspiration estimates. Available water-level and water-chemistry data were considered through 2019.

The information contained herein builds upon and summarizes four other reports describing the Harney Basin hydrologic system. The hydrologic budget is presented in Garcia and others (2022), the geology of the Harney Basin is described in Boschmann (2021), irrigation pumpage is provided in Beamer and Hoskinson (2021), non-irrigation pumpage is summarized in Grondin (2021), and subsurface hydraulic properties are discussed in Grondin and others (2021).

Study Area

The Harney Basin encompasses about 5,240 square miles (mi^2) in southeastern Oregon (fig. 1). The basin covers most of Harney County and includes smaller portions of Grant, Lake, and Crook Counties. The Harney Basin is a closed surface-water basin with three major, perennial streams and numerous smaller, intermittent streams that drain to Malheur and Harney Lakes. The Silvies River and Silver Creek flow southward from the Blue Mountains, and the Donner und Blitzen River flows northward from Steens Mountain; all three flow into the Harney Basin lowlands and terminate into Malheur Lake or Harney Lake. In this study, the Harney Basin lowlands refers to the general mapped extent of Quaternary alluvium (about 1,000 mi^2) within the center of the basin including the floodplains of Silver Creek and the Silvies and Donner und Blitzen Rivers (fig. 1).

The Harney Basin encompasses a high plateau with lowland elevations above 4,000 feet (ft) and adjacent mountains above 9,700 ft. The overall topography is largely a result of fault-block structures, uplift, volcanism, and erosion. Previous studies (Russell, 1903, 1905; Waring, 1908, 1909; Piper and others, 1939; Walker, 1979) describe the Harney Basin as a predominantly volcanic terrain with lowland basin-filling deposits of fluvial-lacustrine origin. The source, depositional environment, grain size, and thickness of the basin-fill sediments vary. The volcanic deposits include numerous eruptive centers, lava flows, and pyroclastic deposits with variable chemical compositions, depositional environments, lateral extents, and thicknesses.

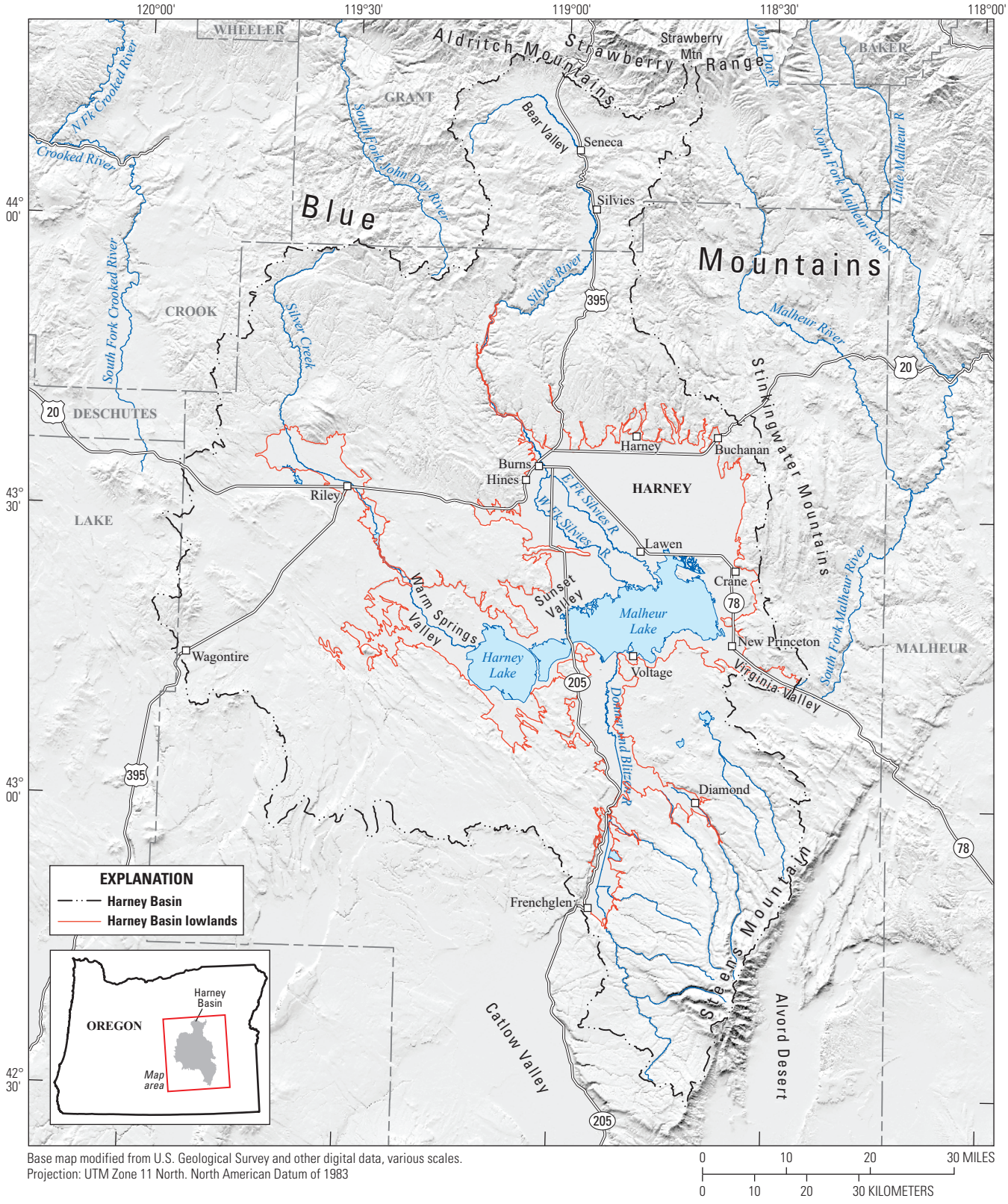

Figure 1. Location and major geographic features of the study area, Harney Basin, southeastern Oregon.

Land cover in the Harney Basin is predominately sagebrush steppe, which covers much of the central and southern areas of the basin. Large areas of greasewood (*Sarcobatus vermiculatus*) and saltgrass (*Distichlis spicata)* surround the many playas and exist just beyond the floodplains of major streams in the lowest elevations of the basin. The sagebrush steppe community transitions to ponderosa pine (*Pinus ponderosa*) forests and mountain meadows in the Blue Mountains uplands in the north and, in the south, transitions to alpine grasslands and meadows on Steens Mountain. Nearly 70 percent of the land in the Harney Basin is publicly owned and managed by various federal and state agencies (fig. 2), including the Bureau of Land Management (BLM), the Forest Service (USFS), the U.S. Fish and Wildlife Service (USFWS), and Oregon Department of State Lands. Most of the rest of the land in the Harney Basin is in private ownership or ownership of the Burns Paiute Tribe. Much of the BLM and USFS holdings are leased for cattle grazing and are predominately in the uplands. The USFWS manages the Malheur National Wildlife Refuge (NWR), an important stopover and nesting location for migratory birds, and includes the areas occupied by Malheur and Harney Lakes. Privately owned land is concentrated in the lowlands of the basin and is largely devoted to grazing and irrigated agriculture (primarily hay production). More than half of the approximately 7,500 basin residents live in the cities of Burns and Hines, with the remainder settled in small communities and on ranches throughout the basin.

The climate of the Harney Basin is semi-arid and characteristic of a high desert region. Mild summers and cool winters are typical, with a broad range in daily and seasonal temperatures. The monthly mean temperature for 1981–2010 varied little by location and elevation, ranging from 27 degrees Fahrenheit (°F) in December to 67 °F in July at the Malheur Refuge Headquarters near Malheur Lake (Malheur Refuge Headquarters, Oregon [355162]; elevation 4,100 ft) and from 25 °F in December to 65 °F in July at the Fish Creek SNOTEL station on Steens Mountain (elevation 7,660 ft) (U.S. Department of Agriculture Natural Resources Conservation Service, 2020; Western Regional Climate Center, 2020). The relative monthly distribution of precipitation is similar across the basin, with the highest amounts falling during winter and the lowest amounts during summer. Total annual precipitation varies markedly across the basin (fig. 3); mean annual precipitation for 1981–2010 was 10 inches (in.) at Malheur Refuge Headquarters and 44 in. at the Fish Creek SNOTEL site (U.S. Department of Agriculture Natural Resources Conservation Service, 2020; Western Regional Climate Center, 2020).

Comparisons between study-period (1982–2016) precipitation and longer-term mean precipitation (1900–2016) highlight the spatial variability within the Harney Basin. To facilitate these comparisons, Garcia and others (2022) used relations between measured precipitation at six sites and estimates from the Parameter-Elevation Relationships on Independent Slopes Model (PRISM; PRISM Climate Group, 2019) for those locations extending back to 1900 to extrapolate the short-term measurements (fig. 4). In the northern uplands at a site near the town of Seneca (fig. 3), mean precipitation during the study period was 7 percent higher than the 116-year (yr) mean. Mean study-period precipitation at sites near Burns (Burns Federal Building) and on the lowlands of the western basin (Squaw Butte) was within 1 percent of the 116-yr mean. At the Double O Ranch site near the center of the Harney Basin just west of Harney Lake, precipitation over the last century has exhibited greater variability than other sites, with few wet or dry periods lasting more than a decade. Study-period precipitation at the Double O Ranch averaged about 9 in. and was equal to the 116-yr mean. On Steens Mountain to the south, mean study-period precipitation at Fish Creek, the highest site, was 9 percent lower than the 116-yr mean (fig. 4). During the 1982–2016 study period, the 1980s and 1990s generally were wetter than the 2000s. With the exception of the Fish Creek site, the 1980s and 1990s were some of the wettest periods during the 116-yr record (fig. 4).

Previous Groundwater Investigations in the Harney Basin

Russell (1903) published the first investigations of groundwater in the Harney Basin, briefly mentioning a few springs and wells in a general report on the hydrogeology of southeastern Oregon. Waring (1909) completed the earliest comprehensive study of hydrology in the Harney Basin, including a discussion of soils, geology, vegetation, and surface and groundwater resources. Piper and others (1939) published an updated analysis of the hydrology of the basin based on a 3-yr study begun in 1928. The study by Piper and others (1939) was the first to recognize and describe several key hydrologic features of the basin, including:

(1) Surface water infiltrating into the Silvies River alluvial fan provided most of the recharge to the basin-fill deposits beneath the northern Harney Basin lowlands.

(2) Evapotranspiration by phreatophytes (deep-rooted plants that consume groundwater) was the primary mechanism for groundwater discharge on the valley floor.

(3) The shallow and deep parts of the groundwater-flow system beneath the northern Harney Basin lowlands often respond differently to recharge and hydrologic stresses.

(4) Prior to any substantial groundwater development, annual fluctuations in groundwater levels in wells penetrating deep into the basin fill were due to the weight of the loading and unloading of the annual springtime freshet water on the ground surface and did not reflect recharge of the deeper sediments.

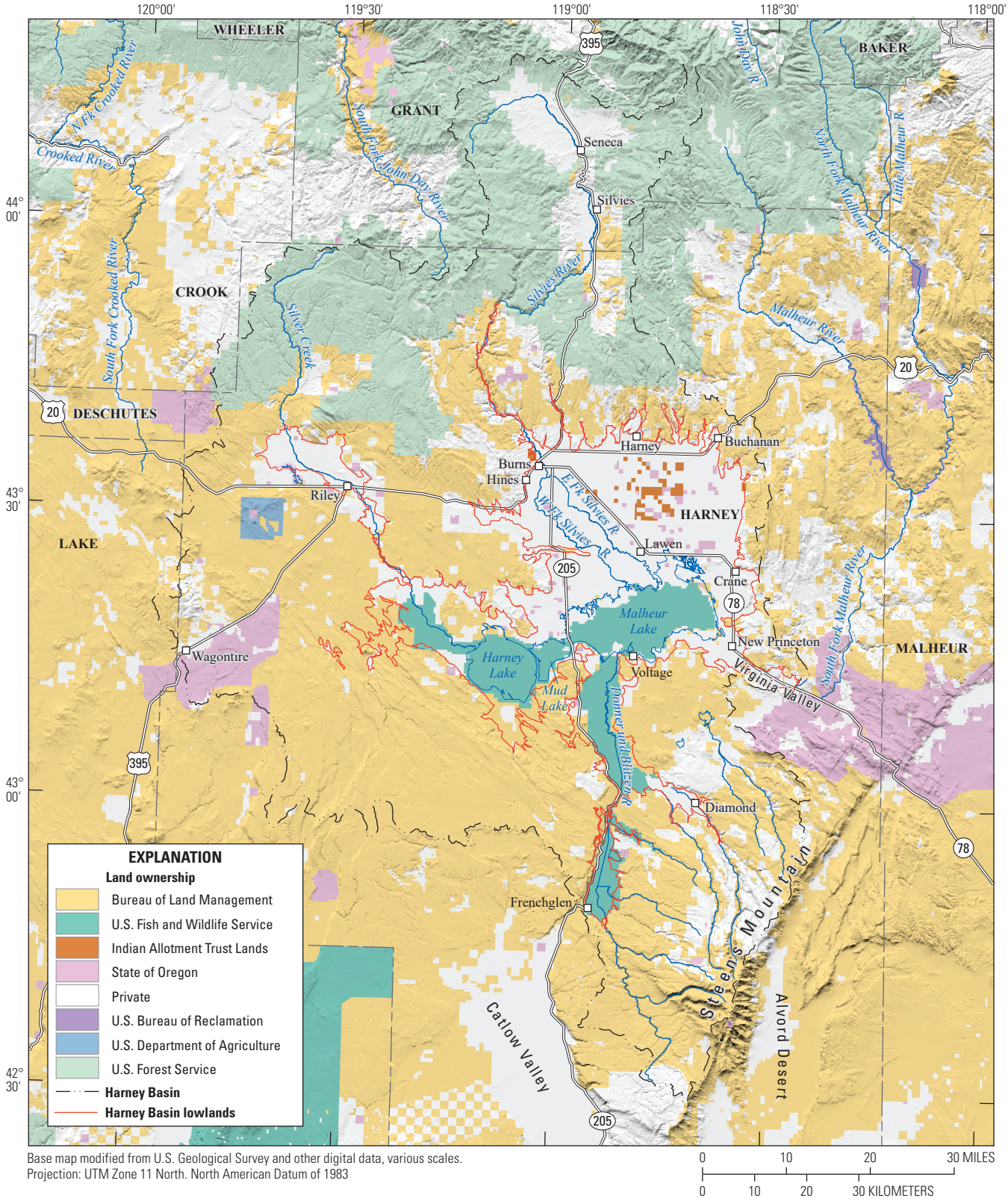

Figure 2. Land ownership in the Harney Basin, southeastern Oregon.

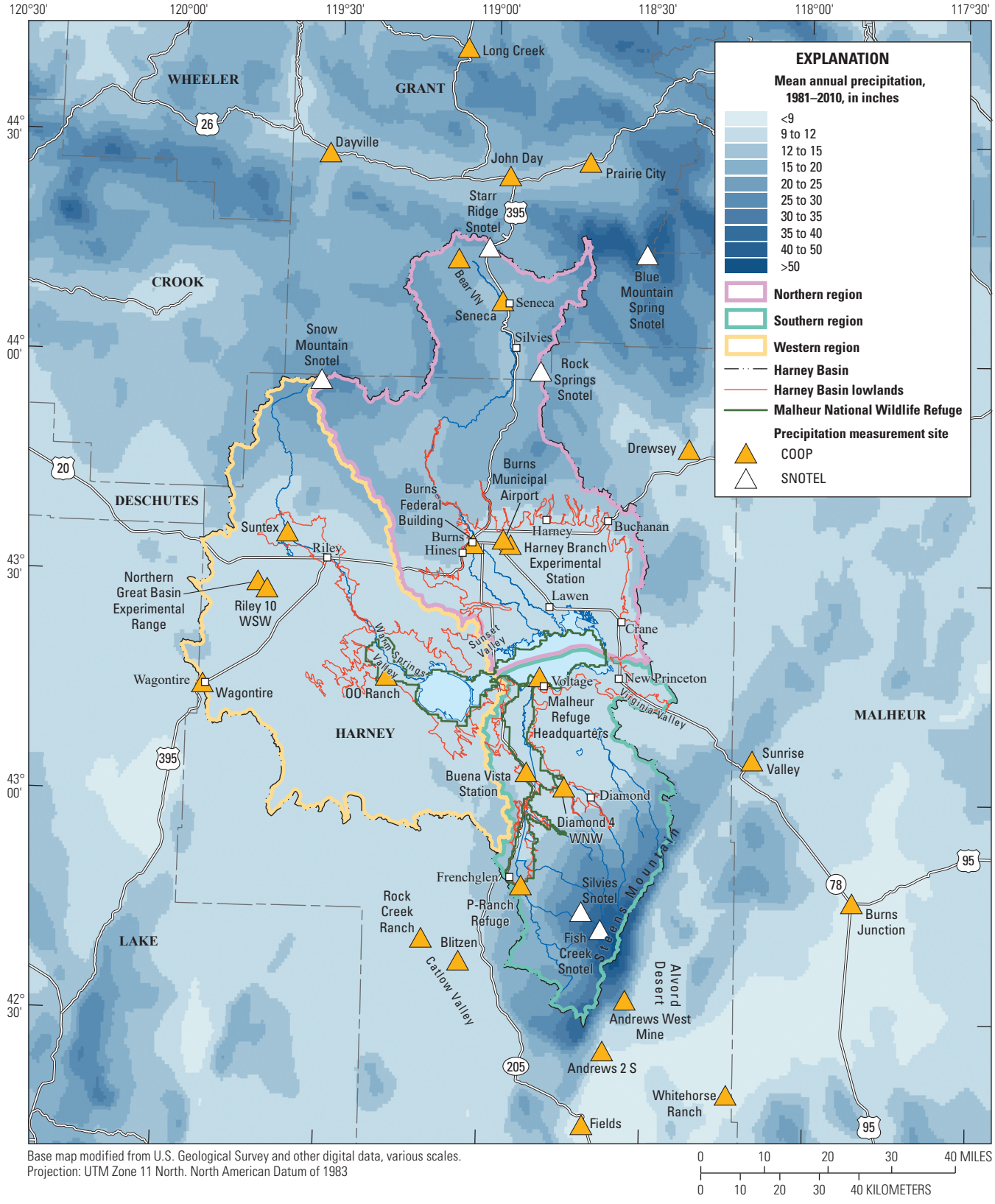

Figure 3. Mean annual precipitation and locations of selected precipitation gages and weather stations, Harney Basin, Oregon, 1981–2010. Data from PRISM Climate Group (2019) and Garcia and others (2022). COOP, National Weather Service Cooperative Observer Program; SNOTEL, National Resources Conservation Service Snow Telemetry.

Figure 4. Measured and estimated annual precipitation at selected sites for 1900–2016, Harney Basin, southeastern Oregon. Modified from Garcia and others (2022).

Piper and others (1939) also made the first estimates of recharge volumes to areas of the Harney Basin lowlands. Robison (1968) used streamflow measurements to estimate basin-wide recharge. Leonard (1970), also working exclusively in the Harney Basin lowlands, developed an updated groundwater-level map for the basin-fill deposits, estimated annual discharge to wells, and characterized the major ion chemistry of the groundwater. Hubbard (1975), in a study of Malheur Lake during 1972–73, concluded that minor seepage from groundwater flowed toward the lake from the southwest and flowed away from the lake toward the north at relatively flat gradients (less than 0.0005 foot per foot [ft/ft]). Reports detailing additional groundwater-level data and groundwater geochemistry for wells in the basin include Gonthier and others (1977), Townley and others (1980), Reed and others (1984a, b), and Gonthier (1985). Aquaveo, LLC (2012), provided updated groundwater-level maps and estimates of groundwater recharge based on a deep-percolation model (Bauer and Vaccaro, 1987) and recommended a program of groundwater-use reporting and future development of a groundwater-flow model of the basin.

Hydrogeologic Framework

Geology controls the storage and flow of groundwater to a considerable extent. The principal factors that influence groundwater flow are the permeability and porosity of the rock or sediment through which it flows. This section describes the geologic framework of the regional groundwater-flow system in the Harney Basin, including a brief description of major geologic units, geologic structure, and geologic factors controlling the flow-system boundaries.

General Geology of the Harney Basin

The Harney Basin is a geologically diverse area underlain by Permian-to-Quaternary rocks that have been deformed by folds and faults as recently as the Holocene (within the last 12,000 yrs) (Walker and Repenning, 1965; Brown and Thayer, 1966b; Greene and others, 1972; Personius and others, 2003). The basin is filled with a sequence of interfingering and faulted volcanic-vent deposits, lava flows, air-fall and ash-flow tuffs, volcanically derived sedimentary rocks, and unconsolidated sediments that rest, at least in part, upon a basement of pre-Cenozoic crystalline and metamorphic rocks (Piper and others, 1939; Walker, 1979). The Harney Basin occupies parts of three physiographic provinces in southeastern Oregon: the northern uplands lie within the southern extent of the Blue Mountains province, the southern uplands extend into the northwest part of the Basin and Range province, and the central basin lowlands comprise the eastern end of the High Lava Plains province (fig. 5) (Dicken, 1950; Walker, 1977; Eaton, 1982).

The Blue Mountains province is a patchwork of late Paleozoic and Mesozoic accreted volcanic arc and oceanic-crustal terranes and associated plutons that have undergone regional uplift as a complexly folded and faulted structural block extending more than 200 miles (mi) across northeastern Oregon into western Idaho and the southeastern corner of Washington (Brooks and Vallier, 1978; Walker, 1990). Rocks of the Blue Mountains province in the northern Harney Basin uplands are the oldest rocks in the basin and include variably deformed and metamorphosed Mesozoic marine sedimentary rocks with subordinate volcanic flows and tuffs (Brooks and Vallier, 1978; Dickinson and Thayer, 1978; Dickinson, 1979; Silberling and Jones, 1984). Permian metamorphic rocks of limited extent have also been mapped in association with the Mesozoic strata (Brown and Thayer, 1977). Combined, these pre-Cenozoic basement rocks form an extensive block that plunges south-southeast and extends at depth beneath the central Harney Basin (Streck, 2002; McClaughry and others, 2019). This deeply eroded basement is unconformably overlain in the northern uplands by late Oligocene to middle Miocene continental volcanic, volcaniclastic, and tuffaceous sedimentary rocks, including lavas of the Columbia River Basalt Group (CRBG) and Strawberry Volcanics (Brown and Thayer, 1966b; Houston and others, 2018; Niewendorp and others, 2018).

The Basin and Range province in southeastern Oregon is the northwesternmost extent of a vast region of the western United States interior undergoing approximately east-west oriented crustal extension expressed as a series of generally north-northeast oriented fault-block mountain ranges and intervening sedimentary basins (Eaton, 1982; Zoback, 1989; Wernicke, 1992; Pezzopane and Weldon, 1993). In the southern Harney Basin uplands, the Steens Mountain fault block has undergone as much as 7,000 ft of vertical displacement across the Steens fault zone (fig. 5) (Hemphill-Haley and others, 2000; Evans and Geisler, 2001). More than 5,000 ft of topographic relief along the eastern escarpment exposes a lower section of late Oligocene and early Miocene volcanic flows and domes, pyroclastic rocks, and sedimentary rocks. These rocks are in turn unconformably overlain by the Steens Basalt—a gently west-northwest dipping sequence of basalt lava flows with an average composite thickness of about 2,000 ft. Steens Basalt lavas, part of the CRBG, form the gently inclined western dip-slope of Steens Mountain and are thought to underlie much of the southern-to-central Harney Basin (Fuller, 1931; Minor and others, 1987; Camp and Ross, 2004; Camp and others, 2013).

The High Lava Plains province is a Miocene-to-Holocene volcanic plateau characterized by widespread basaltic volcanism and a west-northwest migrating trend of silicic volcanism that extends 175 miles (mi) across central and southeastern Oregon from the eastern margin of the Harney Basin to the Cascade Range (fig. 5) (Walker, 1969; Walker, 1974; MacLeod and others, 1975; Jordan and others, 2004). The High Lava Plains province merges gradually into the Basin and Range province to the south, with many structural and volcanic

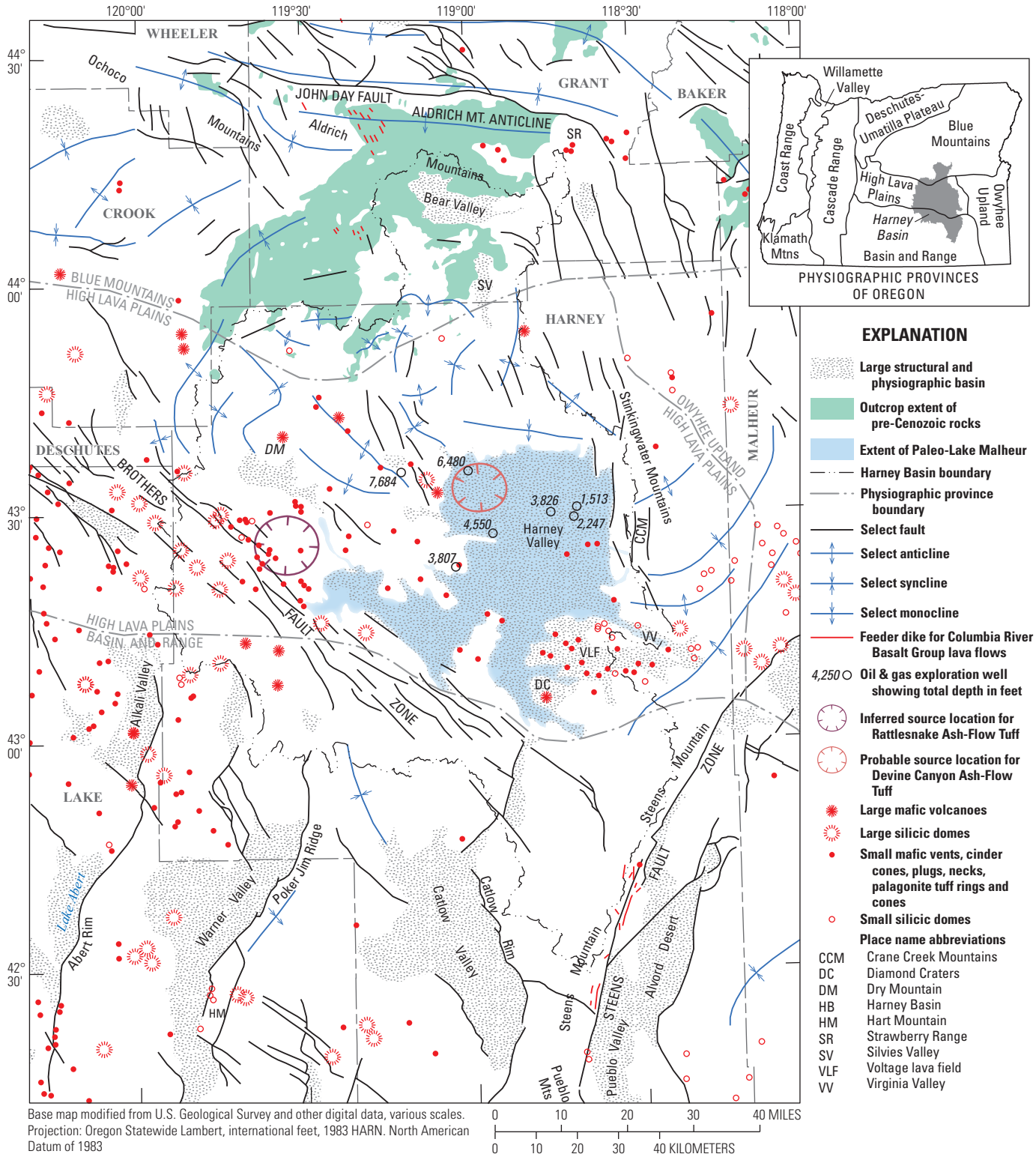

Figure 5. Tectonic overview map showing selected structural and geologic features, Harney Basin, southeastern Oregon. Folds, faults, volcanic features, structural basins, and extent of pre-Cenozoic rocks modified from Walker (1963), Brown and Thayer (1966b), Walker and others (1967), Swanson (1969), Greene and others (1972), and Walker and Repenning (1965). Extent of Paleo-Lake Malheur modified from Snyder and others (1964). Inferred source location for Rattlesnake Ash-Flow Tuff from Streck and Grunder (1995). Probable source location for Devine Canyon Ash-Flow Tuff from Greene (1973). Physiographic provinces of Oregon modified from Dicken (1950) and Walker (1977).

features common to both provinces. In contrast, a relatively sharp boundary separates the High Lava Plains province from the Blue Mountains province to the north (Walker, 1969; Walker and Nolf, 1981). Late Cenozoic rocks of the High Lava Plains province in the central Harney Basin are the product of multiple episodes of bimodal volcanism and subsequent sedimentation. Basaltic and intermediate volcanic rocks occur as lava fields composed of numerous thin compound flows erupted from widely scattered cones and small shield volcanoes. Silicic volcanic rocks occur as numerous dome and flow complexes, three major ash flow sheets, and several minor tuffs. Volcanic rocks of the High Lava Plains province are interbedded with and overlain by weakly to well-indurated fluvial and lacustrine tuffaceous sedimentary rocks that flank the uplands and extend beneath the Harney Basin lowlands (Greene and others, 1972; Walker, 1974; MacLeod and others, 1975; Walker, 1979; Walker and Nolf, 1981; Streck and Grunder, 2012). Structurally, the province is dominated by the Brothers fault zone—a diffuse northwest-trending zone of en échelon normal faults cutting obliquely across the High Lava Plains (Walker, 1969; Lawrence, 1976). The sequence of late Cenozoic volcanic rocks and tuffaceous sediments that make up the bulk of the rocks and deposits filling the basin are overlain in some areas by unconsolidated to poorly consolidated Quaternary fluvial, lacustrine, and aeolian deposits. These younger basin-filling deposits comprise the uppermost part of the fill beneath the Harney Basin lowlands and occupy modern stream channels and floodplains.

Evolution of the Depositional Basin

The depositional evolution of the Harney Basin was driven by volcanic, tectonic, climatic, and surficial processes operating in central and eastern Oregon throughout much of the Cenozoic. The basin began to develop as a large, shallow structural depression and site of deposition and sedimentation by middle to late Miocene (Walker and Swanson, 1968; Walker, 1979) as a result of the combined evolution of the Blue Mountains and Basin and Range provinces and faulting within the Brothers fault zone. Regional deformation began with uplift in the Blue Mountain province after 36 million years before present (Ma; Swanson and Robinson, 1968; Robyn and Hoover, 1982). Uplift in the Blue Mountains along the Aldrich Mountain anticline (fig. 5) originated in the early Oligocene, with rejuvenated anticlinal uplift and development of the John Day fault system in the early to middle Pliocene (Thayer and Brown, 1966). Structural extension of the Basin and Range province in this area was occurring by at least 16.9 Ma ($^{40}Ar/^{39}Ar$ age of basal Steens Basalt flow reported by Moore and others [2018]), as indicated by north-striking Steens Basalt feeder dikes at Steens Mountain. Uplift of the Steens Mountain block along the Steens fault zone had initiated by 10.4 Ma (Johnson, 1995); however, based on outcrop distribution, structural attitude, and paleomagnetic properties of the Devine Canyon Ash-Flow Tuff (fig. 6), substantial topographic relief along the fault zone was likely not present until after the eruption of the tuff at 9.7 Ma (Rytuba and McKee, 1984; Minor and others, 1987; Jordan and others, 2004; Biasi, 2019).

The southwestern margin of the basin is separated from Catlow and Warner Valleys by elevated fault blocks of the Brothers fault zone, while the eastern margin is separated from the Malheur River Basin (plate 1) by north-south oriented fault blocks within the Crane Creek and Stinkingwater Mountains (fig. 5). The subdued western divide is bounded by erosional or volcanic constructional highs dominated by numerous large rhyolitic domes along with younger basaltic vents and lava flows (see locations of large silicic domes and mafic volcanoes in fig. 5). Further development of the structural depression of the Harney Basin may have also been partially due to crustal collapse into evacuated magma chambers associated with the eruption of several late Miocene ash-flow tuffs from calderas now buried beneath the younger basin fill (Walker, 1969; Walker, 1979; Walker and Nolf, 1981). Additional downward crustal flexure and subsidence within the basin has been attributed to crustal loading by mass transfer of mantle magmas to the crust via basaltic injection and volcanism (Ford and others, 2013).

The presence of a closed hydrologic system and lacustrine deposition in a saline, alkaline lake between 9.7 and 7.1 Ma is demonstrated by the distribution of diagenetic-alteration minerals in tuffaceous sedimentary rocks east of Harney Lake (Holmes, 1990; Sheppard, 1993; Sheppard, 1994). This period of sedimentary deposition along with eruption of subaqueous basalt lava flows north of Harney Lake indicates closed basin conditions persisted through at least 2.54 Ma (Greene and others, 1972; Walker, 1979; Jordan and others, 2004).

After 2.54 Ma, exterior drainage to the Columbia River system via the South Fork Malheur River (plate 1) and the Snake River was established through a drainage outlet at Virginia Valley (fig. 5), beginning a period of widespread denudation of the upper part of the basin fill from the central basin (Piper and others, 1939). Wrights Point (plate 1) is a prominent remnant of the uneroded surface where a resistant lava flow, originally emplaced in an ancient stream channel 2.54 Ma (Jordan and others, 2004), protected the underlying sediments from eroding. By about 1.5 Ma the basin floor had been eroded down to its approximate current elevation, based on the distribution of lava flows of the informally named Voltage basalt, which erupted from several vents south of Malheur Lake (fig. 6) as early as 1.47 Ma (Jordan and others, 2004; Sherrod and others, 2012); these flows advanced across Virginia Valley and into the South Fork Malheur River, damming the drainage outlet and once again closing off the Harney Basin from external drainage. This damming began the current period of basin-filling sedimentation, which effectively established the conditions for the present-day groundwater-flow system.

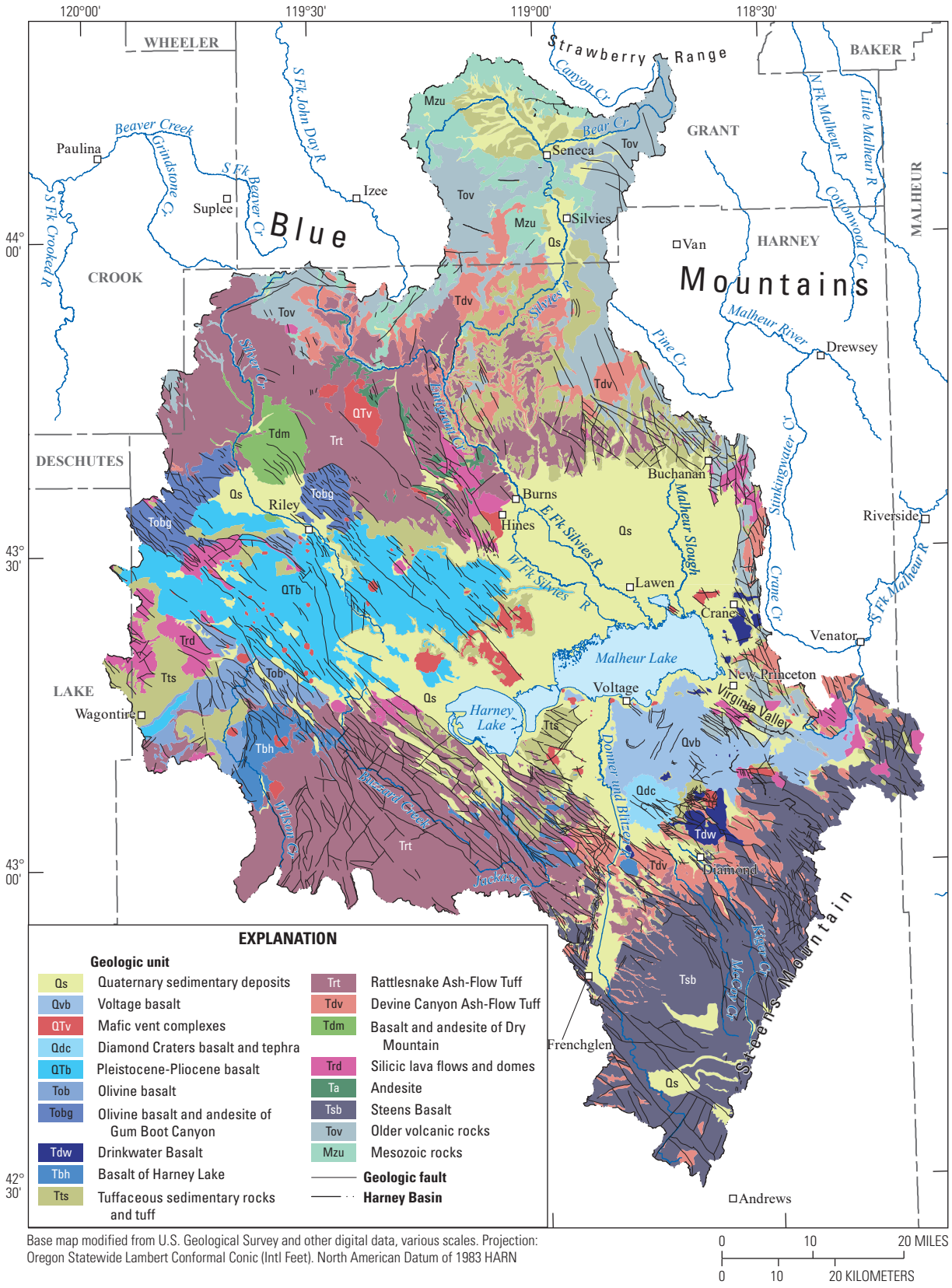

Figure 6. Generalized (*A*) geologic map and (*B*) time-rock chart for generalized geologic map units in the Harney Basin, southeastern Oregon. Map from Boschmann (2021).

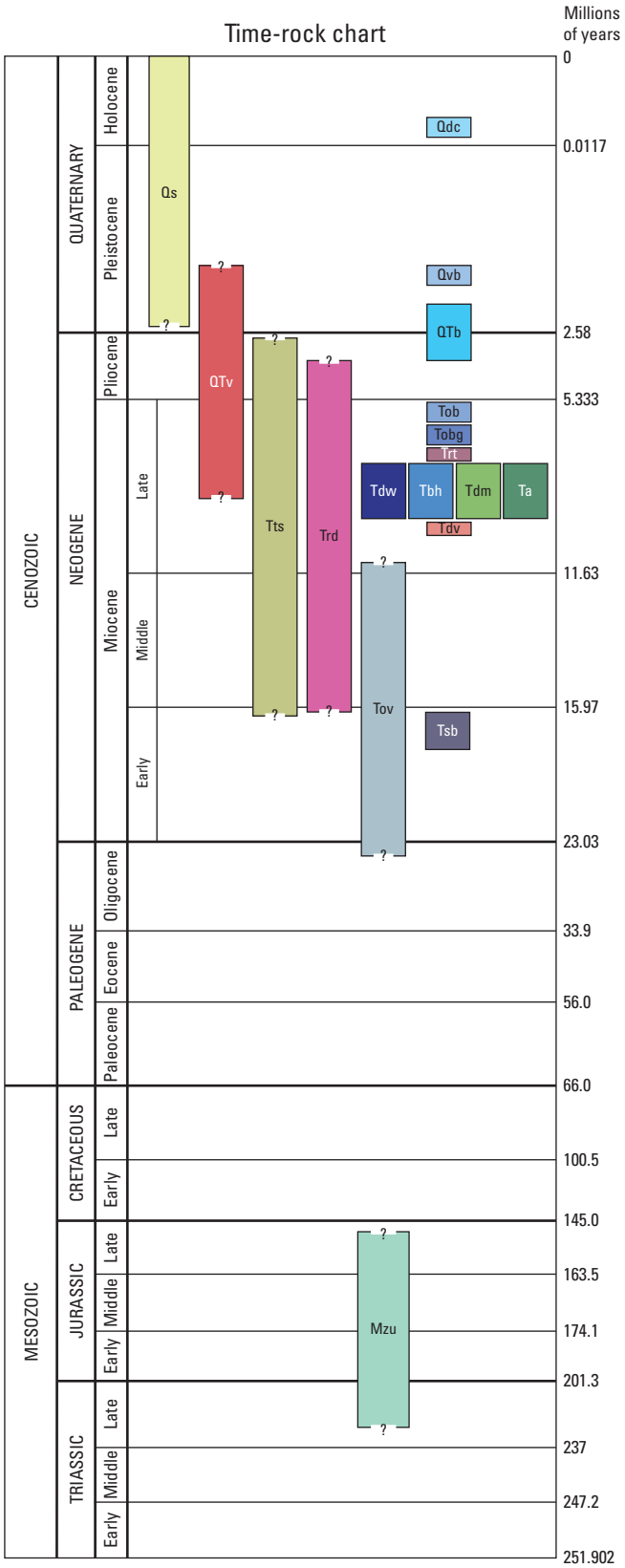

Figure 6.—Continued

Late Quaternary climatic variations in southeastern Oregon resulted in marked lake-level fluctuations under these closed-basin conditions. Paleo-Lake Malheur experienced several high-stand phases beginning as early as 80,000 yrs ago and, at its maximum extent, covered an area greater than 900 mi^2 (Snyder and others, 1964; Dugas, 1998). This period of dominantly closed-basin conditions and sedimentary infilling with scattered volcanic deposition has continued to the present, as modern streams deposit their sediment load and continue building alluvial fans where they enter the lowlands, and interfinger downstream with the finer grained lacustrine deposits, which dominate toward the central part of the basin.

The total thickness of the continental Cenozoic section deposited in the Harney Basin atop the Mesozoic marine rocks is not known with certainty, but it undoubtedly varies considerably across the basin. Metasedimentary xenoliths within the Rattlesnake Ash-Flow Tuff include lithologies similar to those found in the Mesozoic rocks of the Blue Mountains (Streck, 2002), providing the only direct evidence for the presence of these basement rocks beneath the Harney Basin lowlands. Oil and gas well records and related correspondence on file with the Oregon Department of Geology and Mineral Industries clearly indicate that the target formation for the deepest of these wells was the Mesozoic marine strata underlying the Cenozoic section. In 1949, a United Company of Oregon exploration well (HARN0052707; plate 1) just east of Burns penetrated a thick series of interbedded lavas and sedimentary deposits to a depth of 6,480 ft and did not encounter evidence of marine strata in examined samples. Several other oil and gas exploration wells (HARN0052702, HARN0052706; plate 1) deeper than 3,000 ft similarly failed to fully penetrate the Cenozoic section. Seismic and gravity modeling of the High Lava Plains region by Cox and others (2013) indicated that the Cenozoic cover of sediments and volcanic rocks is 3- to 4.5-mi thick beneath the Harney Basin lowlands. Considering these constraints, the Walker (1979) estimate of 3,600- to 4,100-ft-thickness of the Cenozoic section, which was based on field observations and stratigraphic relations, is on the lower end of fill-thickness estimates.

Description of Stratigraphic Units

The stratigraphic nomenclature for Cenozoic rocks in the Harney Basin was updated and formalized in part by Walker (1979); however, a complete and comprehensive stratigraphy was not defined at that time due to the reconnaissance nature of available geologic data. Consequently, many geologic units remain without formalized stratigraphic names. Geologists working in the basin prior to and following Walker (1979) have identified and published more than 100 distinct and mappable geologic units, many of which do not conform to the formalized nomenclature established in 1979.

For the purposes of characterizing the basin-scale stratigraphic and structural framework, a generalized geologic map of the basin was compiled from existing geologic mapping representing nearly 50 yrs of geologic field investigation in the region (fig. 6; Boschmann, 2021). Geologic map units compiled from 14 publications were grouped into 18 generalized units that share similar geologic origins, physical properties, and stratigraphic position. Compilation and generalization of map units endeavored to honor the regional stratigraphic framework of the basin in accord with known constraints, while recognizing the intended application of the compilation as a tool to inform hydrogeological interpretations at the basin scale. For the purposes of assigning stratigraphic units to wells in this study, an additional undifferentiated basin-fill unit was used. The 18 generalized stratigraphic units from Boschmann (2021) and the additional undifferentiated basin-fill unit defined for this study are described below.

Mesozoic Rocks (Mzu)

The oldest rocks exposed in the basin are variably deformed and metamorphosed Upper Jurassic to Upper Triassic marine deposits of the accreted Izee terrane, including interbedded volcanic and tuffaceous mudstone, siltstone, shale, graywacke, calcareous sandstone, conglomerate, limestone, tuff, and minor andesite lavas (Brown and Thayer, 1977; Brooks and Vallier, 1978; Dickinson and Thayer, 1978; Dickinson, 1979; Silberling and Jones, 1984). Minor areas of Miocene intrusive rocks, and Permian to pre-Permian(?) metamorphic rocks of limited extent associated with the Canyon Mountain Complex (Wallace and Calkins, 1956; Brown and Thayer, 1977) are also included with this unit. Exposures of Mesozoic rocks in the basin are limited to the northern uplands (fig. 6); however; they are presumed to form the basement underlying much of the basin at 3–4.5 mi below land surface (Streck, 2002; Cox and others, 2013; McClaughry and others, 2019). The aggregate thickness of Upper Triassic to Upper Jurassic rocks in the region is estimated at nearly 50,000 ft (Brooks, 1979; Dickinson, 1979).

Steens Basalt (Tsb)

Miocene continental flood basalt lavas of the Steens Basalt were erupted from a low, elongate shield volcano centered near the Steens Mountain escarpment where numerous north- and northeast-striking dikes are exposed (fig. 6). More than 100 individual flows with an average composite thickness of about 2,000 ft and a maximum reported thickness of 4,300 ft make up the Steens Basalt. The sequence was largely erupted as compound flows that ranged from 30 to 150 ft thick, though individual flow lobes rarely exceeded 6 ft (Minor and others, 1987; Johnson and others, 1998; Camp and others, 2013). The initial eruption of Steens Basalt occurred by 16.97 ± 0.06 Ma as the earliest pulse of Columbia River Flood Basalt volcanism (Camp and others, 2013; Moore and others, 2018). Steens Basalt lavas have been mapped as far away as 80 mi west of Steens Mountain at Abert Rim and are depicted on some regional maps along the eastern and northern margins of the Harney Basin lowlands (Camp and others, 2013). Based on the widespread distribution, it is presumed that Steens Basalt lavas exist at depth beneath much of the Harney Basin.

Older Volcanic Rocks (Tov)

A thick section of late Oligocene and Miocene volcanic rocks underlies the Devine Canyon Ash-Flow Tuff in the northern and eastern uplands (fig. 6). This unit is primarily composed of basalt and andesite lava flows but also includes rhyolite lava flows and tuffs, rhyodacite and dacite lavas, and interbedded tuffaceous sedimentary deposits. In the northern uplands, this unit is more than 6,500 ft thick (Thayer, 1957) and includes undifferentiated CRBG lavas, Strawberry Volcanics, and Dinner Creek Tuff (Brown and Thayer, 1966a; Greene and others, 1972; Houston and others, 2018; Niewendorp and others, 2018). The unit may also include undifferentiated Steens Basalt in some areas in the eastern part of the basin (Camp and others, 2013).

Devine Canyon Ash-Flow Tuff (Tdv)

This light-gray to greenish-gray, nonwelded to densely welded, crystal-rich rhyolite tuff forms an important stratigraphic marker bed throughout much of the basin (fig. 6). The tuff sheet ranges from a few feet to more than 200 ft thick, with an estimated original extent of more than 7,000 mi^2 (Greene, 1973; Walker, 1979; McClaughry and others, 2019). Greene (1973) proposed a source caldera in the central Harney Basin near Burns based on unit thickness and crystal content distribution. An eruption age of 9.74 ± 0.02 Ma is reported by Jordan and others (2004).

Andesite (Ta)

Fine-grained, dense, and commonly flow-banded andesite and basaltic-andesite lava flows occur as multiple thin flows with a total thickness of a few tens to locally more than 200 ft. These flows erupted from several vent complexes in the uplands northwest of Burns (fig. 6; Greene and others, 1972; Brown and others, 1980b; Brown, 1982; McClaughry and others, 2019). The age of these lava flows is bracketed by the 8.41 Ma Prater Creek Ash-Flow Tuff and 7.1 Ma Rattlesnake Ash-Flow Tuff (Jordan and others, 2004; McClaughry and others, 2019).

Basalt and Andesite of Dry Mountain (Tdm)

Numerous basalt and andesite lava flows erupted from a large shield volcano at Dry Mountain about 7.9 Ma (fig. 6; Greene and others, 1972; Streck and Grunder, 2012). A thickness of 535 ft is penetrated by well HARN0050475 (plate 1), and a 700+ ft section is exposed at the summit scarp; the total thickness is unknown.

Basalt of Harney Lake (Tbh)

This unit is a black to dark-gray olivine-bearing basalt consisting of several 10- to 20-ft-thick flows that combine for about 150 ft of total thickness (Greene and others, 1972; Brown and others, 1980a). The unit is south and west of Harney Lake where it underlies Rattlesnake Ash-Flow Tuff and overlies Devine Canyon Ash-Flow Tuff (fig. 6). A late Miocene age is based on stratigraphic position and $^{40}Ar/^{39}Ar$ ages of 7.68 ± 0.08 Ma and 7.54 ± 0.13 Ma (Jordan and others, 2004).

Drinkwater Basalt (Tdw)

These ridge-capping basalt flows lie along the eastern margin of the basin near Crane and south and east of Diamond Craters (fig. 6). This unit occurs most commonly as a single lava flow, but several flows are found at some locations, with a total thickness ranging from 20 to 200 ft (Greene and others, 1972). An $^{40}Ar/^{39}Ar$ age of 7.25 ± 0.09 Ma is reported for exposures of this unit east of the basin near the South Fork Malheur River (Meigs and others, 2009).

Rattlesnake Ash-Flow Tuff (Trt)

This tuff is a light-brown to red-brown to gray, nonwelded to densely welded, pumice-rich rhyolite tuff that forms an important stratigraphic marker bed throughout much of the basin. The tuff sheet typically ranges from 30 to 100 ft thick with a maximum reported thickness of about 240 ft and an estimated original extent of 13,500 mi^2 (Brown and others, 1980a; Streck and Grunder, 1995). Streck and Grunder (1995) proposed a source caldera in the western Harney Basin on the basis of outcrop, pumice size, and facies distribution as well as flow-direction indicators. An eruption age of 7.093 ± 0.015 Ma is reported by Jordan and others (2004).

Olivine Basalt and Andesite of Gum Boot Canyon (Tobg)

This unit is a medium- to dark-gray, fine- to medium-grained, aphyric and diktytaxitic basalt with groundmass olivine, and medium-gray aphanitic and nonporous andesite with less than 1 percent plagioclase and olivine phenocrysts. Several flows, each a few feet to a few tens of feet thick with a maximum thickness of about 300 ft, are exposed along fault scarps southeast of Dry Mountain (fig. 6; Greene and others, 1972). As mapped by Greene (1972), the unit overlies the Rattlesnake Ash-Flow Tuff, but a $^{40}Ar/^{39}Ar$ age of 7.60 ± 0.11 Ma from southeast of Dry Mountain (Jordan and others, 2004) indicates part of the unit may be older.

Olivine Basalt (Tob)

This unit is a dark-gray to black, fine-grained olivine basalt with some andesite that is more than 300 ft thick in some places. The unit locally includes thin interbeds of tuffaceous sedimentary rock (Greene and others, 1972) and overlies Rattlesnake Ash-Flow Tuff in the southwest part of the basin (fig. 6). A late Miocene age assignment is based on stratigraphic position and a K-Ar age of 6.2 ± 0.8 Ma (Parker and Armstrong, 1972; Feibelkorn and others, 1982).

Silicic Lava Flows and Domes (Trd)

These rocks are medium- to light-gray, pale-red, and reddish-brown, commonly streaked, and flow-banded rhyolite, rhyodacite and dacite with associated vitrophyre and obsidian. The unit occurs as exogenous domes and related flows and plugs widely distributed across the High Lava Plains part of the basin (Greene and others, 1972; Brown and others, 1980a–b). The total thickness of these rocks is unknown but is likely substantially more than 1,000 ft near central dome and vent areas, progressively thinning toward flow margins.

Tuffaceous Sedimentary Rocks and Tuff (Tts)

This unit includes white to buff and pale-brown to yellowish-gray, semi- to well-consolidated lacustrine and fluviatile tuffaceous mudstone, siltstone, sandstone, and conglomerate, with numerous air-fall ash beds and tuffs and occasional thin carbonate and chert beds. The rocks commonly consist of a poorly sorted mixture of pumice, scoria, other rock fragments, plagioclase grains, and glass shards in a clay matrix (Greene and others, 1972; Brown and others, 1980a–b). Locally, the tuffaceous sedimentary rocks and tuffs are diagenetically altered to clay minerals, zeolites, and potassium feldspar (Walker and Swanson, 1968; Walker and Nolf, 1981; Sheppard, 1994). This unit includes all tuffaceous sediments and tuff interbedded with the Rattlesnake and Devine Canyon Ash-Flow Tuffs and includes the 8.41 ± 0.16 Ma Prater Creek Ash-Flow Tuff (Walker, 1979; Jordan and others, 2004). The total composite thickness of this unit is unknown but exceeds 1,800 ft in the central part of the basin and may be nearly 4,000 ft thick in some places. The upper section of the unit is partially equivalent to the Harney Formation of Walker (1979).

Pleistocene-Pliocene Basalt (QTb)

Flows of medium-gray, fine-grained, diktytaxitic, olivine-bearing vesicular basalt occur as a series of thin flows locally separated by thin layers of sedimentary rock (Greene and others, 1972; Brown and others, 1980a, b); including the Wright's Point Member of the Harney Formation (Walker, 1979). The total thickness ranges from a few tens of feet up to several hundred feet. The Pleistocene–Pliocene age assignment is based on $^{40}Ar/^{39}Ar$ ages of 2.83 ± 0.89 Ma, 2.54 ± 0.07 Ma, and 2.2 ± 0.04 Ma (Jordan and others, 2004; Streck and Grunder, 2012).

Voltage Basalt (Qvb)

A unit of medium-gray, vesicular olivine basalt erupted as thin lava flows from numerous vents south and east of Malheur Lake (fig. 6; Greene and others, 1972; Brown and others, 1980a, b). The lava field contains abundant well-preserved flow features such as tumuli and pressure ridges. The unit is at least 310 ft thick at HARN0052607 (plate 1), which is where these lavas dammed the paleo-channel at Virginia Valley; however, elsewhere the thickness is generally less than 200 ft. Jordan and others (2004) reported $^{40}Ar/^{39}Ar$ ages of 1.23 ± 0.05 Ma and 1.47 ± 0.08 Ma.

Mafic Vent Complexes (QTv)

Basaltic to andesitic scoria, cinders, agglomerate, thin flows, and intrusive masses forming lava cones, domes, and small shield volcanoes associated with eruptive centers are related to the following mafic and intermediate volcanic units in the basin: Tov, Tdw, Ta, Tbh, Tobg, Tob, QTb, and Qvb. Locally this unit includes partly consolidated subaqueous deposits of palagonitized basaltic ejecta occurring as tuff and breccia cones and rings and reworked volcanic sediments (Greene and others, 1972; Brown and others, 1980a, b). The thickness varies widely but is up to 500 ft in some places.

Diamond Crater Basalt and Tephra (Qdc)

This unit includes fine- to medium-grained olivine and plagioclase phyric basalt lava flows and tephra including agglomerate, cinders, and ash. The basalt is medium to dark gray and mostly vesicular, forming thin flows with ropy pahoehoe surfaces (Greene and others, 1972; Brown and others, 1980b; Russell and Nicholls, 1987). Many small craters are rimmed with lava spatter, cinders, and bombs. The total thickness of these lavas is estimated at 75–100 ft in the center of the lava field, thinning toward the margins (Peterson and Groh, 1964). The lava field was emplaced sometime between about 7,320–7,790 yrs ago, based on radiocarbon ages and paleomagnetic constraints (Sherrod and others, 2012).

Quaternary Sedimentary Deposits (Qs)

This unit contains unconsolidated to poorly consolidated clay, silt, sand, and gravel of Quaternary age. The deposits originated as alluvium, alluvial fan deposits, colluvium, floodplain deposits, lacustrine deposits, talus, landslide, and other recent sedimentary deposits. This unit includes glacial deposits on Steens Mountain. These deposits are estimated to be up to 300 ft thick, but the thickness varies considerably across the basin (see "Description of Harney Basin Hydrostratigraphic Units" section later in this report).

Undifferentiated Basin Fill Deposits (QTsu)

This unit combines Quaternary sedimentary deposits and tuffaceous sedimentary rocks and tuff beneath the surface of the lowlands for the purposes of correlating stratigraphic units to subsurface formation descriptions on well reports. These units commonly include similar lithologies and have no distinguishing horizon at the contact between the units. In most cases, the individual tuff units are not identified or sufficiently described in well reports so stratigraphic correlation to these units could not be made. The open intervals in about 700 wells in the Harney Basin lowlands were designated QTsu.

Hydraulic Characteristics of Subsurface Materials

The movement and storage of groundwater in geologic units is controlled by hydraulic properties, particularly permeability and porosity. The hydraulic characteristics of geologic materials vary between and within rock types. Descriptions, estimates, and ranges of hydraulic properties of geologic units in the Harney Basin are presented in this section. A more thorough discussion of these key hydrologic characteristics and the methods for determining them can be found in Theis (1935), Cooper and Jacob (1946), Davis and DeWiest (1966), Lohman (1972), Freeze and Cherry (1979), Vorhis (1979), Heath (1983), and Fetter (2001).

An aquifer is a saturated part of the subsurface where groundwater is transmitted through and stored within available open spaces called "pores." Porosity is a measure of the total space of those pores divided by the total volume of rock. An aquifer can be composed of a single rock type or it can include multiple geologic units through which the groundwater moves. Permeability describes the ease with which fluid can move through the pore space and fractures of a geologic material (Lohman, 1972; Winter and others, 1998). Permeability is an intrinsic property of the rock type and is independent of the properties of the fluid in the rock. Deposits with large interconnected open spaces, such as gravel or rubbly lava flows, offer little resistance to groundwater flow and, therefore, commonly have high permeability. In contrast, rocks and sediments with few, small, or poorly connected open spaces, such as clay or unfractured rock, offer more resistance to groundwater flow and, therefore, commonly have low permeability.

The permeability of volcanic rocks varies greatly and depends on primary eruptive features such as vesicles (gas bubbles), lava tubes, or flow brecciation, and on post-eruptive, secondary features such as cooling joints, faulting, alteration, and secondary mineralization. The highly fractured, rubbly zones at the tops and bottoms of basaltic lava flows are commonly highly permeable, whereas the interior of thicker basaltic lava flows generally are dense and have very low permeability. Andesitic and rhyolitic lavas generally have lower primary permeability than basaltic lavas because, during emplacement, these higher-viscosity flows were typically slower-moving and not likely to form an eruptive fabric conducive to groundwater movement. Glass and many minerals in volcanic rocks weather to various clay minerals, which can reduce primary permeability. The original void spaces and secondary fractures in all types of rock can be filled with minerals deposited by circulating groundwater, a process that commonly increases with the age of the rock and that can greatly reduce permeability over time.

The term "hydraulic head," which is the sum of elevation and water pressure divided by the weight density of water, is used to describe potential energy in groundwater-flow systems. Head can be measured as the elevation of the groundwater level in a well, which represents the sum of the elevation and pressure at the open interval of the well. The hydraulic-head gradient is the change in head per unit of distance in a given direction. Head measurements are described using units of distance, such as ft. Gradients are often expressed as a relational pair of units such as foot per foot [ft/ft] or feet per mile [ft/mi].

Where water only partly fills an aquifer, the upper surface of the saturated zone (the water table) is free to rise and decline and is typically represented by the static water level in shallow wells. The water in such aquifers is said to be "unconfined," and the aquifers are referred to as "unconfined aquifers." A map of the water-table elevation helps show the groundwater-head gradient at the top of an unconfined aquifer. Where water completely fills an aquifer that is overlain by a low-permeability unit that restricts the vertical movement of water, the water in the aquifer is said to be "confined." Such aquifers are referred to as "confined aquifers." The head in a confined aquifer is, by definition, greater than the elevation of the top of the aquifer itself. The water level in tightly cased wells open to a confined aquifer stands at the level of the potentiometric surface of the aquifer. In wells open to multiple aquifers, the static water level is some average of the heads in those aquifers.

Many times, the confining beds surrounding confined aquifers can also be considered aquifers. Even though they are less permeable, they can still transmit groundwater, and the system is more properly referred to as "semiconfined." Characterizing an aquifer as confined or semiconfined does not imply that it is not hydraulically connected to other aquifers or to surface water. The terms confined, semiconfined, and unconfined describe the physics of the aquifer response to pumpage at a particular location, and the same stratigraphic unit can be classified differently in different locations depending on the geometry and depth of the layer being considered. In the Harney Basin, groundwater occurs within a single groundwater system that includes various hydraulically connected areas of unconfined and confined layers distinguished by the hydraulic properties of the local hydrostratigraphy.

Estimates of Aquifer Hydraulic Characteristics

The hydraulic characteristics of subsurface materials in the basin have been estimated using data from constant-rate aquifer tests and well-yield tests conducted by well drillers upon completion of new wells (Grondin and others, 2021). A constant-rate aquifer test consists of pumping a well at a known rate and measuring the drawdown and recovery (after pumping ceases) in the groundwater level with time in the pumping well and nearby non-pumping observation wells. The data collected allow generation of a curve showing the drawdown in relation to the amount of time since pumping began. The use of non-pumping observation wells provides evidence for the pumping response in three dimensions. Driller-reported well-yield tests include a pumping rate, test duration, a total drawdown at the end of the test, and the well diameter. Well-yield tests typically consist of a single drawdown measurement taken after a well has been pumped at a specified rate for a specified length of time, typically 1 hour (hr). The well yield per unit of drawdown is determined by dividing the pumping rate at any time during the test by the drawdown at the same time and is referred to as the "specific capacity," which is expressed in units of volume per unit time (such as gallons per minute [gpm]) per unit length [such as ft]). Specific-capacity tests were used to estimate aquifer transmissivity using a method developed by Vorhis (1979).

Transmissivity is a measure of permeability and is defined as the volume of water per unit time that will flow through a unit width of an aquifer perpendicular to the flow direction in response to a unit hydraulic head gradient (Lohman, 1972; Freeze and Cherry, 1979). Transmissivity has units of volume per unit time (such as cubic feet per day) per unit aquifer width (such as ft), which simplifies to length squared per unit time (such as feet squared per day [ft^2/d]). Because the calculated specific capacity may vary with the pumping rate and well construction, it provides a semiquantitative measure of aquifer hydraulic characteristics. Nevertheless, specific-capacity values can be used to evaluate relative differences in hydraulic characteristics between different geographic areas and different hydrogeologic units if data are available from many wells.

Constant-Rate Aquifer Tests

One constant-rate aquifer test conducted in the Harney Basin by OWRD and 41 4-hr, single-well pumping tests submitted to OWRD were available for analysis to estimate transmissivity. Additionally, continuous groundwater-level data from two observation wells near different irrigation (pumping) wells were available. Multiple episodes of groundwater-level drawdown and recovery were captured by the observation-well recorders during each irrigation season which corresponded to the nearby irrigation-well pumping and shut-off periods. Grondin and others (2021) described the tests, analytic methods, and results, and OWRD (2019) contain the test data. For 44 tests in the Harney Basin, estimates of transmissivity ranged from 35 to 17,790 ft^2/d. The lower values were most commonly associated with wells completed in predominantly fine-grained sediments underlying the Harney Basin lowlands. The higher values were most commonly associated with wells intercepting volcanic deposits with high primary permeability, such as HARN0050957 ($T = 15{,}495$ ft^2/d), and wells completed in consolidated sedimentary and volcanic rocks with secondary permeability from fractures, such as HARN0052663 ($T = 9{,}697$ ft^2/d).

Well-Yield Tests

Within a rectangular area of 433 townships encompassing the Harney Basin, 1,451 wells (1,161 within and 290 near but outside the basin) contained data necessary to estimate a transmissivity (Grondin and others, 2021). A single transmissivity calculation was made for each well. Wells where the drawdown during the pumping test was zero (91 wells) were assigned a drawdown of 0.5 ft (half of the estimated measurement error) to ensure the transmissivity calculations yielded finite values. Zero-drawdown wells commonly were associated with young volcanic deposits and were included to avoid introducing a potential bias against wells completed in high-transmissivity aquifers.

Values of transmissivity derived from specific-capacity tests ranged over six orders of magnitude (10^0–10^5 ft^2/d) across the Harney Basin, with values less than 1,000 ft^2/d comprising 50 percent of the results (Grondin and others, 2021). In the Harney Basin lowlands, wells having low transmissivities were intermixed with wells having high transmissivities, indicating that the subsurface materials in those areas are heterogeneous and discontinuous laterally and vertically. Transmissivities greater than 10,000 ft^2/d in the lowlands (about 13 percent of the results) predominantly were determined for wells along the western base of the Stinkingwater Mountains, in wells greater than 150 ft deep, and in areas with young volcanic deposits (fig. 7). Additional discussion of the methods used to determine subsurface hydraulic properties can be found in Grondin and others (2021).

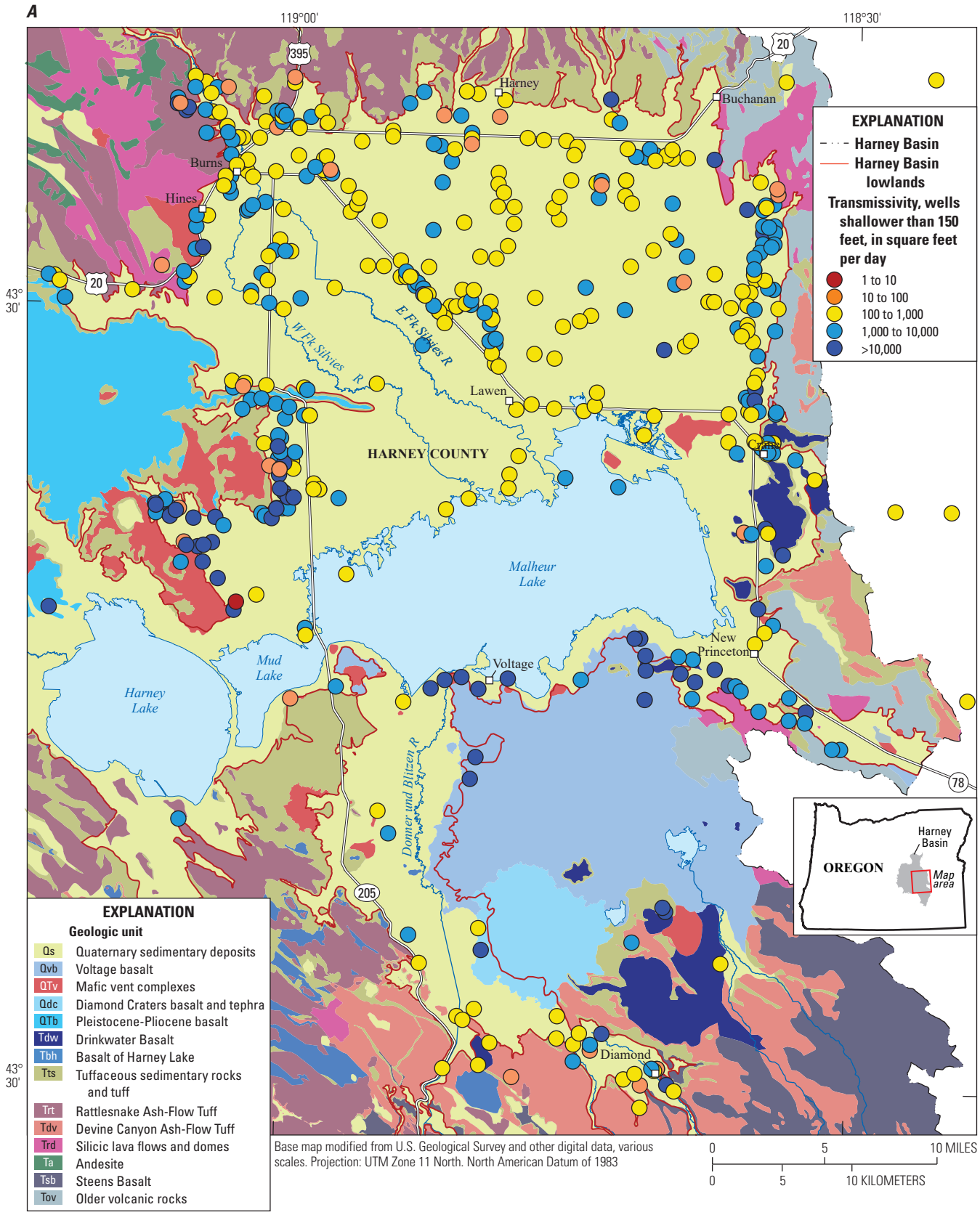

Figure 7. Transmissivity estimates from wells in and around the Harney Basin lowlands, southeastern Oregon. *A*, wells shallower than 150 feet; *B*, wells deeper than 150 feet.

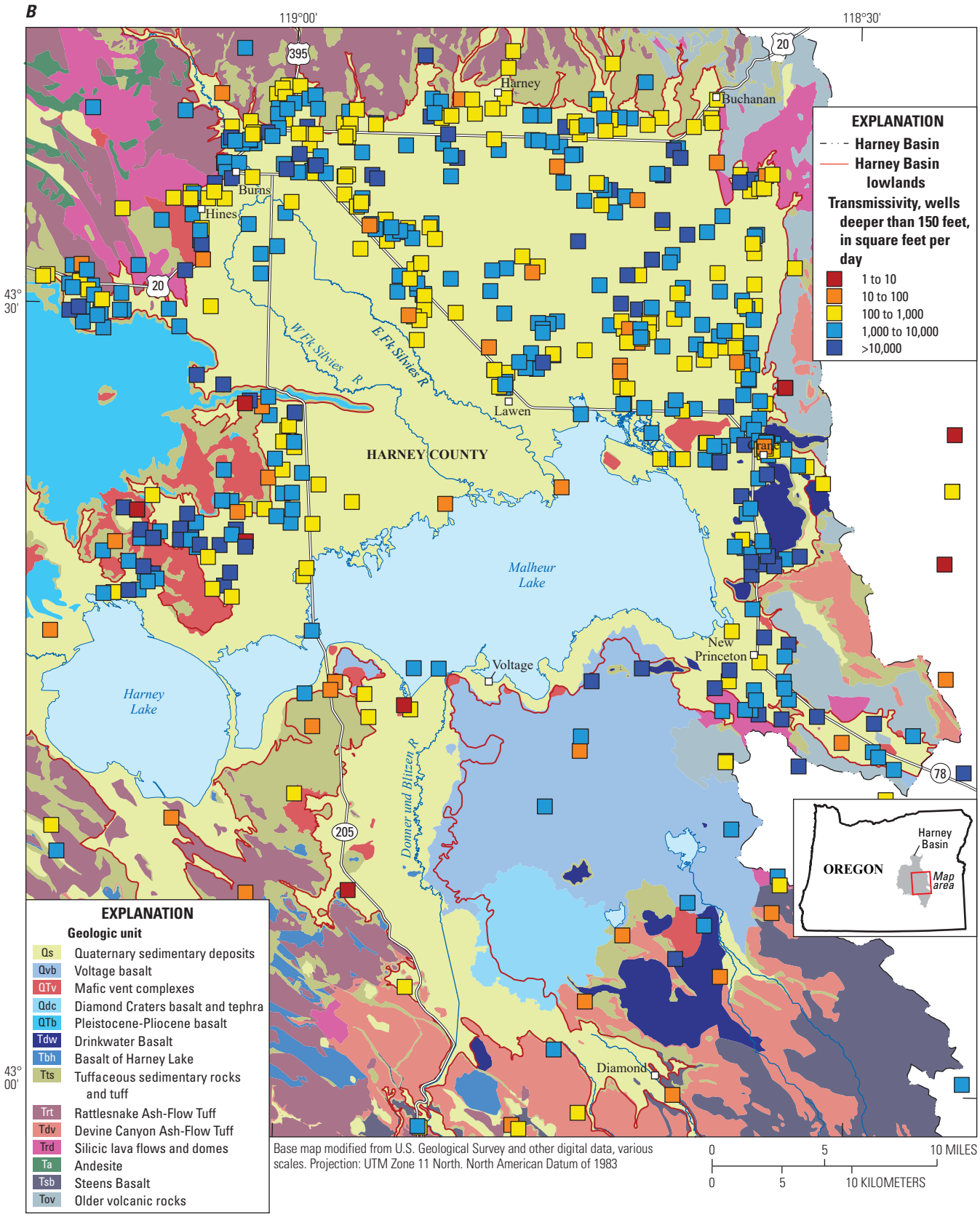

Figure 7.—Continued

Transmissivity of Stratigraphic Units

Transmissivity estimates were made for about 1,000 wells in the Harney Basin. The stratigraphy and open interval for each well with an estimated transmissivity value were interpreted from well reports (Grondin and others, 2021). A well and its corresponding transmissivity were associated with 1 of the 19 stratigraphic units defined for the Harney Basin if the stratigraphic unit comprised 90 percent or more of the open interval of the well.

The highest transmissivity values were associated with young, basaltic lava flows and volcaniclastic deposits, whereas the lowest transmissivity values were associated with the oldest units in the basin, including Mesozoic rocks (Mzu) and the older volcanic units of Steens Basalt (Tsb) and older volcanic rocks (Tov; Grondin and others, 2021). Transmissivity generally increased with decreasing silica content of volcanic units, increasing grain size of sedimentary units, and decreased alteration and induration of geologic units. No transmissivity values were estimated for the Pleistocene-Pliocene basalt (QTb) and Diamond Craters basalt and tephra units (Qdc) because they did not comprise 90 percent or more of the open interval of any well. Grondin and others (2021) reported a complete discussion and presentation of transmissivity values for the Harney Basin stratigraphic units.

Description of Hydrostratigraphic Units

For the purposes of describing regional hydrogeology and for modeling and analyzing groundwater, stratigraphic units are typically grouped into a smaller number of hydrostratigraphic units, which are distinguished and characterized by common hydraulic properties and consist of one or more stratigraphic units that occupy a similar stratigraphic position. The 19 stratigraphic units defined for the Harney Basin were grouped into 9 hydrostratigraphic units (HUs; figs. 8–9; table 1) based on similar ranges of transmissivity, spatial association, and physical properties (Grondin and others, 2021). As with the stratigraphic units, the transmissivity values associated with each HU came from wells where a HU occupies 90 percent or more of the open interval. Characterizing the hydraulic properties of different stratigraphic and hydrostratigraphic units does not imply that groundwater in these units is not hydraulically connected to other units or to surface water. These characterizations are important for describing the physics of groundwater flow and storage within each unit and between each unit. A summary description of each HU follows from oldest (generally deepest) to youngest (most shallow).

Table 1. Grouping of stratigraphic units into hydrostratigraphic units, Harney Basin, southeastern Oregon.

Hydrostratigraphic unit	Identifier	Stratigraphic unit
Younger basin fill (YBF)	Qs	Quaternary sedimentary deposits
Voltage basalt (VB)	Qvb	Voltage basalt
Proximal vent deposits (PVD)	Qdc	Diamond Craters basalt and tephra
	QTv	Mafic vent complexes
High Lava Plains basalt (HLP)	QTb	Pleistocene-Pliocene basalt
	Tob	Olivine basalt
	Tobg	Olivine basalt and andesite of Gum Boot Canyon
	Tdw	Drinkwater Basalt
	Tbh	Basalt of Harney Lake
Older basin fill (OBF)	QTsu	Undifferentiated basin fill deposits
	Tts	Tuffaceous sedimentary rocks and tuff
	Trt	Rattlesnake Ash-Flow Tuff
	Tdv	Devine Canyon Ash-Flow Tuff
Dry Mountain lavas (DML)	Tdm	Basalt and andesite of Dry Mountain
Silicic lava flows and domes (SFD)	Trd	Silicic lava flows and domes
	Ta	Andesite
Upland volcanic rocks (UVR)	Tsb	Steens Basalt
	Tov	Older volcanic rocks
Marine sedimentary rocks (MSR)	Mzu	Mesozoic rocks

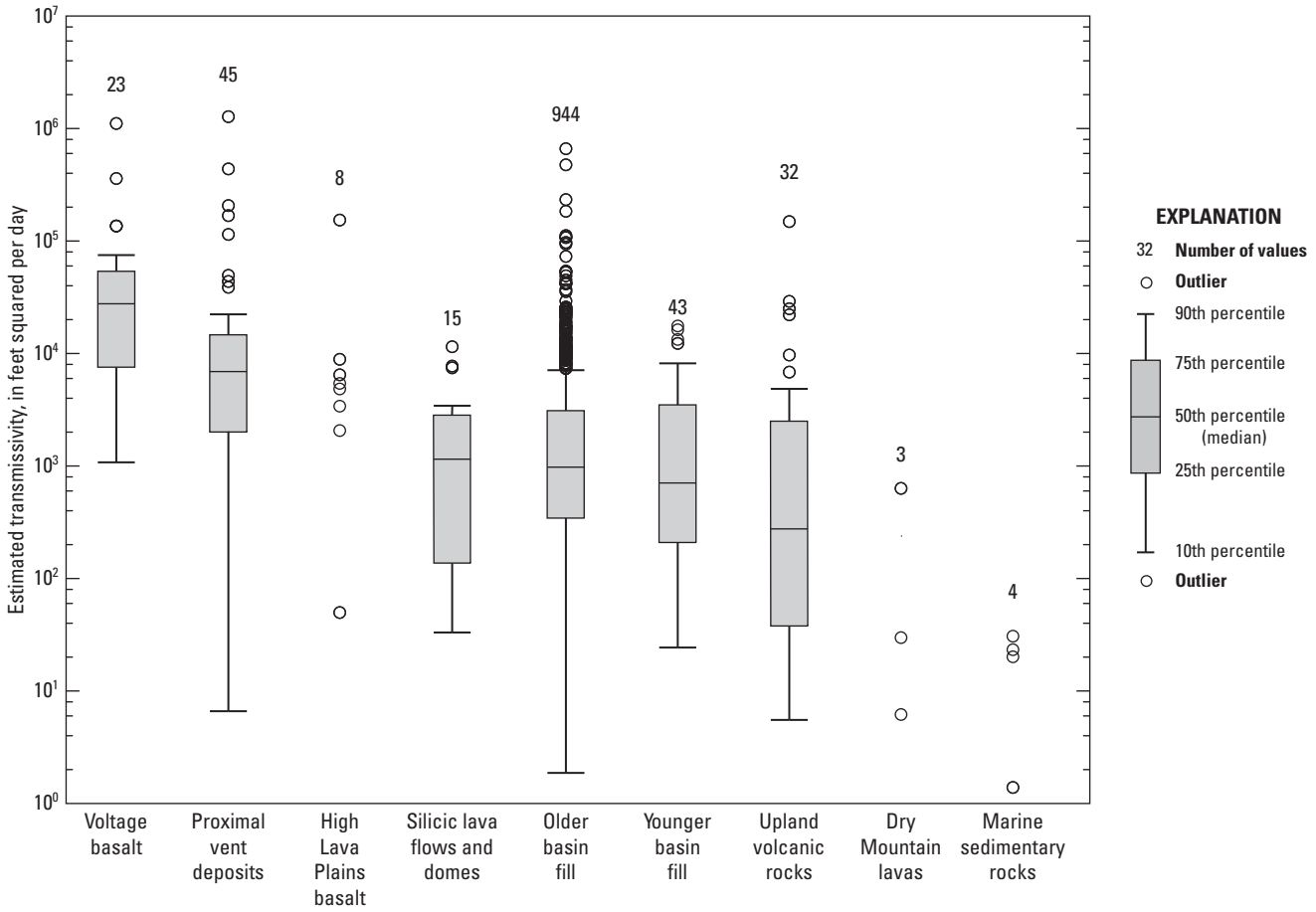

Figure 8. Transmissivity of hydrostratigraphic units, Harney Basin, southeastern Oregon. Modified from Grondin and others (2021).

Marine Sedimentary Rocks (MSR)

Surface exposures of this HU are limited to the northern uplands (fig. 9), but they are thought to form the hydrologic basement underlying much of the basin (Streck, 2002; McClaughry and others, 2019). This unit contains the Mesozoic rocks stratigraphic unit (table 1), which contains mostly marine sedimentary rocks but includes minor amounts of intrusive and metamorphic rocks. For simplicity, this unit will hereinafter be referred to as the "Marine sedimentary rocks HU." This HU is composed of fine-grained lithologies having low permeability. Even where coarse-grained lithologies exist, compaction, cementation, and metamorphism has eliminated much of the permeability. Secondary minerals are common in fracture zones and faults, indicating that much of the permeability created through structural deformation has also been subsequently lost (Brown and Thayer, 1963). In their report on the Mount Vernon quadrangle, Brown and Thayer (1966b) recognized that strata associated with the Marine sedimentary rocks HU in the Aldrich Mountains have low permeability and are unfavorable reservoir rocks for groundwater. The limited number of transmissivity estimates in these rocks (n=4) range from 1.4 to 31 ft^2/d (fig. 8), the lowest of all the HUs.

Upland Volcanic Rocks (UVR)

The Upland volcanic rocks HU forms the base of the Cenozoic section and is extensively exposed in the northern and southern uplands and along the eastern margin of the basin (fig. 9). This HU combines the Steens Basalt (Tsb) and the older volcanic rocks (Tov) (table 1). The thickness is variable, but it reaches a maximum of almost 10,000 ft in the south (Minor and others, 1987) and may be more than 6,500 ft thick in the northern uplands (Thayer, 1957). On the flanks of Steens Mountain, the unit is dominated by thin basalt lava flows with brecciated, vesicular, or clinkery upper and lower crusts and massive, vesicle-poor cores (Bondre and Hart, 2008). Camp and others (2013) observed that sedimentary and tuffaceous interbeds are notably absent in the Steens Basalt.

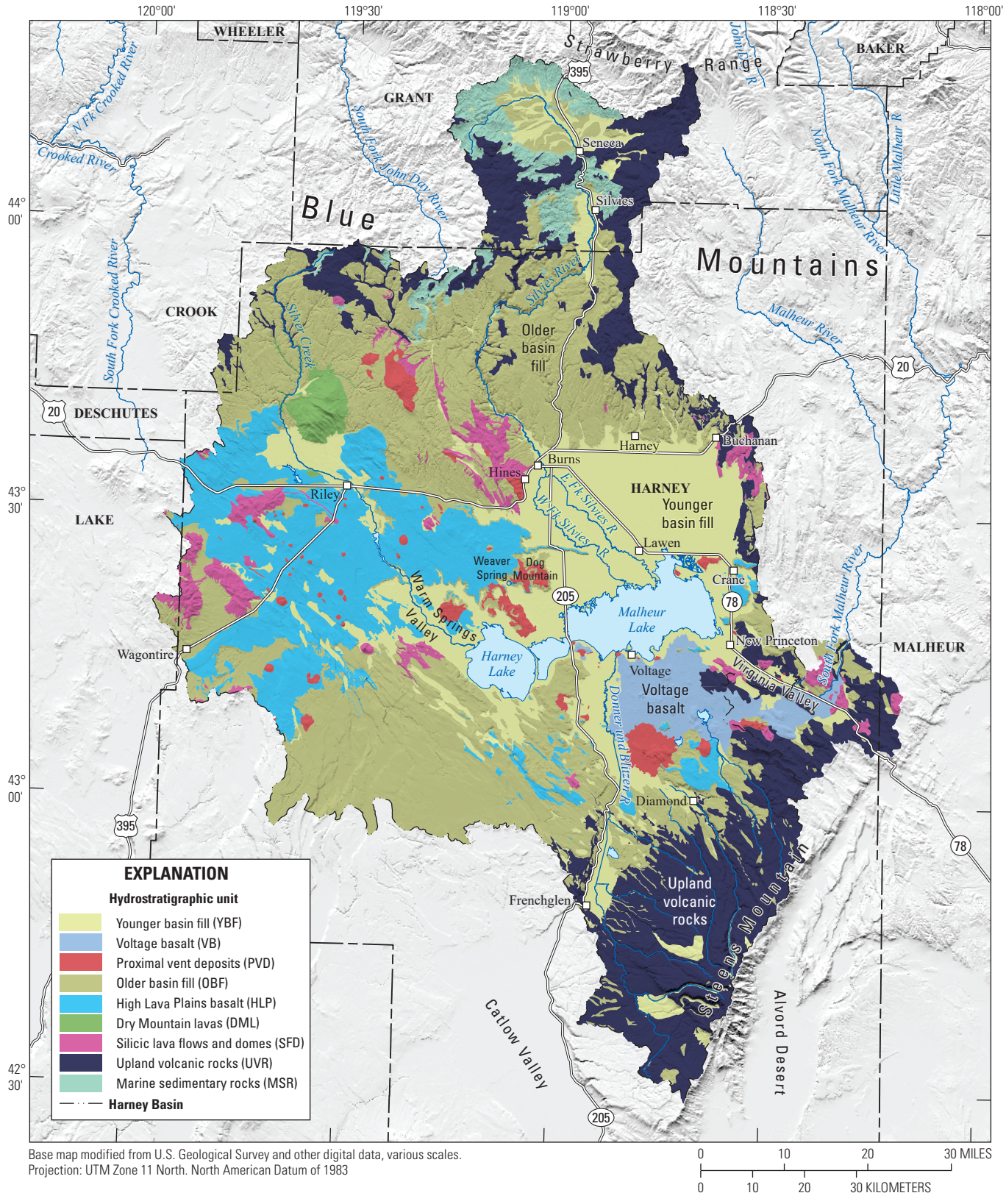

Figure 9. Surficial distribution of the hydrostratigraphic units, Harney Basin, southeastern Oregon.

The contacts between flow units within the Upland volcanic rocks HU are locally welded to varying degrees, and some flows are composed of thinner units whose margins have been annealed (Bondre and Hart, 2008). These flow characteristics may account in part for the relatively low transmissivities observed for wells developed in these rocks. Furthermore, Fuller (1931) described north-south-trending basaltic dikes exposed in valley walls of Steens Mountain. Dikes cut across the gently dipping lava flows that form most of Steens Mountain and generally impede groundwater flow. Transmissivity estimates for the Upland volcanic rocks HU (n=32) have a median value of 280 ft^2/d and an interquartile range of 38–2,500 ft^2/d (fig. 8).

Silicic Lava Flows and Domes (SFD)

The Silicic lava flows and domes HU occurs as widely scattered eruptive centers forming structural and constructional volcanic highs along the margins of the central lowlands (fig. 9). This HU's stratigraphic units of andesite and silicic lava flows and domes (table 1) are typically extruded as thick, highly viscous lava flows and domal masses of generally low permeability. Alteration to clay minerals and secondary silicification further reduces the potential for permeability in these rocks. Primary permeability may occur locally in brecciated bottoms of lava flows and along flow margins. Fragmental deposits associated with explosive eruptions and clastic deposits, including talus breccias and block and ash-flow deposits, may also provide local permeability. Secondary permeability occurs where these rocks are extensively fractured and faulted. The total thickness of these rocks is unknown but is likely substantially greater than 1,000 ft near central dome and vent areas, progressively thinning toward flow margins. Transmissivity estimates for the Silicic lava flows and domes HU (n=15) have a median value of 1,200 ft^2/d and an interquartile range of 140–2,800 ft^2/d (fig. 8).

Dry Mountain Lavas (DML)

The basalt and andesite lavas that form the Dry Mountain lavas HU are 6 mi northwest of Riley, where Dry Mountain rises more than 2,000 ft above Silver Creek (fig. 9). This basaltic and andesitic shield volcano is composed of numerous lava flows with an exposed thickness of more than 700 ft. The total thickness is unknown but is likely considerably more than this exposed portion given the overall size of Dry Mountain. A series of northwest-trending faults cuts through Dry Mountain, creating a stepped graben structure across which substantial extension has occurred. Some of these faults may have been active as recently as middle to late Quaternary (Weldon and others, 2003). The notable lack of springs, minimal surface-water runoff, and anecdotal reports of livestock-watering ponds unable to retain water all indicate that the Dry Mountain lavas should be highly permeable. The limited data available for wells completed in this unit (n=3) have substantially lower than anticipated transmissivity values ranging from 6.1 to 630 ft^2/d (fig. 8). However, these wells are along the lower, unfaulted flanks of the mountain. Exposures of Dry Mountain lavas in the canyon of Silver Creek downstream of McCanlies Road exhibit blocky, poorly connected fractures and jointing and little primary permeability. Secondary permeability likely exists at upper elevations where the unit is faulted.

Older Basin Fill (OBF)

These deposits flank the uplands and extend beneath the Younger basin fill HU under the Harney Basin lowlands (fig. 9). The stratigraphic units that form this HU include tuffaceous sedimentary rocks and tuff, the Devine Canyon and Rattlesnake Ash-Flow Tuffs, and undifferentiated basin fill deposits (table 1). The undifferentiated units were assigned to the Older basin fill HU because in many places the overlying Quaternary sedimentary deposits are relatively thin.

The sedimentary strata within the Older basin fill HU formed in a variety of depositional environments and include fluvial, lacustrine, colluvial, aeolian, and evaporite deposits. The deposits are diverse in physical character, highly lenticular, greatly varied in thickness locally, and grade into sediments of different lithology over short distances. Consequently, the Older basin fill HU sediments have a broad range of permeability depending on the depositional environment, grain size, sorting, depth and duration of burial, compaction, and cementation. In some areas, fine-grained lithologies such as siltstone and claystone can provide sufficient groundwater to irrigation wells through secondary fracturing. The individual ash-flow tuffs also exhibit a wide range of permeability depending on facies variations and alteration. In some locations, secondary minerals fill pore spaces within the various basin-fill lithologies and reduce primary permeability. The combined effect of these depositional and diagenetic processes results in a complex basin-fill unit with highly heterogenous permeability.

The Older basin fill HU varies greatly in thickness. Along the flanks of Steens Mountain and in the northern uplands, the unit thins considerably and pinches out where it laps onto the underlying rocks. The unit thickens substantially toward the central Harney Basin lowlands where it is penetrated by numerous wells to depths greater than 1,000 ft. Drilling records from oil and gas wells within the basin indicate that the deposits may be nearly 4,000 ft thick in some places, although stratigraphic interpretations from the records are ambiguous. Estimates of transmissivity for the Older basin fill HU (n=944) have a median of 980 ft^2/d and an interquartile range of 340–3,000 ft^2/d; however, the entire range spans six orders of magnitude (10^0–10^5 ft^2/d; fig. 8).

High Lava Plains Basalt (HLP)

The High Lava Plains basalt HU is widely exposed at the surface in the western part of the basin and underlies the Younger basin fill HU beneath much of Silver Creek (fig. 9). A few exposures also occur along the southeastern margin of the Harney Basin lowlands and in the faulted uplands south of Harney Lake. This HU contains the stratigraphic units identified as basalt (Pleistocene and Pliocene), olivine basalt, olivine basalt and andesite of Gum Boot Canyon, Drinkwater Basalt, and the basalt of Harney Lake (table 1). These rocks commonly occur as thin compound lava flows with vesicular, brecciated or clinkery zones at flow tops, and vesicular, brecciated basal zones. Columnar and platy jointing are common and thin interbeds of tuffaceous sedimentary rocks occur locally. The jointing, vesicles, breccia zones, and thin, overlapping nature of these flows provide abundant interconnected pore space, and much of the primary permeability remains intact due to the relatively youthful age of the unit. Wells along Silver Creek Valley produce groundwater from this HU with reported yields greater than 1,000 gpm. The thickness of the HU varies widely across the basin, but based on well reports and mapped exposures, the total composite thickness may approach 1,000 ft. The limited number of tests (n=8) for wells completed in this HU have relatively high transmissivities ranging from 50 to 150,000 ft^2/d, with a median of 3,900 ft^2/d (fig. 8).

Proximal Vent Deposits (PVD)

Proximal vent deposits created by fragmentation of magma during explosive eruptions of lava are scattered widely across the High Lava Plains province of the basin (fig. 9). This HU combines mafic vent complexes and Diamond Craters basalt and tephra (table 1). These highly fragmented piles of volcanic material and thin lava flows have abundant interconnected open pore space and commonly have very high permeability. Variations in clast size, sorting, and degree of welding and induration can result in variable permeability. Localized clay-rich altered tuff formed by phreatomagmatic eruptions associated with these deposits results in low-permeability in some areas. Generally, however, proximal vent deposits are among the most permeable rocks in the basin, and many wells completed in these deposits have high yields. The thickness of the Proximal vent deposits HU depends on the overall size of the eruptive center that produced the deposits and proximity to the central part of the eruptive center. Generally, the deposits are thickest at the central part of the eruptive center, thinning toward the margins where they feather out into the surrounding deposits. At the Weaver Spring/Dog Mountain area (Sunset Valley; plate 1), the Proximal vent deposits HU is complexly interbedded with the Older basin fill HU sediments. Here, individual layers of the Proximal vent deposits HU are commonly 20–100 ft thick ranging up to nearly 500 ft thick. The median of the transmissivity estimates for this HU (n=45) is 6,900 ft^{2}d, with an interquartile range of 2,000–15,000 ft^2/d (fig. 8).

Voltage Basalt (VB)

The Voltage basalt HU covers more than 150 mi^2 south and southeast of Malheur Lake (fig. 9). The thin, overlapping lava flows of this HU are commonly rubbly and scoriaceous with abundant blocky, fragmental zones and surface crusts uplifted and fractured by formation of tumuli. Thin, ropy pahoehoe flows fed by large- and small-scale distributary tube systems are also common. The resulting volcanic pile has abundant interior void space and very high permeability. Many wells developing groundwater from this HU can pump greater than 1,000 gpm with minimal drawdown. A total thickness up to 320 ft has been penetrated by wells in the central part of the Voltage basalt HU, but most wells that penetrate through the entire HU encounter the underlying Older basin fill HU after less than 200 ft. Greater thicknesses may exist where these lavas filled in low areas in the paleotopographic surface. The median transmissivity estimate for this HU (n=23) is 28,000 ft^{2}d, the highest median value of all the HUs (fig. 8); the interquartile range for this unit is 7,600–54,000 ft^{2}d.

Younger Basin Fill (YBF)

Consisting of Quaternary sediments deposited after the damming of Virginia Valley by the Voltage basalt about 1.5 Ma (Jordan and others, 2004; Sherrod, 2012), the Younger basin fill HU makes up the uppermost part of the basin fill in the Harney Basin lowlands and occupies modern stream channels and floodplains (fig. 9). The YBF sedimentary strata, which formed in a variety of depositional environments include fluvial, lacustrine, colluvial, aeolian, and evaporite deposits, as well as glacial till and morainal deposits on Steens Mountain. The YBF sediments are commonly unconsolidated but locally semiconsolidated at depth. As observed by Waring (1909), Piper and others (1939), and Leonard (1970), the Younger basin fill HU is generally finer toward the center of the valley where low energy fluvial and lacustrine processes dominate, and coarser toward the margins where higher energy streams enter the valley floor from the upper elevation parts of their catchments.

The Younger basin fill HU sediments are sourced from the same upland lithologies as the Older basin fill HU and therefore can have similar petrologic character and degree of consolidation. This makes the two HUs difficult to distinguish in the subsurface, especially when making interpretations based solely on drillers' formation descriptions listed in well reports. Previous investigators recognized the difficulty of estimating the thickness of the Younger basin fill HU and made their estimates based largely in well reports that were suggestive of consolidation and cementation. Waring (1909) estimated that the Quaternary fill is less than 300 ft thick at most places; Piper and others (1939) estimated that the Quaternary fill is about 100 ft thick within 5 mi of Burns and along the northeastern margin of the valley, thickening to 200–275 ft north of Malheur Lake; and Leonard (1970) suggested that the unconsolidated valley fill has a maximum thickness of about 250 ft. Estimates of transmissivity for the Younger basin fill HU (n=43) have a median of 710 ft^2/d and an interquartile range of 210–3,500 ft^2/d (fig. 8).

Hydrologic Budget

A hydrologic budget provides an accounting of groundwater inflows (recharge), outflows (discharge), and change in storage (which manifests as a change in groundwater levels). In the Harney Basin, recharge processes include infiltration of precipitation, infiltration of streamflow, and infiltration of irrigation water. Limited groundwater-level data indicate that groundwater inflow from outside the Harney Basin is minor. Groundwater discharges naturally through springs, seepage into streams (base flow), evapotranspiration (which includes transpiration by phreatophytes and evaporation from the soil), and groundwater outflow to the Malheur River Basin. Additional groundwater discharge occurs by pumping wells for irrigation, public supply, stock water, and other uses. Prior to development, most of the groundwater discharge was to streams and springs in the uplands and evapotranspiration (ET) in the Harney Basin lowlands. The major groundwater budget components for the Harney Basin during present-day conditions are depicted schematically in figure 10.

If the groundwater budget components were to be measured in any given year, recharge to and discharge from the groundwater system likely would not exactly be equal, and some water would have to be added to or removed from groundwater storage to make up the difference; the difference between recharge and discharge is the change in groundwater storage. This can be represented quantitatively as:

$$Recharge = Discharge \pm Change\ in\ Storage \quad (1)$$

where

Recharge is the total groundwater recharge,
Discharge is the total groundwater discharge, and
Change in Storage is the total change in groundwater storage per time in the Harney Basin.

A series of above-average precipitation years would result in recharge exceeding discharge and an increase in the amount of groundwater in storage. Conversely, a series of below-average precipitation years would result in discharge exceeding recharge and a decline in groundwater storage. Changes in groundwater storage typically manifest as a rise or decline in the elevation of the water table or hydraulic head. Although the pre-development groundwater budget likely was not in balance in any particular year, when averaged across years or decades, the change in groundwater storage was equal to zero and the long-term mean budget was in balance.

The mean annual groundwater budget for current conditions in the Harney Basin (1982–2016) was assessed and reported by Garcia and others (2022). Groundwater recharge to the lowlands was estimated as 173,000 acre-ft/yr (table 2), and the annual groundwater discharge from the lowlands was estimated as 283,000 acre-ft/yr (table 3). Under current conditions, the annual groundwater discharge exceeds annual recharge by 110,000 acre-ft/yr, indicating that the hydrologic budget is out of balance because the change in groundwater storage is not zero. The major perturbation to the groundwater budget since pre-development conditions is groundwater pumpage, primarily for irrigation. Garcia and others (2022) estimated that during 2017–18 the mean amount of groundwater pumped for all purposes was 152,000 acre-ft/yr, 95 percent of which was for irrigation. About 8,000 acre-ft/yr of pumped groundwater returns as recharge, more than 7,000 acre-ft/yr beneath irrigated fields and 900 acre-ft/yr from other non-irrigation groundwater uses.

A summary of the various components of the hydrologic budget are provided in the following sections of the report. A detailed description of the development of each component is provided by Garcia and others (2022).

Table 2. Estimated mean annual groundwater recharge components by region, Harney Basin, southeastern Oregon, 1982–2016.

[Modified from Garcia and others (2022). Regions are shown in figures 1 and 11. Recharge estimates are rounded to two significant figures for values below 100,000, and three significant figures for values above 100,000. **Geographic position**: position of water-bearing units receiving recharge. Groundwater inflow from uplands: upland recharge that flows through the subsurface and recharges lowland groundwater, computed as upland recharge minus upland base flow and spring flow]

Geographic position	Recharge source water	Mean annual recharge by region (acre-feet per year)			
		Northern	Southern	Western	Harney Basin
Upland	Precipitation and snowmelt	86,000	157,000	45,000	288,000
Lowland	Groundwater inflow from uplands	9,000	20,000	20,000	49,000
	Streamflow (natural) [1, 2]	40,000	900	18,000	59,000
	Streamflow (irrigation)	24,000	26,000	7,300	57,000
	Groundwater irrigation and other uses[3]	4,800	1,200	2,200	8,200
	Lowland Total	78,000	48,000	47,000	173,000

[1]Includes a part of upland runoff and base flow.

[2]Includes channel losses from irrigation canals.

[3]From irrigation and other groundwater uses. Estimate is basin-wide, but more than 90 percent of the groundwater use occurs in lowlands.

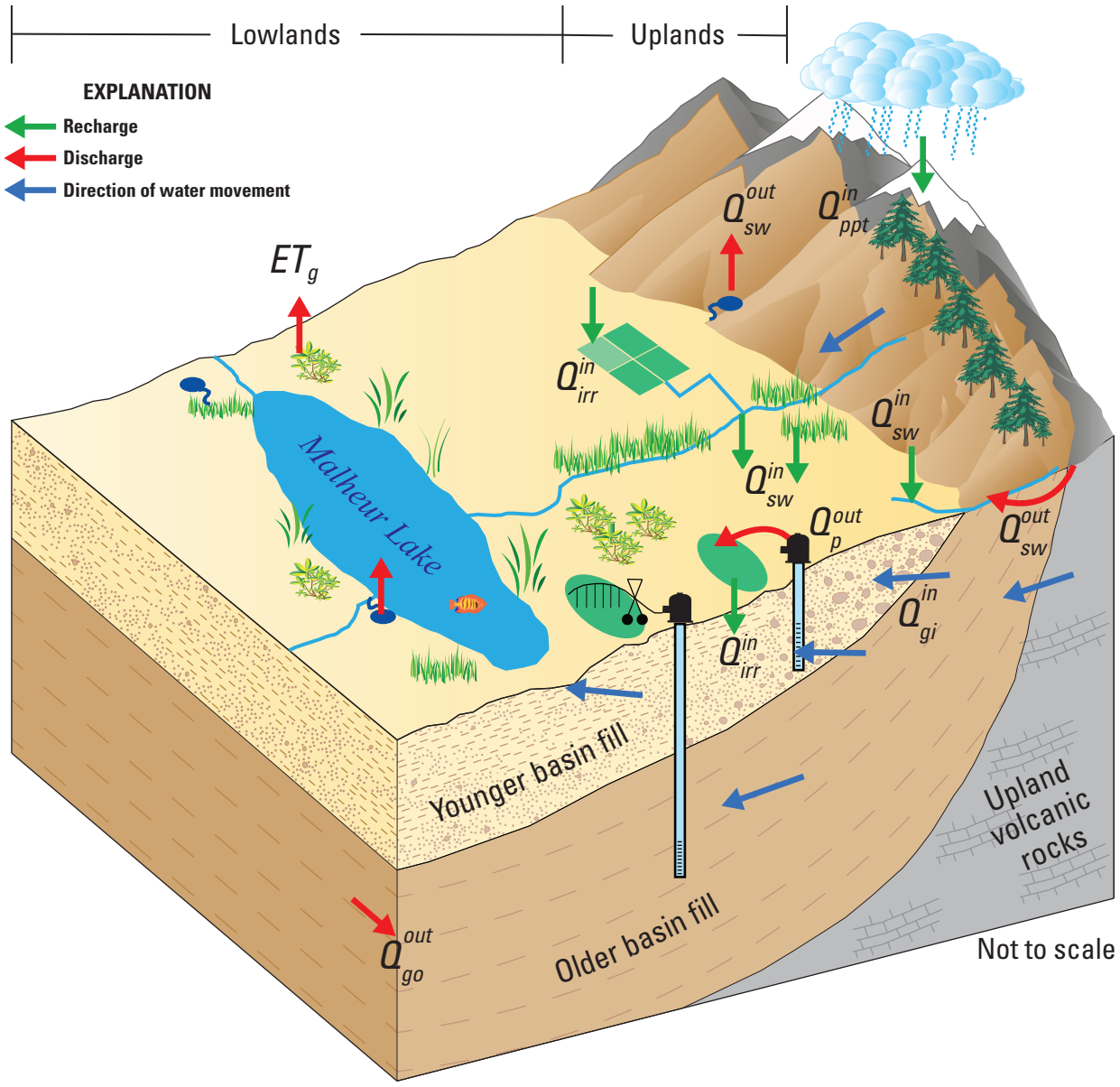

Figure 10. Schematic block diagram of groundwater recharge and discharge and direction of water movement, Harney Basin, southeastern Oregon. Recharge and discharge components are from equations 2 and 3 and include: Q^{in}_{ppt}, upland recharge from precipitation and snowmelt; Q^{in}_{sw}, lowland recharge from surface water; Q^{in}_{irr}, lowland recharge from irrigation water and other non-irrigation water use; Q^{in}_{gi}, lowland recharge from groundwater inflow from uplands; ET_g, groundwater discharge through evapotranspiration; Q^{out}_{sw}, groundwater discharge to surface water; Q^{out}_{p}, groundwater discharge through pumpage; and Q^{out}_{go}, groundwater outflow to Malheur River Basin.

Table 3. Estimated mean annual groundwater discharge components by region, Harney Basin, southeastern Oregon, 1982–2016.

[Modified from Garcia and others, 2022. Values represent the mean of input ranges. Discharge estimates are rounded to two significant figures for values below 100,000, and three significant figures for values above 100,000. Discharge totals are summarized by column and row and therefore might differ. Regions are shown in figure 11. Values presented in parentheses are accounted for in other estimate totals. **Geographic position**: position of water-bearing units where recharge and discharge occur. **Mean annual discharge by region**: Values represent the mean of input ranges. **Abbreviations**: ET, evapotranspiration; MRB, Malheur River Basin; <, less than; —, not estimated]

Geographic position	Component	Mean annual discharge by region (acre-feet per year)			
		Northern	Southern	Western	Harney Basin
Upland	Base flow	75,000	125,000	25,000	225,000
	Springs[1]	2,000	12,000	22	14,000
	Upland total	**77,000**	**137,000**	**25,000**	**239,000**
Lowland	Springs	530	[2]8,900	[3](25,000)	8,900
	ET_g(natural)[4]	64,000	20,000	35,000	119,000
	Diffuse flux to lakes[5]	(44)	(60)	(630)	(730)
	Groundwater flow–MRB	—	3,100	—	3,100
	Total without pumpage	64,000	32,000	35,000	131,000
	Irrigation pumpage[6,7]	81,000	22,000	42,000	145,000
	Non-irrigation pumpage[7]	6,100	470	400	7,000
	Total pumpage	87,000	22,000	43,000	152,000
	Lowland total	151,000	54,000	78,000	283,000

[1]Estimates represent discharges unaccounted for in base-flow estimates and include current and historical spring discharge measurements.

[2]Mean of measurements made during 1907–1980

[3]Summation of current and historical measurements.

[4]ET from natural areas. Includes ET of spring discharge and ET from spring-irrigated agriculture that otherwise would be lost as ET from natural areas.

[5]Sum of groundwater fluxes toward Malheur and Harney Lakes. Estimates accounted for in ET_g (natural) estimates.

[6]2017–18 average groundwater pumpage.

[7]Values include pumpage from the full basin but most occurs in lowland areas.

Overview of the Detailed Groundwater Hydrologic Budget

The detailed groundwater budget for the entire Harney Basin can be represented quantitatively as:

$$Q_{ppt}^{in} + Q_{sw}^{in} + Q_{irr}^{in} = ET_g + Q_{sw}^{out} + Q_p^{out} + Q_{go}^{out} + \Delta S_{gw}, \quad (2)$$

and for the Harney Basin lowlands as:

$$Q_{gi}^{in} + Q_{sw}^{in} + Q_{irr}^{in} = ET_g + Q_{sw}^{out} + Q_p^{out} + Q_{go}^{out} + \Delta S_{gw} \quad (3)$$

where

Q_{ppt}^{in} is groundwater recharge from infiltration of precipitation and snowmelt through soils and permeable bedrock (occurs in upland areas only),

Q_{sw}^{in} is groundwater recharge from infiltration of surface water (streams, floodwater, and lakes),

Q_{irr}^{in} is groundwater recharge from infiltration of irrigation water (surface water and groundwater) and pumpage for non-irrigation groundwater use,

ET_g is groundwater discharge through ET by phreatophytes and bare soil,

Q_{sw}^{out} is groundwater discharge to surface water (streams, springs, and lakes),

Q_p^{out} is groundwater discharge through pumpage,

Q_{go}^{out} is groundwater discharge through groundwater outflow from the Harney Basin to the Malheur River Basin,

ΔS_{gw} is change in groundwater storage, and

Q_{gi}^{in} is groundwater flow from uplands to lowlands.

The movement of groundwater in the Harney Basin and its relation to specific groundwater budget components can be illustrated by considering the fate of upland precipitation and snowmelt, which is the primary source of all groundwater in the basin (fig. 10). Upland precipitation and snowmelt that is not lost to ET or as direct runoff to streams infiltrates through the soil and into the geologic deposits underlying upland areas (Q_{ppt}^{in}). Part of this upland recharge moves directly through the subsurface from the upland deposits into the deposits underlying the adjacent Harney Basin lowlands (Q_{gi}^{in}). Another part of this upland recharge discharges in the uplands as springs or as base flow to streams (Q_{sw}^{out}), and a relatively small amount of this water is lost as ET (ET_g). Streams exiting the uplands convey a mixture of groundwater discharged as base flow and direct runoff of precipitation and snowmelt, and the infiltration of a part of this water recharges deposits underlying the Harney Basin lowlands (Q_{sw}^{in}; fig. 10). The minor part of streamflow that reaches Malheur and Harney Lakes evaporates or recharges the underlying lowland deposits. Most groundwater in the lowlands ultimately discharges in the lowlands as ET (ET_g) or through pumpage (Q_p^{out}; fig. 10); a very small proportion exits the Harney Basin as groundwater outflow (Q_{so}^{out}).

Surface-water and groundwater development in the Harney Basin has altered regional recharge and discharge components of the water budget (Garcia and others, 2022). Upland recharge from direct infiltration of precipitation and snowmelt likely is similar to predevelopment conditions, whereas infiltration of streamflow and floodwater in the Harney Basin lowlands likely has been altered to some extent by surface-water diversions for irrigation beginning in the late 1800s. Similarly, groundwater discharge in the uplands is largely similar to predevelopment conditions, but groundwater discharge in the lowlands has been changed substantially by pumpage.

Garcia and others (2022) divided the Harney Basin into three analysis regions based on topography of the uplands and groundwater flowpaths near the center of the basin to ease comparison of groundwater recharge and discharge volumes and to evaluate groundwater development through time. The three regions are (1) the northern region, which includes the areas of the Harney Basin lowlands and the uplands north and east of Malheur Lake, including the entire Silvies River drainage, (2) the western region, which includes the lowland and upland areas north, south, and west of Harney Lake, including the entire Silver Creek drainage, and (3) the southern region, which includes the areas south and southeast of Malheur Lake, including all of Steens Mountain, the Donner und Blitzen River drainage, and Virginia Valley (fig. 11). The regions represent generalized connected groundwater recharge and should discharge, but not be considered separate flow systems (Garcia and others, 2022).

Groundwater Recharge

The principal natural recharge areas in the Harney Basin are the (1) uplands of the Blue Mountains and Steens Mountain and the (2) floodplains of the Silvies River, Donner und Blitzen River, Silver Creek, and the smaller streams entering the Harney Basin lowlands. The principal recharge mechanisms in the Harney Basin are infiltration of precipitation and snowmelt, streamflow loss through channel seepage, infiltration of the annual springtime freshet floodwater across the inundated lowland areas, and infiltration of irrigation water. In upland areas where the soil and underlying hydrostratigraphic units have low permeability (for example, areas underlain by the MSR and UVR HUs; figs. 8–9), infiltrating precipitation tends to flow along shallow groundwater flowpaths to nearby streams and springs; little precipitation infiltrates deeply in these settings. These areas typically have well-developed stream networks to convey rainfall and snowmelt that cannot

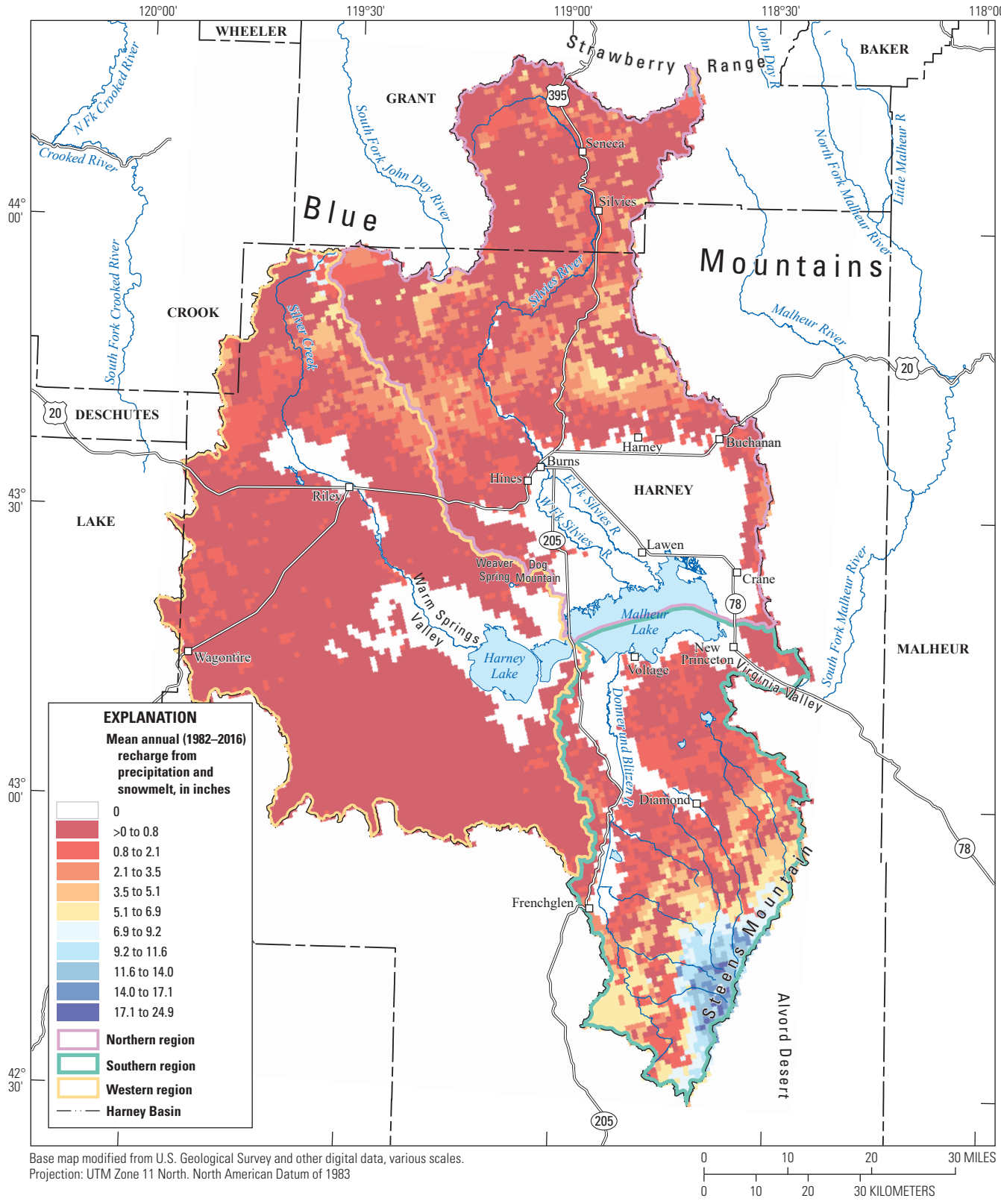

Figure 11. Location of recharge evaluation regions and distribution of estimated mean annual upland groundwater recharge from direct infiltration of precipitation and snowmelt, Harney Basin, southeastern Oregon, water years 1982–2016. Map modified from Garcia and others (2022).

infiltrate. In areas where the soil and underlying geologic deposits have high permeability (for example, areas underlain by the HLP HU; figs. 8–9), a larger proportion of precipitation infiltrates, groundwater flowpaths are typically longer and deeper, and stream networks tend to be poorly developed due to the lack of runoff. Substantial groundwater inflow to the Harney Basin from the surrounding groundwater basins is unlikely; however, water-level data are insufficient to rule out the possibility of a small amount of inflow.

Upland Groundwater Recharge

Recharge from precipitation and snowmelt (Q_{ppt}^{in}) primarily occurs in the uplands owing to higher precipitation amounts in these areas. About 288,000 acre-ft/yr of precipitation and snowmelt recharges the Harney Basin uplands and represents about 8 percent of the approximately 3.4 million acre-ft/yr of mean annual precipitation in the uplands (Garcia and others, 2022). Expressed as a depth of water uniformly distributed across upland areas, mean annual recharge is about 1.3 in. Of the remaining precipitation that falls in the Harney Basin uplands, 2.7 million acre-ft/yr (79 percent) returns to the atmosphere through ET, about 290,000 acre-ft/yr (about 9 percent) runs off as overland flow to streams, and about 130,000 acre-ft/yr (4 percent) is lost during winter to snow sublimation or is blown out of the basin (Garcia and others, 2022). The estimate of recharge from upland precipitation is largest in the southern region draining Steens Mountain and smallest in the western region, which has the lowest average upland elevation and precipitation of the three regions (fig. 3).

Recharge in the uplands was estimated using a soil-water-balance model (fig. 11; Garcia and others, 2022; Corson-Dosch and Garcia, 2022). Soil-water-balance models simulate the spatial and temporal distribution of recharge by partitioning residual precipitation into direct runoff, ET, soil water storage, and recharge; residual precipitation is the part of total precipitation that reaches the ground after accounting for ET of precipitation intercepted by the tree canopy. Input datasets include gridded daily climate data from GridMET (Abatzoglou, 2012), soil properties from the Soil Survey Geographic Database (SSURGO) and The Digital General Soil Map (STATSGO2; Soil Survey Staff, 2018), land cover from Oregon Biodiversity Information Center (2010). Additional details about input datasets and model development are provided in Corson-Dosch and Garcia (2022) and Garcia and others (2022).

Lowland Groundwater Recharge

Groundwater recharge to subsurface deposits beneath the Harney Basin lowlands totaled 173,000 acre-ft/yr (Garcia and others, 2022). Recharge to the Harney Basin lowlands includes groundwater inflow from upland rocks, infiltration of surface water (from natural flooding and irrigation), infiltration of applied pumpage for irrigation and other uses, and minor lake-water infiltration. Recharge from precipitation in the lowlands is negligible or non-existent due to low precipitation, high ET demand, and widespread low-permeability deposits. Recharge to the Harney Basin lowlands was 78,000 acre-ft/yr in the northern region, 48,000 acre-ft/yr in the southern region, and 47,000 acre-ft/yr in the western region (table 2).

The largest source of lowland recharge in the northern region was surface water (82 percent), with a lesser contribution from groundwater inflow from upland areas (12 percent) and reinfiltration of pumpage (6 percent). In the southern region, most lowland recharge (56 percent) was from surface water, with groundwater inflow from upland areas providing most of the rest (42 percent); 3 percent was from the reinfiltration of pumpage. In the western region, lowland recharge was mostly sourced from surface water (53 percent) and groundwater inflow from upland areas (42 percent); 5 percent was from the reinfiltration of pumpage. Lake-water infiltration was negligible; estimated less than 100 acre-ft/yr (Garcia and others, 2022).

During 1982–2016, lowland recharge by groundwater inflow from uplands (Q_{gi}^{in}) totaled about 49,000 acre-ft/yr (Garcia and others, 2022). Groundwater inflow from uplands represents the net recharge of upland areas, or the difference between groundwater recharge from precipitation and snowmelt and groundwater discharge to streams and springs.

Infiltration of streamflow and floodwater provides recharge between the upland-valley margins and Malheur and Harney Lakes (fig. 12), but most likely recharges within a few miles of the upland-valley margins where streamflow and floodwater infiltrate through the relatively coarse, unconsolidated surficial deposits surrounding the periphery of the lowlands (Piper and others, 1939). Surficial deposits in the lowlands generally become finer within a few miles from the upland-valley margins, which limits the infiltration of surface water and, hence, groundwater recharge.

The area where surface water infiltrates in the lowlands varies from year-to-year and depends on the size of the snowpack accumulated during the previous winter. During the annual springtime freshet, the Silvies River, Donner und Blitzen River, Silver Creek, and other smaller streams often overtop their channels, and floodwater spreads across the surrounding land. In years of normal and lower-than-normal precipitation, the floodwater largely is managed by a network of ditches to provide irrigation to near-stream native grass meadows across the lowlands, including the Malheur NWR; infiltration largely is limited to the stream channels and areas receiving irrigation water. In years of exceptionally large runoff (for example, 2017), floodwaters are difficult to manage and inundate substantial parts of the floodplains surrounding the major rivers and streams (fig. 12) for many months, and a substantial amount of floodwater reaches Malheur and Harney Lakes. In all years, most of the floodwater delivered by the annual freshet is consumed by ET, and only a small fraction percolates downward and recharges the groundwater system. Recharge from streamflow in the lowlands averaged 116,000 acre-ft/yr and was estimated by Garcia and others (2022) as the difference between streamflow and spring flow issuing from upland areas to lowland areas and (a) streamflow to Malheur and Harney Lakes, (b) ET of natural, overbank flooding, and (c) ET of streamflow used for irrigation.

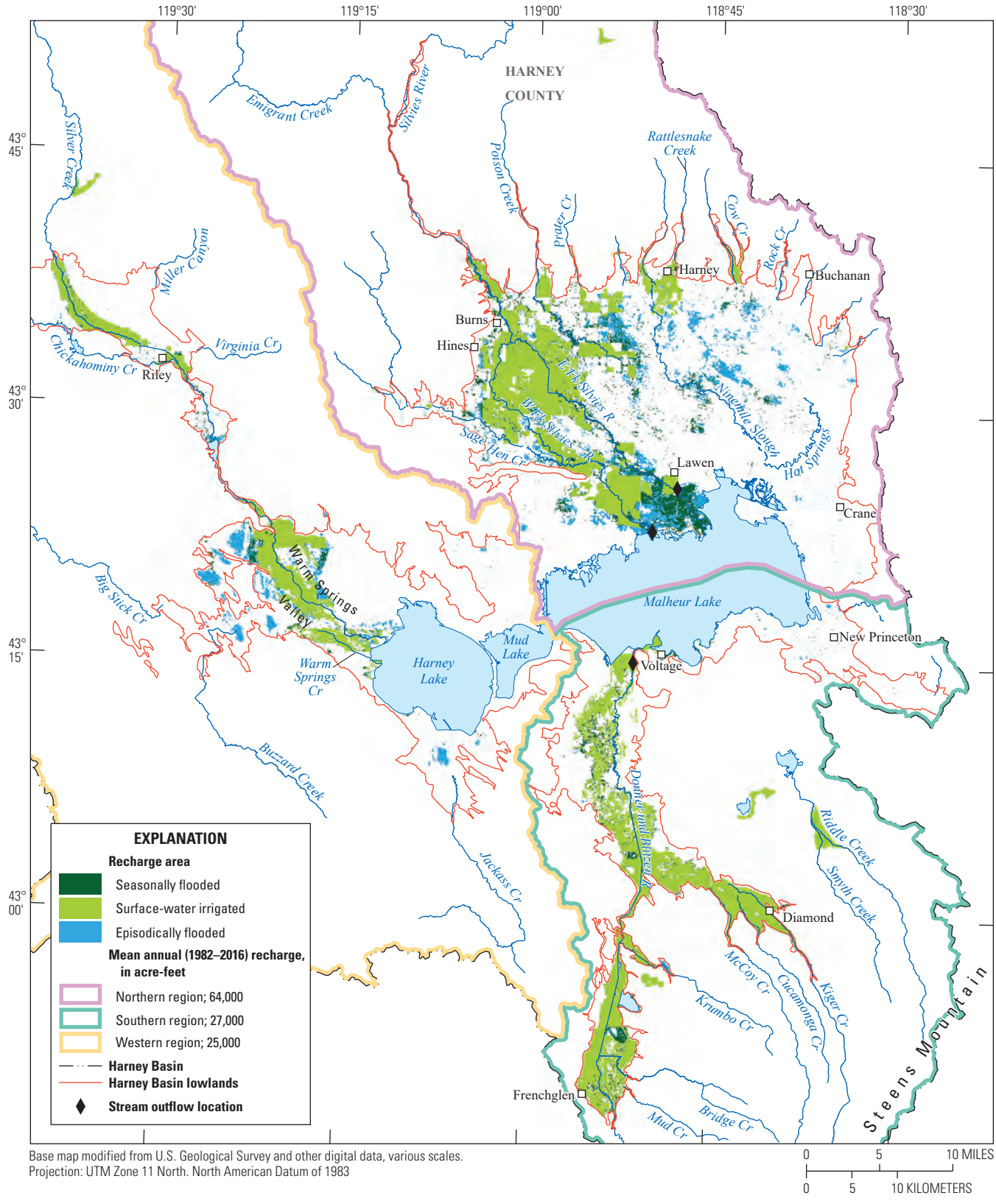

Figure 12. Location and volume of recharge from infiltration of surface water beneath streams and surface-water-flooded areas, Harney Basin, southeastern Oregon. Map from Garcia and others (2022).

Recharge from applied irrigation water (Q_{irr}^{in}) on groundwater-irrigated fields on the Harney Basin lowlands was estimated as 8,200 acre-ft/yr (Garcia and others, 2022). Garcia and others (2022) estimated 5–13 percent of applied groundwater irrigation reinfiltrated as recharge. The rate of recharge under groundwater-irrigated fields reflects greater irrigation efficiencies associated with center-pivot sprinkler systems when compared to flood irrigation used in surface-water irrigated fields (13–17 percent expected to reinfiltrate). Because most of the efficiency losses in groundwater-irrigated fields are attributed to wind losses before irrigation water reaches the land surface, little excess water remains to become recharge.

A minimal amount (about 200 acre-ft/yr) of lake water is estimated to recharge lowland deposits to the north of Harney Lake and to the northwest and east of Malheur Lake. This amount was estimated using hydraulic head gradients near the lakes and geochemical evidence that indicates some groundwater flow toward areas of irrigation pumpage, but the recharge volume was likely within the estimate uncertainty (Garcia and others, 2022) and therefore was not included in lowland recharge estimates.

Groundwater Discharge

The principal mechanisms of natural groundwater discharge in the Harney Basin include discharge to surface water (streams, springs, and lakes), ET by phreatophytes, and groundwater outflow to the Malheur River Basin. A large amount of groundwater discharge also occurs by pumpage, nearly all of which occurs in the Harney Basin lowlands. Groundwater discharge in the uplands and lowlands are accounted for and discussed separately because a portion of the upland groundwater discharge to streams and springs reinfiltrates in the lowlands and constitutes an important source of recharge in the lowlands. Groundwater discharge from the Harney Basin uplands was estimated as 239,000 acre-ft/yr. Groundwater discharge in the Harney Basin lowlands was estimated as 283,000 acre-ft/yr: 151,000 acre-ft/yr in the northern region, 54,000 acre-ft/yr in the southern region, and 78,000 acre-ft/yr in the western region (table 3; Garcia and others, 2022). Estimates of groundwater discharge from individual mechanisms are discussed in more detail in the following sections.

Discharge through Evapotranspiration by Natural Vegetation

Groundwater ET (ET_g) is the most important mechanism for the natural discharge of groundwater in the lowland areas within the Harney Basin. The estimated mean annual volume of groundwater ET from more than 400,000 non-irrigated acres across the Harney Basin lowlands totaled 119,000 acre-ft (table 3), which was 42 percent of the total groundwater discharge in the lowlands (Garcia and others, 2022). This estimate represents the average of two Landsat-based remote-sensing methods (Laczniak and others, 2008; Beamer and others, 2013) applied within a groundwater ET area (GETA) centered on Malheur and Harney Lakes (fig. 13). Both methods incorporate groundwater ET measurements from similar vegetation in other basins within the Great Basin and were applied in the Harney Basin using 23 years of Landsat data. The GETA boundary is the transition from topographically upgradient xeric shrubs and a thicker unsaturated zone (typically 20 ft below land surface or more) to a downgradient mix of xeric and phreatophytic shrubs and a thinner unsaturated zone. The GETA was mapped using aerial imagery, a digital elevation model, groundwater-level data, vegetation maps, and field observations of land cover (Garcia and others, 2022). Natural groundwater ET estimates represent mean annual conditions within the Harney Basin GETA during 1987–2015 and are assumed to represent discharges during the 1982–2016 study period.

Mean annual groundwater ET from natural vegetation varied among the three regions: 64,000 acre-ft in the northern region, 20,000 acre-ft in the southern region, and 35,000 ac-ft in the western region. In northern and western region lowlands, groundwater ET fully accounts for non-pumping discharge, while in the southern region it accounts for about two-thirds of the natural discharge. Groundwater ET in the northern and southern regions is predominantly through root-water uptake from the water table or capillary fringe, whereas western region groundwater ET is largely ET of spring flow.

Discharge to Surface Water

Discharge to surface water (Q_{sw}^{out}) is the primary mechanism for the natural discharge of groundwater in the uplands and the second most important mechanism in the lowlands. It includes discharge to springs, seepage into streams (base flow in gaining streams), and seepage into Malheur and Harney Lakes. Groundwater discharge to surface water in the uplands was estimated to be 239,000 acre-ft/yr. Total discharge to surface water in the Harney Basin lowlands from all mechanisms is estimated to be about 35,000 acre-ft/yr (Garcia and others, 2022). Each mechanism is discussed in more detail in the following sections.

Discharge to Springs

Discharge to springs in the uplands of the Harney Basin is substantial. Thousands of springs are mapped across the Blue Mountains and Steens Mountain, but few have discharge measurements. The lack of measurements does not present a problem for developing the water budget, however, because groundwater discharging to upland springs either evapotranspires in meadows and wetlands or it contributes to upland streamflow. Both upland ET and upland streamflow are quantified and the contribution of upland spring discharge is included in those estimates.

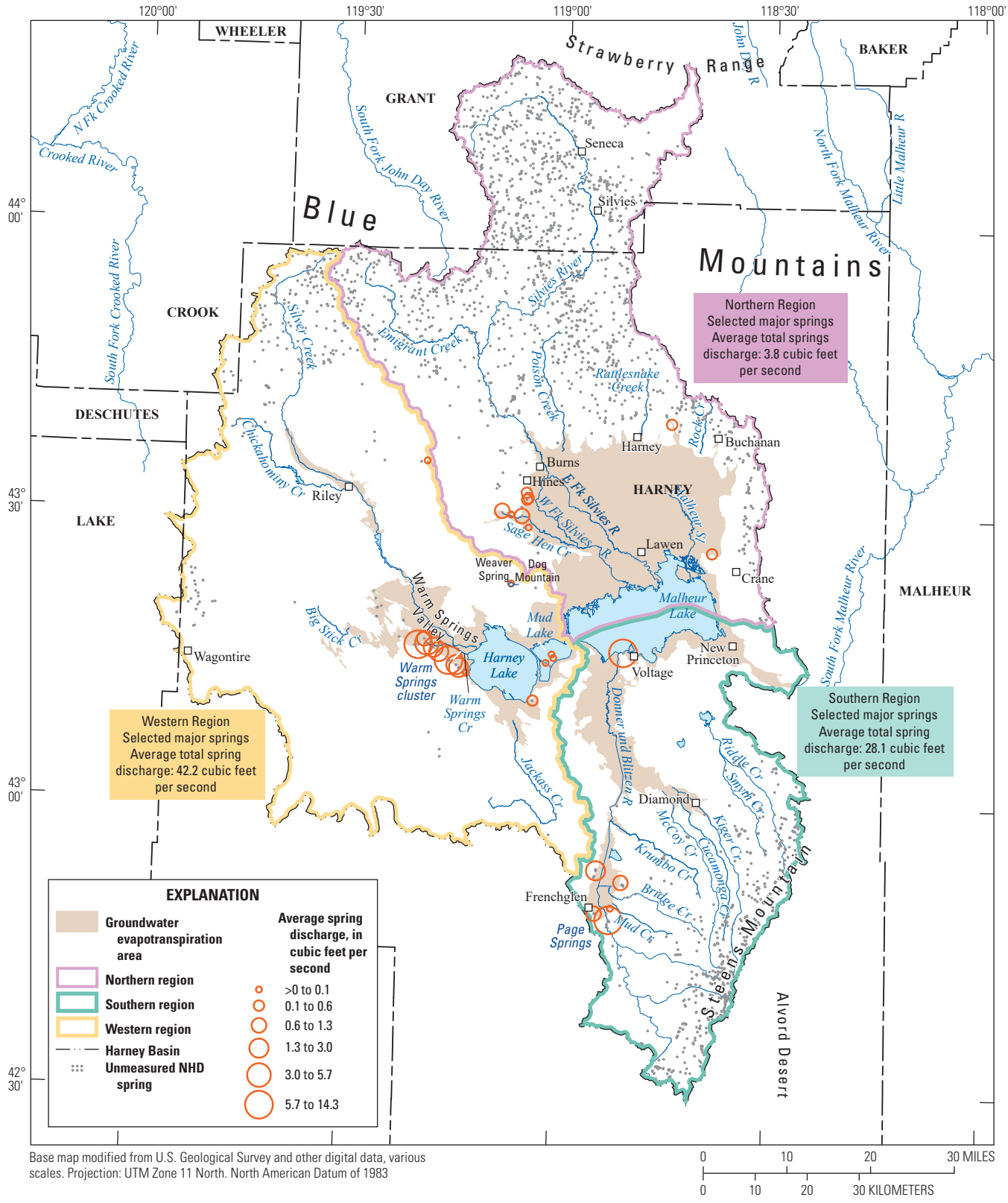

Figure 13. Location and mean discharge rate of selected major springs, summed by region (1903–2017), and unmeasured springs from the National Hydrography Dataset (NHD), Harney Basin, southeastern Oregon. Map from Garcia and others (2022).

Natural groundwater discharge to selected springs in the Harney Basin lowlands totals about 34,000 acre-ft/yr (table 3), most of which emerges in Warm Springs Valley (fig. 13; Garcia and others, 2022). Spring-flow estimates were compiled from previously published studies, and from measurements of selected springs in Warm Springs Valley made in July 2017 by OWRD. Spring-flow measurements were limited and primarily from the early 1900s and those made for this study. The spring-discharge estimates provided herein assume that spring flow has not changed appreciably since the early 1900s and the mean of the irregularly spaced measurements represents the long-term mean (Garcia and others, 2022). Discharge to springs in Warm Springs Valley measured in 2017 totaled 23,500 acre-ft/yr, accounted for about 96 percent of estimated spring discharge in the western region, was within 10 percent of the mean annual groundwater ET estimate for the Warm Springs Valley area (21,600 acre-ft/yr; Garcia and others, 2022), and within 11 percent of the 1931 discharge estimate of Piper and others (1939).

Discharge to Streams

About 225,000 acre-ft/yr of groundwater discharges as base flow to streams in upland areas of the Harney Basin (table 3). Upland discharge is highest in the southern region and lowest in the western region, which is the driest of the three regions (Garcia and others, 2022). Groundwater discharge to streams in the lowlands was considered negligible because streams in the northern and western lowland regions are mostly losing water and contributing to groundwater recharge and, in the southern region, base-flow gains between Frenchglen and Diamond Lane were likely offset by streamflow losses farther downstream (Garcia and others, 2022).

Groundwater discharges to streams in areas where the stream water-level elevation is lower than the elevation of the water table in the adjacent aquifer. Groundwater discharge to stream channels can occur at discrete points–essentially underwater springs–but more often occurs as diffuse seepage through the streambed sediments. Groundwater discharge in upland areas provides most of the late-summer flow in perennial streams in the Harney Basin and is a key component of streamflow during the rest of the year.

Groundwater discharge to streams in the Harney Basin was estimated using a multistep approach to account for base flow in gaged and ungaged watersheds during 1982–2016. Mean annual streamflow across all major surface-water drainages conveying water from the mountainous uplands to the valley lowlands and for select streams flowing from the valley lowlands to Malheur and Harney Lakes was extended or estimated for the study period. For streams with more than 1 yr of continuous record, base-flow estimates from graphical hydrograph separation and summer low-flow estimates were averaged over the period of record and scaled to the study period using a composite of measured and extended streamflow records (Garcia and others, 2022). Adequacy of using the mean base flow from graphical hydrograph separation and summer low-flow estimates was validated using chemical hydrograph separation in two watersheds where multi-year chemical data exist. Base flow for ungaged streams was estimated as the product of mean annual extended or estimated streamflow during 1982–2016 and the average ratio of base flow-to-total flow estimated at nearby gaged streams. Additional details of the techniques, locations, and limitations are detailed in Garcia and others (2022).

Discharge to Malheur and Harney Lakes

Direct measurements of groundwater flow into Malheur and Harney Lakes were not available, so estimates of discharge to the lakes were made by calculating the Darcy groundwater flux using the mapped groundwater gradient and estimates of near-lake sediment permeability (Garcia and others, 2022). Estimates of groundwater flow into and out of Malheur Lake are small — about 100 acre-ft/yr toward the lake from the north and south and about 50 acre-ft/yr away from the lake toward areas of groundwater decline east and west of the lake, yielding a net groundwater discharge of about 60 acre-ft/yr into Malheur Lake for a lake-stage elevation of about 4,094 ft. At Harney Lake, the estimates indicate that about 630 acre-ft/yr of groundwater flows toward the lake from the east, south, and west sides, and about 160 acre-ft/yr flows northward away from the lake toward the Weaver Spring/Dog Mountain area of groundwater decline, yielding a net groundwater discharge of 470 acre-ft/yr into Harney Lake for a lake-stage elevation of about 4,084 ft. Lake-flux estimates are considered approximations owing to uncertainty of the thickness and permeability of the near-lake sediments; but discharge estimates in Harney Lake are similar (within 15 percent) to groundwater ET estimates within the Darcy-flux analysis area (Garcia and others, 2022). In the water budget, groundwater discharge to lakes was accounted for in the estimates of lowland groundwater discharge to ET.

Discharge to Adjacent Basins

Groundwater discharge as subsurface outflow to the Malheur River Basin through Virginia Valley was estimated to be about 3,100 acre-ft/yr (Garcia and others, 2022). The estimate of the discharge component (Q_{go}^{out}) was made by calculating the Darcy groundwater flux using the mapped groundwater hydraulic-head gradient and estimates of the permeability and cross-sectional area through which groundwater is moving. The permeability estimate is the median transmissivity of the highly permeable Voltage basalt HU (28,000 ft^2/d; fig. 8) that underlies parts of Virginia Valley (fig. 9). Groundwater discharge to any other adjacent basins is not indicated by any hydrologic data collected to date in other areas of the Harney Basin.

Discharge to Wells

Total groundwater pumpage (Q_p^{out}) for irrigated agriculture and for all non-irrigation uses for 2017–18 was estimated to be about 152,000 acre-ft/yr (table 3). Pumpage in the lowlands accounts for 92 percent of the total pumpage in the Harney Basin and accounts for about 54 percent of all groundwater discharge from the Harney Basin lowlands (Garcia and others, 2022). Irrigated agriculture accounts for 95 percent of the total pumpage. Most groundwater is pumped from the Harney Basin lowlands north of Malheur and Harney Lakes from the Younger and Older basin fill HUs. Most groundwater withdrawn by irrigation pumpage is consumed by plants and lost to the atmosphere as ET, although a small amount (5–13 percent; see the "Recharge from Irrigation" section) reinfiltrates and recharges the groundwater-flow system beneath irrigated fields. In contrast, much of the pumpage for private domestic wells returns to the groundwater system by infiltration from septic systems.

Pumpage for Agricultural Irrigation

Groundwater pumpage for irrigation in the Harney Basin lowlands was about 145,000 acre-ft/yr during 2017–18. Garcia and others (2022) reported that pumpage estimated by Beamer and Hoskinson (2021) was largest in the northern region (81,000 acre-ft/yr), followed by the western region (42,000 acre-ft/yr) and the southern region (22,000 acre-ft/yr). Groundwater pumpage for agricultural irrigation has increased considerably since the early 20th century when the first estimate was compiled. In the 1930s, pumpage for irrigation was about 1,000 acre-ft/yr (Piper and others, 1939) and was primarily withdrawn from wells less than 100 ft deep. By the end of the 1960s, groundwater pumpage for irrigation was about 7,900–10,700 acre-ft/yr, and the depth of recently completed irrigation wells routinely exceeded 300 ft (Leonard, 1970). Since the late 1960s, the number of irrigation wells in the Harney Basin has nearly tripled, but groundwater-use measurements and data reporting for irrigation are sparse. Because few direct measurements exist for the study period, groundwater pumpage for irrigation was calculated from remotely sensed measurements of ET from groundwater-irrigated fields, which were scaled by a locally derived irrigation efficiency (Beamer and Hoskinson, 2021). A time series of selected years during 1991–2018 was used to capture the increase in groundwater irrigation that began in the early 1990s. Selected years were those (1) having the most cloud-free May–September Landsat scenes, (2) having available imagery for mapping field boundaries, (3) having at least one clear scene per month during the growing season, and (4) representing a range of wet-to-dry water years (Beamer and Hoskinson, 2021). A mean irrigation efficiency of 70 percent was estimated using the ratio of the measured growing season net ET volume and reported pumpage volume for 59 paired fields and wells.

Groundwater pumpage for irrigation in the Harney Basin increased substantially during 1991–2018 from 51,000 acre-ft/yr in 1991 (about 20,200 acres for groundwater-irrigated fields and 10,400 acres for fields irrigated with groundwater and surface water) to 145,000 acre-ft/yr during 2017–18 (about 57,900 acres for groundwater-irrigated fields and 16,200 acres for groundwater and surface water; figs. 14–15). The largest rate of change occurred during 2010–17. Most of the increase occurred on newly established fields (about 43,500 acres) using only groundwater to irrigate—the fields have no primary or supplemental surface-water irrigation right (Beamer and Hoskinson, 2021). The groundwater volume pumped for fields irrigated with a combination of surface water and groundwater has remained relatively constant since 2000 (fig. 15; Beamer and Hoskinson, 2021).

Pumpage for Non-Irrigation Uses

Groundwater pumped for non-irrigation uses in the Harney Basin accounts for about 5 percent of total pumpage and includes municipal water-supply systems, private small-community water-supply systems, rural domestic uses, privately and publicly supplied livestock water and commercial-industrial uses (fig. 16). About 1,700 wells supply the water. Groundwater pumped for non-irrigation uses totaled about 6,900 acre-ft/yr, with about 6,000 acre-ft/yr consumed and about 900 acre-ft/yr returned to groundwater as recharge (Grondin, 2021). Non-irrigation pumpage was assumed to represent the 1982-2016 study period. The largest non-irrigation groundwater uses include pumpage in the northern region that supplies the cities of Burns and Hines (2,200 acre-ft/yr) and pumpage for commercial-industrial uses (about 2,000 acre-ft/yr). Pumpage for rural domestic use and livestock each account for roughly 20 percent of non-irrigation pumpage and small community systems account for about 1 percent of non-irrigation pumpage.

Groundwater Elevations and Flow Directions

Spatial variations in hydraulic head provide the driving force for groundwater flow. Head is expressed as its height above a common datum (usually feet above mean sea level), and groundwater flows from areas of high head toward areas of low head. The change of head with vertical or horizontal distance is referred to as the "hydraulic head gradient," or simply "head gradient." Head generally is a subdued expression of topography and is highest in upland areas and lowest in valleys and other lowland areas. Lateral head gradients drive groundwater flow horizontally, whereas vertical head gradients drive it downward or upward within the groundwater system that can include multiple saturated stratigraphic units with differing hydraulic properties. Vertical head gradients are downward in recharge areas and upward in discharge areas.

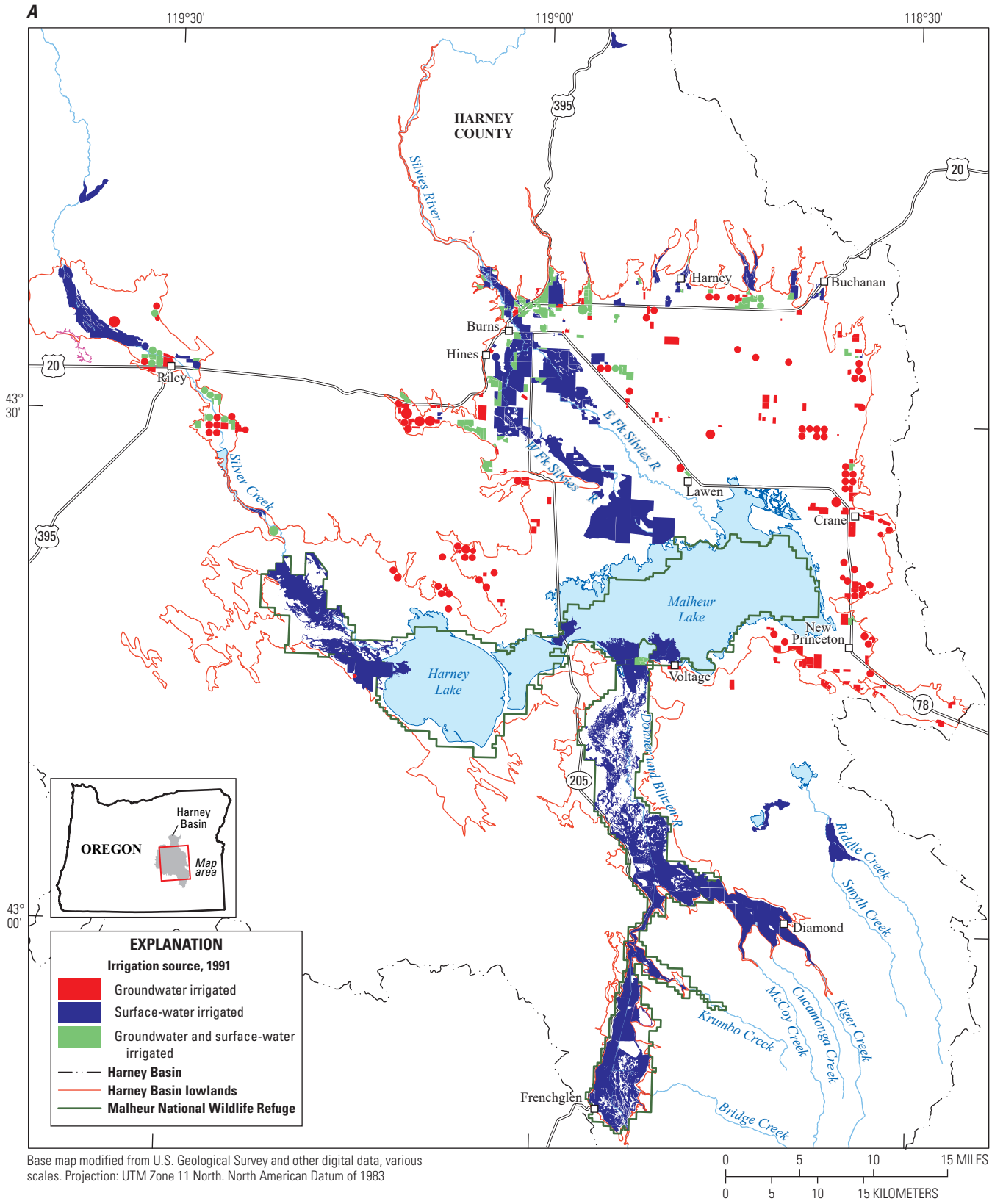

Figure 14. Irrigated fields categorized by irrigation source type in (*A*) 1991 and (*B*) 2018, Harney Basin, southeastern Oregon. Map from Garcia and others (2022).

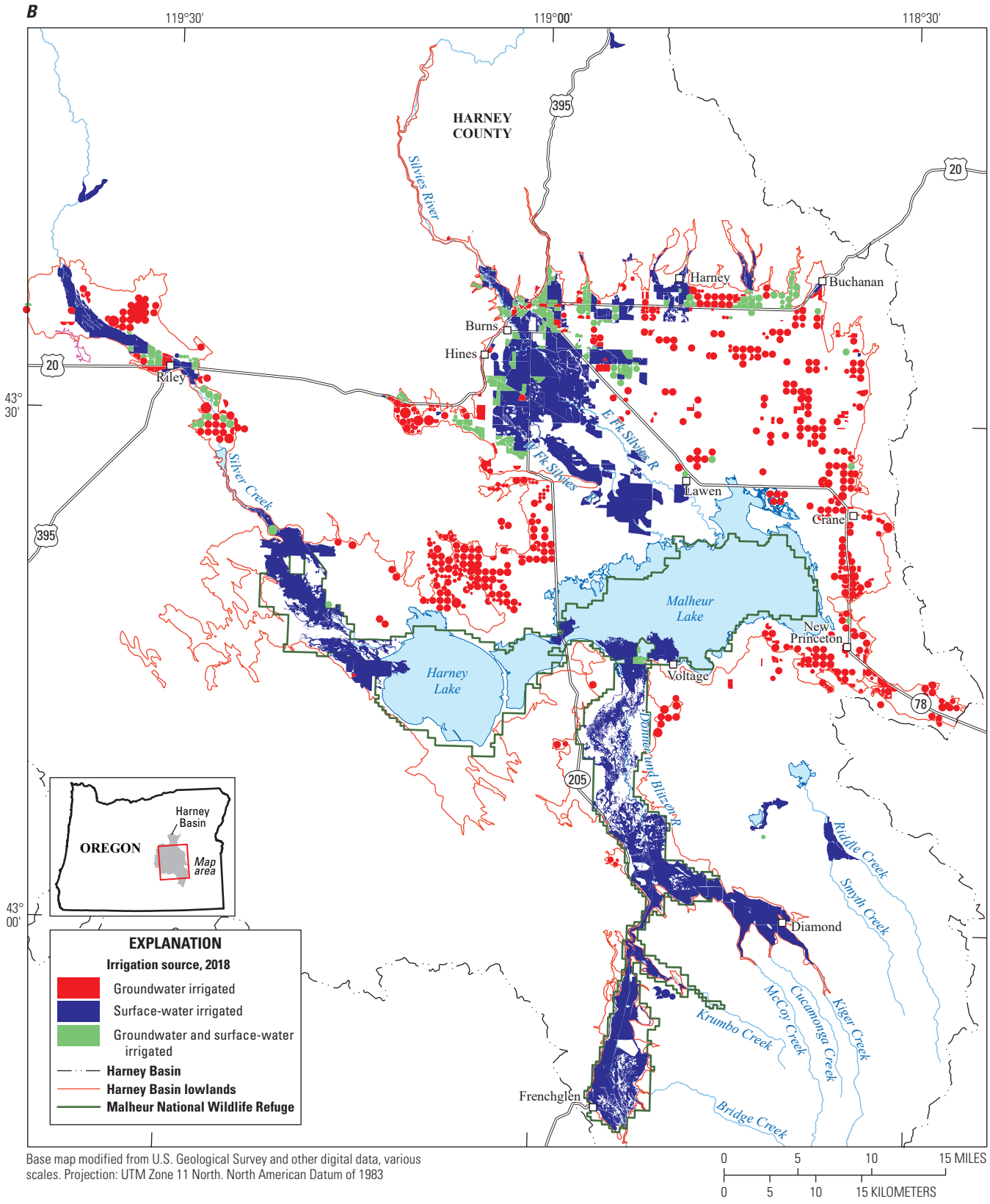

Figure 14.—Continued

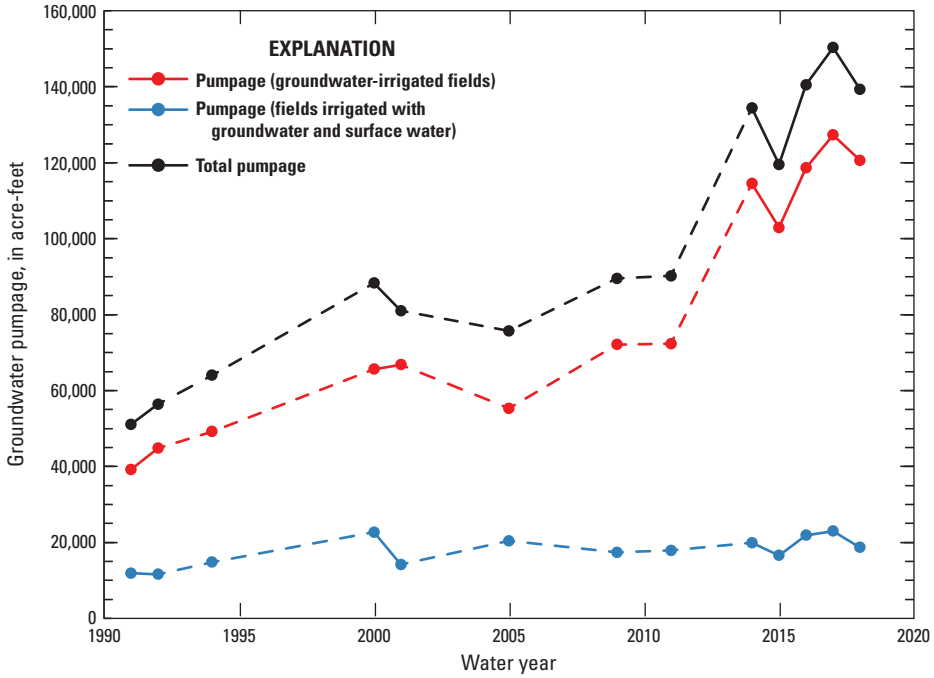

Figure 15. Total groundwater pumpage for irrigation, Harney Basin, southeastern Oregon, water years 1991–2018. Graph from Beamer and Hoskinson (2021).

The non-pumping or static water level in a well provides a measure of the average hydraulic head of the saturated interval penetrated by the open interval of the well. In recharge areas where vertical head gradients are typically downward, the elevation of the groundwater levels in wells decreases (becomes deeper) with increasing well depth. In discharge areas where vertical head gradients are typically upward, the elevation of the groundwater levels in wells increases (becomes shallower) with increasing well depth. If the head elevation in a well exceeds land-surface elevation, the well will flow at land surface. Such wells are commonly referred to as "flowing artesian wells."

Groundwater Flow

Understanding the three-dimensional distribution of hydraulic head within the groundwater system is critical to determining the directions of groundwater flow. A "potentiometric surface" is the representation of head at a particular depth in a groundwater-flow system. The water table is a unique potentiometric surface that reflects the head at the top of the unconfined part of the system. Two potentiometric surfaces (Gingerich and others, 2021) were developed for this report, one reflecting conditions in the shallow, generally unconfined part of the system (plate 2), and the other representing a deeper and generally confined part of the system (plate 3). For the remainder of this report, the term "water table" is used to describe the distribution of head in the shallow, generally unconfined parts of the Harney Basin groundwater-flow system, and the term "potentiometric surface" is used when discussing head conditions in the deeper, generally confined part of the system. The water-table map was developed using groundwater-level measurements from shallow wells (generally less than 100 ft deep in the lowlands) and the elevations of springs and gaining stream reaches and constrained by the elevation of the land surface. The deeper potentiometric-surface map was developed using measurements from wells generally more than 100 ft deep in the lowlands. The hydraulic-head distributions depicted in plates 2–3 are generalizations. The large study area, availability of water-level measurements, distribution of wells across the Harney Basin, and resource limitations for the study precluded mapping all the complexities of the head distribution. Contours are most detailed and have 10-ft intervals (with the exception of the 4,095-ft contour) in the Harney Basin lowlands where data are more abundant and the land surface is relatively flat. Groundwater heads of 4,200 ft or more were mapped using 500-ft contour intervals and generally coincided with upland areas where wells are sparse and groundwater head is primarily controlled by topography.

The head data for most wells used to develop the head maps were collected by measuring the groundwater level at those wells during February–March 2018, when groundwater levels were near their annual maximum elevation and were largely recovered from the drawdown that occurred during the 2017 irrigation season. The groundwater-level measurements collected for this study are maintained by the OWRD and can be accessed using their Groundwater Information System webpage (Oregon Water Resources Department, 2019).

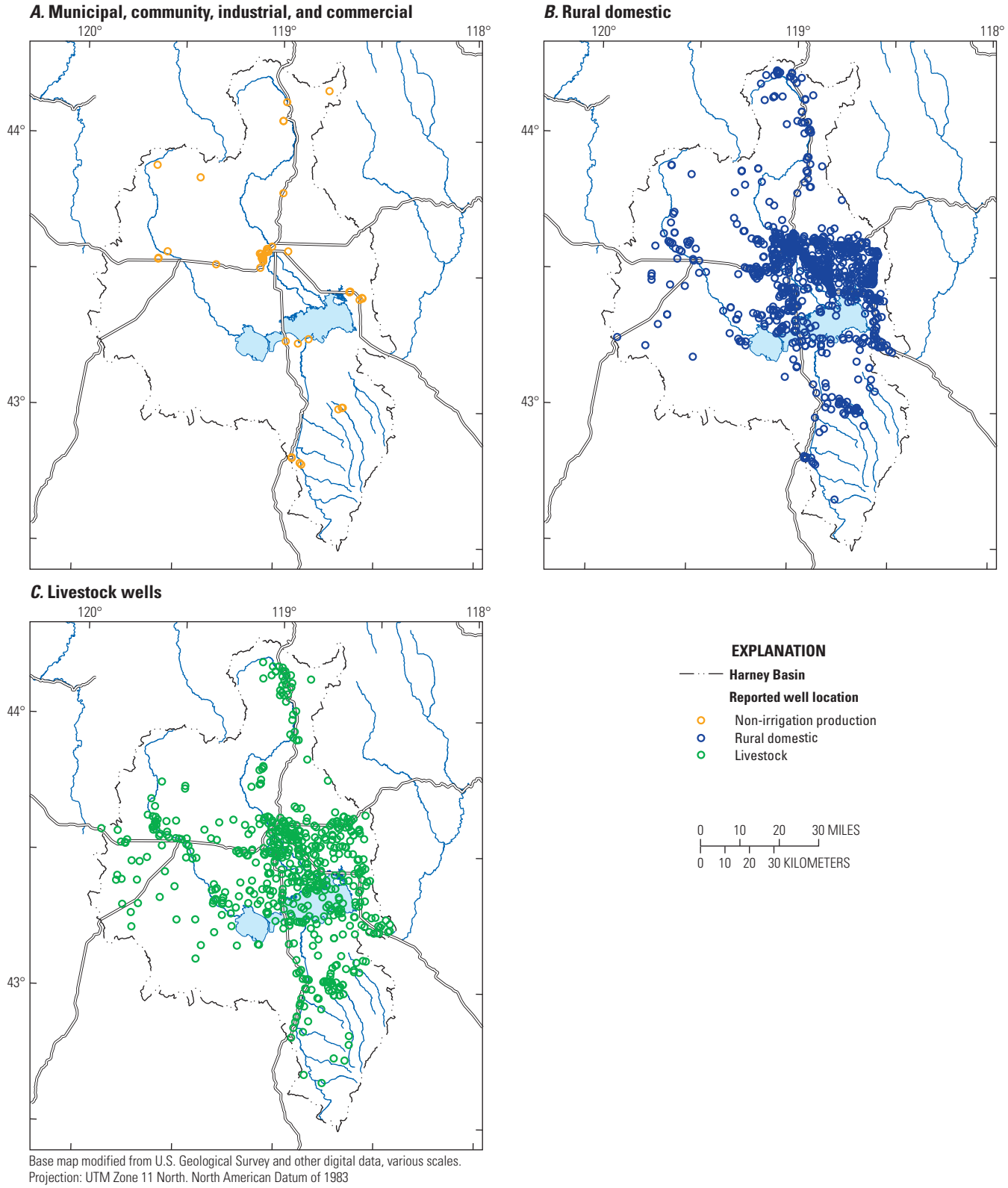

Figure 16. Distribution of (*A*) municipal, community, commercial-industrial, (*B*) rural domestic, and (*C*) livestock wells with water well reports filed with the Oregon Water Resources Department, Harney Basin, southeastern Oregon Locations modified from Grondin (2021).

In areas that were distant from major pumping centers and where no other data were available, older groundwater-level measurements made by USGS and OWRD and groundwater levels recorded in well reports were used to constrain the head maps. Groundwater-level measurements collected by OWRD and USGS were collected using the same standardized procedures to ensure accuracy and consistency of measurements (Cunningham and Schalk, 2011). Springs and gaining streams provided additional information about the hydraulic-head distribution at the water table and provided the major source of data used to construct the water-table map in upland areas. Spring and stream elevations were obtained from light detection and ranging (LiDAR) surveys or topographic maps. Losing stream reaches and land-surface elevation were used to constrain the head elevations of the water table across the Harney Basin.

The highest heads in the Harney Basin occur in areas that have the highest elevations— Steens Mountain in the south and the Blue Mountains in the north (plate 2). Upland groundwater generally flows toward upland stream valleys and toward the Harney Basin lowlands. From Steens Mountain, groundwater flows westward and northward toward the Donner und Blitzen River, Malheur Lake, and Virginia Valley. The northwest dip of the Steens Basalt favors the flow of groundwater recharged atop Steens Mountain into the Harney Basin; however, the movement of a small amount of water recharged within the Harney Basin study area boundary eastward toward the Alvord Desert cannot be ruled out with the existing data. In the Blue Mountains, groundwater generally flows toward the Silvies River, Silver Creek, and their many tributaries, and southward toward Harney and Malheur Lakes. Within the Younger and Older basin fill HUs underlying the Harney Basin lowlands, groundwater generally flows toward Malheur and Harney Lakes. A small amount of groundwater flows eastward through the Voltage basalt HU in Virginia Valley and into the Malheur River Basin.

Numerous geologic faults have been mapped across the Harney Basin study area, and undoubtedly many unmapped faults cut the soft sediments filling the central basin. The effect of faulting on groundwater movement is complex and poorly understood. Faults have been documented to act as barriers that restrict groundwater movement, conduits that enhance movement, and in many cases seem to have no effect at all on the movement of groundwater (Bredehoeft and others, 1992; Bense and van Balen, 2003; Mayer and others, 2007). Although many parts of the Harney Basin are geologically faulted, the available groundwater-level data did not show any abrupt groundwater-level offsets, which would be evidence that faults are affecting groundwater flow. However, the presence of springs coincident with many mapped faults appears to indicate that faults may locally enhance permeability.

Groundwater pumpage for irrigation has caused large, localized depressions in groundwater levels of up to 100 ft under the Harney Basin lowlands. The depressions have changed groundwater-flow directions from pre-development conditions. Three Harney Basin areas with a combined area exceeding 140 mi^2 have experienced groundwater-level declines exceeding 40 ft relative to pre-development conditions: (1) near the Weaver Spring/Dog Mountain area, (2) in the northeastern floodplains along Highway 20 (best illustrated in plate 3), and (3) near Crane. Areas of more modest groundwater-level decline (about 10 ft) were identified in the Virginia Valley area and the Silver Creek floodplain north of Riley (plate 3). Smaller areas of groundwater-level depression have also formed around individual wells or groups of wells throughout the Harney Basin lowlands. Areas of decline are discussed in more detail in the section of this report titled "Description of Harney Basin Groundwater-Flow System."

Vertical Groundwater Gradients

The natural, undisturbed vertical head gradient varies across the Harney Basin. In the uplands, the gradient generally is downward in locations outside stream valleys where recharge occurs and upward in valleys with perennial streams where groundwater discharges to the streams. In the Harney Basin lowlands, the vertical gradient is generally downward near the mountain front area and the adjacent, lower elevation, gently dipping plain transitioning to upward near the center of the basin surrounding Malheur and Harney Lakes.

Groundwater pumping has increased the magnitude of the vertical head gradient to varying degrees in many areas of the Harney Basin lowlands. Generally, higher pumping-induced gradients develop in areas with lower vertical permeability and lower gradients develop in areas with higher vertical permeability. For example, groundwater levels in a collocated pair of observation wells (HARN0052234, HARN0052235; plate 1) near Lawen highlight a relatively high downward vertical gradient that provides the potential for water movement from the shallow to the deep part of the groundwater-flow system. Here, the vertical gradient increases seasonally with pumping in the deeper sediments. Well HARN0052234 is completed in relatively less-permeable deposits of the shallower Younger basin fill HU and HARN0052235 is completed in the deeper Older basin fill HU (specifically, the Rattlesnake Ash-Flow Tuff). The groundwater level at the shallow well (open interval: 4,049- to 4,028-ft elevation; 55- to 76-ft depth) only fluctuates 1–2 ft seasonally, whereas the groundwater level in the deep well (open interval: 3,654- to 3,633-ft elevation; 450- to 471-ft depth) fluctuates about 60 ft each year (fig. 17). The seasonal pumping cycle creates a downward gradient for groundwater movement that fluctuates between 0.06 ft/ft in winter and 0.21 ft/ft in summer (calculated as the difference in groundwater level between the wells divided by the difference in open-interval midpoint from the shallow to the deep well). The large vertical head gradient and muted groundwater-level response in the shallow well relative to the deep well are caused by the permeability contrast between the shallow and deep deposits. Similar seasonal fluctuations in the downward vertical gradient were observed in response to irrigation pumpage between Buchanan and Crane and along the Blue Mountain front between Prater Creek and Mahon Creek.

To the northeast of Dog Mountain (plate 1), more wells pump from the shallow part of the basin fill than from the deeper part, resulting in an upward groundwater-head gradient. The upward pumping-induced gradient at HARN0052629 (open interval: 4,044- to 4,021-ft elevation and 82- to 105-ft depth) and HARN0052606 (fig. 17; open interval: 3,644- to 3,620-ft elevation and 482- to 506-ft depth, respectively) fluctuates from 0.04 ft/ft in winter to 0.05 ft/ft in summer, which is comparatively small relative to the 0.15 ft/ft difference between seasonal fluctuations near Lawen. A smaller seasonal fluctuation likely indicates lower permeability contrast between shallower and deeper wells in the area northeast of Dog Mountain relative to the Lawen area. The vertical gradient prior to the onset of groundwater development in this area is not known; therefore, determining if pumpage has reversed or augmented the natural vertical gradient is not possible.

At a three-well cluster (HARN0052749, HARN0052748, HARN0052747) installed in the floodplain between the East Fork Silvies River and West Fork Silvies River (fig. 2), the vertical head gradient generally is small (about 0.01 ft/ft) and changes direction during the year (fig. 17). These three wells have open intervals of 4,124- to 4,112-ft elevation (11- to 23-ft depth), 4,035- to 4,009-ft elevation (100- to 126-ft depth), and 3,622- to 3,592-ft elevation (513- to 543-ft depth); the upper two wells are screened in the Younger basin fill HU, and the deepest well is screened in the Older basin fill HU (specifically, the Rattlesnake Ash-Flow Tuff). The lithology in the Younger basin fill HU is mainly a mixture of clay and sand. In late autumn, the gradient is neutral to downward in the upper sediments (from HARN0052749 to HARN0052748) and upward in the deeper part of the system (from HARN0052747 to the other two wells), converging on the intermediate depth sediments where most of the groundwater pumping in the area is occurring. As pumping effects wane during winter and pressure loading and recharge from surface-water flooding begins in the springtime, the gradient changes to downward throughout the entire section of basin fill (from HARN0052749 to the other two wells). Once pumping begins again, the gradients toward the intermediate depth from the upper and lower wells are re-established.

A relatively small downward vertical groundwater gradient also was observed in a pair of observations wells in the southern part of the Weaver Spring/Dog Mountain area completed in the high-permeability Proximal vent deposits HU (HARN0052630 and HARN0052631). The downward head gradient at the wells (open interval: 3,987- to 3,963-ft elevation [167- to 191-ft depth] and 3,692- to 3,668-ft elevation [462- to 486-ft depth], respectively) remains about 0.01 ft/ft throughout the seasonal pumpage cycle (fig. 17). This type of vertical head gradient and groundwater-level response is observed in areas where the high-permeability deposits extend from the surface to depth. Groundwater throughout the southern Weaver Spring/Dog Mountain vicinity behaves in a manner similar to what is observed at HARN0052630 and HARN0052631.

Similar to the Weaver Spring/Dog Mountain area, a pair of observation wells in Virginia Valley completed in the high-permeability Voltage basalt HU (HARN0052608 and HARN0052607) also exhibit a relatively low vertical groundwater gradient. Here, groundwater levels are very similar in the shallow and deep wells open to the Voltage basalt HU at elevations of 4,003- to 3,979-ft elevation (117- to 141-ft depth) and 3,773- to 3,749-ft elevation (347- to 371-ft depth), respectively, which is consistent with a relatively high vertical permeability in the Voltage basalt HU at this location (fig. 17). A slight downward gradient, less than 0.01 ft/ft, is induced in summer when pumpage is greatest.

Historically, flowing artesian wells were found in many areas of the Harney Basin. Flowing wells occur where the head at the well open interval is higher than the elevation of the land surface at the well; a situation commonly associated with groundwater under some level of confinement by overlying low-permeability deposits. Piper and others (1939) noted flowing artesian wells near Hines, Sodhouse Spring, Sunset Valley, and Warm Springs Valley (figs. 1, 13). The original flowing wells noted by Piper and others (1939) have been lost and therefore unavailable for remeasurement. Near Mud Lake, HARN0001455 (525 ft deep) was observed flowing in 1979 and during this study. Near Buchanan, HARN0000722 (615 ft deep) was flowing in September 1969 (Leonard, 1970) but had static water-level measurements between 0.05 and 47 ft below ground surface during this study (Oregon Water Resources Department, 2019).

Groundwater-Level Fluctuations

Hydraulic head fluctuates with time in response to external stresses, the largest and most important of which are variations in natural groundwater recharge and groundwater pumpage. Head fluctuations are manifest as variations in groundwater levels in wells and variations in groundwater discharge to springs and to streams as base flow. Periodic measurements of static groundwater levels in wells were used to understand how natural variations in recharge and groundwater pumpage affect groundwater levels in wells throughout the basin.

Multiple groundwater-level measurements collected by OWRD and USGS are available for many wells in the Harney Basin for periods ranging from less than 2 yrs to more than 80 yrs (Oregon Water Resources Department, 2019). The measurements have been made at intervals ranging from once every 2 hrs using automated recording devices to manual measurements made a few times a year or decade. The groundwater-level data from these wells provide an understanding of the dynamic nature of the groundwater-flow system throughout the basin.

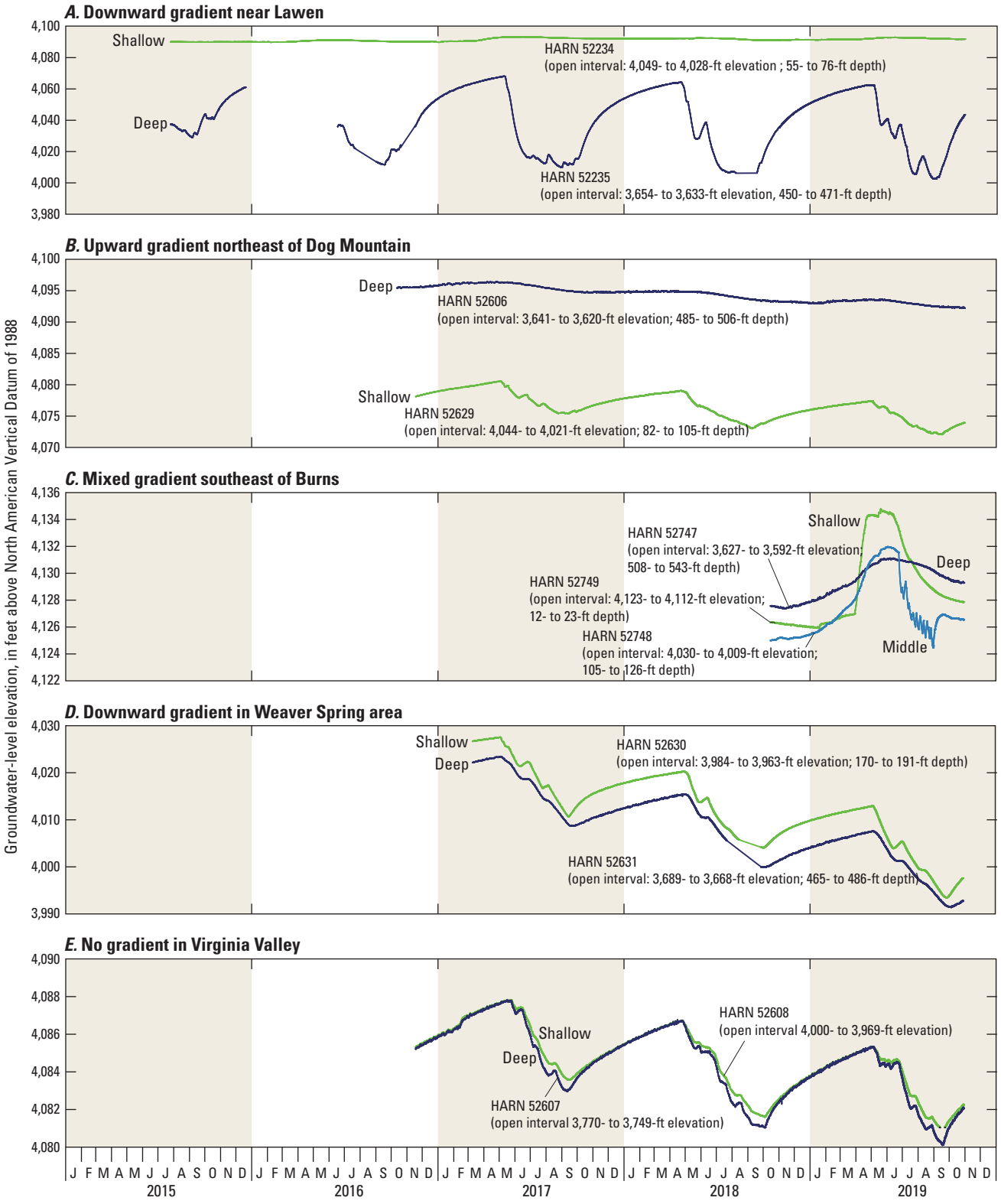

Figure 17. Groundwater levels at selected well pairs showing vertical gradients during 2015–19, the Harney Basin, southeastern Oregon. Well locations shown on plate 1; *A*, downward gradient near Lawen. *B*, upward gradient northeast of Dog Mountain. *C*, mixed gradient southeast of Burns. *D*, downward gradient in Weaver Spring area. *E*, no gradient in Virginia Valley.

Response to Precipitation and Streamflow

Changes in precipitation, both seasonal and year-to-year, affect recharge from direct infiltration of precipitation and from infiltration of runoff. In the Harney Basin, groundwater levels typically rise when snowmelt and surface-water infiltration provide a pulse of recharge and freshet waters pond across the Harney Basin lowlands causing an increase in pore pressure in the underlying sediments. Groundwater levels decline after the freshet waters subside and during the onset of pumpage for irrigation in summer months. The magnitude of the seasonal response to recharge in a well varies with the amount of springtime runoff (which itself varies with snowpack volume), proximity of a well to a stream or flooded area, the depth of the well, and the local hydrostratigraphy.

The influence of seasonal surface-water flow on the groundwater-flow system is most apparent in groundwater-level records from wells that are either continuously monitored or measured monthly or quarterly. The influence of elevated streamflow and overbank flooding during the springtime freshet are evident in groundwater-level records from wells in the Harney Basin lowlands north of Malheur Lake (fig. 18). Groundwater levels increase owing to increases in stream-channel seepage, infiltration of flood waters, and increases in pore pressure in the aquifers from the weight of flood waters on the surface. However, determining the relative contributions of infiltration and pressure response to the groundwater-level rise at a well is difficult due to insufficient information on (1) the volume and depth of surface-water flooding around the observation wells and (2) the compressibility, porosity, and lithology of the sediments penetrated by each well. Later sections of this report present geochemical evidence that precludes rapid infiltration of freshet water as the cause of the observed springtime rise in groundwater levels across much of the Harney Basin lowlands (refer to sections "Geochemical Evaluation of Recharge, Flowpaths, and Residence Time" and "Description of Harney Basin Groundwater-Flow System"). Those data support the observations and conclusions Piper and others (1939) made about the response of the water levels in deeper parts of the aquifers in the northern Harney Basin lowlands.

The response of the groundwater-flow system to the springtime freshet varies across the Harney Basin lowlands owing to the degree of aquifer confinement in the Younger and Older basin fill HUs. As an example, well HARN0000440 (fig. 18) is within 100 ft of a spur of Poison Creek slough, has an open interval 35–120 ft below ground surface, and is completed in gravel, sand, and clay. The groundwater level in this well rises rapidly within 1–2 days after streamflow peaks in the Silvies River. A rapid rise in groundwater level at HARN0000440 is evident in 2016, 2017, and 2019 when peak flow in the Silvies River was greater than 1,000 cubic feet per second (ft^3/s) but not evident in 2018, a drier year, when peak flow was less than 300 ft^3/s (fig. 18). That response, in which the groundwater level increases after a certain flow threshold is met, indicates that flow in a nearby channel was likely overtopping its bank or a levee and spilling out onto the floodplain near the well. Flooding likely does not result in recharge by direct downward infiltration at this site because the upper 12 ft of the well was drilled through clay (according to the well report). Rather, the observed rise in the groundwater level at this well is most likely due to compression of the floodplain sediments by the weight of the flood water. Layers of clay between 0- and 12- and 30- and 50-ft deep likely produce semi-confining conditions in layers of sand and gravel from 12- to 30-ft deep. Later in each season, sustained head at the well is likely from lateral spreading of recharge through the more permeable layers from channel losses. The periodic water-level records from shallow wells HARN0050891 (open interval 28–40 ft deep), HARN0050460 (open interval 50–68 ft deep), and HARN0050719 (open interval 50–77 ft deep) show similar responses to springtime runoff conditions (fig. 18). These wells have clay layers 12-, 48-, and 50-ft thick, respectively, overlying the layers that the wells are open to, indicating semiconfined to confined conditions.

The groundwater-level record from HARN0050719 (fig. 18) shows a groundwater-level increase likely due mainly to the overlying pressure of flooded surface water on a confined part of the groundwater-flow system. Here, during a site visit on April 18, 2017, at least 1 ft of flooded water from the expansion of nearby Malheur Lake surrounded the well. At that time, the groundwater level in the well had increased by about 16 ft since the previous measurement 3 months prior, when no flooding was present. Because of the 50 ft of low-permeability clay above the open interval of the well, rapid infiltration of recharging surface water to the groundwater-flow system is highly unlikely. Furthermore, the specific conductance (SC; a measure of salinity) of the water measured in the well was more than 10 times higher than historical measurements of SC from the East Fork Silvies River near Lawen (Hubbard, 1975; Rinella and Schuler, 1992), indicating that the surface water was not entering the well casing and directly recharging the aquifer open to the well. Therefore, the nearly immediate 16-ft rise in groundwater level is interpreted as primarily a pressure response caused by the weight of the floodwater covering the area around the well and secondarily attributed to some recharge of surface water to the groundwater-flow system somewhere upgradient of the well.

Wells HARN0051736 (open interval 60- to 103-ft depth) and HARN0052234 (open interval 55- to 76-ft depth), which are on the periphery of the Silvies River floodplain, show a small, gradual groundwater level increase each springtime, similar to each other but more subdued than in the shallower wells. Again, the response indicates semiconfined to confined conditions as the wells penetrate 46- and 52-ft-deep clay layers below land surface, precluding rapid same-season recharge near the well.

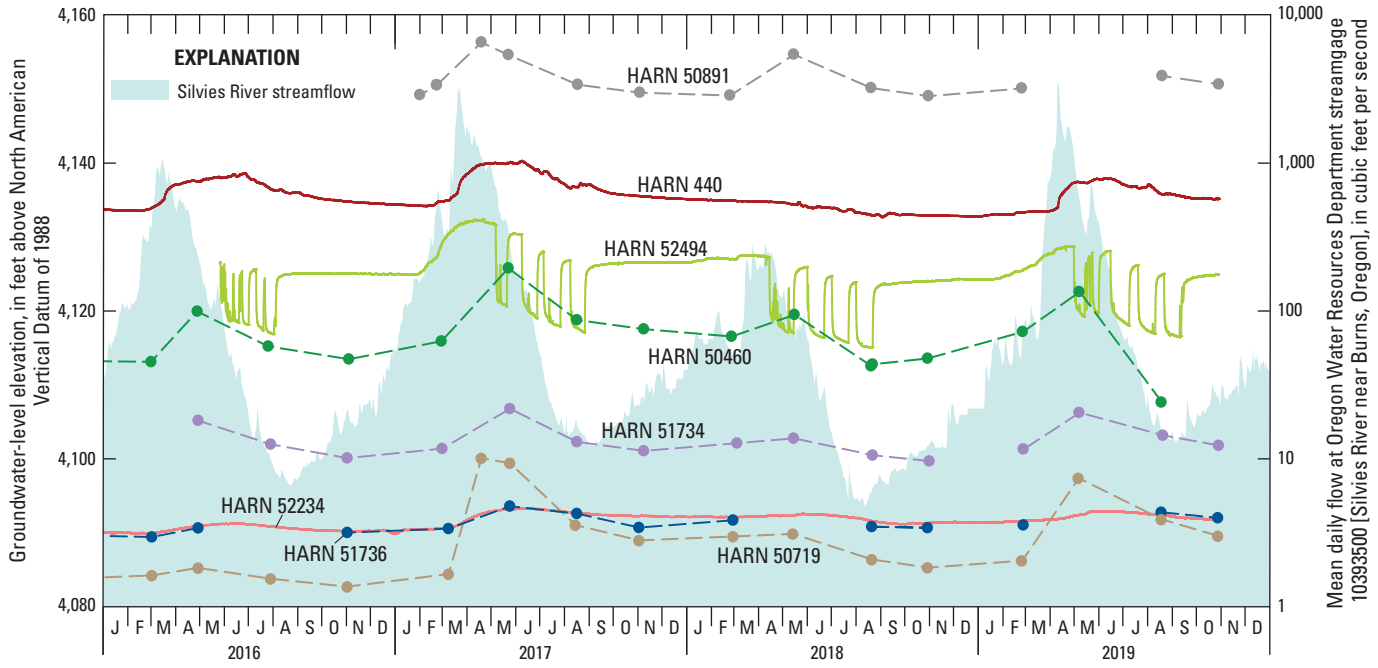

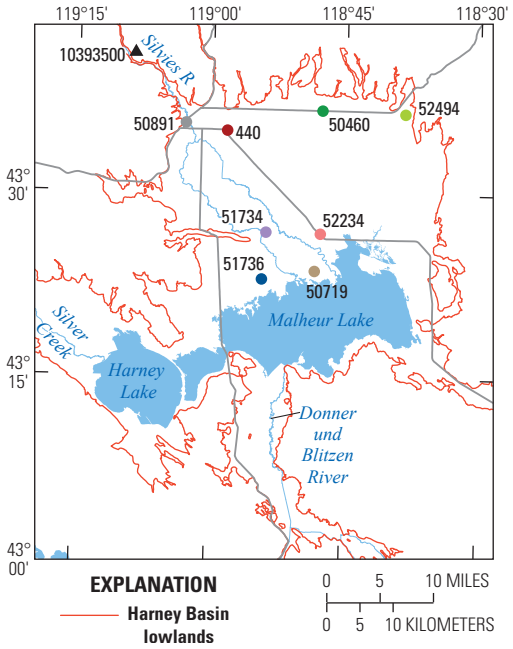

Well HARN number	Open interval depth, in feet	Clay interval depths, in feet
440	35–120	0–12; 30–50
50460	5–68	2–50
50719	50–77	0–50
50891	28–40	17–29
51734	60–103	1–45; 60–70; 85–103
51736	60–103	0–6; 14–60
52234	55–76	0–47
52494	124–142	0–12; 27–124

Figure 18. Groundwater-level responses to springtime surface-water runoff in selected wells, well information, and mean daily flow at streamgage 10393500 (Silvies River near Burns; Oregon Water Resources Department) during 2016–19, Harney Basin, southeastern Oregon. Well HARN number: Oregon State designation numbers (see "Well- and Spring-Identification System" section in front matter of this report). NAVD1988, North American Vertical Datum of 1988.

The water-level record from HARN0052494 (open interval 124- to 142-ft depth) includes a pumping signal from nearby irrigation wells, but a seasonal response beginning around the end of January is also apparent (fig. 18). The well penetrates 109 ft of clay above the open interval and is in an area that does not generally experience springtime flooding, so this response is likely not due to direct recharge infiltration but rather to a pressure response to recharge to a layer of the Older Basin fill HU that may surface upgradient from the well. Geochemical evidence (discussed below in the section titled "Geochemistry to support groundwater-flow interpretation") supports the conclusion that little or no modern water is present at depth in this area.

To understand the effect of decadal precipitation variations on groundwater levels, wells in areas unaffected by pumpage are needed. However, in the Harney Basin, long-term records of groundwater levels in areas unaffected by pumpage are limited to wells in areas where groundwater is likely affected by nearby surface-water conditions, making interpretation of the data problematic. The late winter (January–April) groundwater-level record at HARN0000874 (a 17-ft-deep well in the Younger basin fill HU) generally shows the groundwater-level increasing several feet (fig. 19) during periods of increased annual precipitation in the 1950s and 1960s (such as 1953, 1957, 1964, 1968), likely because of nearby flooding from high flows in Sage Hen Creek and the Silvies River following periods of higher precipitation and subsequent larger freshets. No nearby surface-water records are available for comparison. In the northern uplands, two shallow long-term groundwater-level records are available from wells (HARN0000009 and GRAN0000800) open to the Younger basin fill HU. The HARN0000009 record shows late winter groundwater-level increases in response to the wet period around 1983, but other increases and declines in either record are not clearly relatable to precipitation. Because these wells are proximal to streams, the effects of precipitation variation on the groundwater-level record are complicated by the effects of surface-water flooding through natural flooding or managed irrigation. In the future, monitoring of groundwater levels in wells unaffected by nearby surface water would provide better information on water-level response to interannual variations in precipitation.

Response to Pumpage

When a well is pumped, the groundwater level near the well declines due to the removal of groundwater from storage. In sediments that are generally uniform, a roughly cone-shaped depression centered on the well develops on the potentiometric surface and expands until the change in the head gradient is sufficient to redirect groundwater flow toward the well equal to the pumping rate. After pumping ceases, the groundwater level begins to recover. Hydraulic characteristics, the rate and duration of pumping, the possible presence of flow boundaries, and the number of wells affecting the groundwater level in each area are key factors that determine the magnitude of groundwater-level fluctuations caused by pumping and the rate of recovery after pumping ceases. Where wells are completed in low-permeability aquifer material, pumping-induced groundwater-level fluctuations can be large, but effects are spatially limited due to physical constraints of moving water through materials with limited permeability. These large drawdowns may interfere with the operation of nearby wells. If the long-term average pumping rate in a saturated geologic unit or composite of units exceeds the rate at which recharge can replenish the unit(s), the water removed from storage by pumping is not fully replaced. In these areas, groundwater levels will not recover to their pre-pumping level, and long-term groundwater-level declines will occur. Long-term regional declines in groundwater levels attributable to years of groundwater-storage depletion by pumpage are evident in hydrographs of late winter groundwater levels from many areas in the Harney Basin lowlands. Some areas of the Harney Basin have experienced long-term groundwater-level declines of more than 100 ft. Long-term groundwater-level trends are discussed in the section titled “Description of Harney Basin Groundwater-Flow System.”

Seasonal groundwater-level fluctuations from pumpage, mainly for irrigated agriculture, typically range from a few feet to more than 100 ft and occur in many areas of the Harney Basin lowlands. These pumpage effects can best be seen in the hydrographs for observation wells with continuous groundwater-level records (fig. 20). Hydrographs for these wells generally exhibit a rapid drawdown during late springtime when pumpage commences and continued, gradual drawdown during the summer growing season. When pumps are shut off at the end of the growing season, groundwater levels begin to recover and rise gradually throughout the autumn, winter, and early springtime. Hydrographs from some observation wells are dominated by pumping cycles of a single nearby well or well cluster (for example, the regular variations seen in HARN0052494), whereas hydrographs from many others show the combined influence from many pumping wells (for example, the broad declines and rises seen in HARN0052619 and HARN0052235).

Site HARN0052494 is an observation well about 15 ft from an irrigation well drilled into the Older basin fill HU in the northeastern corner of the Harney Basin lowlands. The hydrograph shows initial drawdown followed by periodic recovery and drawdown cycles related to times when pumpage stops for alfalfa (*Medicago sativa L.*) cutting (fig. 20). Each pumpage cycle causes a 9–10 ft drawdown response followed by partial recovery after pumpage stops. On a year-to-year basis, groundwater levels in this well generally do not fully recover by the beginning of the following irrigation season. This year-to-year decline of 4–5 ft indicates the volume of water being removed from storage each irrigation season is larger than can be replenished by recharge prior to the following season. Because the open interval of this observation well is 124–142 ft below the ground surface and the well penetrates clay in all but 6 ft of the overlying sediments, the groundwater-level record reflects the head in a relatively deep confined part of the groundwater-flow system. Presently, no evidence indicates an appreciable water-level decline in the shallow unconfined part of the system near this well (plate 2).

The groundwater-level record for HARN0052534 in the western part of the Weaver Spring/Dog Mountain area, completed in the Older basin fill HU, shows a similar pattern as HARN0052494 (fig. 20). The pumping-cycle response in observation well HARN0052534 is muted compared to HARN0052494, likely because the nearest pumping well is more than 1,800 ft away and, potentially, the hydraulic properties in this location are different. During 2017–19, the rate of decline at the well was about 1.5 ft/yr.

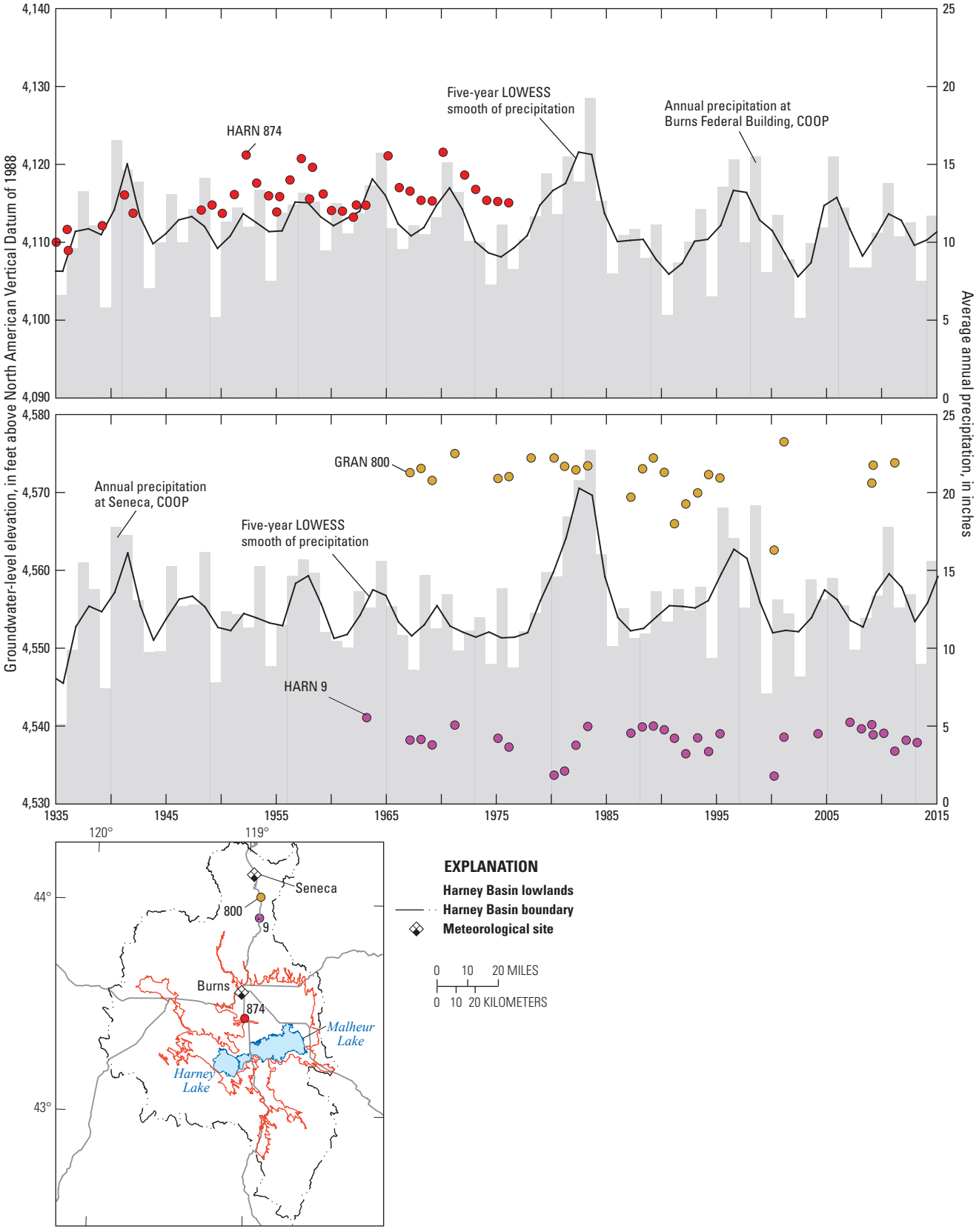

Figure 19. Groundwater levels measured January–April at selected wells and annual precipitation during 1935–2014, Harney Basin, southeastern Oregon.

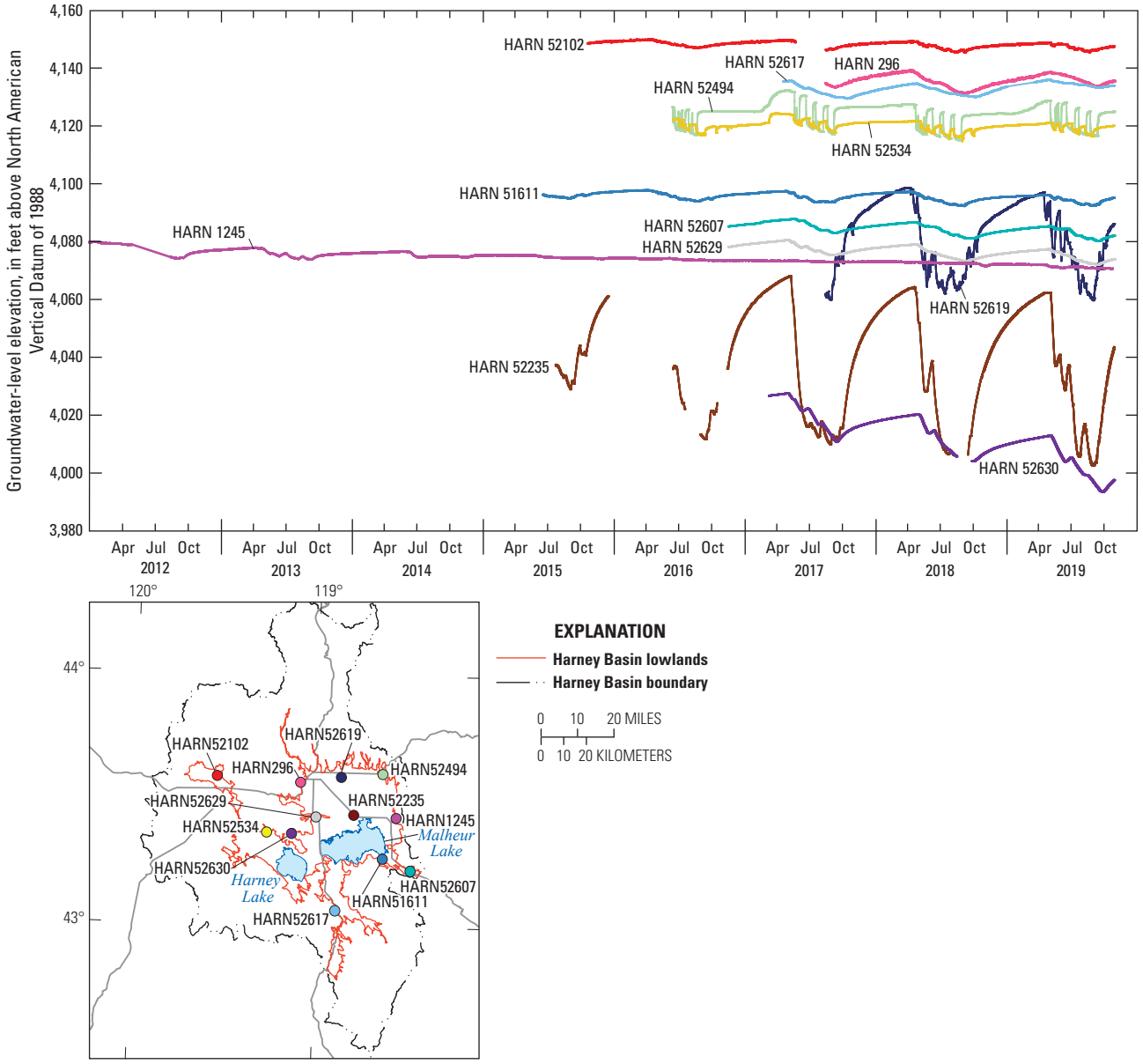

Figure 20. Groundwater-level elevations at selected observation wells showing pumpage effects in the Harney Basin, southeastern Oregon 2012–19. NAVD1988, North American Vertical Datum of 1988.

Observation wells HARN0052235 and HARN0052619 show the largest seasonal response to groundwater pumpage measured at any of the wells with continuous groundwater-level records. Well HARN0052235 is completed in the Older basin fill HU (specifically, the Rattlesnake Ash-Flow Tuff) in the center of the Harney Basin lowlands near Lawen. The seasonal pumpage-driven groundwater-level fluctuations observed in this well are about 60 ft each year (fig. 20). The hydrograph of HARN0052235, which has an open interval 450–471 ft below ground surface, shows the head in a confined part of the groundwater-flow system. The closest irrigation wells that might be responsible for the observed fluctuations are about 1.3–1.5 mi away, demonstrating the way in which large pumpage effects can propagate long distances under confined conditions with small storage properties. During 2017–19, the rate of decline at the well was nearly 3 ft/yr.

Well HARN0052619 is nearly 11 mi northwest of HARN0052235, and it is open to the Older basin fill HU from 190 to 390 ft below ground surface. Water-level data for HARN0052619 show a similar pattern of head response to pumpage stresses as HARN0052235, but the seasonal fluctuations are smaller, about 35 ft (fig. 20). Numerous irrigation wells within 2 mi of this well extract groundwater from similar depths in the northern Harney Basin lowlands.

Geochemical Evaluation of Recharge, Flowpaths, and Residence Time

Geochemical tracers are useful for developing and refining an understanding of groundwater-flow systems, including determining groundwater recharge sources, rate of movement, and residence time. They also can assist in confirming and refining groundwater flowpaths developed from groundwater-level maps. Water samples were collected from 194 sites within and near the Harney Basin during October 2016–October 2019 and analyzed for carbon-14 (^{14}C), tritium (^{3}H), and stable isotopes of water (fig. 21). The three tracers were not collected at all sites. One or more tracer samples were collected from 104 wells, 52 springs, 35 streams, Moon Reservoir, Malheur Maar, and the groundwater table exposed in Malheur Cave. Thirty-two sites were sampled 2 or more times during the study to characterize seasonal and interannual variability, including 17 springs, 9 wells, and 6 streams. Background on the use and interpretation of the three tracers and a discussion of sample-collection methods are provided in appendix 1.

Based on the multi-tracer evidence, much of the deep groundwater in the uplands and most of the groundwater in the Harney Basin lowlands was recharged in the late Pleistocene to mid-Holocene (about 30,000–5,000 yrs ago) when climatic conditions in the northern Great Basin were cooler and wetter than today (Benson, 1981; Benson and others, 1990; Dugas, 1998; Cohen and others, 2000; Oldow and Singleton, 2008; Lyle and others, 2012; Hudson and others, 2017). These results are consistent with the ancient water identified from wells and springs in other paleolake basins throughout the Great Basin (Thomas and others, 1996; Smith and others, 2002; Gardner and Heilweil, 2014). In the following discussion, the results for the three tracers are discussed. In the subsequent section ("Description of Harney Basin Groundwater-Flow System"), tracer results are synthesized and discussed alongside the physical hydrology for selected areas of the Harney Basin.

Carbon-14 and Stable Carbon Isotope Ratio

Samples for ^{14}C and stable carbon isotope ratio ($\delta^{13}C$; the isotope ratios are reported as delta [δ] values expressed as parts per thousand [permil, or ‰]) in dissolved inorganic carbon (DIC) were collected from 19 sites across the Harney Basin—13 wells and 6 springs (fig. 21*A*; Gingerich and others, 2022). Values of ^{14}C ranged from 0.5 percent modern carbon (pmC) to 98.0 pmC (fig. 22*A*; Gingerich and others, 2022), and the calibrated ^{14}C age ranged from less than (<) 500 to more than 45,000 yrs before sample date. Generally, the youngest ^{14}C ages were from samples in the uplands and on the periphery of the Harney Basin lowlands, though older groundwater also was found in the uplands. Most groundwater samples in the Harney Basin lowlands had a ^{14}C age greater than 8,000 yrs (fig. 21*A*; Gingerich and others, 2022).

Fifteen of the samples (all six springs and nine wells) were not influenced or were minimally influenced by the addition of DIC enriched in carbon-13 (^{13}C) and depleted in ^{14}C relative to soil gas (fig. 22*A*); the ^{14}C ages calculated for these samples were accepted as reasonable estimates of the mean age of the groundwater sample. In four samples, evidence for a moderate to substantial addition of DIC enriched in ^{13}C and depleted in ^{14}C is present, likely CO_2 from biogenic methanogenesis in the groundwater-flow system. The ^{14}C ages calculated for these samples overestimate the radiocarbon age of the sample owing to the dilution of atmospherically derived ^{14}C with a ^{14}C-dead source produced within the groundwater-flow system. The rationale for these conclusions is discussed in the rest of this section.

Accurate determination of the ^{14}C age requires an understanding of the processes that determine the ^{14}C activity in recharging groundwater and processes other than radioactive decay that may alter the ^{14}C activity during transit through the groundwater-flow system. The ^{14}C age of DIC in a groundwater sample is calculated as follows:

$$t = -8{,}267 \times \ln\left(\frac{A_t}{A_o}\right) \quad (4)$$

where

t is time, in years since recharge,
A_t is the measured ^{14}C activity of DIC in the sample, in percent modern carbon; and
A_0 is the initial activity of ^{14}C at the time of recharge, in percent modern carbon.

The initial ^{14}C activity of DIC in recharge (A_0) is about the same as the ^{14}C activity of atmospheric CO_2 at the time of recharge if no mineralogical DIC is added to the sample in the soil and unsaturated zone. Because A_0 can only be measured for modern recharge, the atmospheric reconstruction of ^{14}C in CO_2 over the previous 50,000 yrs is used as a surrogate (Hua and others, 2013; Reimer and others, 2016; fig. 23). In reality, the ^{14}C activity of DIC in soil water is about 2 percent less than the ^{14}C activity of atmospheric CO_2 at the time of recharge owing to fractionation processes affecting ^{14}C in the soil zone (Clark and Fritz, 1997); however, that difference is typically ignored because the actual fractionation is not measured at most study sites (and was not measured in the Harney Basin), cannot be measured for ancient samples, and is within the uncertainty of the reconstructed atmospheric ^{14}C activity. For the samples collected in the Harney Basin for this study, the uncertainty introduced by ignoring this fractionation is small (110–170 yrs) relative to the sampled median ^{14}C age of 8,659 yrs. No evidence for the addition of mineralogical DIC during recharge that would have diluted the atmospheric ^{14}C activity with ^{14}C-dead DIC was found, and therefore A_0 was assumed equal to the atmospheric ^{14}C activity at the time of recharge for the samples collected in the Harney Basin. The evidence against the addition of mineralogical DIC is discussed below.

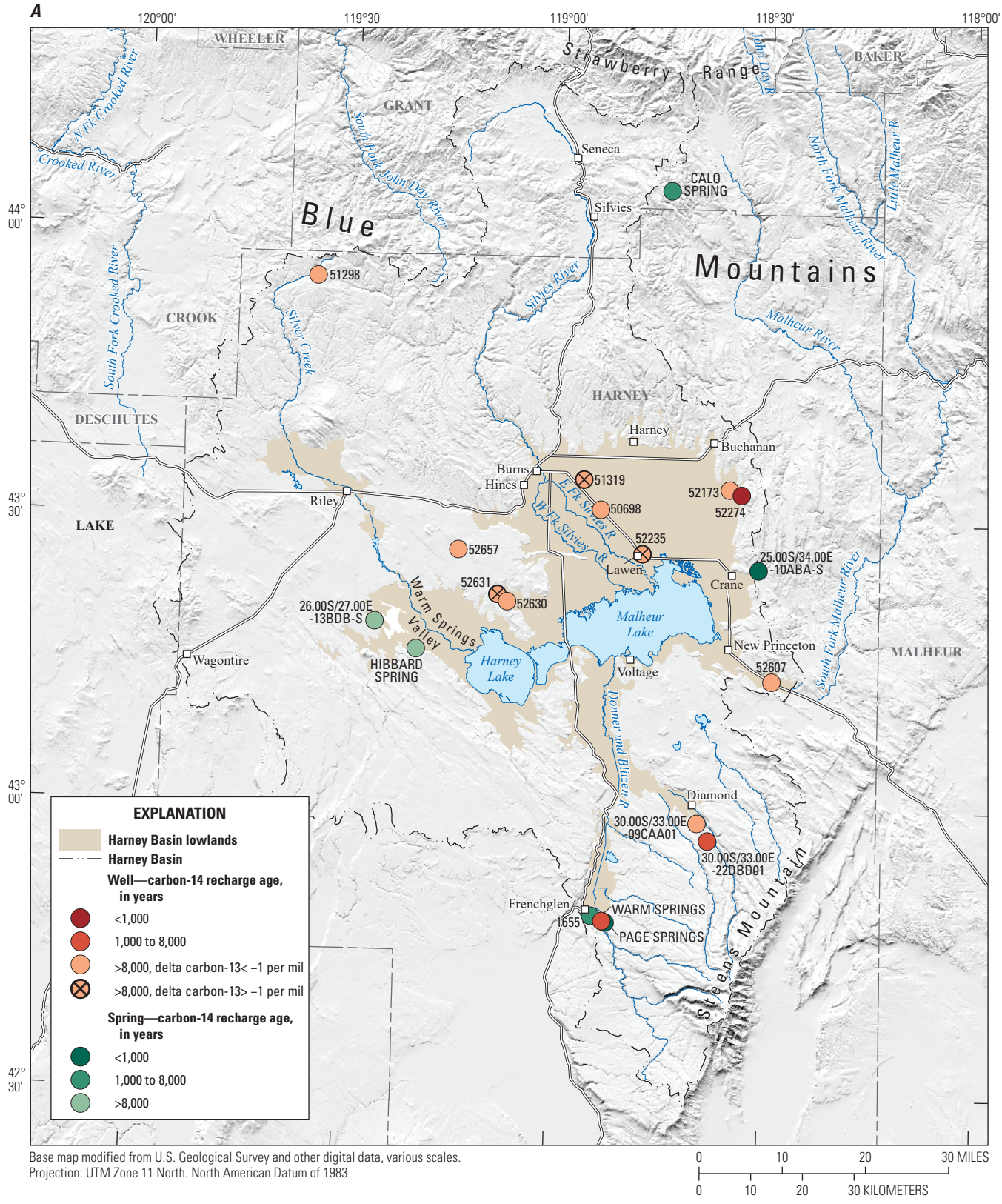

Figure 21. Sites sampled for (*A*) carbon-14, (*B*) tritium, and (*C*) stable isotopes of water, Harney Basin, southeastern Oregon.

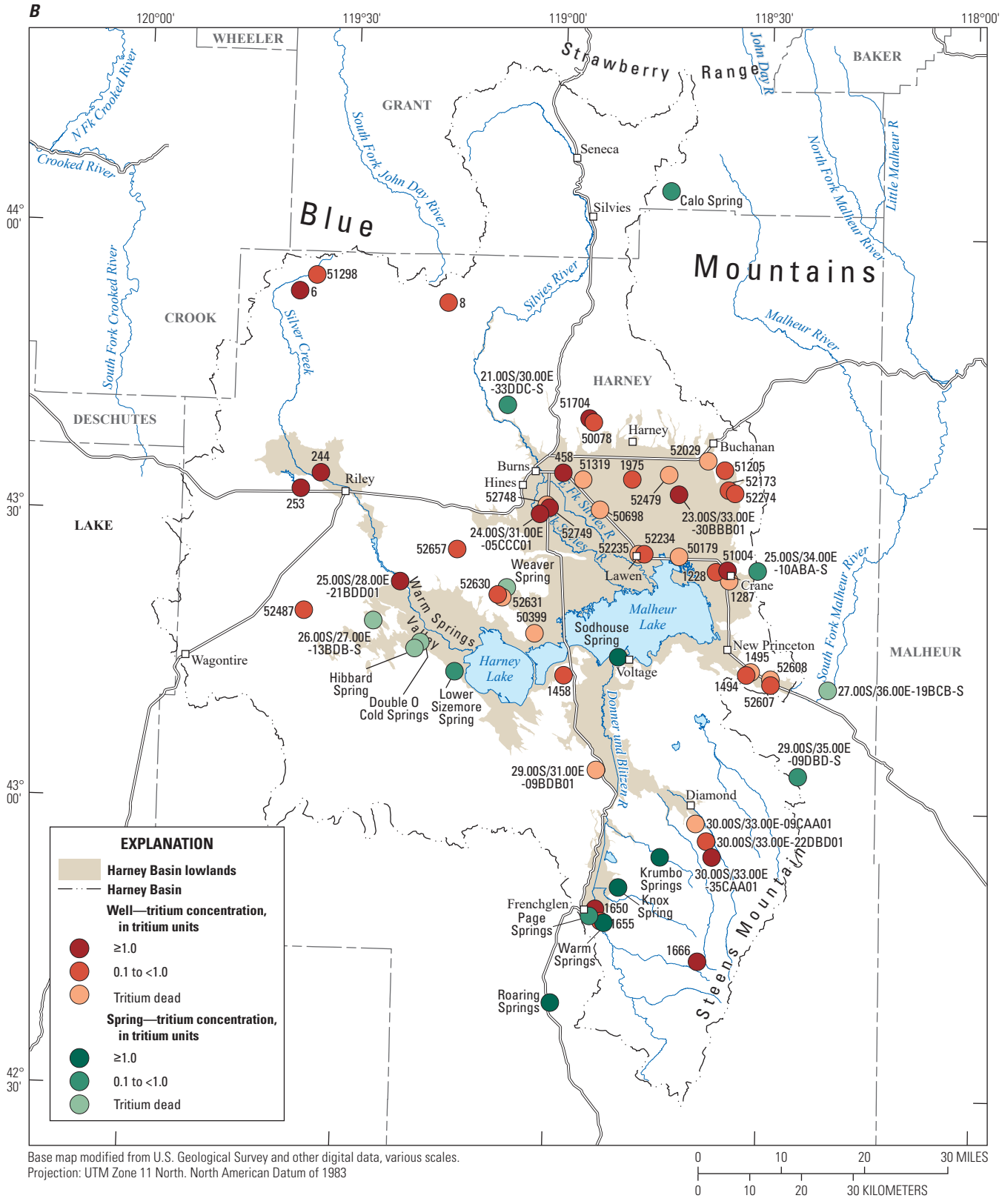

Figure 21.—Continued

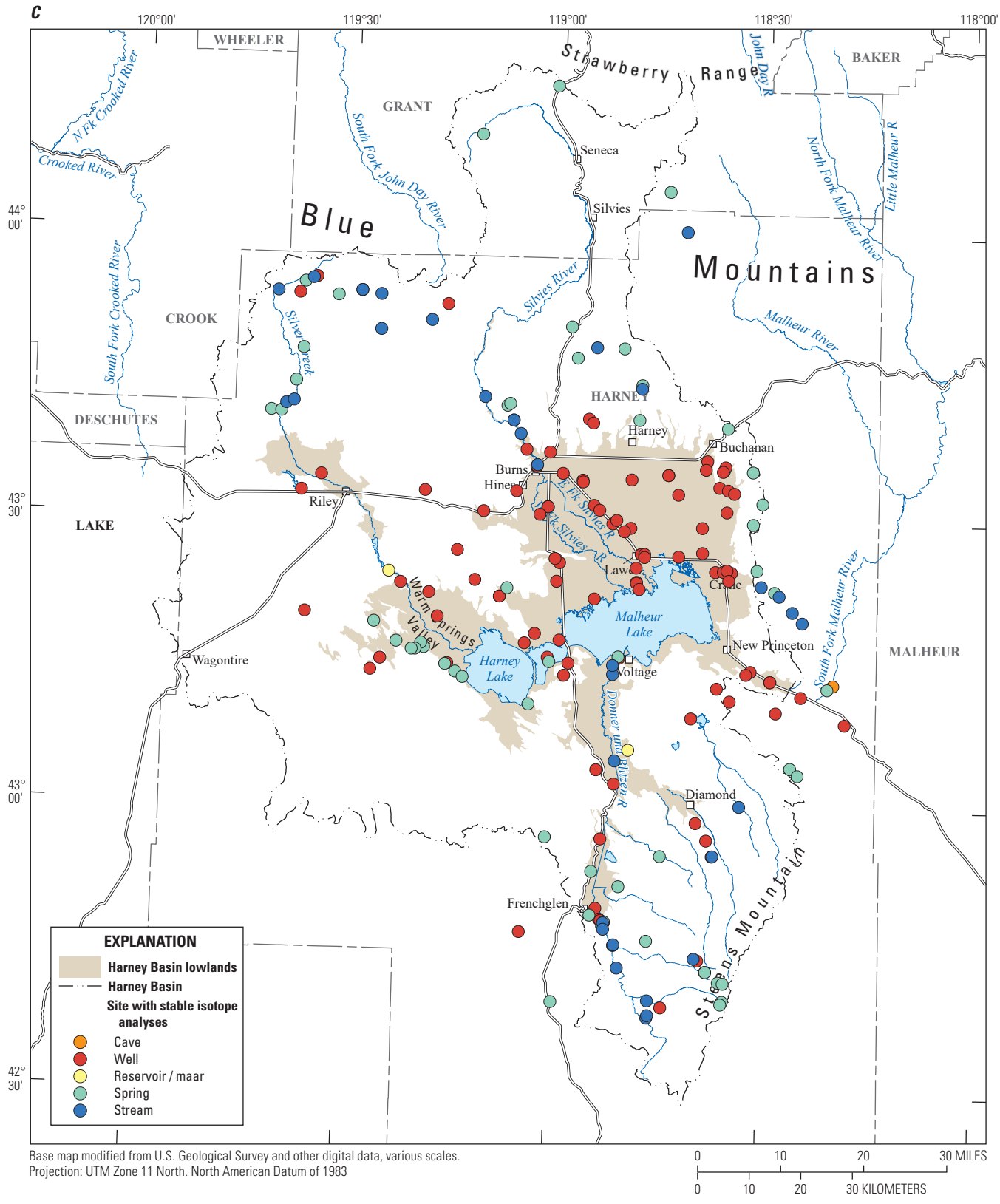

Figure 21.—Continued

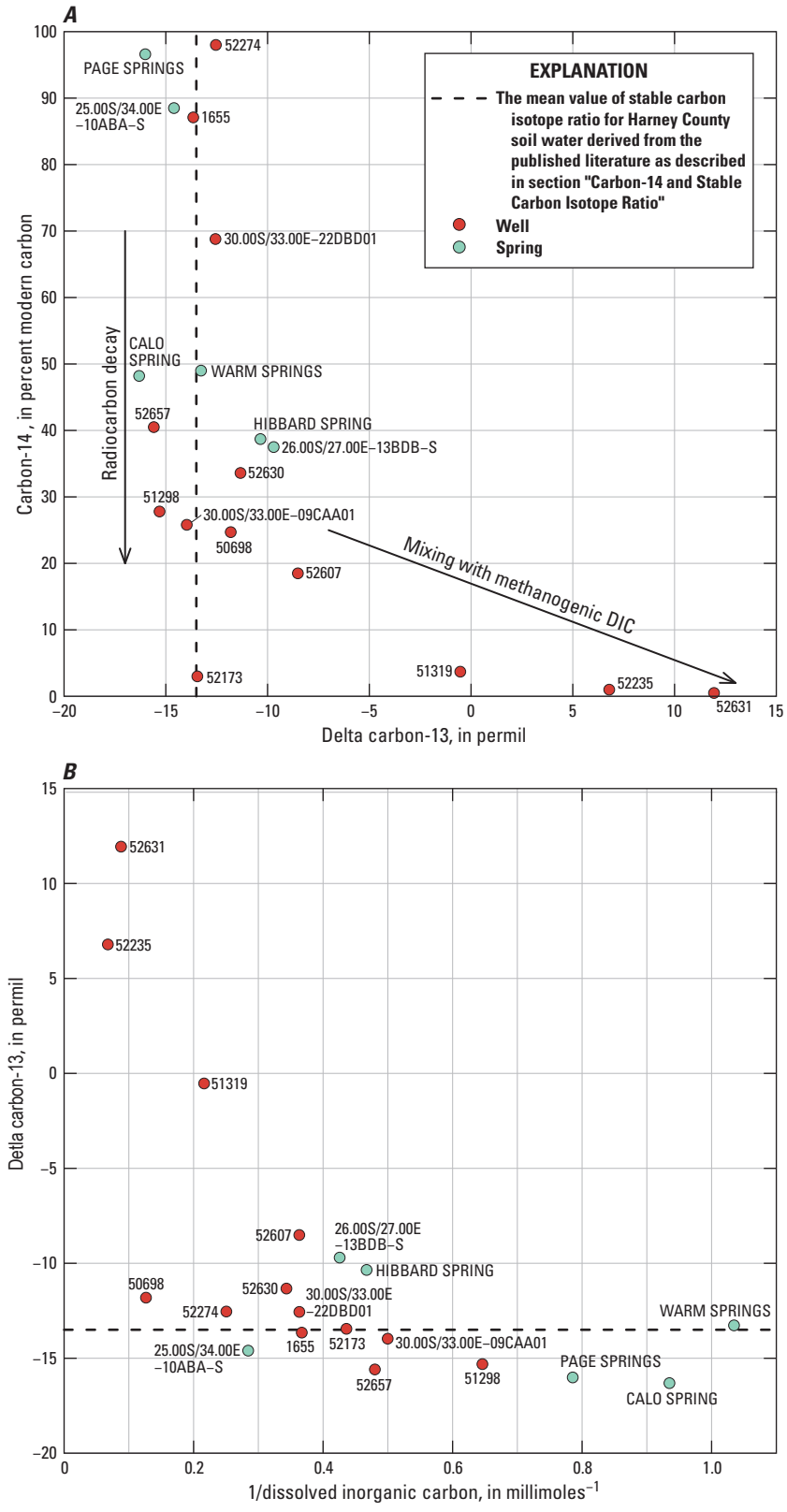

Figure 22. Relation between (*A*) stable carbon isotope ratio and carbon-14 and (*B*) stable carbon isotope ratio and dissolved inorganic carbon, Harney Basin, southeastern Oregon. DIC, dissolved inorganic carbon.

The addition of mineralogical carbon in the unsaturated zone or during transit through the groundwater-flow system can be assessed by comparing the measured $\delta^{13}C$ of DIC of a sample with estimates of the initial $\delta^{13}C$ of DIC resulting from fractionation of atmospheric ^{13}C in the unsaturated zone. The $\delta^{13}C$ ratio of DIC in recharge is initially determined by the $\delta^{13}C$ of the soil gas at the place of recharge, values of which have been compiled from a literature review and reported by Clark and Fritz (1997). In mid-latitude biomes (such as Harney County) dominated by plants using the C3 photosynthetic pathway, the $\delta^{13}C$ of soil CO_2 averages -23 ‰ (Clark and Fritz, 1997).

As an independent check on the mean value reported by Clark and Fritz (1997), the $\delta^{13}C$ of soil CO_2 was calculated from a database of plant $\delta^{13}C$ compiled from the literature by Kohn (2010) and published fractionation values; a value of -22 ‰ was obtained using this method, corroborating the mean value of Clark and Fritz (1997). The dataset compiled by Kohn (2010) was filtered to include only mid-latitude studies (30–45° north or south latitude) with a reported mean annual precipitation less than 300 millimeters; filtering resulted in 50 measurements from 18 different studies. The median plant $\delta^{13}C$ was -26 ‰, with a range of -27 to -23 ‰. Decomposition of plant organic matter by soil microbes results in soil CO_2 gas with a similar $\delta^{13}C$ to the local plant communities. CO_2 gas in the soil fractionates as it diffuses from the soil to the atmosphere, leaving the soil gas enriched by about 4 ‰ compared to the local plant communities (Cerling and others, 1991; Dörr and Münnich, 2016). Accounting for diffusive fractionation, the median $\delta^{13}C$ of CO_2 soil gas determined from Kohn's compilation is -22 ‰.

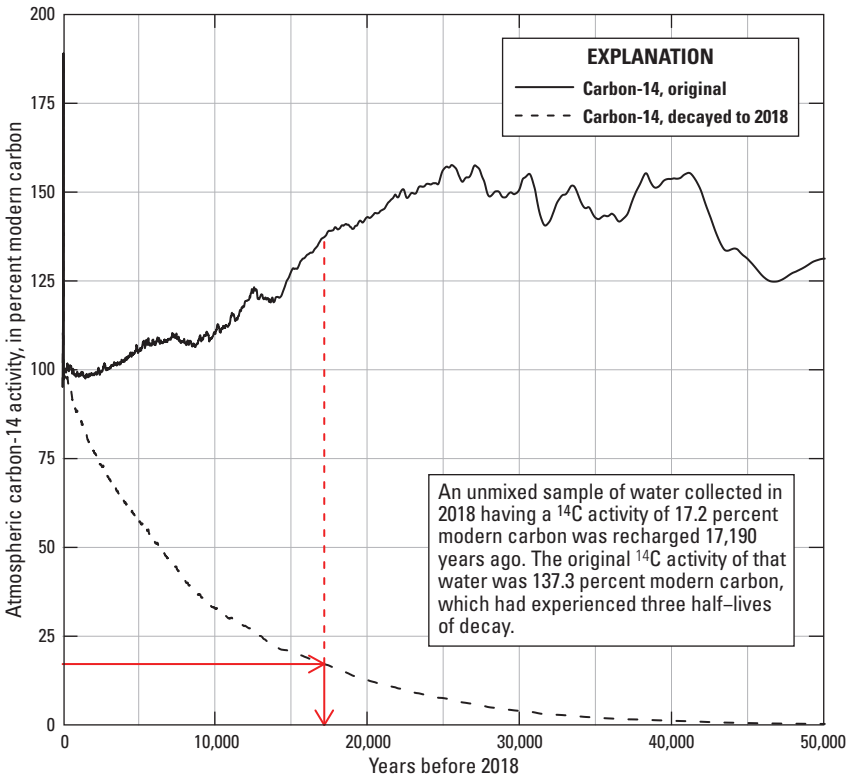

Figure 23. Reconstruction of atmospheric carbon-14 (^{14}C) activity for the previous 50,000 years. The atmospheric activity data were obtained from an updated version of Jurgens and others (2012) that used the IntCal13 ^{14}C reconstruction (Reimer and others, 2016). The dashed line shows the value of the original ^{14}C activity decayed to the year 2018 and reflects the ^{14}C activity that would be measured in a sample of water collected in 2018. The narrow peak in ^{14}C activity near year zero on the x-axis is from atmospheric testing of nuclear weapons during the mid-20th century.

These two similar, independent estimates for $\delta^{13}C$ of soil gas CO_2 values were used to estimate the initial $\delta^{13}C$ of DIC for the Harney County samples. The dissolution of soil CO_2 gas in water and its subsequent dissociation into HCO_3^- and CO_3^{2-} further fractionates ^{13}C. The gas-DIC fractionation process is temperature dependent (Plummer and Glynn, 2013) and results in about a 9 ‰ enrichment relative to the soil CO_2 at 7 °C, the mean annual air temperature at Burns Municipal Airport (Western Regional Climate Center, 2020). Applying a 9 ‰ enrichment to the two literature-provided estimates of soil gas $\delta^{13}C$ (-23 ‰ and -22 ‰), yields an expected initial soil water DIC $\delta^{13}C$ of -14 ‰ to -13 ‰.

The potential for addition of other sources of DIC, and therefore dilution of A_0, was evaluated by comparing the expected mean DIC $\delta^{13}C$ values of soil water (-14 ‰ to -13 ‰) to the DIC $\delta^{13}C$ measured in the samples from the Harney Basin. The median $\delta^{13}C$ of samples from the Harney Basin is -12.6 ‰. Excluding the three samples having $\delta^{13}C$ greater than -1 ‰ (discussed below), the median $\delta^{13}C$ is -13.4 ‰, which is within the two estimates of the $\delta^{13}C$ ratio of soil DIC provided from the literature. Because the $\delta^{13}C$ ratio of these 16 samples is similar to the estimated soil water DIC derived solely from atmospheric CO_2 (fig. 23), little or no DIC is concluded to have been added to these samples from sources enriched or depleted in $\delta^{13}C$ relative to DIC derived from atmospheric vapor. And, because no evidence for substantial contributions of DIC from a source other than atmospherically derived DIC in these 16 samples is apparent, no major contribution of ^{14}C in these 16 samples from any DIC source other than the atmosphere is expected. Therefore, the use of the reconstructed atmospheric ^{14}C activity for A_0 in the calculation of ^{14}C age is justified.

The three samples having $\delta^{13}C$ greater than -1 ‰ are greatly enriched in ^{13}C relative to the other samples (fig. 22*A*) and relative to the atmosphere, indicating the addition of DIC highly enriched in ^{13}C while in the subsurface. The three samples also have three of the four largest DIC concentrations (fig. 22*B*). The sample from HARN0052607 may have a measurable but small addition of non-atmospheric DIC. Although the $\delta^{13}C$ ratio from HARN0052607 (-8.5 ‰) is not substantially different from that of the next lowest (-9.7 ‰) and the DIC concentration is similar to most other samples, the concomitant enrichment in ^{13}C and depletion in ^{14}C that conforms to an exponential relation that includes the three highly enriched samples indicates a potential relation with those samples (fig. 22*A*). As discussed by Han and others (2014), an exponential relation between $\delta^{13}C$ and ^{14}C among samples from the same area is characteristic of mixing between atmospherically derived DIC and a ^{14}C-dead source of DIC enriched in $\delta^{13}C$. The calculated ^{14}C age of samples that have experienced mixing with a ^{14}C-dead source will be older than the actual age of the sample. Han and others (2014) discussed a method to back out the actual age, but the small number of samples in the Harney Basin (n=3) that are unequivocally mixed precludes the application of the technique. A qualitative estimate can be obtained for the samples from the Harney Basin: The age bias is directly related to the amount of ^{14}C-dead DIC added to the groundwater sample, which can be assessed by the magnitude of the $\delta^{13}C$ ratio. Therefore, the sample most enriched in ^{13}C (HARN0052631) will have a greater age bias than a less-enriched sample, such as HARN0051319. Small amounts of non-atmospheric DIC may have been added to other samples; however, the addition cannot be distinguished from the natural variability expected in the initial $\delta^{13}C$ of soil DIC (Clark and Fritz, 1997) and would not substantially change the ^{14}C-age estimates.

Potential sources of subsurface DIC enriched in ^{13}C include carbonate minerals, geogenic CO_2, and methanogenic CO_2. Of these sources, only methanogenic CO_2 is sufficiently enriched in ^{13}C to explain the enriched values measured in the samples from the Harney Basin. DIC from carbonate minerals and geogenic CO_2 typically have a $\delta^{13}C$ less than 0 ‰ (Clayton and Degens, 1959; Talbot, 1990; Cerling and Quade, 1993; Clark and Fritz, 1997), so the $\delta^{13}C$ of DIC in groundwater containing significant contributions from these sources will be elevated above soil gas, but generally considerably less than 0 ‰ unless the geologic sources overwhelmingly dominate the DIC. The presence of measurable ^{14}C activity indicates that has not occurred. In contrast, $\delta^{13}C$ of DIC in groundwater containing CO_2 produced during methanogenesis generally exceeds 0 ‰ and commonly exceeds +10 ‰ (Han and others, 2012, 2014; Plummer and Glynn, 2013). Methanogenesis requires highly reducing conditions, evidence of which was found at the three wells where $\delta^{13}C$ was greater than -1 ‰, including (1) sulfate concentrations less than 2.1 milligrams per liter (mg/L) (range: <0.2–2.1), (2) dissolved oxygen concentration ≤ 2.0 mg/L (range: 0.7–2.0), and (3) nitrate concentrations less than 0.005 mg/L (nitrate not detected at any site). In contrast, at the other eight sites with ^{14}C analyses, sulfate ranged from 5.0 to 89.5 mg/L (median = 27.9 mg/L), dissolved oxygen ranged from <0.2 to 8.1 mg/L (median = 3.25 mg/L), and nitrate ranged from <0.005 to 2.7 mg/L (median = 0.025 mg/L). The analyses of sulfate, dissolved oxygen, and nitrate were obtained from the Oregon Department of Environmental Quality (2021). Dissolved gas samples were not collected at any sites to confirm the presence of methane, nor was the qualitative presence or absence of hydrogen sulfide odor recorded during sampling. Additional evidence for the potential for methanogenic DIC comes from the distribution of the three sampled wells compared to the other sample locations; specifically, no pattern to the occurrence was observed: these wells are in three different areas of the basin, the wells are not among the shallowest nor the deepest, other wells completed in the same depth range show no evidence of additional DIC, and the groundwater temperature ranges from cool (12.3 °C) to warm (23.9 °C) with other wells falling within that same range. The lack of a pattern is indicative of isolated, unique locations in the groundwater-flow system where conditions for methanogenesis were favorable.

Tritium

Tritium (^3H) is a radioactive isotope of hydrogen that is useful for discriminating groundwater recharged before about 1953 from groundwater recharged after about 1953. Samples for ^3H were collected from 60 sites across the Harney Basin—44 wells and 16 springs (fig. 21*B*; Gingerich and others, 2022). The ^3H concentration ranged from <0.1 to 4.3 TU. Samples without detectable ^3H (a state called "tritium dead") comprised 19 of the 60 samples (32 percent). Tritium was detected at less than 1 TU in 22 samples (37 percent) and at 1 TU or greater in 19 samples (32 percent). Generally, sites where ^3H was greater than or equal to (≥) 1 TU were in the uplands, along the mountain front, near reservoirs, and wells less than 200 ft deep. Samples that were tritium dead generally were collected from the center of the Harney Basin lowlands, Warm Springs Valley, deep wells along the mountain front, and Virginia Valley. Tritium-dead samples were collected from seven wells less than 200 ft deep, including one less than 100 ft deep (HARN0050698), indicating that well depth alone is not a good predictor of tritium-dead groundwater in the Harney Basin.

Tritium enters the groundwater as a tritiated water molecule ($^3H^1HO$) with a concentration similar to the concentration of tritium in atmospheric water vapor at the time of recharge. Because ^3H is radioactive (half-life of 12.32 yrs), the ^3H concentration of the recharged water decreases over time. The atmospheric concentration history is highly non-monotonic with a large peak in the 1960s owing to atmospheric testing of nuclear weapons which, combined with uncertainty in the initial concentration due to radioactive decay, makes assigning a precise recharge date using a single ^3H sample impossible. Nevertheless, certain characteristics of ^3H make it an attractive and useful age-dating tool for groundwater. First, because the water itself is the target of the analysis (as opposed to something dissolved in the water such as calcium), sample collection is resistant to contamination and the analytical results are robust and straightforward to interpret. Second, the natural background concentration of ^3H in the atmosphere prior to the beginning of atmospheric testing of nuclear weapons is no longer detectable with the analytical methods used for this study. These ^3H characteristics mean that groundwater in a tritium-dead sample can be definitively assigned a date of recharge prior to 1953, whereas the presence of ^3H in a sample provides firm evidence that some fraction of the water in the sample was recharged after 1953. In subsequent discussions, water recharged prior to 1953 is referred to as "pre-modern" and water recharged after 1953 is referred to as "modern." The presence of modern water in a sample is a useful indicator of areas of active recharge and of the circulation depth of recent recharge. Additional background on the use of ^3H for dating groundwater can be found in app. 1.

In addition to a simple presence-absence, the ^3H concentration can be used to evaluate the proportion of pre-modern groundwater in a sample. Most samples collected from a well or spring are a mixture of groundwater that recharged at separate times and that followed different flowpaths to the sampling location (fig. 24). These complex mixtures of groundwater can be conceptualized as relatively simple, two-component mixtures, in which one component is pre-modern (tritium dead) and the other component is modern and has a ^3H concentration equal to the flow-weighted mean ^3H concentration from all flowpaths containing modern groundwater that are intercepted by the well or spring. In principle, the range of potential modern flow-weighted mean ^3H concentrations is bounded by the maximum and minimum post-1953 atmospheric ^3H concentration decayed to the sampling date. In reality, the range is much smaller because dispersion processes preclude recharge from a single year from traveling through the unsaturated zone and groundwater-flow system without

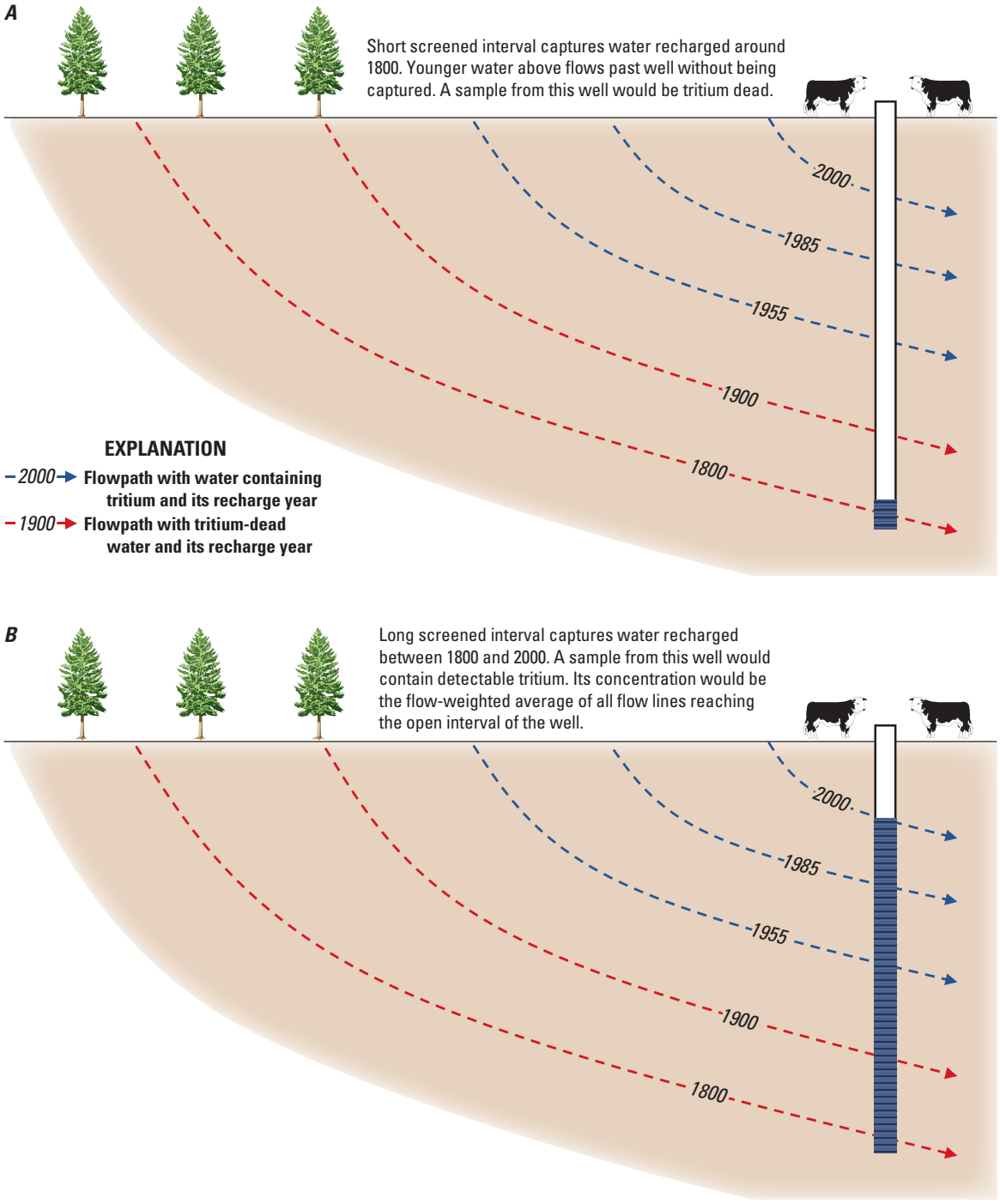

Figure 24. Groundwater flowpaths and the effect on tritium concentration in a well casing having (*A*) a short open interval and (*B*) a long open interval.

mixing with water from other recharge years. A plausible range of two-component mixtures was developed using seven different ^{3}H concentrations for the modern component (fig. 25). The seven values were calculated as the 2-yr mean atmospheric ^{3}H concentration (decayed to 2018) for each decade starting in 1955. These seven modern end-member concentrations were mixed with a tritium-dead end-member representing the pre-modern component. The steep slope of the 1965 mixing line results from the high concentrations of ^{3}H in atmospheric water vapor due to atmospheric testing of nuclear weapons (fig. 1.1). The shaded area encompassed by the mixing lines in figure 25 represents the range of plausible ^{3}H values and fractions of pre-modern groundwater; mixtures in the unshaded area of the plot are impossible or highly improbable for reasons already discussed. A broad range of age mixtures are possible for a measured ^{3}H concentration greater than about 1 TU but are considerably more limited for measured ^{3}H concentrations less than 1 TU. For example, a sample having a measured ^{3}H concentration of 3 TU could contain no pre-modern groundwater at all (with a mean recharge year around 1995), or it could be a mixture of about 94-percent pre-modern groundwater with about 6 percent modern groundwater having a mean recharge year of 1965, or the mixture could lie anywhere between the two extremes. In contrast, in a sample having a measured ^{3}H concentration of 0.5 TU, at least 80 percent and as much as 98 percent of the groundwater in the sample must be pre-modern. As the ^{3}H concentration approaches the analytical limit of detection (0.1 or 0.2 TU depending on lab performance metrics), confidence in the proportion of groundwater recharged prior to 1953 in the sample increases. Thus, in addition to the simple presence-absence of ^{3}H as an indicator of pre-modern or modern groundwater, it is also possible to evaluate the proportion of pre- and post-1953 groundwater in a sample.

In figure 25, the mixing line for 1985 describes the minimum fraction of pre-modern groundwater that can be in a sample. Using that line, the frequency distribution of the minimum fraction of pre-modern groundwater in the 60 ^{3}H samples from the Harney Basin was developed (fig. 26). In 43 ^{3}H samples (72 percent), at least half the water in the sample was pre-modern; in 29 samples (48 percent), 90 percent of the water in the sample was pre-modern; and in 19 samples (32 percent), no indication of any modern groundwater was present. Only 11 samples (18 percent) could potentially contain no pre-modern groundwater.

Although ^{3}H can be used to identify and constrain the amount of pre-modern groundwater in a sample, the age of that component is known only to have been recharged prior to 1953. This limitation can be overcome at sites where ^{3}H and ^{14}C were collected if a relation exists between the two tracers and cautiously extrapolated to other sites where ^{3}H was collected without a corresponding ^{14}C sample. At all 19 sites where ^{14}C was collected, ^{3}H was also collected and a statistically significant, relatively strong correlation was identified between ^{3}H concentration and ^{14}C age (Spearman's rho = 0.74, p-value = 0.0003). The relation is similar when considering only the 16 sites without clear evidence for additions of methanogenic DIC (Spearman's rho = 0.72, p-value = 0.0017). At these 19 sites, the ^{3}H concentration decreases as the ^{14}C age of the groundwater increases, providing evidence that the average age of the pre-modern component is quite old (fig. 27) and also providing additional evidence that mixing of pre-modern and modern groundwater is common in the Harney Basin. Development of a predictive relation between ^{3}H and ^{14}C to quantify the age of the pre-modern groundwater fraction was not possible owing to the large variability in ^{14}C ages younger than 5,000 yrs. However, some useful general estimates can be made. Generally, in samples in which the ^{3}H concentration is less than 1 TU and greater than about 0.3 TU, the mean age of the pre-modern component likely is more than 1,000 yrs and less than 10,000 yrs old. And, in samples in which the ^{3}H concentration is less than 0.3 TU, the mean age of the pre-modern component is at least 10,000 yrs old. These general guidelines help constrain the age of the three ^{14}C samples that had $\delta^{13}C$ greater than -1 ‰ – all three samples were tritium dead, which is consistent with an age of at least 10,000 yrs old. Although the ^{14}C-based ages in these three samples are biased high owing to the addition of ^{14}C-dead carbon after recharge, the groundwater in those samples likely is older than 10,000 yrs.

Stable Isotopes of Water

Samples for the analysis of stable isotopes of water were collected from 194 sites within and near the Harney Basin (fig. 21*C*) and included 104 wells, 52 springs, 35 streams, Moon Reservoir, Malheur Maar, and the groundwater table exposed in Malheur Cave. Samples generally plot to the right of the Global Meteoric Water Line (GMWL; see app. 1 for discussion of the GMWL and stable isotopes) (fig. 28). Wells had the largest range in values, springs had a somewhat smaller range, and streams were most limited in their range of values. The least-squares regression (LSR) fit through all stable isotope samples has a slope of 5.7, which is less than the slope of the GMWL (slope = 8.0) and indicative of non-equilibrium evaporative processes affecting the evolution of water in the area (Clark and Fritz, 1997). Three samples are highly evaporated (delta hydrogen-2 [$\delta^{2}H$] greater than -100 ‰; see app. 1 for discussion of δ notation); however, removing them does not appreciably affect the slope of the LSR (slope=5.9). Similarly, the slopes of LSR lines fit through samples of the three major groups of sites were not appreciably different from one another (5.7 for wells, 5.4 for springs, and 5.2 for streams) or from the LSR slope through all the samples. The general rightward shift of all samples relative to the GMWL and the LSR slope less than the GMWL likely results from several processes, including evaporation during canopy interception (Claassen and Downey, 1995), evolution of the snowpack (Sommerfield and Friedman, 1991; Cooper, 1998; Sokratov and Golubev, 2009), and subcloud evaporation during precipitation. Some samples experienced additional evaporative fractionation owing to prolonged exposure in reservoirs, wetlands, stream channels, and ephemeral ponds created during the springtime freshet.

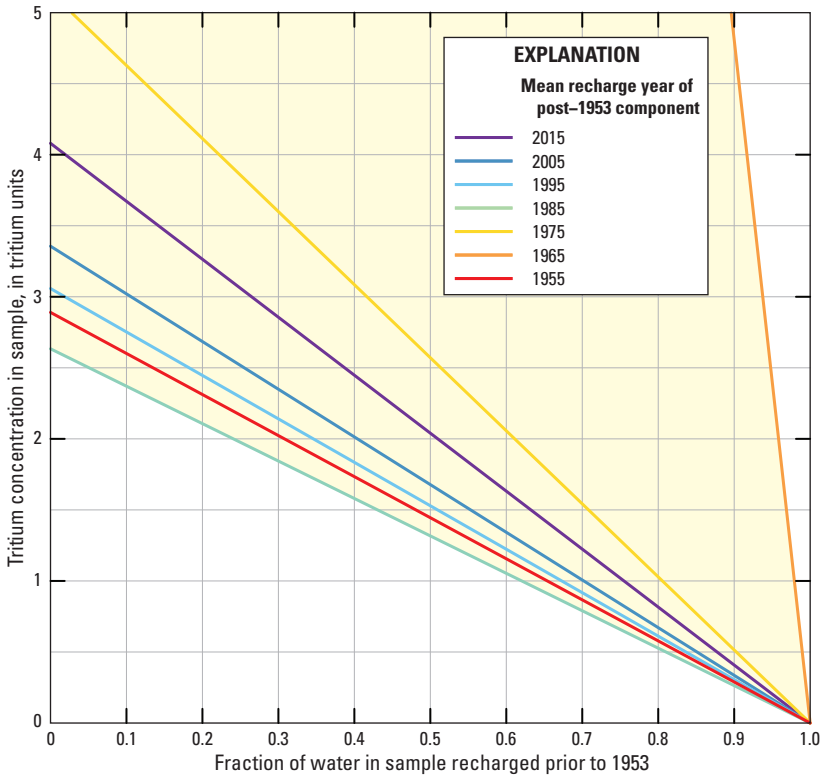

Figure 25. Mixing lines for two-component mixtures of groundwater, where one component is tritium-dead groundwater recharged prior to 1953 and the second component contains tritiated groundwater that was recharged after 1953, Harney Basin, southeastern Oregon. The shaded area shows the range of plausible mixtures.

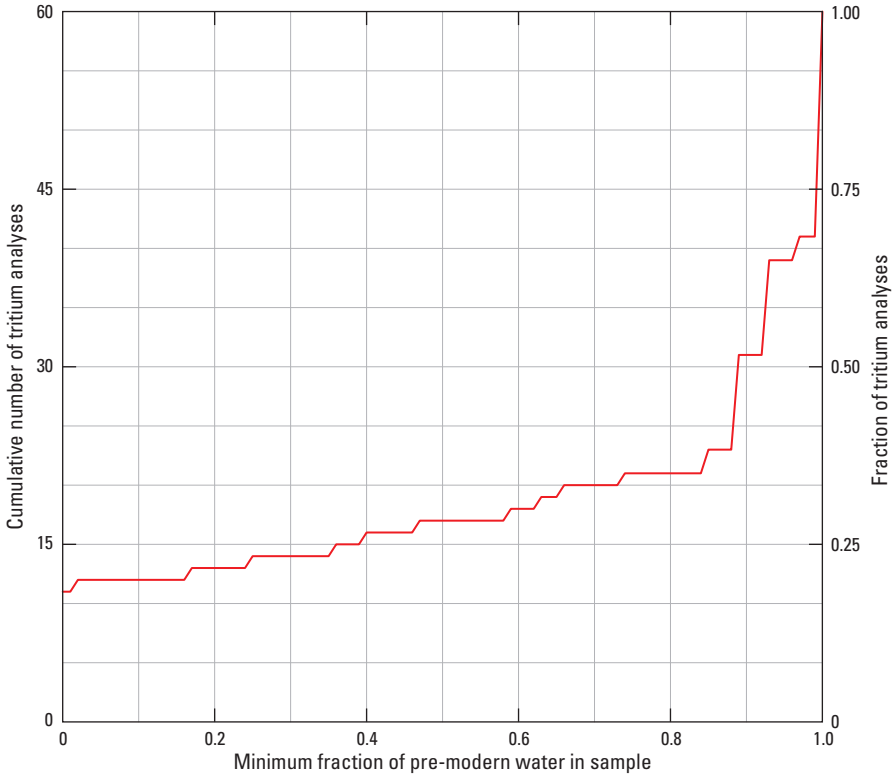

Figure 26. Cumulative distribution of the minimum fraction of water recharged prior to 1953 in tritium samples from the Harney Basin, southeastern Oregon. The minimum fraction was calculated from the binary mixing model developed for a mixture of water recharged in 1985 and prior to 1953 (shown in fig. 25).

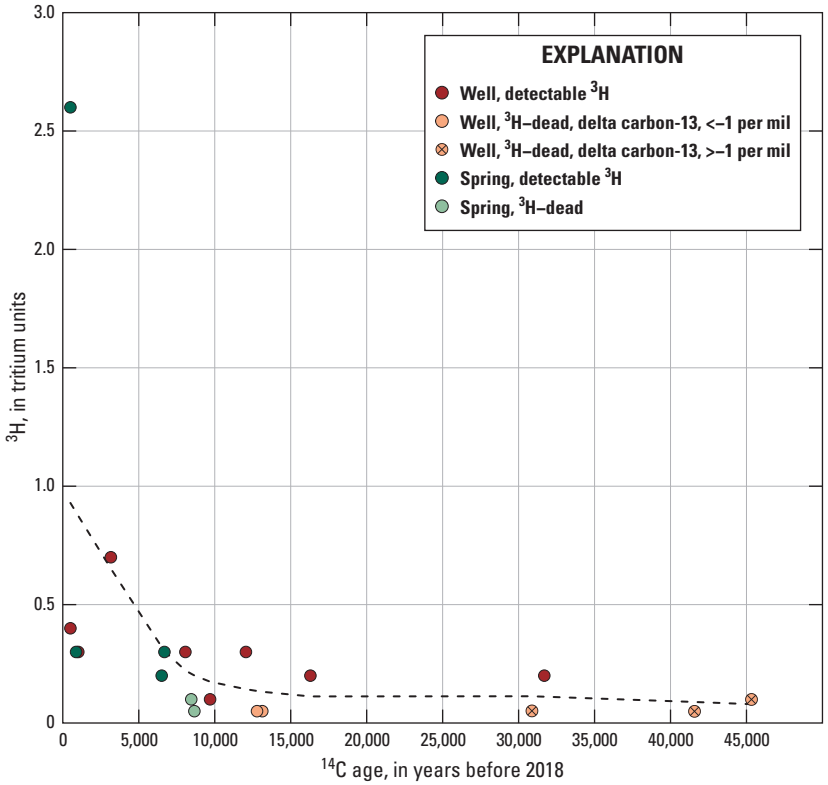

Figure 27. Relation between tritium (^3H) and carbon-14 (^{14}C), Harney Basin, southeastern Oregon. The black, dashed curve is a locally weighted scatterplot smoothing (LOWESS) model smooth through all the data. <, less than; >, greater than.

The position of a sample relative to the GMWL is often expressed by the deuterium excess (eq. 5).

$$deuterium\ excess = \delta^2H - 8 \times \delta^{18}O \quad (5)$$

Because the slope of a line fit through samples evaporated from the same source water is less than the slope of the GMWL, samples that have experienced more evaporation will plot further from the GMWL than less-evaporated samples. Expressed in terms of deuterium excess, less-evaporated samples will have a value closer to 10, whereas more-evaporated samples will be less than 10; highly evaporated samples will have a negative value of deuterium excess.

A high degree of correlation exists between δ^2H and $\delta^{18}O$ owing to the physics of the major isotopic fractionation processes (fig. 28; Clark and Fritz, 1997); therefore, the subsequent discussion of stable isotopes of water generally will refer only to the δ^2H analysis for conciseness and also because of the potential for geothermal systems to introduce small but measurable increases in $\delta^{18}O$ (Smith and others, 2002).

Relation Between Deuterium, Tritium, and Carbon-14

The understanding of the distribution of groundwater age in the Harney Basin can be expanded by incorporating the δ^2H results into the previous analysis of ^3H and ^{14}C. Little overlap in the range of δ^2H values between fully pre-modern groundwater and potentially fully modern groundwater is present (fig. 29). The δ^2H value in samples containing potentially fully modern groundwater (fraction = 0.0) ranged from -106 to -122 ‰, except for one highly evaporated sample from a shallow well near Delintment Lake (δ^2H = -84 ‰; HARN0000006 on plate 1). The δ^2H value in samples containing fully pre-modern groundwater (fraction = 1.0) ranged from -119 to -139 ‰, so the overlap between potentially fully modern and fully pre-modern is -119 to -122 ‰. Therefore, fully modern groundwater likely has δ^2H greater than -119 ‰, whereas pre-modern groundwater likely has δ^2H less than -122 ‰. Using δ^2H greater than -119 ‰ as an indicator of fully modern is consistent with the only long-term measurements of water stable isotopes in precipitation from the Harney Basin, which had a long-term, volumetrically weighted mean δ^2H value of -115 ‰ (Friedman and others, 2002). The deduced ranges of δ^2H in modern and pre-modern groundwater also are

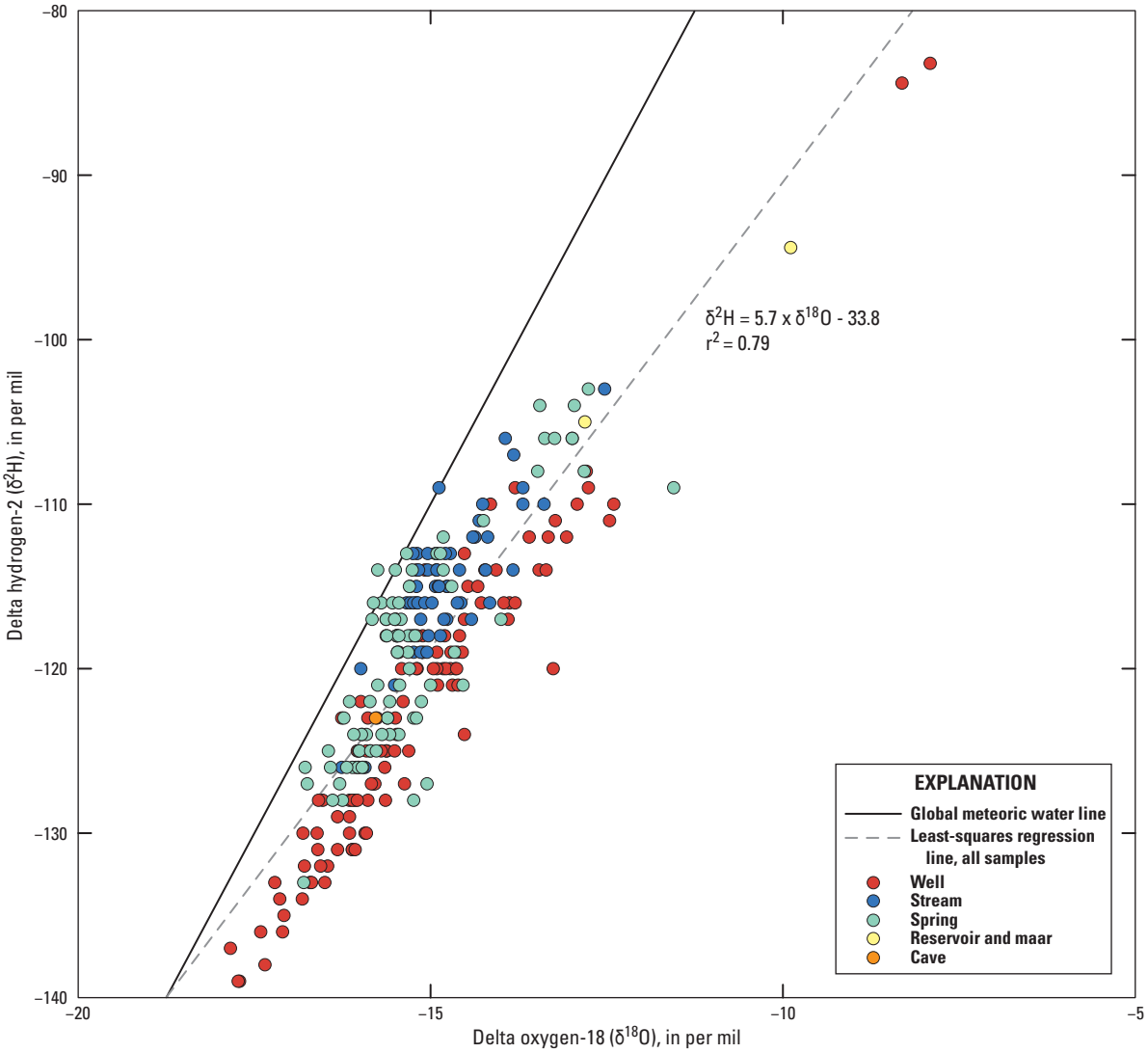

Figure 28. Stable isotopic composition of water sampled in and near the Harney Basin, southeastern Oregon, 2016–19.

consistent with samples where the minimum fraction of pre-modern groundwater is between 0.0 and 1.0 (fig. 29): most tritiated samples fall in the area bounded by the upper and lower ranges of the two groups (dashed blue lines in figure), and the δ^2H value of the sample generally decreases as the minimum fraction of pre-modern water increases.

The analysis of the relation among ^{14}C, ^{3}H, and δ^2H supports the use of δ^2H as a semiquantitative age indicator in the Harney Basin study area. Its use requires the recognition and acknowledgment that many groundwater samples in the study area are mixtures of modern and pre-modern water as demonstrated by samples having detectable ^{3}H and yet have ^{14}C ages that are many thousands of years old (fig. 27). The relation between the minimum fraction of pre-modern groundwater and δ^2H (fig. 29) provides further evidence that mixtures of old and young water are common.

The use of δ^2H as a semiquantitative age tracer can be generalized and simplified as follows: (a) δ^2H greater than -119 ‰ is a good indicator that most of the groundwater in the sample is modern (recharged after 1953) with larger values (up to about -105 ‰) generally corresponding to a larger fraction of modern groundwater in the sample; (b) δ^2H less than -122 ‰ is a good indicator that most of the groundwater in the sample is pre-modern (recharged prior to 1953) with more negative values generally corresponding to a larger fraction of pre-modern groundwater in the sample. A simplified terminology will be adopted for the remainder of the report for discussion purposes: samples having δ^2H greater than -119 ‰ will be referred to as "predominately modern," and samples having δ^2H less than -122 ‰ will be referred to as "predominantly pre-modern."

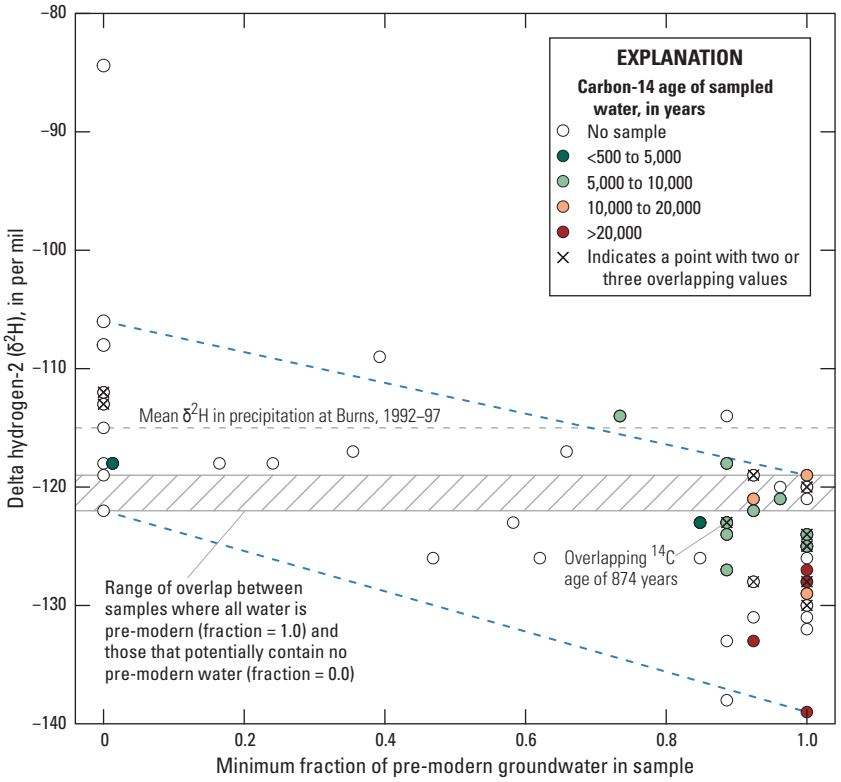

Figure 29. Relation between delta hydrogen-2 [δ^2H] and the minimum fraction of pre-modern groundwater in a sample (as determined by its tritium concentration), Harney Basin, southeastern Oregon. Dashed blue lines represent upper and lower range of δ^2H in mixtures of fully pre-modern groundwater (fraction = 1.0) and potentially fully modern groundwater (fraction = 0.0) based on measured values. <, less than; >, greater than.

Tracer Relations Within Groups of Sites: Streams, Springs, and Wells

Streams

The δ^2H values of most stream samples fall within the range of predominantly modern groundwater described above and provide additional confidence for use of δ^2H as a semiquantitative age surrogate in the Harney Basin (fig. 30; table 4). Seven stream samples plot in the range where predominantly modern and predominantly pre-modern groundwater overlap (-122 ‰ ≤ δ^2H ≤ -119 ‰ [≤, less than or equal to]). The three samples that plot in the range of predominantly pre-modern groundwater were sampled during summer baseflow conditions and are from streams supplied by upland springs having an isotopic composition similar to or less than the stream composition. The geochemical evidence from springs associated with these three streams indicates substantial amounts of pre-modern water supply these systems and is discussed in more detail below.

Most of the water in Thousand Springs Creek (434032119062700; δ^2H = -123 ‰; plate 1) originates from a complex of springs about 2 mi upstream of the sampling location. Two spring orifices in the complex (21.00S/30.00E-33DDC-S and 21.00S/30.00E-34CCA-S [plate 1]) were sampled for stable isotopes and had δ^2H values of -126 ‰ and -125 ‰, respectively. Tritium was collected from 21.00S/30.00E-33DDC-S and had a concentration of 1.0 TU, indicating a minimum pre-modern water fraction of about 0.6 (fig. 25). The slightly higher δ^2H value at the stream sampling location (relative to the spring complex samples) indicates evaporation or mixing with water having a substantially higher δ^2H occurred between the spring complex and stream-sampling location. Curry Gordon Creek (USGS site 434032119062600; δ^2H = -126 ‰; plate 1) drains the region immediately to the east of Thousand Springs Creek and had a δ^2H value similar to water issuing from the spring complex that sustains Thousand Springs Creek. Although the spring complex feeding Curry Gordon Creek could not be accessed for this study, spring water from the complex is likely the dominant source of water to Curry Gordon Creek and is largely responsible for the measured δ^2H value in the stream. Similar to Thousand Springs Creek, numerous springs have been mapped in the headwaters of Curry Gordon Creek and aerial imagery of the spring-discharge areas shows large meadows with active springbrooks during the summer. The aerial imagery also indicates that the watershed transitions to a drier juniper-sage dominated landscape downstream of the

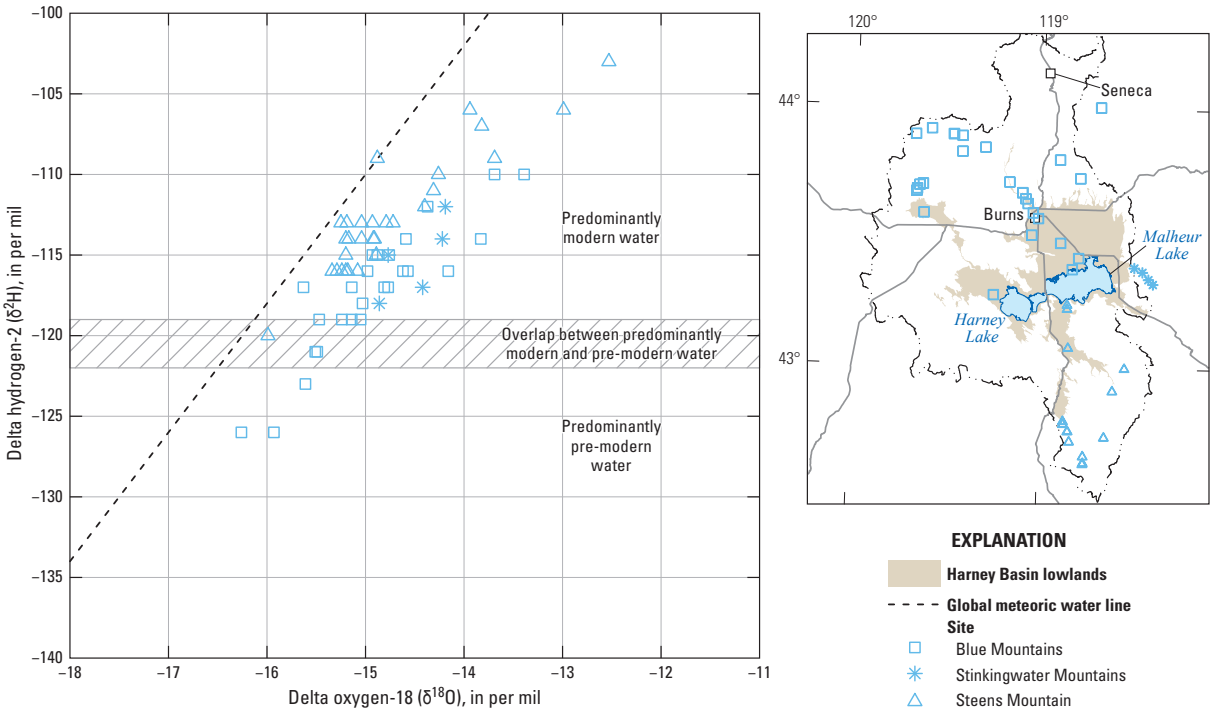

Figure 30. Stable isotopes of water in stream water samples from within and adjacent to the Harney Basin, southeastern Oregon. Plot symbols designate groups of sites sharing the same primary upland water source based on surface-water catchments; sites that could not be confidently assigned to an upland water source were placed in the group named "central basin/southwest uplands." The axis scales were reduced relative to figure 28 to improve detail.

Table 4. Number of stable isotope samples by site type and range of delta hydrogen-2 [δ^2H] values, Harney Basin, southeastern Oregon.

[Site types having fewer than five samples are not shown in table. ‰, per mil]

	Greater than -119 ‰ (predominantly modern)	-119 ‰ to -122 ‰	Less than -122 ‰ (predominantly pre-modern)
Streams	50	7	3
Springs	41	12	29
Wells	33	22	58

headwater spring complex. The USGS 1:24,000 scale topographic map of the area (Poison Creek quadrangle) indicates Curry Gordon Creek is perennial up to the headwater spring complex and shows only one small tributary between the spring complex and the sampling location. The third stream plotting in the fully pre-modern area on figure 29, Wolf Creek (440034118415200; δ^2H = -126 ‰; plate 1), drains the Blue Mountains just east of the Harney Basin. Like the other two streams just discussed, numerous headwater springs and spring complexes are mapped within the Wolf Creek watershed and the USGS 1:24,000 scale topographic maps (Magpie Table quadrangle and Jump-Off Joe Mountain quadrangle) show perennial streams up to the headwater springs. Spring-related vegetation could not be assessed with aerial imagery owing to the dense forest cover in the watershed. One spring in the Wolf Creek headwater area (Calo Spring [plate 1]) was sampled for stable isotopes, ^3H, and ^{14}C. The tracer values from Calo Spring all were consistent with predominantly old pre-modern water: δ^2H = -127 ‰, ^3H = 0.3 TU, and a ^{14}C age of 6,689 yrs; the trace amount of ^3H detected in the sample indicates a small amount of modern water reaches the spring. The discharge of old groundwater from Calo Spring and others in the upper Wolf Creek watershed likely are responsible for the highly negative δ^2H observed in the stream sample from Wolf Creek.

Springs

Unlike streams, the stable isotope values of spring samples span nearly the entire range of non-highly evaporated values (δ^2H <-100 ‰) observed in samples collected for this study (fig. 31; table 4). All springs in the Steens Mountain group plot within the range of predominantly modern groundwater or in the overlap range between predominantly modern and predominantly pre-modern groundwater. In contrast, springs in the Blue Mountain group generally plot in the predominantly pre-modern or in the modern/pre-modern overlap area of figure 31; only 8 out of 38 samples plot in the range where groundwater is predominantly modern. In the Blue Mountain group of springs, no systematic difference was observed between springs in the uplands (11 samples; 8 unique sites; median δ^2H = -123 ‰) and those in the Harney Basin lowlands (27 samples; 18 unique sites; median δ^2H = -123 ‰). The contrast between springs in the Steens Mountain group and the Blue Mountain group likely reflects differences in the underlying geology of the two areas, with a large proportion of modern water in the Steens Mountain group of springs likely associated with higher permeability geologic units. Similar to the Blue Mountain group, springs in the Stinkingwater Mountain group spanned a large range of stable isotope values, ranging from predominantly modern to predominantly pre-modern (fig. 31). Springs in the central basin/southwest uplands group all plotted in the predominantly pre-modern region, which likely reflects the large distance between these springs and major sources of recharge in the Harney Basin.

Wells

Stable isotope values from wells had the largest range of any group of samples (figs. 28, 32). The large range was driven by two highly evaporated samples from shallow wells adjacent to surface-water features and reflect seepage from those evaporative bodies. Well HARN0000006 (104 ft deep) is drilled less than 200 ft downgradient from the shore of Delintment Lake (plate 1). When drilled, HARN0000006 had a static groundwater level 32 ft below land surface, which was at the same elevation (5,544 ft) as the lake at its maximum depth. Well HARN0051086 (60 ft deep) is about 3,000 ft northwest of The Narrows (plate 1), which separates Malheur Lake from Mud Lake. The head gradient of the groundwater table in this region is from Malheur Lake toward the northwest (plate 2).

Excluding the two highly evaporated samples, the range of stable isotope values from wells was similar to that observed in spring samples (figs. 28, 32). In contrast to the samples from springs, however, more than half of the samples from wells had δ^2H less than -122 ‰, indicating that samples from wells generally contained a larger fraction of old water than samples from springs (table 4). Only 29 percent of the well samples contained predominantly modern groundwater (δ^2H >-119 ‰). As observed with the spring samples, wells in the Steens Mountain area generally plot in the predominantly modern or in the overlapping modern-pre-modern area of figure 32; only two samples from the Steens Mountain area contained predominantly pre-modern water. Wells in the Blue Mountain area are relatively uniformly distributed across the range of non-highly evaporated δ^2H values, while most wells in the Stinkingwater Mountains and the central basin/southwest uplands areas plot in the predominantly pre-modern part of figure 32. Additional discussion of regional patterns in well geochemistry will be addressed in the next section of the report (“Description of Harney Basin Groundwater-Flow System”).

Generally, δ^2H decreased with increasing well depth (fig. 33), indicating that groundwater age tends to increase with depth across the Harney Basin. The relation was stronger among wells in the Harney Basin lowlands than among wells in the uplands. Among lowland wells that plot in the area of predominantly modern groundwater in figure 33 (n=17), most samples (76 percent) are from wells less than 100 ft deep, and only one sample is from a well deeper than 200 ft. In contrast, among lowland wells that plot in the area of predominantly pre-modern groundwater in figure 33 (n=32), most samples are from wells deeper than 100 ft (78 percent), and many are from wells deeper than 200 ft (44 percent). Although the regression through the data from the upland wells is considerably poorer, the same general distribution is observed among upland wells. Among upland wells that plot in the area of predominantly modern groundwater in figure 33 (n=7), only two (29 percent) were deeper than 200 ft. In contrast, among upland wells that plot in the area of predominantly pre-modern groundwater in figure 33 (n=15), 11 (73 percent) were deeper than 200 ft. The considerable regional variability encompassed in figure 33 is explored and discussed in more detail in the section titled “Description of Harney Basin Groundwater-Flow System.”

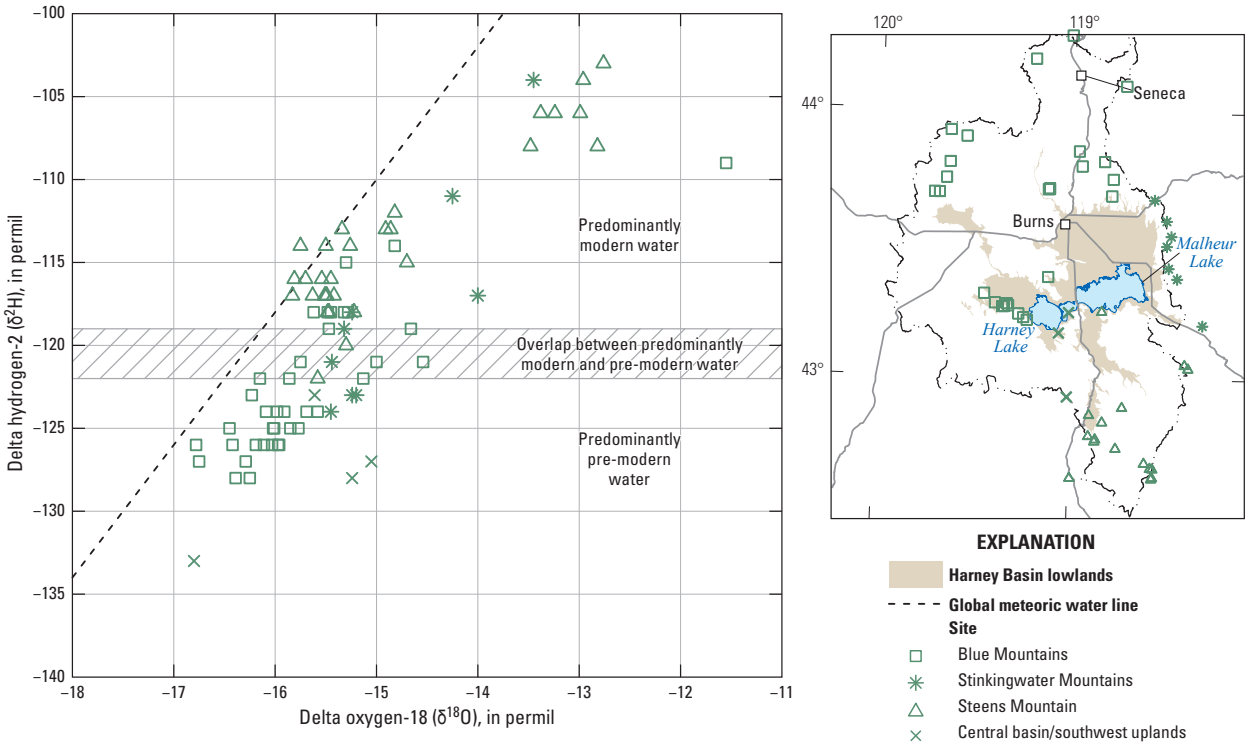

Figure 31. Stable isotopes of water in spring samples from within and adjacent to the Harney Basin, southeastern Oregon. Plot symbols designate groups of sites sharing the same primary upland water source based on surface-water catchments; sites that could not be confidently assigned to an upland water source were placed in the group named "central basin/southwest uplands." The axis scales were reduced relative to figure 28 to improve detail.

Greater topographic variability in the uplands obscures the relation between δ^2H and well depth. For example, two upland wells with depths greater than 300 ft plot in the predominantly modern water area of figure 33, but after adjusting for topography, they both plot closer to the main body of data in the figure. Near Frenchglen, HARN0001655 (325 ft deep; uncased hole from 22 ft) is located on a peninsula of upland material situated about 80 ft higher than the surrounding lowlands; however, the groundwater level at the time it was drilled (87 ft below land surface) was only about 7 ft below the elevation of the adjacent lowlands. Well HARN0001650 (100 ft deep; uncased from 98 ft) is located in the lowlands approximately 1.5 mi north of HARN0001655 and had a similar groundwater level at the time it was drilled (8 ft below land surface); additionally, the elevation of the midpoint of the saturated open interval of the two wells is nearly identical: 4,105 ft in HARN0001655 and 4,099 ft in HARN0001650. After adjusting the plotting position of HARN0001655 upward by 80 ft (its height above the lowlands) in figure 33, it would plot much closer to other wells. Similarly, HARN0001548 (578 ft deep) is drilled close to the top of a butte rising nearly 300 ft above the surrounding lowlands about 9 mi northeast of Diamond Craters. This well had a groundwater level 403 ft below land surface in March 2018–about 100 ft below the elevation of the surrounding lowlands. It too plots much closer to other wells after adjusting the plotting position for the approximately 300 ft of topographic relief.

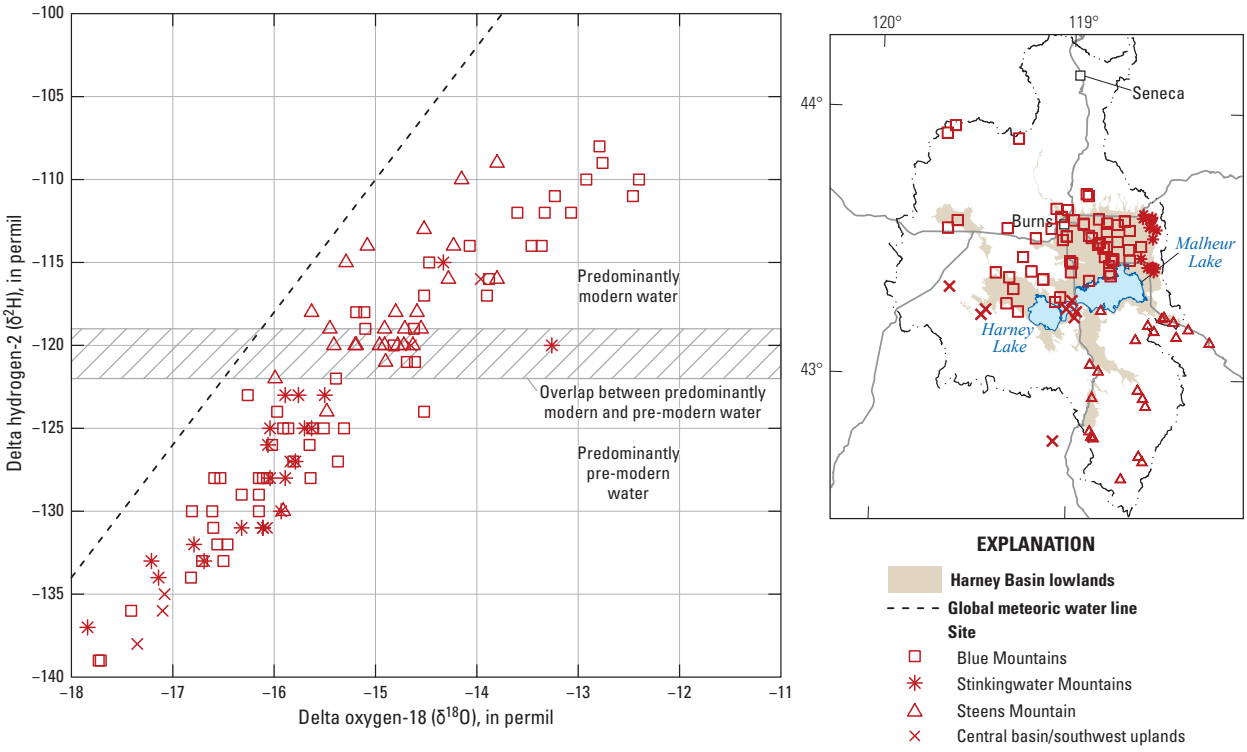

Figure 32. Stable isotopes of water in well-water samples from within and adjacent to the Harney Basin, southeastern Oregon. Plot symbols designate groups of sites sharing the same primary upland water source based on surface-water catchments; sites that could not be confidently assigned to an upland water source were placed in the group named "central basin/southwest uplands." The axis scales were reduced relative to figure 28 to improve detail. The two highly evaporated samples shown on figure 28 (delta hydrogen-2 [δ^2H] values greater than -100 per mil [‰]) were omitted to improve detail.

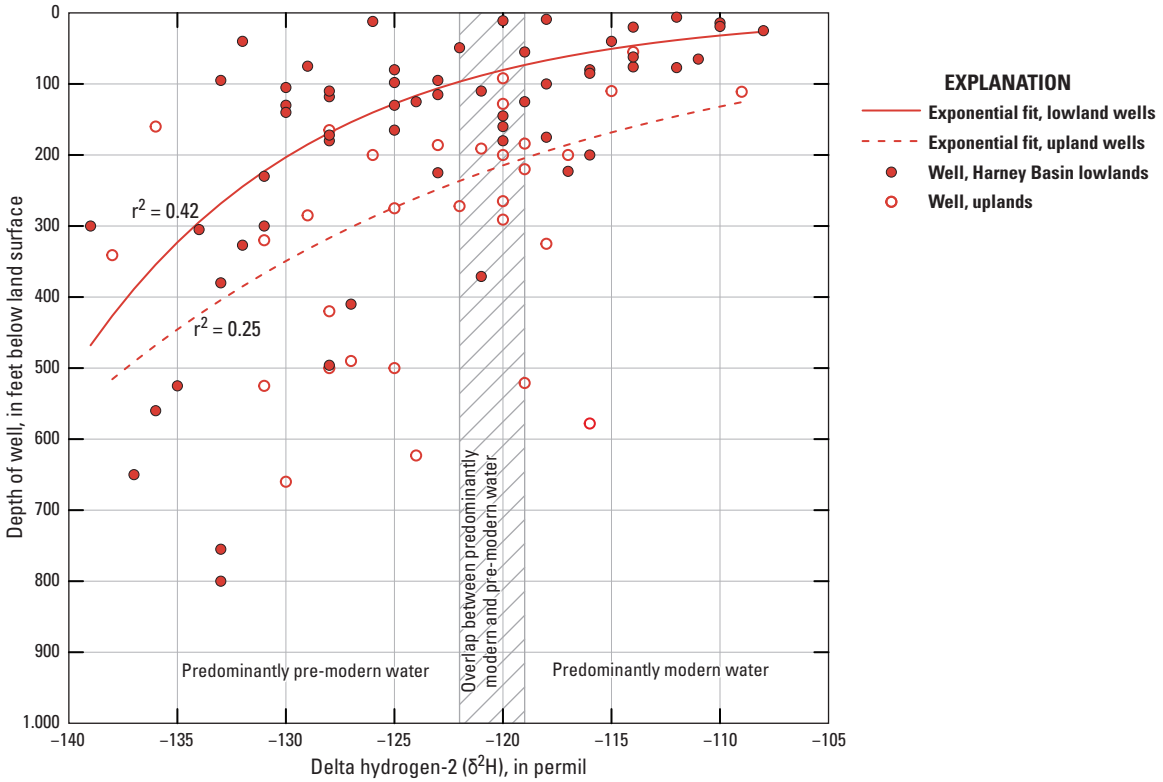

Figure 33. Relation between delta hydrogen-2 [δ^2H] and well depth in well-water samples from within and adjacent to the Harney Basin, southeastern Oregon. The two highly evaporated samples shown on figure 28 (δ^2H values greater than -100 per mil [‰]) were omitted to improve detail.

Description of the Harney Basin Groundwater-Flow System

Groundwater in the Harney Basin occurs within a single groundwater-flow system that includes several distinct yet hydraulically connected areas of interest distinguished by local hydrostratigraphy, location in the basin-wide groundwater-flow system, and local rate and magnitude of recharge and discharge. In this section, the hydrogeology of selected areas of the Harney Basin is described in greater detail to illustrate how their distinguishing factors influence groundwater flow.

Low-Permeability Uplands

Upland areas underlain by hydrostratigraphic units with generally low permeability comprise about 60 percent of the Harney Basin. The water table in the uplands is typically within 100 ft of ground surface due to relatively high precipitation and low permeability, which inhibits rapid movement of groundwater through the rocks and sediments. The most widespread hydrostratigraphic units underlying the uplands are the Marine sedimentary rocks HU, the Upland volcanic rocks HU, the Older basin fill HU, and the Silicic lava flows and domes HU. In these generally low-permeability units, most recharge from infiltrating snowmelt and rainfall flows along subsurface pathways that are relatively shallow and short and discharges to the surface as springs and base flow of gaining streams. The abundance of upland springs (more than 2,500 springs listed in the National Hydrography Dataset) and gaining streams, and the pervasive low permeability of upland rocks, is typical of a topographically controlled groundwater-flow system (Tóth, 1963). About 83 percent of recharge to the uplands discharges to upland springs and streams. The streamflow generated in the uplands from precipitation runoff, spring flow, and stream base flow is an important source of recharge where it flows onto the Younger and Older basin fill HUs in the lowlands at the base of the mountain front.

An estimated 17 percent of the upland recharge moves through the groundwater-flow system in the upland mountain block and directly recharges the basin fill beneath the lowlands. Movement of groundwater through the upland mountain block is slow and takes thousands of years to reach the lowland basin fill due to the low permeability of the upland geologic deposits. Evidence for the slow movement of groundwater through these rocks is provided by ^{14}C ages from six upland wells across the Harney Basin which ranged from about 1,000 to about 45,000 yrs (median = about 8,900 yrs; Gingerich and others, 2022). Two of these wells were tritium dead and ^3H was detected at less than 1 TU in the other four wells. Eleven additional upland wells with ^3H analyses had a

median value of 1.8 TU; none were tritium dead (Gingerich and others, 2022). Four of the 11 wells had ^{3}H greater than 3 TU, indicating most of the water in those samples was modern; the depth of these wells ranged from 50 to 184 ft. In contrast, 5 of the 11 wells had ^{3}H less than 1 TU, indicating most of the water in those samples was pre-modern; the depth of these five wells ranged from 165 to 420 ft. Lastly, 22 additional wells had only stable isotope samples (Gingerich and others, 2022). Among these, 10 had values of $\delta^{2}H$ that indicate the water was predominantly pre-modern ($\delta^{2}H$ <-122 ‰), 8 had values of $\delta^{2}H$ that were in the overlapping range of predominantly pre-modern and predominantly modern water (-122 ‰ ≤ $\delta^{2}H$ ≥ -119 ‰), and 4 had values of $\delta^{2}H$ that indicated the water was predominantly modern ($\delta^{2}H$ greater than [>] -119 ‰). The median depth of these three groups of wells was 410, 243, and 89 ft, respectively. Collectively, the geochemical data support the concept of a topographically controlled groundwater-flow system in the upland areas of the Harney Basin. The uplands can generally be characterized as having a shallow (less than 150 ft deep), active, predominantly modern groundwater flow with limited and slow movement of groundwater at increasing depths within the rocks and sediment of the mountain block.

Wells in the uplands are sparse, so groundwater-flow directions are inferred mostly from spring elevations and stream-valley topography. The water table generally is a subdued expression of topography—the water table is at or near the ground surface at springs and in stream valleys and deeper below the ground surface upslope from these features (plate 2; fig. 34). In the few available wells in the uplands, depths to groundwater are several tens to a few hundred feet below the ground surface depending on the depth of the well (fig. 34) In upland recharge areas, the vertical groundwater gradient is generally downward; groundwater levels in deeper wells are lower than in shallower wells.

Groundwater levels in the low-permeability uplands typically are highest in springtime after winter precipitation and springtime snowmelt have provided recharge to and increased head in the groundwater-flow system. They go down throughout the rest of the year. Wells in the uplands may be productive locally, but overall, low permeability leads to localized seasonal groundwater-level declines when pumped. Pumping shallow upland wells captures groundwater that would have discharged locally to nearby springs, provided base flow to streams, or recharged the deep upland groundwater system. In contrast, pumping deeper upland wells captures groundwater that otherwise would have traveled through the mountain block and discharged to larger upland streams farther downgradient or directly to the lowland basin fill at the base of the mountain front.

Donner und Blitzen River Floodplain

The relatively narrow floodplain of the Donner und Blitzen River extends more than 30 mi from the community of Frenchglen, at the base of Steens Mountain, to Voltage, at the southern edge of Malheur Lake. Less than 5 mi at its widest point, the floodplain is constrained by high ridges to the west and by gently sloping uplands to the east. Most of the floodplain lies within the boundaries of the Malheur NWR. South of approximately Diamond Lane (latitude 43.045 degrees north), and including the Diamond Valley, the floodplain is underlain by deposits of the Younger basin fill HU, Older basin fill HU, and Upland volcanic rocks HU. Diamond Valley is the floodplain for Kiger, Cucamonga, and McCoy Creeks, and merges with the Donner und Blitzen River floodplain southwest of Diamond Craters (plate 1). North of approximately Diamond Lane, the Voltage basalt HU and Proximal vent deposits HU are overlain by the Younger basin fill HU, and the entire sequence is underlain by the Older basin fill HU (fig. 35). Along a 3-mi reach of the Donner und Blitzen River between Krumbo Creek and Diamond Lane, the Donner und Blitzen River floodplain is less than 0.25 mi wide. The interaction between the uplands, the river, and the underlying groundwater-flow system differ north and south of this constriction.

South of Diamond Lane, the head gradient between the uplands and low-lying areas causes groundwater to move toward the river valley and northward toward Malheur Lake (plate 2). Upland groundwater diffusely discharges into the basin fill underlying the Donner und Blitzen River floodplain and discharges through numerous small and large springs surrounding the floodplain; discharge from these springs augments flow in the Donner und Blitzen River. Geochemical data indicate that recently recharged groundwater circulates to a depth of at least 100 ft below the Donner und Blitzen River floodplain south of Diamond Lane (fig. 36) – HARN0001650 (100 ft deep; ^{3}H = 2.0 TU; $\delta^{2}H$ = -118 ‰). The depth to which predominantly modern groundwater circulates in the floodplain sediments is not known owing to a lack of data from deep wells, although the $\delta^{2}H$ value from HARN0052440 (125 ft deep; $\delta^{2}H$ = -124 ‰) is in the range of predominantly pre-modern groundwater and indicates circulation may not be much greater than 100 ft. Several relatively large-volume springs surround the southern floodplain and discharge predominately modern groundwater, including Page Springs (^{3}H = 2.6 TU; ^{14}C age <500 yrs), Knox Spring (^{3}H = 2.7 TU), and Krumbo Springs (^{3}H = 3.6 TU). These springs demonstrate the presence of young groundwater in the uplands near the floodplain and provide evidence that the young groundwater underlying the floodplain originates as infiltration from the surrounding uplands rather than infiltration from the Donner und Blitzen River. The relatively constant flow in the river along this reach precludes substantial losses from the river to the groundwater-flow system.

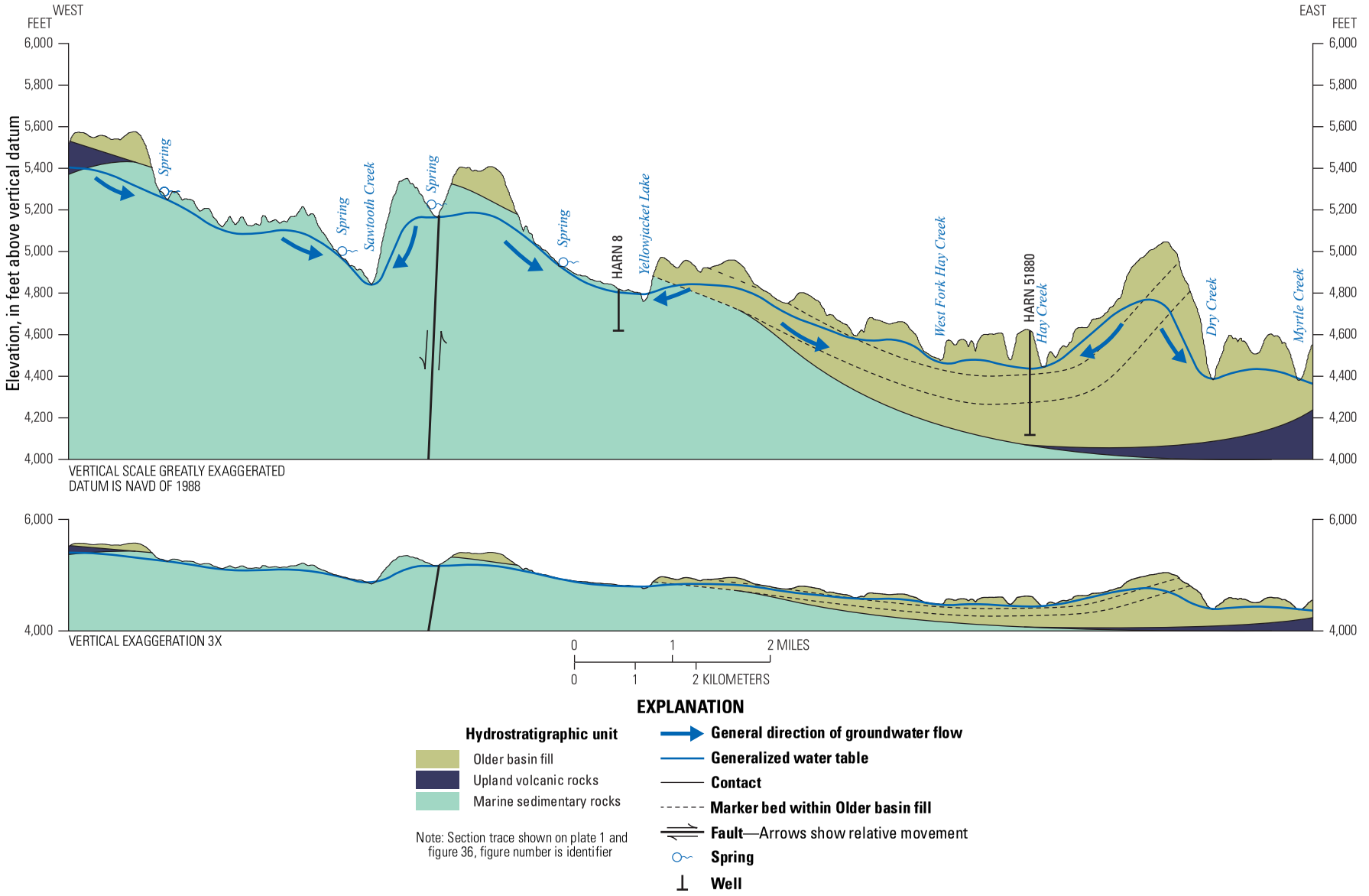

Figure 34. Schematic hydrogeologic cross section of the low-permeability uplands in the Blue Mountains, Harney Basin, southeastern Oregon. Section trace is shown on plate 1.

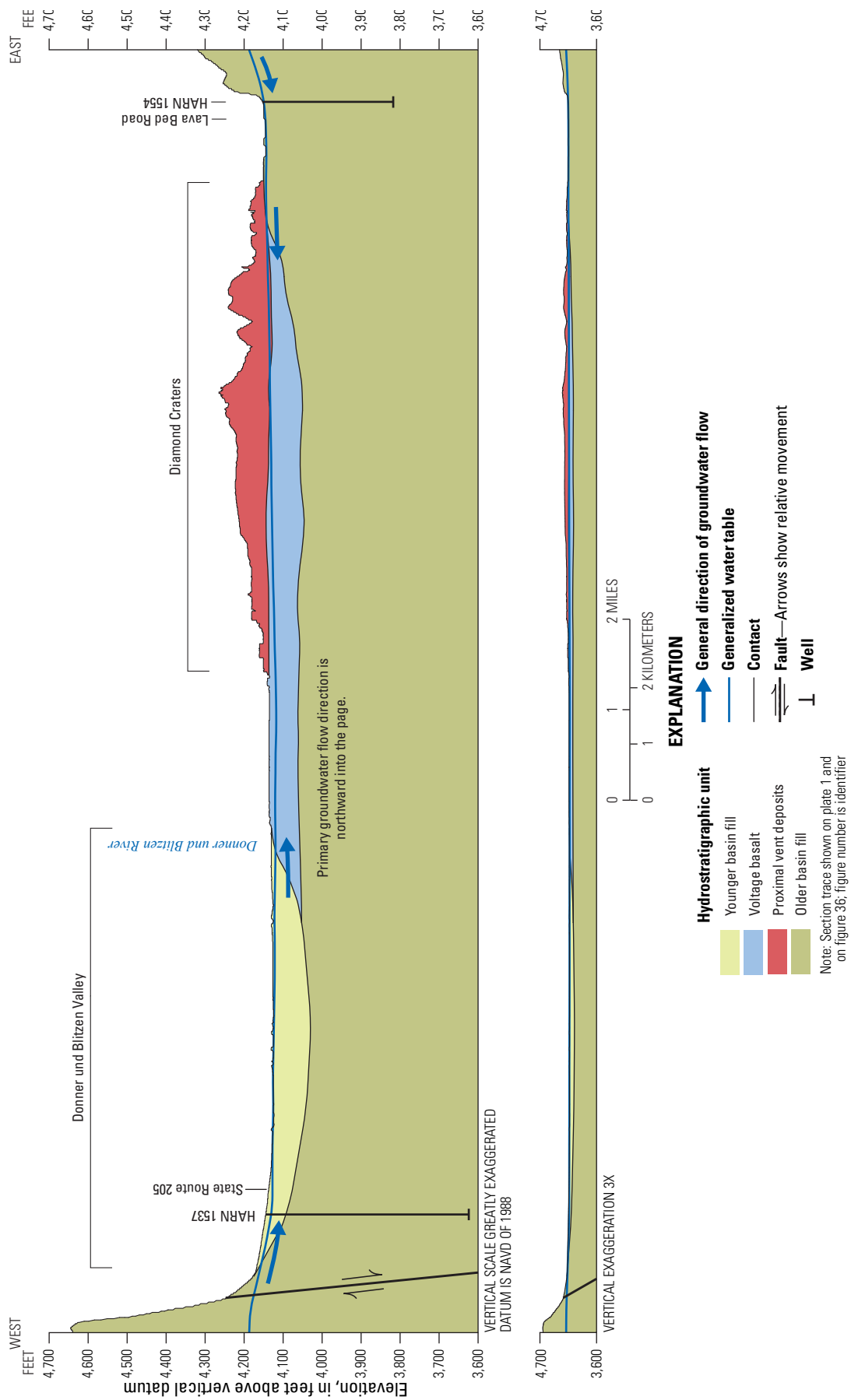

Figure 35. Schematic hydrogeologic cross section of the northern Donner und Blitzen River floodplain, Harney Basin, southeastern Oregon. Section trace is shown on figure 36.

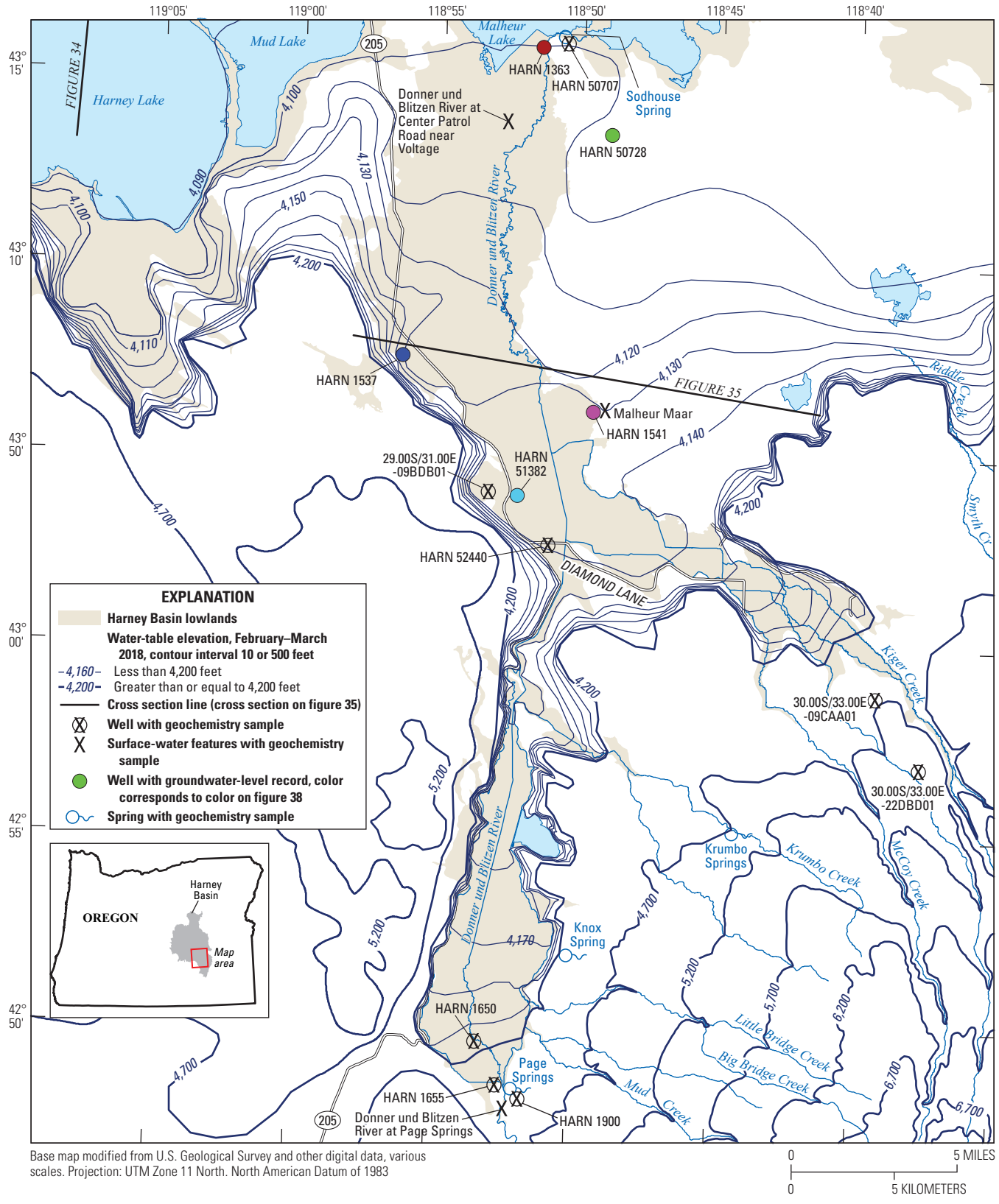

Figure 36. Location of selected groundwater-level and geochemistry sites, Donner und Blitzen River floodplain, Harney Basin, southeastern Oregon.

In contrast to the southern floodplain, north of Diamond Lane the groundwater-level data indicate that the Donner und Blitzen River recharges the Younger basin fill HU underlying the floodplain via seepage loss through the streambed. Additional recharge to the Younger basin fill HU likely occurs in the flooded wetlands of the Malheur NWR to the east and west of the river. The connection between the river and underlying groundwater-flow system is evident in the relation among stable isotope samples collected from sites in the Donner und Blitzen River floodplain (fig. 37). Samples from the Donner und Blitzen River at Page Springs (424808118520100; blue squares) plot closer to the GMWL, whereas samples from the river at Center Patrol Road (431407118512501; blue asterisks) lie along an evaporation line with a slope of 4.7. Although some evaporation likely occurs along the main stem of the river, the evaporative signal in the river water at Center Patrol Road primarily results from the diversion of river water and its distribution across the wetlands of the Malheur NWR, which is subsequently returned to the river. The two most evaporated samples from the river at Center Patrol Road were collected in July 2017 and July 2018. Samples from three groundwater sites in the northern floodplain fall along the same evaporative line: Sodhouse Spring (10401600; green crosses), Malheur Maar (430615118490100; yellow diamond), and HARN0050707 (111 ft deep; dark red circle). All these groundwater samples plot between the most and least evaporated of the river samples collected at Center Patrol Road. The stable isotopic composition of groundwater samples from the northern floodplain contrast with those from nearby wells outside the floodplain (light red circles); no plausible mechanism exists to evolve the isotopic composition of the non-floodplain groundwater samples to a composition observed in samples from the northern floodplain groundwater samples. Collectively, the groundwater-level and geochemical data indicate that groundwater in the northern Donner und Blitzen River floodplain is recharged by the infiltration of water from the Donner und Blitzen River, within the mainstem channel and in the surrounding, seasonally flooded wetlands of the Malheur NWR.

The losing reach in the river begins west of Diamond Craters, about where the 4,130-ft water-table contour crosses the river and continues downstream to Malheur Lake (plate 2). West of the Donner und Blitzen River, groundwater flows northward toward Malheur Lake; 2 mi west of the river, westward movement of groundwater is limited by relatively high uplands that are underlain by the relatively low-permeability Older basin fill HU (figs. 7–8). East of the river, groundwater flows northeastward toward Malheur Lake, moving through the high-permeability Voltage basalt HU and the Proximal vent deposits HU associated with the geologically young Diamond Craters volcanic field (figs. 7–8). Transmissivity estimates indicate that deposits underlying the floodplain assigned to the Younger and Older basin fill HUs are much less permeable than the young lavas and vent deposits comprising the Voltage basalt HU and Proximal vent deposits HU to the east of the floodplain (figs. 7–8).

In much of the Donner und Blitzen River floodplain, groundwater levels in shallow wells are less than 10 ft below the ground surface. Compared with other areas of the Harney Basin, relatively few wells are in the floodplain, and most are shallow, low-production stock wells; few long-term groundwater-level records exist. During 2015–19, wells east of the floodplain (for example, HARN0050728 in fig. 38), nearer to areas with more deep irrigation wells, have declined 3–6 ft. Seasonal fluctuations are about 2–5 ft/yr, and the limited records indicate annual trends in late winter groundwater levels might correspond to nearby pumpage and to fluctuations in the water level of Malheur Lake (fig. 38).

Silver Creek Floodplain: Suntex to Harney Lake

The Silver Creek floodplain begins where Silver Creek exits the uplands near Dry Mountain, about 10 mi northwest of Riley, and extends southeastward to Harney Lake (plate 1). A broad plateau south of Highway 20 separates the upper floodplain from the lower floodplain. Moon Reservoir occupies a canyon cut through this plateau by Silver Creek. In the upper Silver Creek floodplain, relatively low-permeability surficial sedimentary deposits (Younger basin fill HU) overlie a higher-permeability lithologic sequence (High Lava Plains basalt HU, Dry Mountain lavas HU, and more-permeable sections of Older basin fill HU) penetrated by many of the wells in the area (fig. 39). Well reports indicate that wells near the head of the floodplain penetrate the higher-permeability sequence about 200–300 ft below ground surface, but farther downstream, near Highway 20, the higher-permeability rocks are penetrated as shallow as 50 ft below the surface. The high-permeability sequence is at least 300-ft thick in the deepest wells; however, no wells appear to penetrate through the sequence, so the maximum thickness is unknown. The primary permeability of the high-permeability zone likely is enhanced by faulting along the Brothers fault zone (figs. 5 and 40), which parallels the course of the Silver Creek floodplain from Dry Mountain down to Harney Lake. Deposits of the Younger basin fill HU underlying the lower Silver Creek floodplain differ from those in the Younger basin fill HU underlying the upper floodplain. Wells penetrating Younger basin fill HU deposits under the upper floodplain contain a higher proportion of coarse sands and gravels, whereas Younger basin fill HU deposits underlying the lower Silver Creek floodplain are dominated by fine-grained materials, such as fine sand and silt with an increasing abundance of lacustrine clays near to Harney Lake. Lithologic descriptions in well reports from the lower Silver Creek floodplain more closely resemble those found on many well reports from the central Harney Basin lowlands north of Malheur Lake. Well reports from the eastern portion of the lower floodplain describe cinders and basalt, which are related to deposits associated with the Proximal vent deposits and High Lava Plains basalt HUs exposed on Freeman Butte (fig. 40; plate 1). In the central and western portions of the lower floodplain, thin layers of sand and gravel,

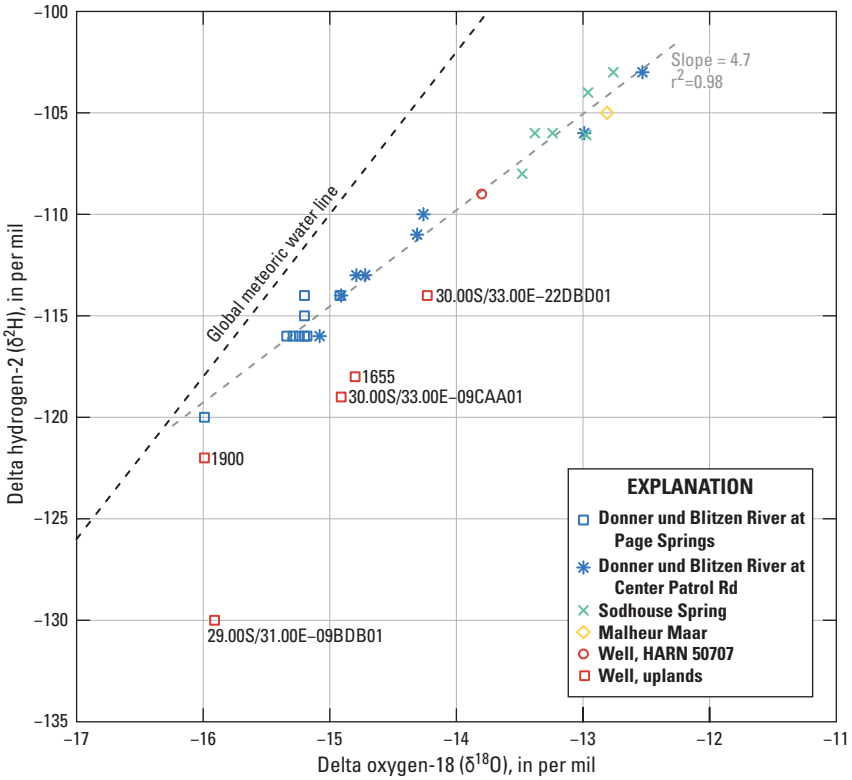

Figure 37. Stable isotopic composition of selected sites from the Donner und Blitzen River floodplain and surrounding uplands, Harney Basin, southeastern Oregon.

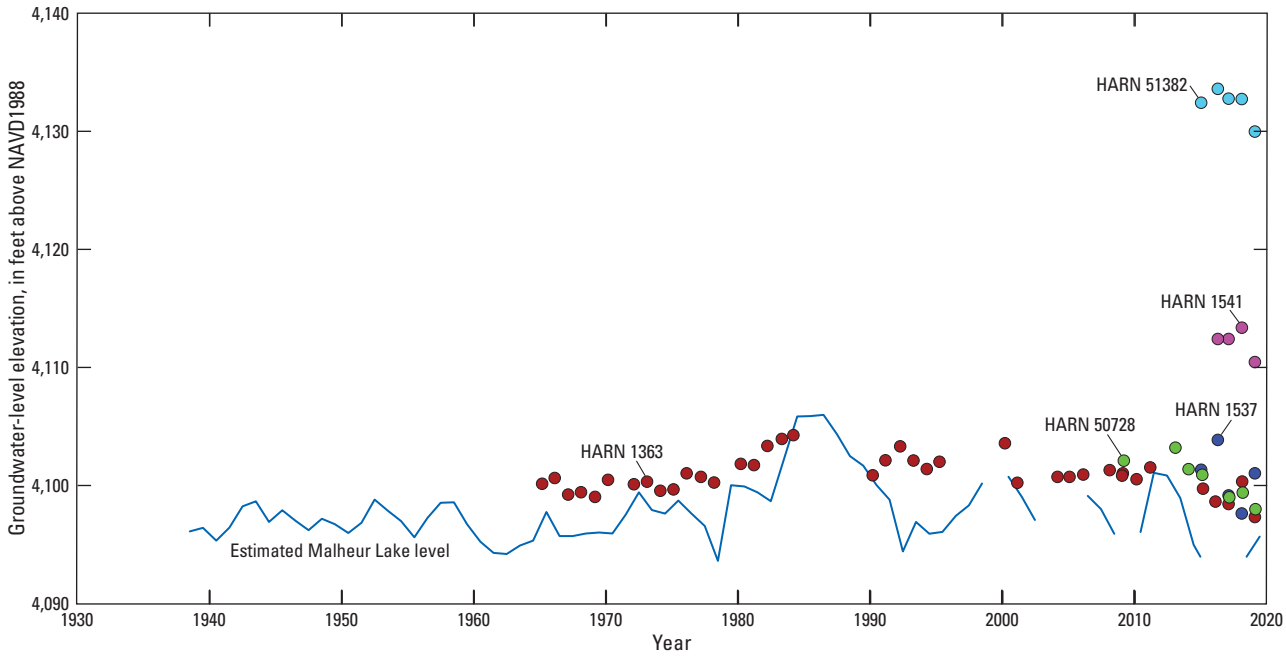

Figure 38. Groundwater levels during January–April at selected wells in the Donner und Blitzen River floodplain, Harney Basin, southeastern Oregon. Estimated Malheur Lake level from U.S Fish and Wildlife Service unpublished data. Colored dots correspond to well locations shown on figure 36.

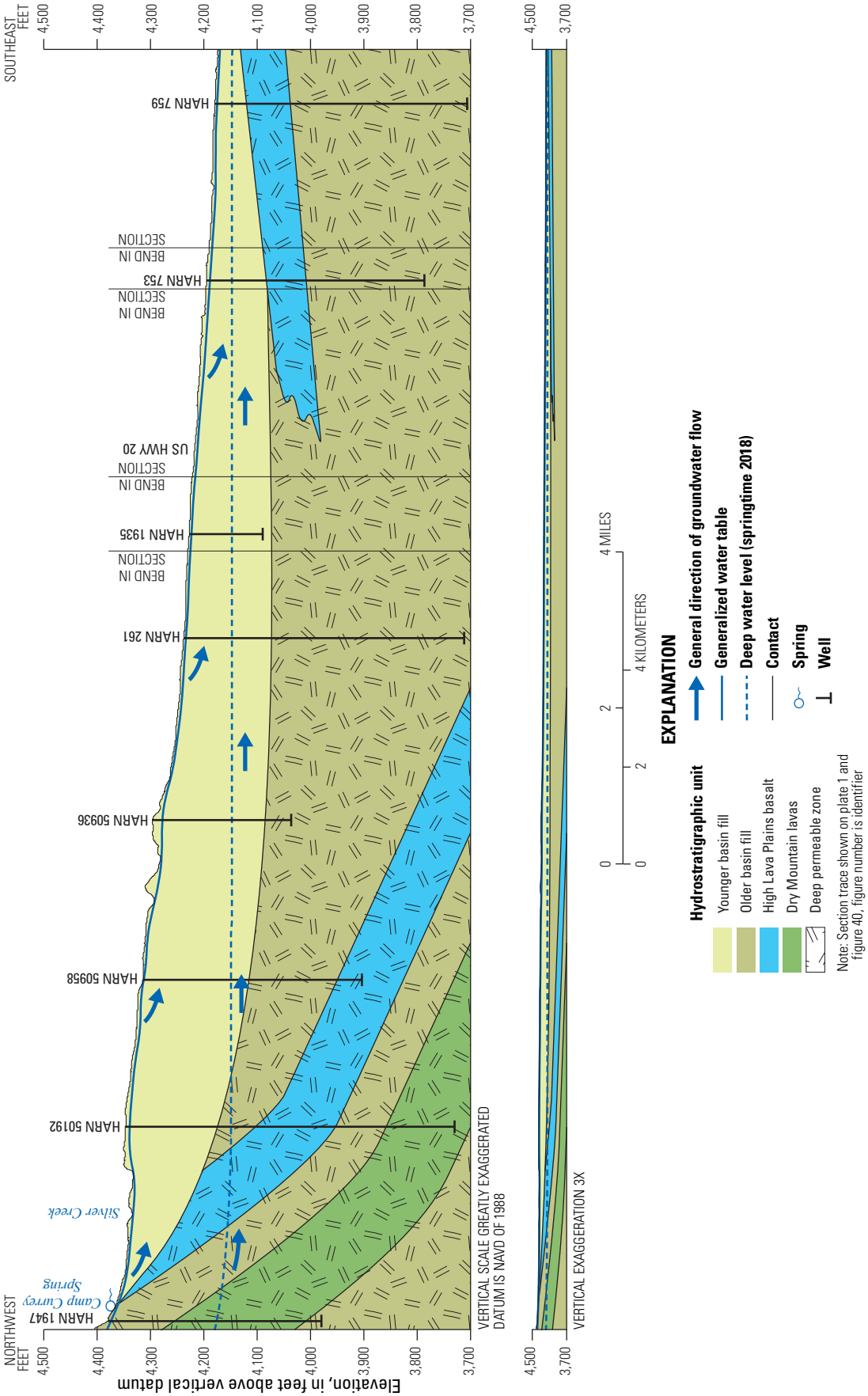

Figure 39. Schematic hydrogeologic cross section of upper Silver Creek floodplain, Harney Basin, southeastern Oregon. Section trace shown is on figure 40.

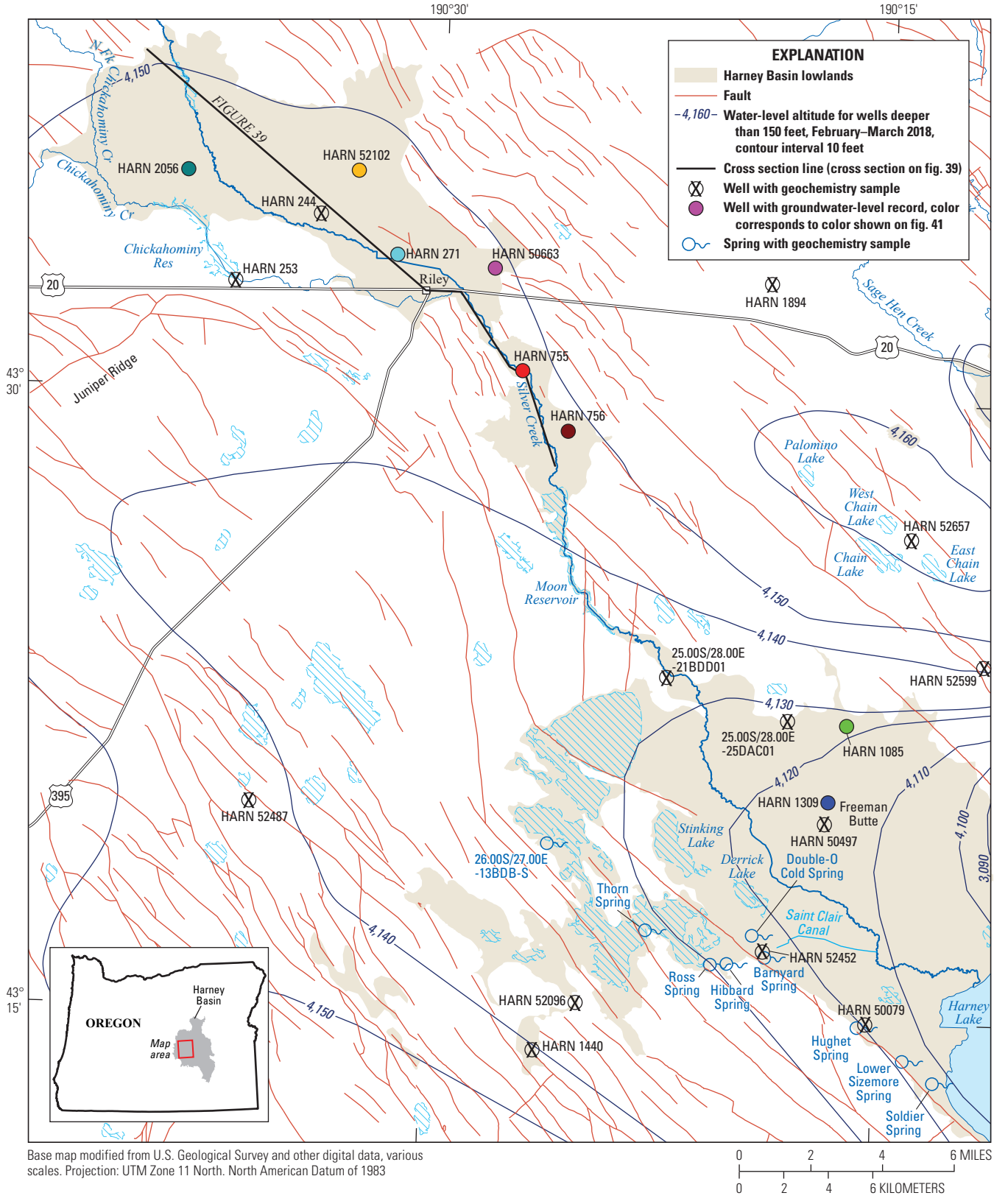

Figure 40. Location of selected groundwater-level and geochemistry sites, Silver Creek floodplain area, Harney Basin, southeastern Oregon.

likely deposited by Silver Creek, are interbedded with fine-grained material. Excluding some wells near Freeman Butte, well yields noted in well reports from the lower Silver Creek floodplain tend to be lower than those noted in the upper Silver Creek floodplain. The plateau separating the upper and lower floodplains is capped with a veneer of High Lava Plains basalt HU underlain by tuffaceous sediments and rock associated with the Older basin fill HU; exposures of these materials can be seen in the canyon walls of Moon Reservoir and at Cote Grade 3.1 mi east of Moon Reservoir where Double O Road drops from the plateau onto the lower floodplain (plate 1).

Recharge to the rocks beneath the Silver Creek floodplain comes from infiltration of water from springtime freshet flooding, seepage from Silver Creek, deep infiltration of irrigation water in the upper and lower Silver Silver Creek floodplain, and infiltration from the low-permeability uplands to the north and west (Garcia and others, 2022; plates 2–3). Infiltration of surface water in the upper Silver Creek floodplain is substantial. Excluding the springtime freshet period, in most years Silver Creek streamflow (August mean monthly flow at Silver Creek below Nicholl Creek near Riley, OR, is 1.9 ft^3/s; Garcia and others, 2022, table 9) fully infiltrates upstream of Highway 20, and the streambed is dry the remaining distance to Moon Reservoir. The presence of tritium in shallow groundwater along the length of the Silver Creek floodplain attests to the importance of surface-water infiltration as a source of recharge. In the upper floodplain, tritiated water was identified in a sample from a 110-ft well about 3 mi northwest of Riley (4.2 TU; HARN0000244; fig. 40) and in a sample from a 200-ft well downgradient from Chickahominy Reservoir (1.7 TU; HARN0000253; fig. 40). In the lower floodplain, tritiated water was detected in a sample from a well (depth unknown) approximately 2.5 mi downgradient from Moon Reservoir (1.6 TU; 25.00S/28.00E-21BDD01; fig. 40). The δ^2H values for the two tritiated wells in the upper floodplain are in the range of predominantly modern groundwater (HARN0000244: -118 ‰; HARN0000253: -117 ‰). The deuterium excess in HARN0000244 (+2.9 ‰) indicates that the water has experienced little evaporation, whereas the deuterium excess in HARN0000253 (-0.8 ‰) indicates it has undergone modest evaporation and likely reflects infiltration of surface water stored in Chickahominy Reservoir. Among five wells in the lower floodplain, four have evidence of moderate to substantial evaporation in their values of deuterium excess (-0.8 ‰ to -7.4 ‰). The most evaporated samples were from two wells closest to Moon Reservoir–25.00S/28.00E-21BDD01 (depth unknown; deuterium excess = -6.9 ‰) and 25.00S/28.00E-25DAC01 (depth unknown; deuterium excess = -7.4 ‰)–and likely reflect recharge of irrigation water that was previously stored in the reservoir.

Two wells adjacent to springs in the Warm Springs Valley area of the lower floodplain were sampled. Well HARN0052452 (depth unknown) is adjacent to Barnyard Spring, and the SC, temperature, and stable isotope values of the spring and the well are nearly identical, indicating that they share a similar source of recharge. A similar correspondence in chemistry was observed between HARN0050079 (55 ft deep) and Hughet Spring. Relative to samples from the two wells near Moon Reservoir, samples from the wells near Barnyard Spring and Hughet Spring are considerably less evaporated and have SC values one-half to one-third of those near Moon Reservoir. This result points to at least two recharge mechanisms to wells in the lower floodplain–infiltration of surface water from applied irrigation water that was stored in Moon Reservoir and a source associated with the line of springs emerging along the fault-bounded Warm Springs Valley; the hydrology of springs in Warm Springs Valley is explored in more detail below. A third recharge mechanism in the lower Silver Creek floodplain is indicated by the sample from HARN0050497 (140 ft deep), drilled about 11 mi southeast of Moon Reservoir. The δ^2H value from this well is considerably more negative (-130 ‰) than the other four wells in the lower floodplain (-109 ‰ to -125 ‰) and consistent with predominantly pre-modern water (fig. 29). The elevated SC (738 microsiemens per centimeter [µS/cm]) and deuterium excess (-0.8 ‰) in the sample from well HARN0050497 indicated a modest amount of evaporation occurred prior to recharge and may reflect the natural ponding, evaporation, and infiltration of freshet water that was the primary recharge mechanism to much of the lower floodplain for the millennia prior to water development in the Harney Basin. This recharge process is discussed fully in the "Silvies River and Poison Creek Floodplains" section, where more data are available with which to evaluate spatial patterns in groundwater chemistry.

In the most distal parts of the lower floodplain, groundwater discharge dominates as numerous springs emerge around the margins of Harney Lake and along a fault scarp bounding the southwestern edge of Warm Springs Valley (fig. 40). The groundwater travel time from the recharge area to two of the major springs in the lower floodplain is around 8,500 yrs based on the ^{14}C age from Hibbard Spring (8,453 yrs) and from spring 26.00S/27.00E-13BDB-S (8,659 yrs). Considering the stability and volume of flow from these springs, the principal recharge area for these springs is most likely the upper Silver Creek floodplain. Based on the ^{14}C age and an estimated total direct line travel distance of 26–36 mi from the upper floodplain, the mean groundwater velocity is about 0.03–0.05 foot per day. Other springs in the northwestern part of the Warm Springs Valley likely share a similar recharge area and flow history. Ross, Double O Cold, and Barnyard Springs were not sampled for ^{14}C but had stable isotope values nearly identical to Hibbard Spring and 26.00S/27.00E-13BDB-S, and Double O Cold Springs was tritium dead. Thorn Spring also is in the northwestern part of the Warm Springs Valley (fig. 40) but has a considerably lower flow volume than the other springs that were visited, and the stable isotope values indicated its water had experienced substantial evaporation (deuterium excess = -16.6 ‰). Three springs were sampled in the southeastern part of Warm Springs Valley (Hughet, Lower Sizemore, and Soldier Springs; fig. 40) and had δ^2H values in the overlapping range of predominantly pre-modern and predominantly

modern water (-122 ‰ to -119 ‰); a trace amount of ^{3}H (0.2 TU) was detected at Lower Sizemore Spring, indicating that the water was predominantly premodern with a small amount of modern recharge. Most of the groundwater issuing from these southeastern springs likely is of the same origin and age as those in the northwestern part of Warm Springs Valley with the addition of a small amount of local, more recent recharge from the lower Silver Creek floodplain.

Groundwater levels in shallow wells completed in the Younger basin fill HU indicate that the water table is no more than a few tens of feet below ground surface in the upper Silver Creek floodplain and generally within 10 ft of land surface in the lower Silver Creek floodplain (plate 2). Groundwater levels measured during drilling of wells that penetrate through the Younger basin fill HU beneath the upper Silver Creek floodplain and a well with cascading groundwater (HARN0052473; plate 1) show that the hydraulic head in these deposits decreases with depth, indicating that groundwater is flowing downward through the alluvial sediments of the Younger basin fill HU, providing further evidence of recharge in this area.

Most wells in the upper Silver Creek floodplain that penetrate through the Younger basin fill HU into the underlying High Lava Plains basalt and permeable Older basin fill HUs encounter a uniform groundwater-level elevation of about 4,150 ft (fig. 39; plate 3). The abundance of wells encountering near uniform groundwater-level conditions indicates that the permeability of these units is relatively high over an area possibly as much as 150 mi^2. Groundwater levels in these high-permeability rocks fluctuate only about 3–4 ft annually (for example, HARN0052102; fig. 20) in response to local groundwater pumpage. Although limited in number, transmissivity estimates from wells completed in the High Lava Plains basalt HU are among the largest in the Harney Basin (fig. 8). The transmissivity of the Older Basin Fill HU encountered here is also likely high. Groundwater levels typically are highest at the end of April after winter precipitation and springtime snowmelt has provided recharge. After the onset of pumpage for irrigation, groundwater levels decline until late August or September when irrigation usually stops. Groundwater levels recover during autumn and winter until the next irrigation cycle begins. The long-term record of late winter groundwater levels in these deeper units shows that groundwater levels were relatively steady during 1960–90 but were declining about 0.5 ft/yr during 2015–19 (fig. 41). Overall, groundwater levels have declined less than 10 ft since 1980. No record of long-term groundwater levels is available for the shallow Younger basin fill HU along the upper Silver Creek floodplain.

Deep groundwater beneath the upper Silver Creek floodplain flows to the south and east toward a broad trough beginning near western Juniper Ridge and stretching downgradient toward Warm Springs Valley and Harney Lake (fig. 40; plate 3). This flow direction is likely enhanced by the fabric of NW-SE trending faults of the Brothers fault zone, which may increase permeability in that direction. Continued groundwater withdrawal and development in the upper Silver Creek floodplain ultimately will reduce groundwater discharge to the lower floodplain, including springs of

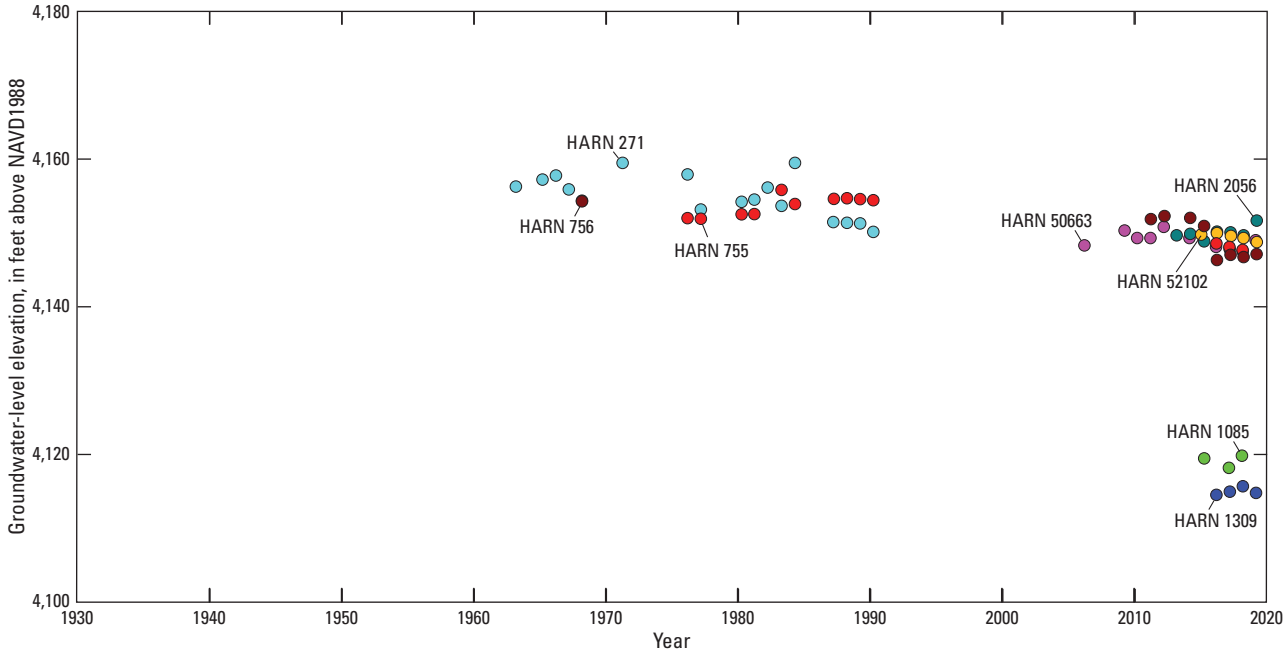

Figure 41. Groundwater levels during January–April at selected wells in the Silver Creek Valley, Harney Basin, southeastern Oregon, 1930–2020. Colored dots correspond to well locations shown on figure 40. NAVD1988, North American Vertical Datum 1988.

the Warm Springs Valley. Groundwater levels at two wells in the lower Silver Creek floodplain near Freeman Butte (HARN0001085 and HARN0001309; fig. 40) were stable; however, no groundwater-level data for these wells are available prior to 2014. Long-term groundwater-level data are not available from any wells in the lower Silver Creek floodplain, so groundwater-level trends cannot be evaluated. Likewise, no measurable decrease in flow from springs in the Warm Springs Valley was observed between the early 20th century (Piper and others, 1939) and the period of this study; however, long-term records of flow on which to robustly calculate trends also are lacking.

Weaver Spring/Dog Mountain

Dog Mountain and the NW-SE trending ridge south of Weaver Spring are composed of highly permeable material assigned to the Proximal vent deposits HU and comprise a 140-mi^2, locally productive part of the Harney Basin groundwater-flow system as much as 500 ft thick. Irrigation wells drilled into these rocks are generally high yielding. The productive Proximal vent deposits HU in this area is surrounded by deposits having much lower permeability. To the east and south, the area is bounded by deposits of the Younger basin fill HU overlying deposits of the Older basin fill HU, while to the north and west the area is bounded by deposits of the Older basin fill HU that are capped with a veneer of the High Lava Plains basalt HU (fig. 9). Weaver Spring discharges southward-flowing groundwater emanating from the low-permeability Older basin fill HU underlying the plateau north of the area (fig. 42).

Three decades of intensive groundwater withdrawal in this area has removed groundwater from storage and led to a widespread area of declining groundwater levels (plates 2–3). Because the surrounding hydrostratigraphic units have much lower permeability, they cannot supply groundwater at a sufficient rate to replace groundwater extracted from the high-permeability deposits. The subsurface extent of the Proximal vent deposits HU is greater than the surface expression shown on the surficial geologic map (fig. 9). Well reports and specific-capacity tests indicate that these deposits likely extend several miles beyond the mapped boundary and lie beneath the Younger basin fill HU to the east and south. The mapped extent of the area with large groundwater-level declines coincides with the inferred subsurface extent of the Proximal vent deposits HU (plates 2–3).

Prior to the beginning of extensive groundwater development in this area in the 1990s, the water table in the Weaver Spring/Dog Mountain area was about 15–40 ft below the ground surface, depending on local topography, and had remained relatively steady since about 1960 when groundwater-level data collection in this area began (figs. 43–44). During 1993–2012, late winter groundwater levels declined about 2 ft/yr (HARN0001990 in figs. 43–44); however, since 2016, late winter groundwater levels declined as much as 8 ft/yr (HARN0001094 in figs. 43–44). Large declines in water levels due to groundwater withdrawal have been documented across the Weaver Spring/Dog Mountain area, and the water table has been lowered to more than 140 ft below ground in some places (plate 2). Because the heads in this unit have been lowered even more than in the overlying units (plate 3), wells that penetrate to depths greater than about 300 ft likely penetrate a deeper, semiconfined, higher-permeability, higher-yield layer of the Proximal vent deposits HU. Heads in this deeper unit have been lowered below 4,000-ft elevation, the lowest values measured anywhere in the basin apart from the east end of Virginia Valley where groundwater exits the basin. Prior to groundwater development, the natural direction of groundwater flow through this area was from the northern plateau southward toward Harney Lake and Mud Lake; the bed of Harney Lake (about 4,085-ft elevation) was the lowest discharge area in this part of the basin (Piper and others, 1939). The hydraulic head in the Weaver Spring/Dog Mountain area of decline is now nearly 90 ft lower (3,993-ft elevation at HARN0052630 in September 2019) than the bed of Harney Lake. Groundwater-level maps (fig. 42; plates 2–3) indicate that the large depression in groundwater hydraulic head and steep groundwater gradients are likely inducing groundwater flow from all directions including from Malheur, Mud, and Harney Lake toward the central area of the depression.

Groundwater levels in the Weaver Spring/Dog Mountain area typically are highest at the end of April and sharply decline with the onset of pumping for irrigation. Shallow and deep groundwater levels fluctuate only about 15 ft annually (HARN0052631in fig. 17*D*) in response to groundwater pumping (additional evidence that the productive unit has a relatively high permeability). Groundwater levels go down until irrigation stops and the onset of phreatophyte senescence in late summer to mid-autumn and slowly rise through autumn and winter until the next irrigation cycle begins (HARN0052630 in fig. 17*D*). However, groundwater levels do not recover to the same elevation as the previous winter. Year-to-year declines are largest near the center of the cone of depression and smaller on the periphery.

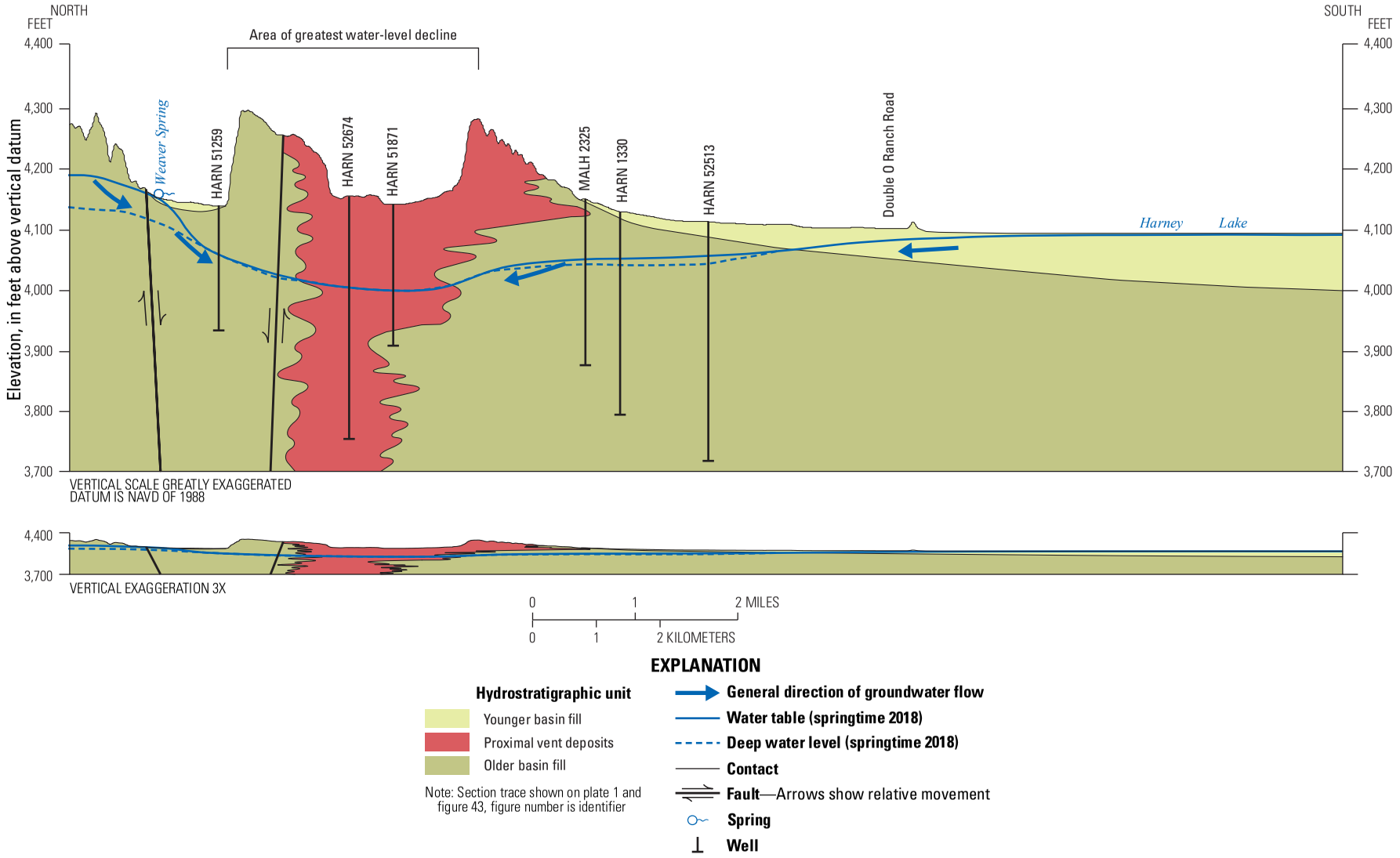

Figure 42. Schematic hydrogeologic cross section of the Weaver Spring Area, Harney Basin, southeastern Oregon. Section trace shown on figure 43.

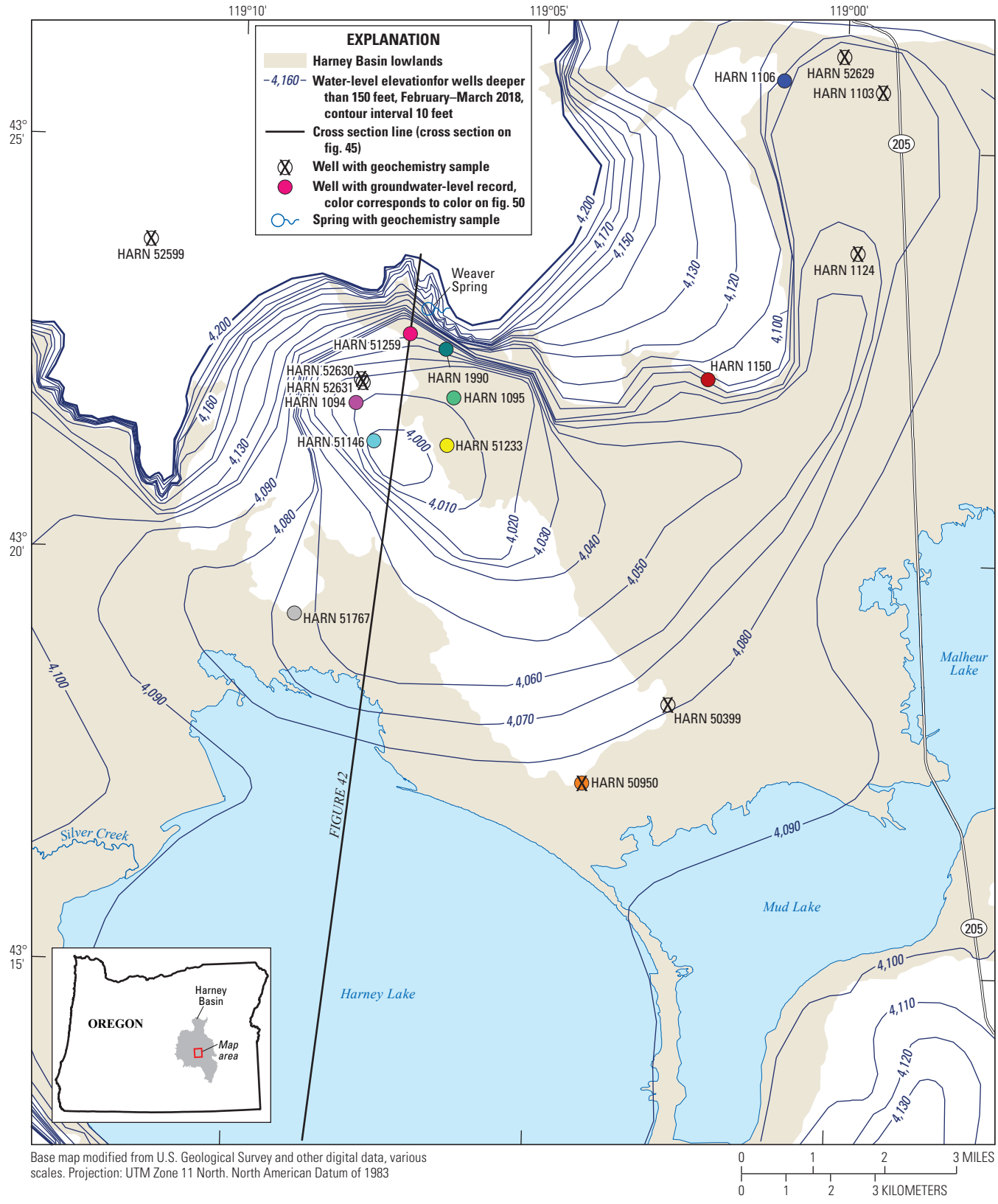

Figure 43. Locations of selected groundwater-level and geochemistry sites, Weaver Spring/Dog Mountain area, Harney Basin, southeastern Oregon.

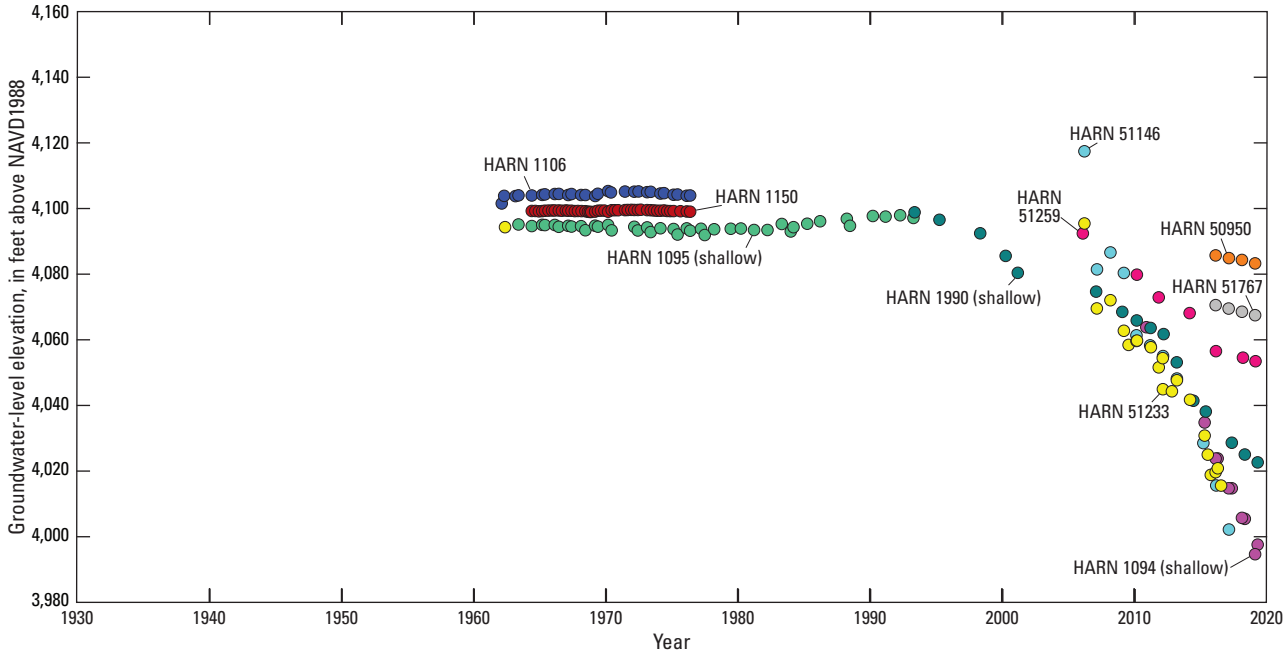

Figure 44. Groundwater levels during January–April at selected wells in the Weaver Spring/Dog Mountain area, Harney Basin, southeastern Oregon. Colored dots correspond to well locations shown on figure 43.

Recharge to this heavily stressed area of the Harney Basin is limited owing to its distance from the primary sources of precipitation in the Blue Mountains and Steens Mountain and due to it being surrounded by low-permeability deposits. The widespread distribution of pre-modern water across the Weaver Spring/Dog Mountain area reflects this combination of distance and geology. Water discharging from Weaver Spring (432258119065201) was tritium dead, as were two of the three ^{3}H samples from wells in the area (fig. 43)–HARN0052631 (490 ft deep) and HARN0050399 (110 ft deep). In the third well–HARN0052630 (190 ft deep)– ^{3}H was detected at the detection level of 0.1 TU. Two of these well samples also had ^{14}C analyses, which yielded ^{14}C ages of about 9,700 yrs (HARN0052630) and about 45,000 yrs (HARN0052631). At HARN0052631, the elevated $\delta^{13}C$ value provides evidence for the addition of dead carbon in the subsurface and the calculated ^{14}C age is too old; however, it likely exceeds 10,000 yrs (refer to fig. 27 and accompanying discussion in the "Tritium" section of the "Geochemical Evaluation of Recharge, Flowpaths, and Residence Time" section). The $\delta^{2}H$ values for Weaver Spring and the three well samples ranged from -121 to -128 ‰ and were consistent with a large portion of pre-modern water in these samples (fig. 29). Stable isotope samples were collected from five additional wells in this area: three wells had $\delta^{2}H$ values in the range of predominantly pre-modern water (HARN0052599, 500 ft deep, -125 ‰; HARN0052629, 105 ft deep, -130 ‰; HARN0001103, 40 ft deep, -132 ‰), one well (HARN0001124, 110 ft deep, -121 ‰) fell in the overlapping range of figure 29, and one well (HARN0050950, 65 ft deep, -111 ‰) had a $\delta^{2}H$ value in the range of predominantly modern water. The last well is about 1.5 mi from Harney Lake and Mud Lake; the stable isotopes indicate the sample is more evaporated than others from the Weaver Spring/Dog Mountain area and it likely is a mixture of local groundwater and lake water (which has $\delta^{2}H$ of -25 ‰ to -44 ‰; Rinella and Schuler, 1992) and corroborates the head gradients (plates 2–3), which show the capture of water from the lakes due to lowered groundwater levels in this area. The geochemical data demonstrate that very little young water recharges the Weaver Spring/Dog Mountain area and indicate that the groundwater-level recovery during autumn and winter is owing to movement of old groundwater from the plateau and surrounding low-permeability Younger and Older basin fill HUs rather than infiltration of local precipitation, which is meager (less than 9 in. annually; fig. 3).

Silvies River and Poison Creek Floodplains

In the Harney Basin lowlands, beneath the floodplains of Silvies River and Poison Creek (plate 1), groundwater flows in the Younger and Older basin fill HUs (fig. 45). Most of the Younger basin fill HU in this area consists of material deposited by coalescing alluvial fans along the course each stream follows as they enter the Harney Basin lowlands from the uplands. The permeability of these basin fill deposits varies greatly with location and depth. Coarser-grained, moderately permeable deposits (primarily sand and small gravel) grade distally into finer grained, less-permeable deposits (primarily silt and clay) along the main stream channel toward Malheur Lake as heavier, coarse-grained material drops from suspension near the mountain front owing to the decrease in river gradient (and loss of energy) with increasing distance from the Blue Mountains. Natural, seasonal overbank flooding and managed flood irrigation convey stream water laterally away from the main stream channels, and a similar loss of energy results in deposits that grade from coarser- to finer-grained sediment laterally away from the main stream channels. Over the course of hundreds or thousands of years, sediment aggradation and flood scouring have caused the primary channels of Silvies River and Poison Creek to migrate, which has created a complex, heterogenous distribution of coarse- and fine-grained deposits in the subsurface near the mountain front; deposits generally become more uniformly fine grained with increasing distance from the Blue Mountains.

The water budget and geochemical evidence indicate some groundwater flow from the low-permeability uplands in the north into the deposits underlying the Harney Basin lowlands (discussed above in the section "Low-permeability uplands"). However, most of the recharge to groundwater underlying the Silvies River/Poison Creek floodplain is from surface water infiltrating through the lowland sediments near the mountain front during the springtime freshet and subsequent irrigation season as indicated by the water budget (refer to "Hydrologic Budget" section and Garcia and others [2022]) and the geochemical data. The SC of groundwater samples collected from the Silvies River/Poison Creek floodplain generally decreases with depth (fig. 46). The relation differs between samples collected from wells in the upper floodplain (north of Hutchensen Lane; fig. 47) and lower floodplain (south of Hutchensen Lane), with samples from the lower floodplain generally being more saline. The strong correlation between SC and deuterium excess (a measure of evaporation; fig. 48) indicates that the increased SC values predominantly are due to evaporative concentration of natural dissolved minerals rather than dissolution and infiltration of surficial salts or agricultural chemicals. The high SC groundwater most likely is due to the infiltration of ponded freshet water that has been concentrated by evaporation over the weeks or months that it sits on the surface. Applied surface-water irrigation infiltrates much more rapidly and therefore experiences less evaporation demand prior to recharge. The higher SC in the lower floodplain wells is likely due to a combination of lower infiltration rates and greater evaporative concentration in areas underlain by low-permeability lacustrine sediments.

Despite the importance of surface-water infiltration to recharge in this area, the geochemical data indicate that the infiltration and circulation of modern recharge is limited and generally restricted to the upper 100 ft. The data also indicate that most of the groundwater underlying the Silvies River/Poison Creek floodplain is thousands of years old. This ancient groundwater was recharged during wetter climatic phases of the late Pleistocene and early Holocene and is moving through the groundwater-flow system very slowly. In the upper floodplain, six wells were sampled for tritium (fig. 47). Three were tritium dead–(HARN0051319 (300 ft deep), HARN0052748 (130 ft deep), HARN0050698 (75 ft deep)– and three had ^{3}H greater than 2.7 TU–HARN0000458 (49 ft deep), HARN0052749 (25 ft deep), 24.00S/31.00E-05CCC01 (6 ft deep). Based on the ^{3}H data, the shallowest indication of fully pre-modern water is 75 ft, and the deepest indication of predominantly modern water is 49 ft. Two ^{14}C samples were collected from wells in the upper floodplain – HARN0051319 and HARN0050698; both were tritium dead and had ^{14}C ages exceeding 13,000 yrs. In the lower floodplain, two wells near Lawen were sampled for ^{3}H – HARN0052234 (76 ft deep) and HARN0052235 (496 ft deep) and one for ^{14}C (HARN0052235). ^{3}H was detected in the shallow well at 0.3 TU, indicating that the water is predominantly pre-modern; the deeper well was tritium dead and had a ^{14}C age of more than 41,000 yrs. The ^{14}C age likely is biased old owing to the addition of ^{14}C-dead carbon in the subsurface ($\delta^{13}C$ = +6.79 ‰), but as previously discussed, is likely at least 10,000 yrs old (refer to fig. 27 and accompanying discussion). The stable isotope results from wells in the upper floodplain–the six noted above plus five additional wells without ^{3}H or ^{14}C–are consistent with the ^{3}H and ^{14}C results and indicate predominantly modern water is only found at depths less than 50 ft (fig. 49*A*); similarly, predominantly pre-modern water is found at depths as shallow as about 75 ft. Stable isotope samples from wells in the lower floodplain generally support the same conclusions; however, the results are muddied by the widespread evaporation of groundwater in the lower floodplain which has shifted the $\delta^{2}H$ values toward more positive values. When the lower floodplain $\delta^{2}H$ values were adjusted along an evaporative slope of 4.7 (the slope determined for sites in the Donner und Blitzen River floodplain; fig. 37) such that their deuterium excess was equal to +3.5 ‰ (the median of the three largest values of deuterium excess observed in wells having pre-modern water in the upper Silvies River/Poison Creek floodplain), the relation between $\delta^{2}H$ and depth was similar to wells in the upper floodplain (fig. 49*B*) and indicated that most of the groundwater below about 75 ft is predominantly pre-modern.

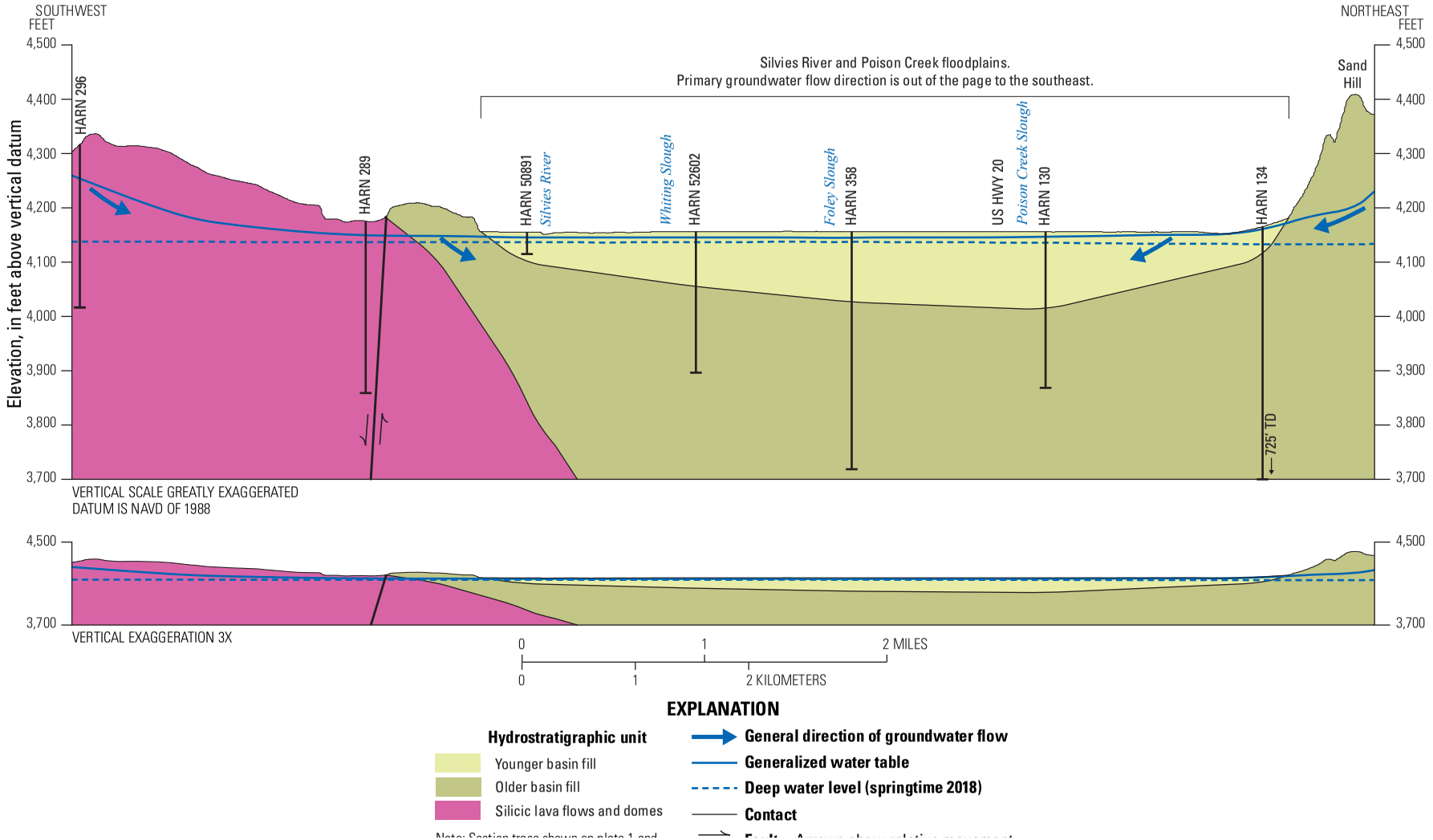

Figure 45. Schematic hydrogeologic cross section of the Silvies River/Poison Creek floodplain, Harney Basin, southeastern Oregon. Section trace shown on figure 47.

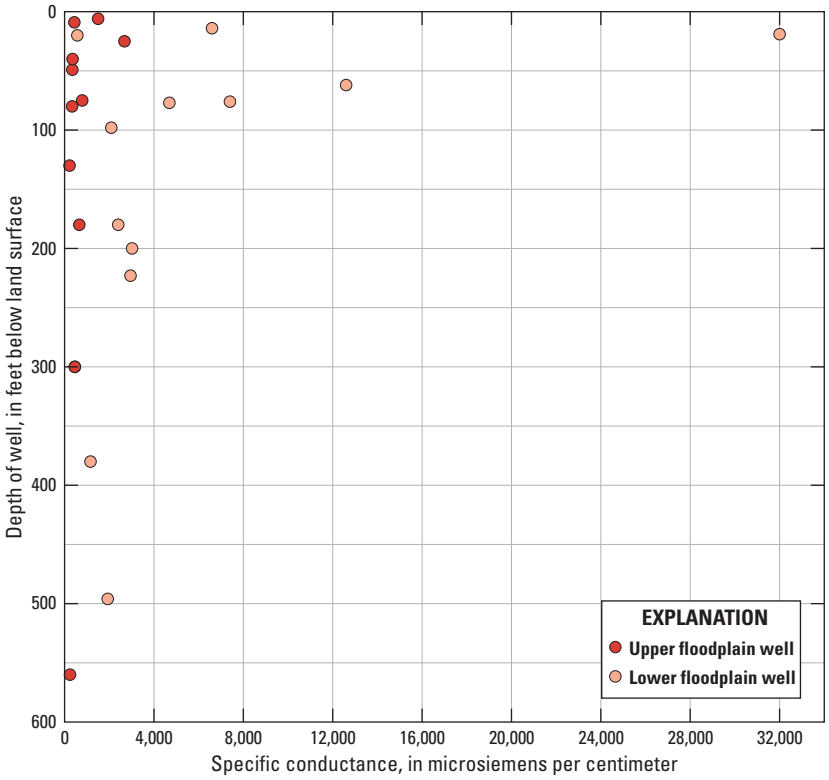

Figure 46. Relation between specific conductance and depth in wells in the Silvies River/Poison Creek floodplain between Burns and Malheur Lake, Harney Basin, southeastern Oregon.

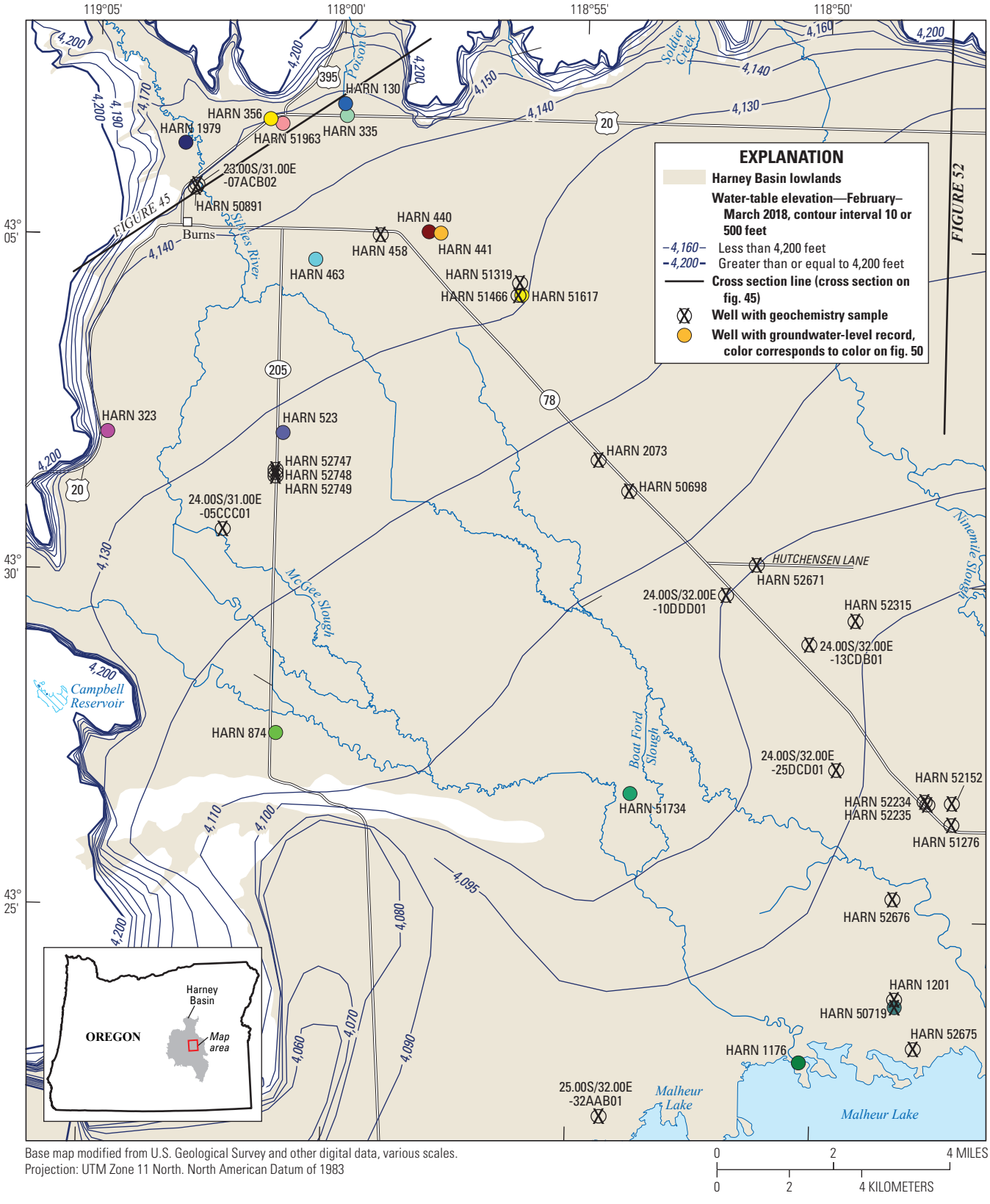

Figure 47. Location of selected groundwater-level and geochemistry sites, Silvies River/Poison Creek floodplain between Burns and Malheur Lake, Harney Basin, southeastern Oregon.

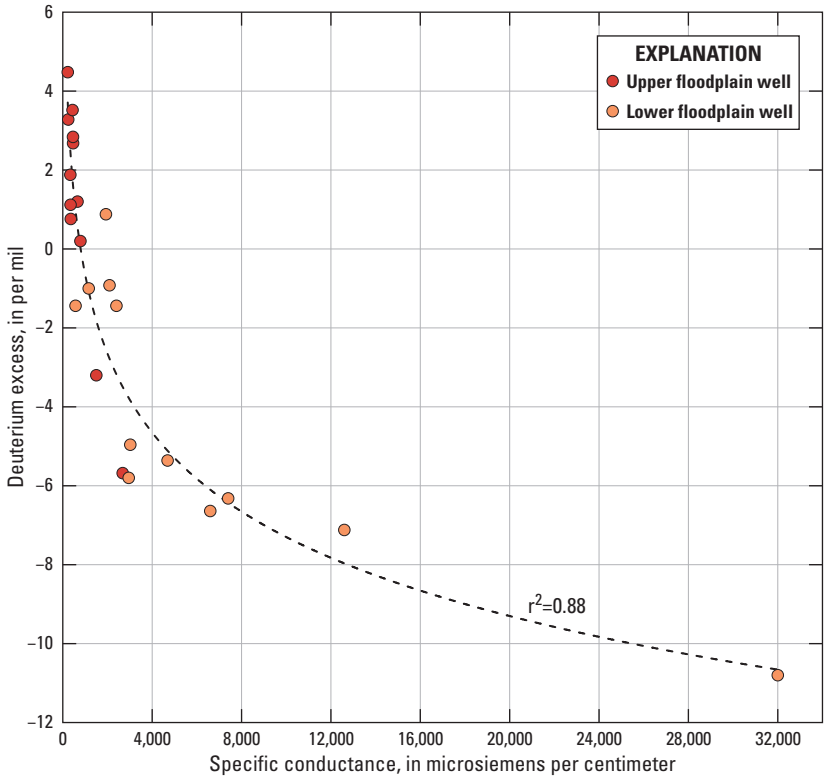

Figure 48. Relation between specific conductance and deuterium excess in wells in the Silvies River/Poison Creek floodplain between Burns and Malheur Lake, Harney Basin, southeastern Oregon.

In shallow wells open to the Younger basin fill HU throughout the floodplain, groundwater levels generally are 5–20 ft below the ground surface. The transmissivity of shallow wells in this area generally decreases away from the mountain front (fig. 7*A*). The water table (plate 2) follows topography and indicates that groundwater flows southeast toward Malheur Lake. The deep groundwater-level contours (plate 3) also show a similar gradient toward Malheur Lake. Wells deeper than about 150 ft in the Silvies River/Poison Creek floodplain commonly encounter higher-permeability layers (for example, HARN0000279, HARN0000478, HARN0001979; plate 1), likely in the Older basin fill HU, and consequently have higher yields (fig. 7). Some of these higher-permeability layers may be continuous with higher-permeability layers encountered in the uplands northwest of Burns. For example, three wells (HARN0050462, HARN0051724, HARN0051292; plate 1) in the uplands drilled into the Older basin fill HU or underlying Silicic lava flows and domes HU near the northwest extent of the Silvies River/Poison Creek floodplain also encountered relatively high-permeability layers with relatively high groundwater yields, typically at a depth below 4,050-ft elevation. Groundwater levels in these upland wells near Burns are about the same as wells drilled into more permeable units beneath the lowlands. The continuity and extensiveness of the higher-permeability layers is unknown, but groundwater-level data indicate their likely presence.

Lowland wells near the mountain front in the Silvies River/Poison Creek floodplain have groundwater levels near land surface that have shown small declines in response to increased pumpage over the previous 50 yrs. For example, HARN0000335 and HARN0000130 (fig. 47) are adjacent wells completed at different depths in different HUs (open from elevations of 4,143 to 4,139 ft [10- to 14-ft depth] and 4,133 to 4,028 ft [25- to 130-ft depth], respectively). From 1940 to 1960, their annual peak groundwater levels largely paralleled each other. Between 1960 and 1970, pumping from the deeper sediments increased and groundwater levels in the deeper well declined, whereas the shallow well continued the previous trend with some response to climatic variations (fig. 50). Similar responses are apparent in another shallow/deep well pair, HARN0000440 and HARN0000441 (open from elevations of 4,097 to 4,027 ft [50- to 120-ft depth] and 3,927–3,586 ft [220- to 561-ft depth], respectively), farther south on the floodplain. Overall, long-term groundwater-level declines are relatively small. During 2015–19, late winter groundwater levels in the shallow well were commonly 4–6 ft below 1960–75 late winter groundwater levels (HARN0000440 in fig. 50). In the deep well, groundwater levels during 1960–75 were about the same as in the shallow well; however, late winter groundwater levels had declined 16–18 ft by 2015–19 (HARN0000441 in fig. 50).

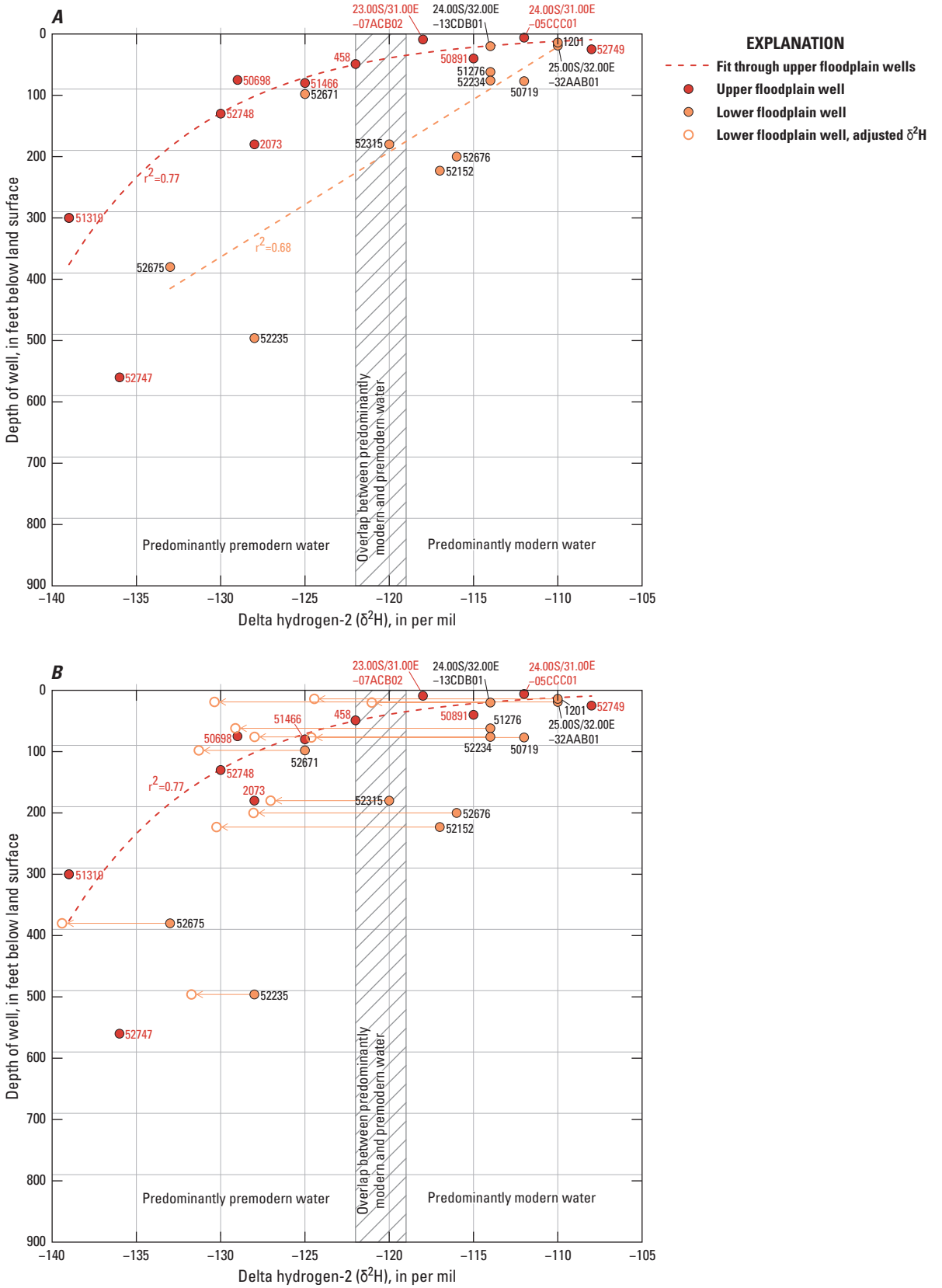

Figure 49. Relation between delta hydrogen-2 [δ^2H] and well depth in wells in the Silvies River/Poison Creek floodplain between Burns and Malheur Lake, Harney Basin, southeastern Oregon. (*A*) Shows the measured δ^2H value for all wells and (*B*) shows the measured δ^2H value for wells in the upper floodplain and the δ^2H value for wells in the lower floodplain adjusted to a deuterium excess of +3.5 per mil (‰) along an evaporative slope of 4.7.

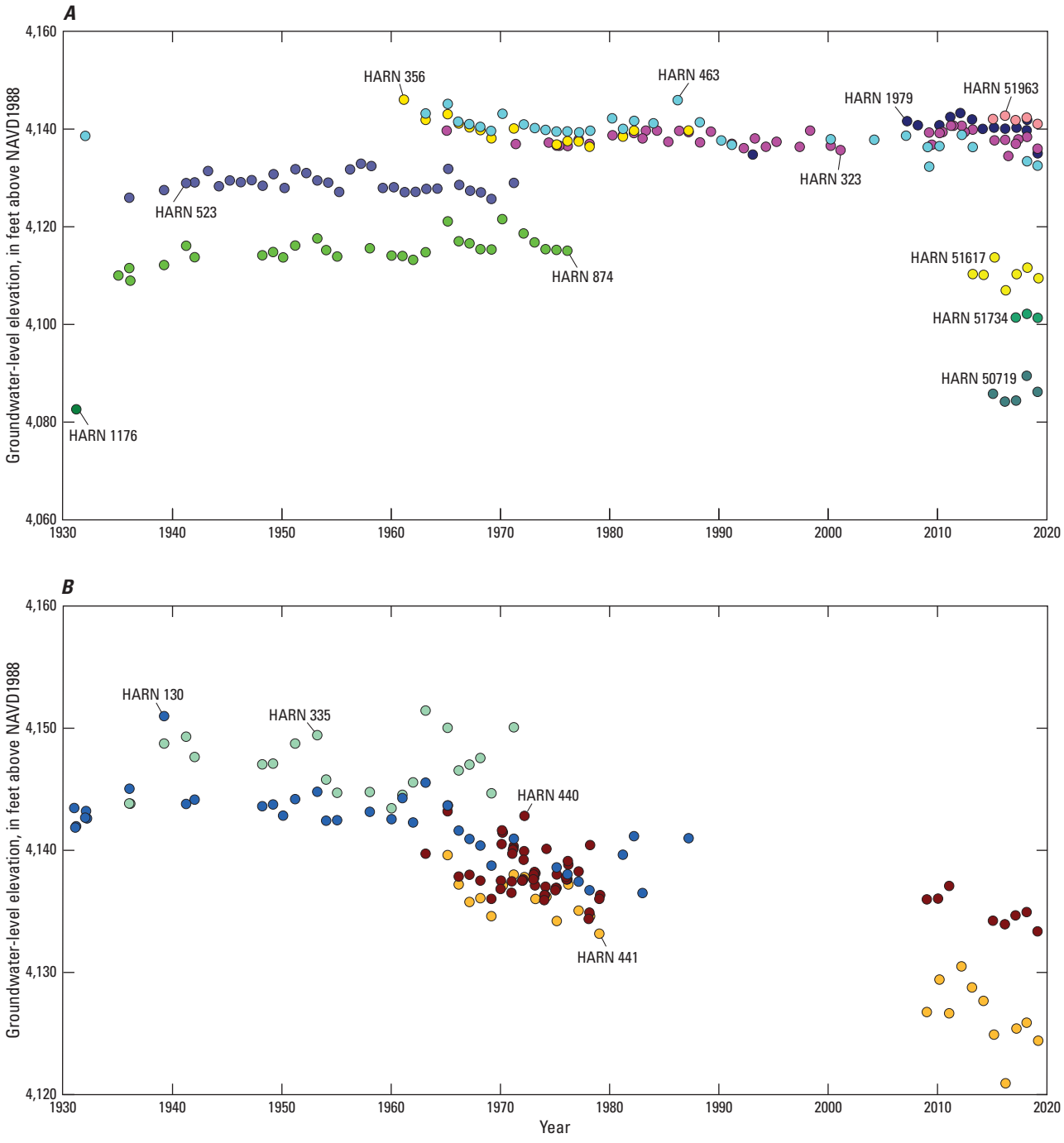

Figure 50. Groundwater levels during January–April at selected A) single and B) paired wells in the Silvies River/Poison Creek floodplain, Harney Basin, southeastern Oregon. Colored dots correspond to well locations shown on figure 47. NAVD1988, North American Vertical Datum of 1988.

Southeastward in the floodplain, the late winter groundwater levels in the shallower and deeper parts of the basin fill are nearly coincident, likely because of the lesser amount of groundwater pumping from the deeper fill in this area. Groundwater levels in three wells at the Eastern Oregon Agricultural Research Center monitoring wells (HARN0052749, HARN0052748, and HARN0052747 in fig. 17) open to the basin fill at elevations of 4,124–4,112, 4,035–4,009, and 3,622–3,592 ft, respectively, were all within 2.2 ft of each other on March 1, 2019, with the deepest well having the highest groundwater level and hence indicating an upward groundwater gradient. During the irrigation season, the gradients shift toward the zone of likely greatest groundwater pumping, to which the middle-depth well (HARN0052748) is open.

Close to stream channels and associated sloughs that receive diverted surface water, groundwater levels in wells (such as HARN0000440 in fig. 19) are influenced by increased surface-water flow and irrigation flooding. Groundwater levels are highest in late May or June and recede throughout the year, reaching the lowest level in January–February. Streamflow in the Silvies River (USGS streamgage 10393500 [Silvies River near Burns, Oregon]) typically peaks each year during March–May, preceding the highest groundwater levels in wells by about a month (fig. 19). On the edge of the uplands, away from the Silvies River and Poison Creek channels, seasonal groundwater-level fluctuations are about 5 ft (HARN0000296 [open from elevations of 4,097 to 4,027 ft; 140- to 305-ft depth] in fig. 20) and typically are highest in April due to autumn and winter recovery from pumpage and possibly recharge from winter precipitation. Groundwater levels are drawn down with the onset of irrigation in springtime and trend downward through summer until the end of the irrigation season and the onset of phreatophyte senescence in late summer to mid-autumn. Groundwater levels then recover during the autumn and winter until the following year's drawdown begins due to the onset of springtime irrigation pumping.

The springtime rise in groundwater levels in wells in the Silvies River/Poison Creek floodplain is predominantly owing to increased overburden pressure that freshet floodwater exerts above the Younger and Older basin fill HUs. The springtime rise in groundwater levels is unlikely due to immediate (a few days to weeks) recharge to the groundwater-flow system by rapid infiltration of surface water, as evidenced by groundwater geochemistry results. In the upper Silvies River floodplain, groundwater at the water table from a well (24.00S/31.00E-05CCC01; fig. 47) near the river was predominantly modern; however, the SC was about seven times higher (1,500 µS/cm) than surface water from Silvies River near Burns, and the value of deuterium excess (-3.2 ‰) indicates that the groundwater had undergone substantial evaporation. The time required to evaporate this water precludes immediate recharge to the water table. The much-finer silt and clay deposits encountered in this part of the floodplain preclude rapid infiltration, allowing evaporation of ponded surface water before recharge occurs. Other water-table wells (24.00S/32.00E-13CDB01, 25.00S/32.00E-32AAB01, HARN0001201; fig. 47) in the lower floodplain show a similar evaporative history. Evidence for localized, rapid recharge in the upper floodplain near Burns is provided by one water-table well (23.00S/31.00E-07ACB02; fig. 47). This well, less than 100 ft from the Silvies River, shows the presence of predominantly modern water, with an SC value similar to water from Silvies River near Burns, at the water table. The value of deuterium excess of this sample (+3.5 ‰) indicates that the water underwent little evaporation before infiltrating as channel loss through the coarser sediments near the river. The potential for immediate recharge exists for the areas that have efficient hydraulic connection with stream channels near the uplands where rivers and streams have deposited coarser sediments.

The groundwater-level data in the Sage Hen Valley area (a tributary valley to the Silvies River) were insufficient to determine estimates of long-term trends in groundwater level (fig. 51). Water levels demonstrate a groundwater gradient eastward from the uplands toward the Silvies River floodplain (plate 2). Expanded monitoring is needed to establish trends in groundwater levels in this area.

Floodplains from Prater Creek to Mahon Creek

Along the northern edge of the Harney Basin lowlands, groundwater moves through the Younger and Older basin fill HUs. Most of the Younger basin fill HU in this area consists of material deposited by coalescing alluvial fans along the course each stream follows as it enters the Harney Basin lowlands from the uplands (fig. 52). As was discussed in the Silvies River/Poison Creek area, the permeability of the Younger basin fill HU is highly variable depending on location and depth. Along each stream, coarser-grained, moderately permeable alluvial deposits near the mountain front grade into finer-grained, less-permeable deposits longitudinally with the stream channel into the valley and laterally away from the stream channel. Here, the Older basin fill HU consists of a heterogenous mixture of alluvial and volcanic deposits of varying permeabilities.

Groundwater levels in shallow wells throughout the floodplain are generally 5–20 ft below the ground. The water table (plate 2) follows topography and indicates that groundwater flow is southward toward Malheur Lake. The water budget (refer to "Hydrologic Budget" section and Garcia and others [2022]) and geochemistry indicate some groundwater flow from the low-permeability uplands located to the north into the deposits underlying the Harney Basin lowlands. However, most modern recharge to the Harney Basin lowlands north of Malheur Lake originates from surface water infiltrating through alluvial sediments in the floodplains of this area and the adjoining Silvies River/Poison Creek area.

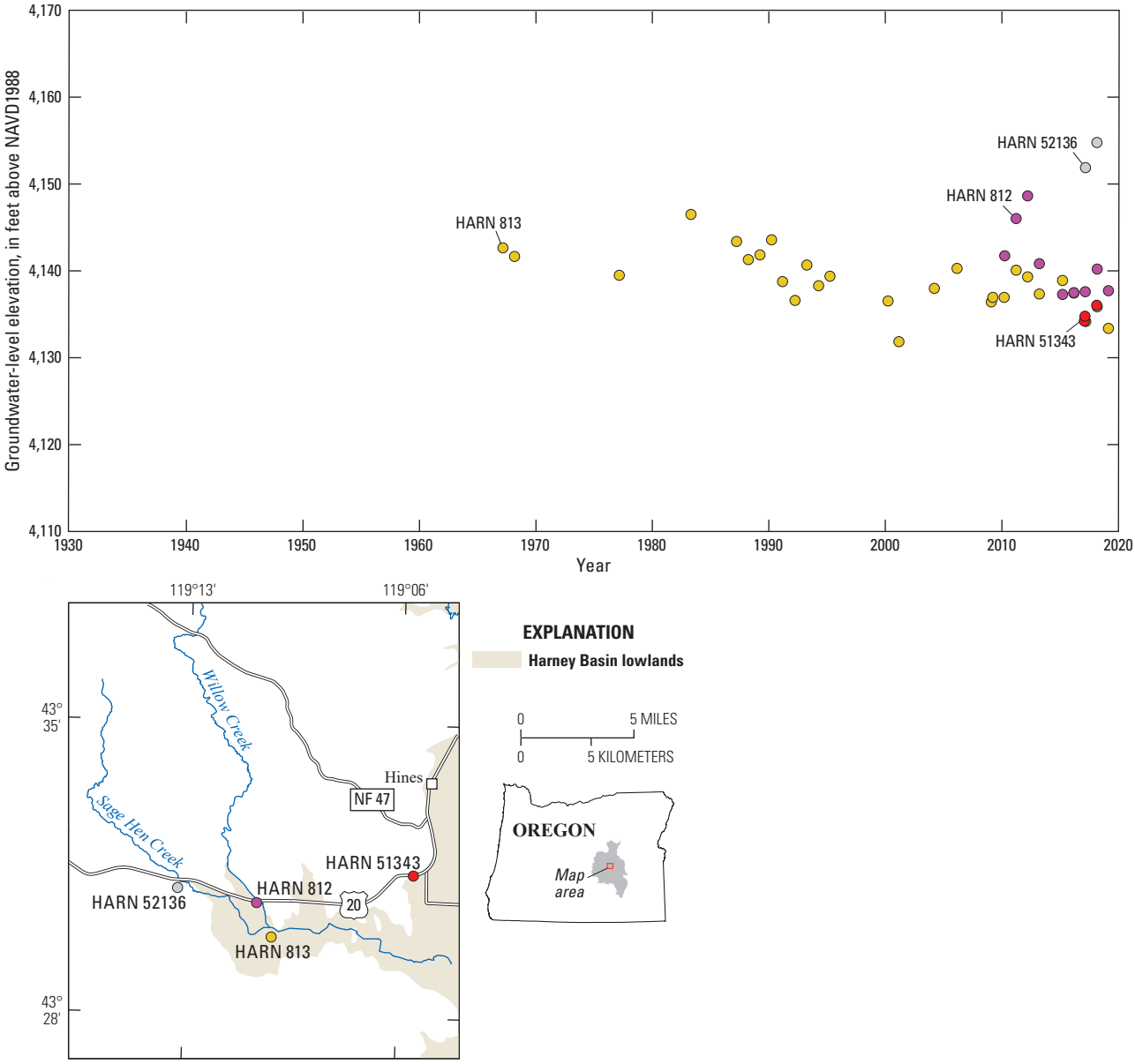

Figure 51. Groundwater levels during January–April at selected wells near Sage Hen Valley, Harney Basin, southeastern Oregon, 1930–2020. NAVD1988, North American Vertical Datum of 1988.

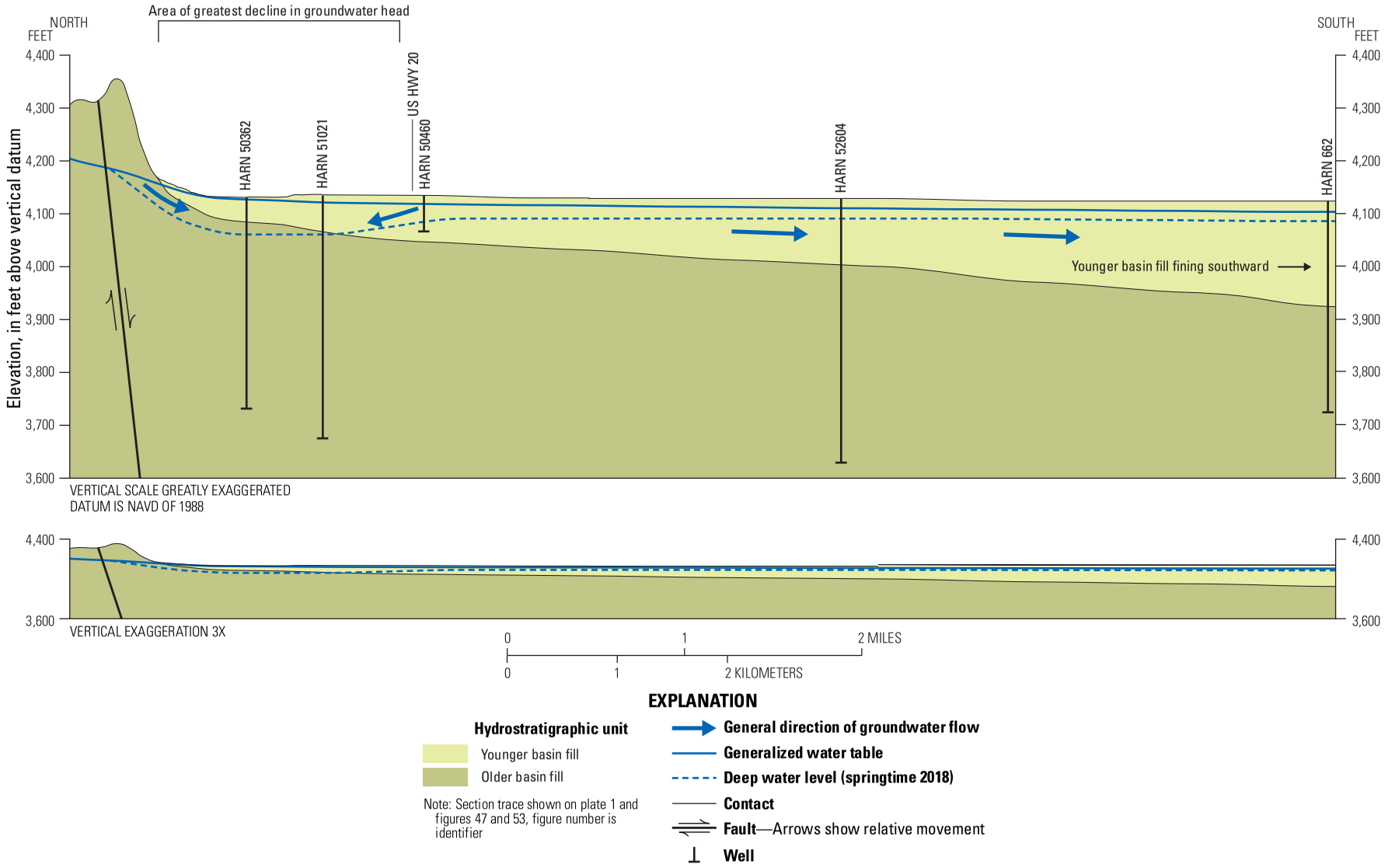

Figure 52. Schematic hydrogeologic cross section of floodplains from Prater Creek to Mahon Creek, Harney Basin, southeastern Oregon. Section trace shown on figure 53.

Although infiltration of freshet water is the principal source of recharge in this area, the geochemical data indicate that the volume of this recharge is limited. Six wells were sampled for ^{3}H in this area (fig. 53). Two of the well samples were tritium dead–HARN0052029 (165 ft deep) and HARN0052479 (230 ft deep). Three wells had ^{3}H less than 1 TU–HARN0001975 (95 ft deep), HARN0052274 (95 ft deep), and HARN0052173 (800 ft deep)–indicating they are pumping predominantly pre-modern groundwater (fig. 25). Tritium was detected in the last well (23.00S/33.00E-30BBB01; 12 ft deep) at 1.4 TU, indicating that the groundwater at the top of the water table either was wholly recharged prior to 1960 (fig. 1.1) or is a mixture of a small amount of recent recharge and predominantly pre-modern groundwater (fig. 25). The trace amount of ^{3}H detected in the 800-ft-deep well (HARN0052173) likely reflects the contribution of groundwater from the upper part of the long open interval of this well, which extends from 105 to 800 ft below land surface. The ^{14}C ages determined for two wells in this area– HARN0052274 (<500 yrs) and HARN0052173 (31,691 yrs)–substantiate the vertical age stratification observed in the ^{3}H data and attest to the ancient age of the deep groundwater in this area. The stable isotope results from eight wells in this area (the six wells with ^{3}H plus two additional wells) also support the presence of predominantly pre-modern water at all depths throughout the groundwater-flow system (fig. 54). The vertical distribution of groundwater ages observed in this region is similar to that observed in the Silvies River/Poison Creek floodplain–namely, a thin layer of predominantly modern groundwater resting atop a large body of predominantly pre-modern groundwater. The thickness of the layer of predominantly modern water in this area is substantially thinner than was observed in the Silvies River/Poison Creek floodplain (as evidenced by largely pre-modern water at a depth of 12 ft in well 23.00S/33.00E-30BBB01) and is attributed to the considerably smaller volume of freshet water that floods this area each year. Infiltration of irrigation water is not likely a substantial contributor to recharge in this area because irrigation is predominantly by center-pivot sprinklers, which have small infiltration losses (Beamer and Hoskinson, 2021; Garcia and others, 2022); additional sampling for ^{14}C or other atmospheric gas tracers (for example, sulfur hexafluoride or chlorofluorocarbons) from shallow wells in this area could help determine if reinfiltration of irrigation water occurs in any appreciable amount.

Similar to the upper Silvies River/Poison Creek floodplain, groundwater in the floodplains from Prater Creek to Mahon Creek generally has relatively low salinity (median SC = 531 µS/cm) and is not highly evaporated (median deuterium excess = +3.0 ‰), which likely is owing to its limited upland precipitation catchment and its proximity to the upland mountain front which provides drainage (infiltration and overland) and prevents large amounts of freshet water from sitting on the surface for extended periods of time. The highest SC (3,340 µS/cm) and greatest degree of evaporation (deuterium excess = -0.8 ‰) were observed in a water-table well situated about midway between the mountain front and Malheur Lake: 23.00S/33.00E-30BBB01 (12 ft deep).

Seasonal groundwater-level fluctuations in wells less than 100-ft deep drilled into the Younger basin fill HU are about 6–10 ft, with the highest levels in May and the lowest levels in August (for example, HARN0050460 [open from elevations of 4,085 to 4,067 ft; 50- to 68-ft depth] in fig. 19). Presently, late winter groundwater levels in the deeper wells completed in the Older basin fill HU are 20 ft to more than 90 ft lower than in shallower wells completed in the overlying Younger basin fill HU (compare plates 2–3), resulting in a downward groundwater head gradient. Seasonal groundwater-level fluctuations in the deeper Older basin fill HU are greatest where groundwater pumpage is highest. North of Highway 20, deep groundwater levels seasonally fluctuate as much as 110 ft (for example, HARN0050766; plate 1), and, farther south, groundwater levels fluctuate about 30–40 ft, with the lowest groundwater levels reached in August (for example, HARN0052619 in fig. 20). At well HARN0050362 (open to the Older basin fill HU 80–405 ft below ground surface), March groundwater-levels declined nearly 5 ft/yr during 2008–18 (fig. 55) to as much as 30 ft below the level of Malheur Lake (4,094-ft elevation in 2019).

Similar to the Silvies River area, the springtime groundwater-level rise in wells in in the floodplains from Prater Creek to Mahon Creek is not due to immediate infiltration of surface water. Rather, as indicated by the ancient age of the groundwater, the observed rise in groundwater level in wells is owing to the increased loading that freshet floodwater exerts on the Younger and Older basin fill HUs.

Pumpage in in the floodplains from Prater Creek to Mahon Creek has lowered the late winter groundwater levels in the Older basin fill HU more than 60 ft (plate 3). Although data from shallow wells are sparse, indications are that the pronounced depressions in groundwater level of the deeper part of the groundwater-flow system are greatly subdued near the water table (plate 2). The muted decline at shallow depths likely is because of the low vertical permeability of the sediments overlying the heavily pumped deeper units. Late winter water levels at HARN0000547 (open to the Younger basin fill HU 60–93 ft below ground surface; fig. 55) were relatively stable from 1960 to 1980; however, since 1980, water levels have declined by about 10 ft. At HARN0050362, late winter groundwater levels have declined about 40 ft since 2010. The pumpage-induced depression in hydraulic head in this area has changed groundwater gradients and flow directions. North of Highway 20, the natural southward groundwater-flow direction has been reversed, causing groundwater to flow northward toward the areas of pumpage (plate 3). The natural southward flow direction resumes about 2–3 mi south of Highway 20. Pumpage north of Highway 20 effectively captures most of the limited recharge from stream infiltration and from groundwater flow entering this area from the uplands through deep groundwater flowpaths that otherwise would have provided recharge to deep wells in the Harney Basin lowlands south of Highway 20.

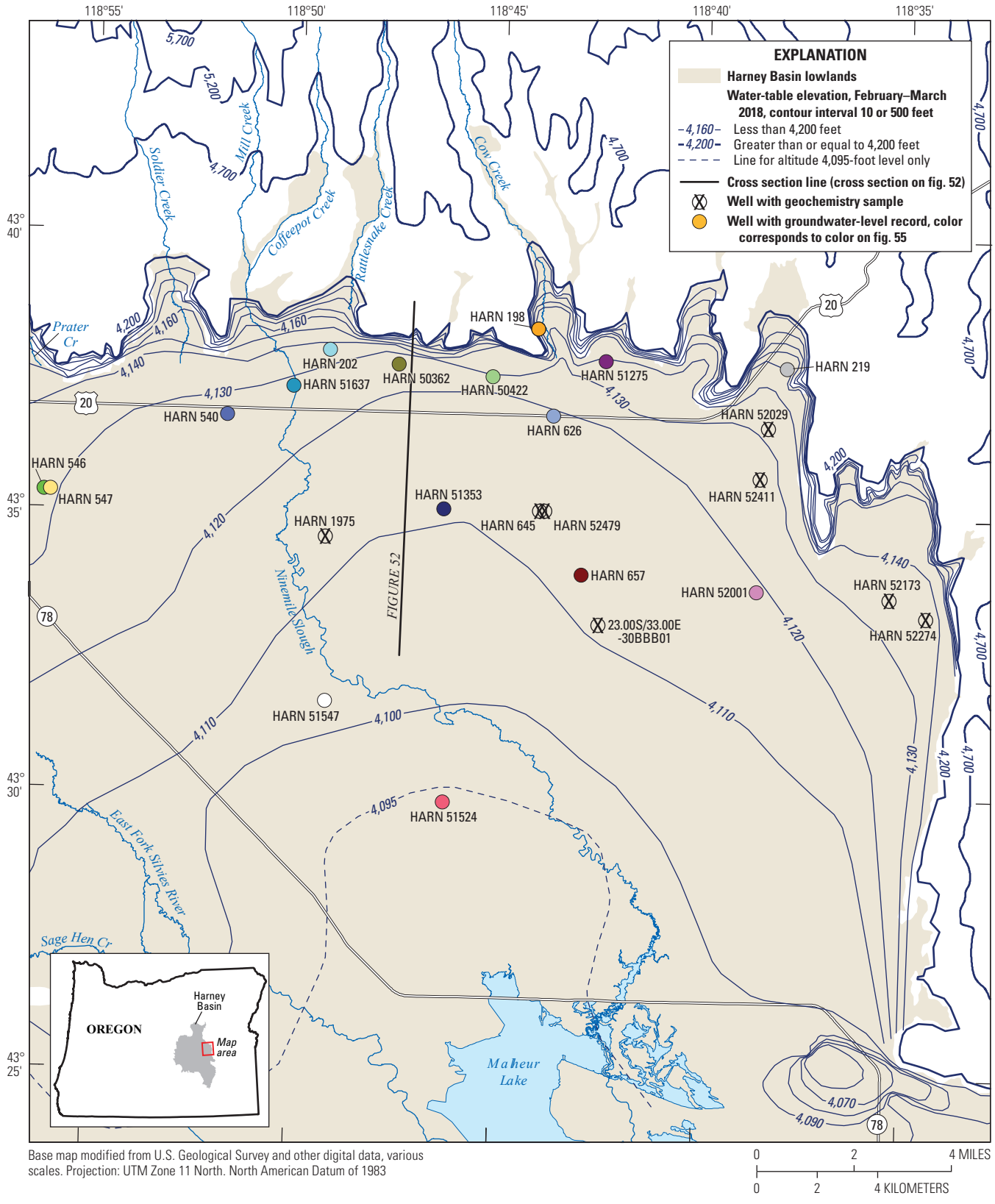

Figure 53. Location of selected groundwater-level and geochemistry sites, Prater Creek to Mahon Creek floodplain area, Harney Basin, southeastern Oregon.

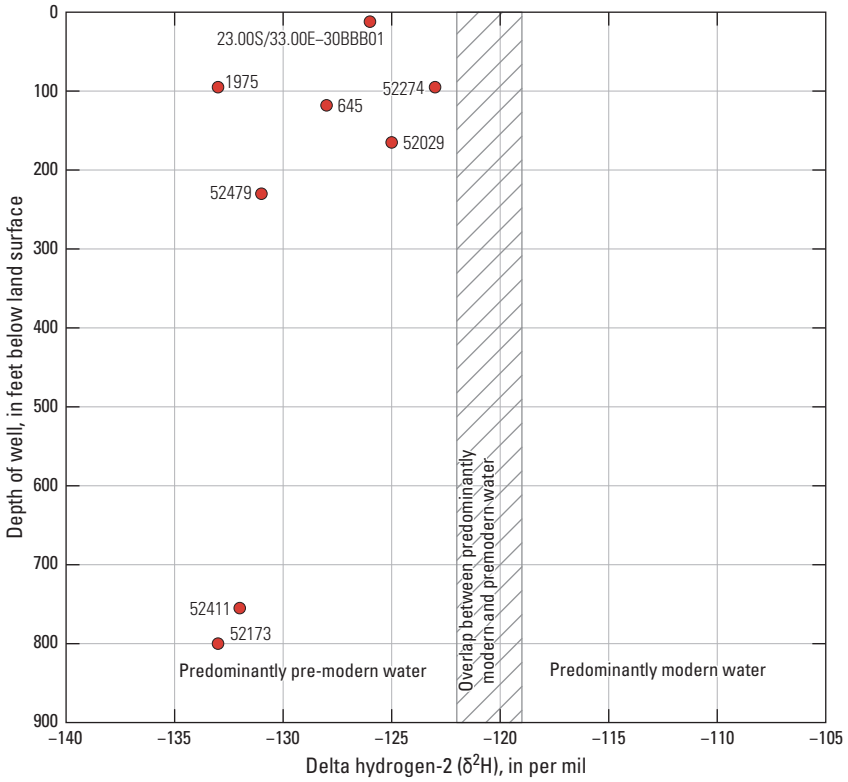

Figure 54. Relation between delta hydrogen-2 [δ^2H] and well depth in wells in the floodplain of the northeastern Harney Basin lowlands, southeastern Oregon.

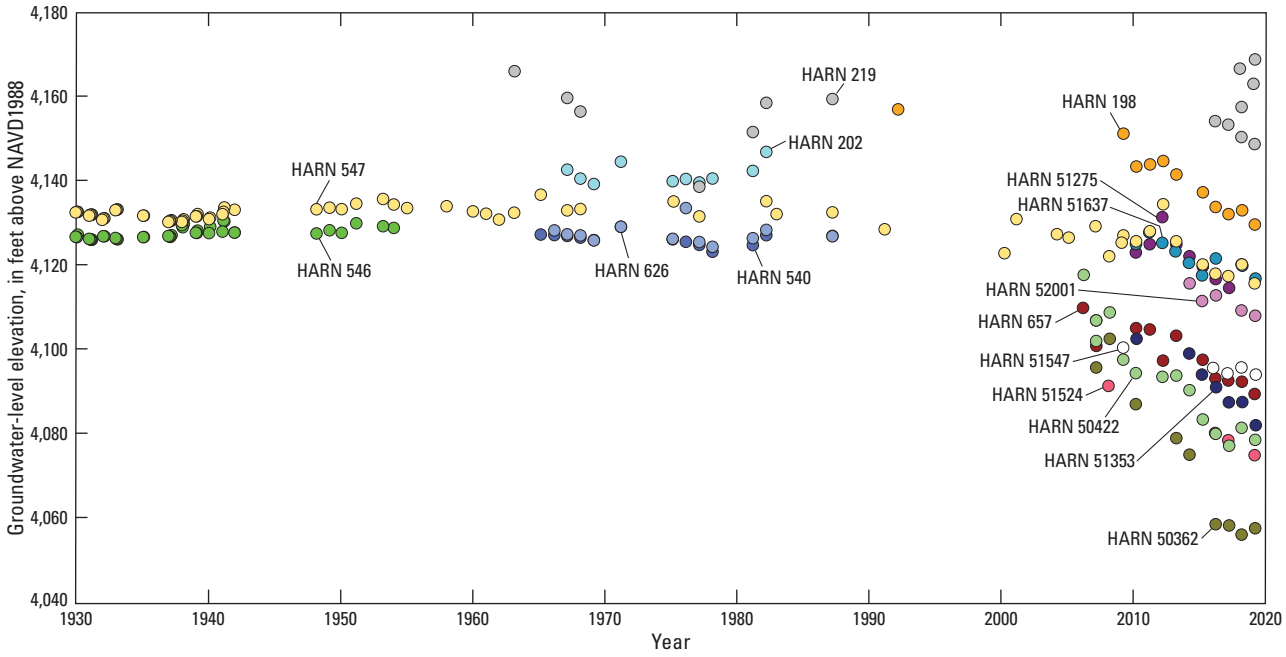

Figure 55. Groundwater levels during January–April at selected wells in the floodplains from Prater Creek to Mahon Creek, Harney Basin, southeastern Oregon. Colored dots correspond to well locations shown on figure 53. NAVD1988, North American Vertical Datum 1988.

Crane

Relatively permeable areas of the Younger and Older basin fill HUs along the eastern margin of the Harney Basin lowlands provide groundwater to many of the irrigation wells near the town of Crane. Westward toward the center of the basin, the Younger basin fill HU deposits become increasingly finer-grained, and well yields decrease considerably (fig. 7). Well reports indicate that the highest-yield strata are coarser-grained sediments (sand and gravel) and layers of basalt immediately west of the mountain front of the Stinkingwater Mountains (fig. 56). The high-permeability sands and gravels described in well reports may be locally derived alluvial fan deposits from the adjacent Stinkingwater Mountains or deposits from streams that once flowed through this part of the basin. Some wells west of Warm Springs Butte have penetrated westward-thinning, productive layers of more-permeable sediment and lava flows associated with a Proximal vent deposits HU emanating from the butte. Well HARN0051587 (yield = 4 gallons per minute per foot of well), about 0.25 mi northwest of Warm Springs Butte, penetrates about 80 ft of black sand, claystone, and basalt (fig. 56; plate 1), but 0.75 mi farther west at HARN0001934 (yield = 0.4 gallons per minute per foot of well; not shown on cross section) only 5 ft of black sand is penetrated, indicating that the volcanic deposits thin toward the north and west. The permeability of consolidated sediments and volcanic units in the area may be enhanced by north-trending faulting associated with the uplift of the Stinkingwater Mountains to the east (fig. 6).

Several miles south of Crane, the Drinkwater Basalt (part of the high-transmissivity High Lava Plains basalt HU which caps Crane Butte) is down-dropped beneath the Harney Basin lowlands by north-trending faults and is buried by basin fill deposits. Although no geochemical identification from well cuttings has been made, some of the high-yield wells likely produce from the Drinkwater Basalt.

The Crane area is far from any major recharge source, and only a few small intermittent streams flow into the Harney Basin lowlands from the nearby uplands. Recharge to this area is limited because rainfall on the eastern uplands is about 12–15 in/yr, and the catchment area for streams flowing into the Harney Basin extends only about 3–4 mi to the east. The lack of appreciable local recharge is apparent in geochemical samples collected in the area, which indicated a limited amount of modern groundwater. Four wells were sampled for ^{3}H (fig. 57). Samples from HARN0001287 (130 ft deep) and HARN0050179 (327 ft deep) were tritium dead, indicating that they contain entirely pre-modern groundwater. Samples from HARN0001228 (300 ft deep; 0.2 TU) and HARN0051004 (115 ft deep; 1.1 TU) had detectable ^{3}H. The groundwater from HARN0001228 was at least 90 percent pre-modern water, and the groundwater from HARN0051004 was at least 60 percent pre-modern (fig. 26), providing evidence for some modern recharge in the Crane area. However, the large proportion of pre-modern water in these two wells, particularly HARN0051004, which is less than 100 ft deep and is within 1 mi of the upland mountain front, along with tritium-dead water from a 130 ft deep well within 2.5 mi of the mountain front (HARN0001287), indicates that the amount of modern recharge is very small. The stable isotope results from these four wells and six others in the Crane area are consistent with the ^{3}H results: they provide no evidence for substantial amounts of modern water and indicate that the age of the groundwater increases with depth (fig. 58). The shallowest well (24.00S/33.00E-27CCC01, 11 ft deep) was the only one that had a $\delta^{2}H$ value in the range that could potentially be predominantly modern; however, the SC (6,810 µS/cm) and deuterium excess (-13.92 ‰) strongly indicated it has experienced substantial evaporation meaning its original $\delta^{2}H$ value was much lower and fully in the range of predominantly pre-modern water.

The water-table map (plate 2) indicates that groundwater flows generally southwest toward Malheur Lake. Groundwater pumpage has led to several areas of depressed groundwater levels, causing a localized reversal of flow direction toward these pumping centers. Prior to about 1980, groundwater levels in shallow wells throughout the area were generally 10–20 ft below the ground surface. In March 2019, the groundwater level was more than 35 ft lower in some places, such as at HARN0001245 (fig. 59). Groundwater levels from wells greater than about 150 ft deep show a more extensive area of decline in a north-south orientation (plate 3) owing to the prevalence of high-capacity irrigation wells pumping from the deeper, more-permeable basin fill deposits. Historically, groundwater levels in the basin fill deposits near and to the east of Crane may occasionally have been high enough to allow some flow of groundwater eastward through the Crane Creek Gap south of the Crane Creek Mountains. Presently, however, groundwater flows westward from the gap into the Harney basin.

As observed elsewhere in the Harney Basin, the highest groundwater levels in the Crane area occur in March–May after over-winter recovery from pumpage, limited wet-season recharge, and pressure response from the loading of freshet water on the surface. The lowest groundwater levels occur in August–September and correspond to the end of the irrigation season and the onset of phreatophyte senescence. Seasonal groundwater-level fluctuations in shallow wells near pumping areas are typically about 6–10 ft. Well HARN0001245 (open to the Younger basin fill HU from elevations of 4,098 to 3,978 ft; 40- to 160-ft depth) had seasonal fluctuations in this range during 2007–14, but they diminished to less than 0.5 ft. after 2014, when nearby pumpage for irrigation was stopped, reportedly owing to declining groundwater yield in the supply wells (fig. 20). In contrast, seasonal groundwater-level fluctuations are larger in deeper parts of the basin fill. For example, annual fluctuations exceeded 40 ft during 2016 and 2017 at HARN0051722 (open to the Older basin fill HU from elevations of 3,832 to 3,730 ft; 288- to 390-ft depth). As observed in the northeastern Harney Basin lowlands, groundwater levels in the Crane area were relatively steady until about 1980. Water levels appear to decline after 1980, but data are sparse until 2010. During 2010–19, late winter groundwater levels declined 7–20 ft, or about 1–2 ft/yr (fig. 59), in monitored wells across the Crane area.

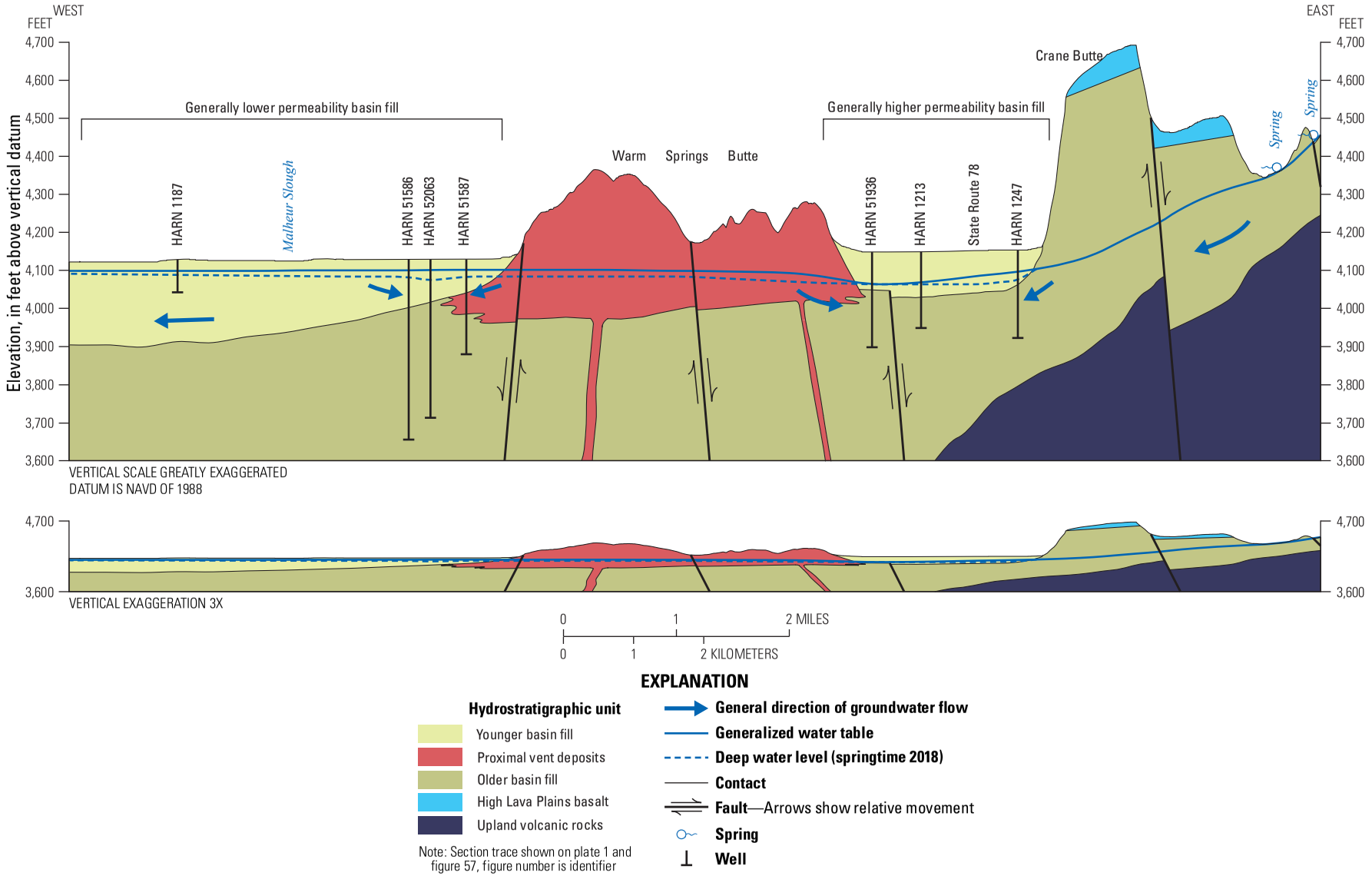

Figure 56. Schematic hydrogeologic cross section of Crane area, Harney Basin, southeastern Oregon. Section trace shown on figure 57.

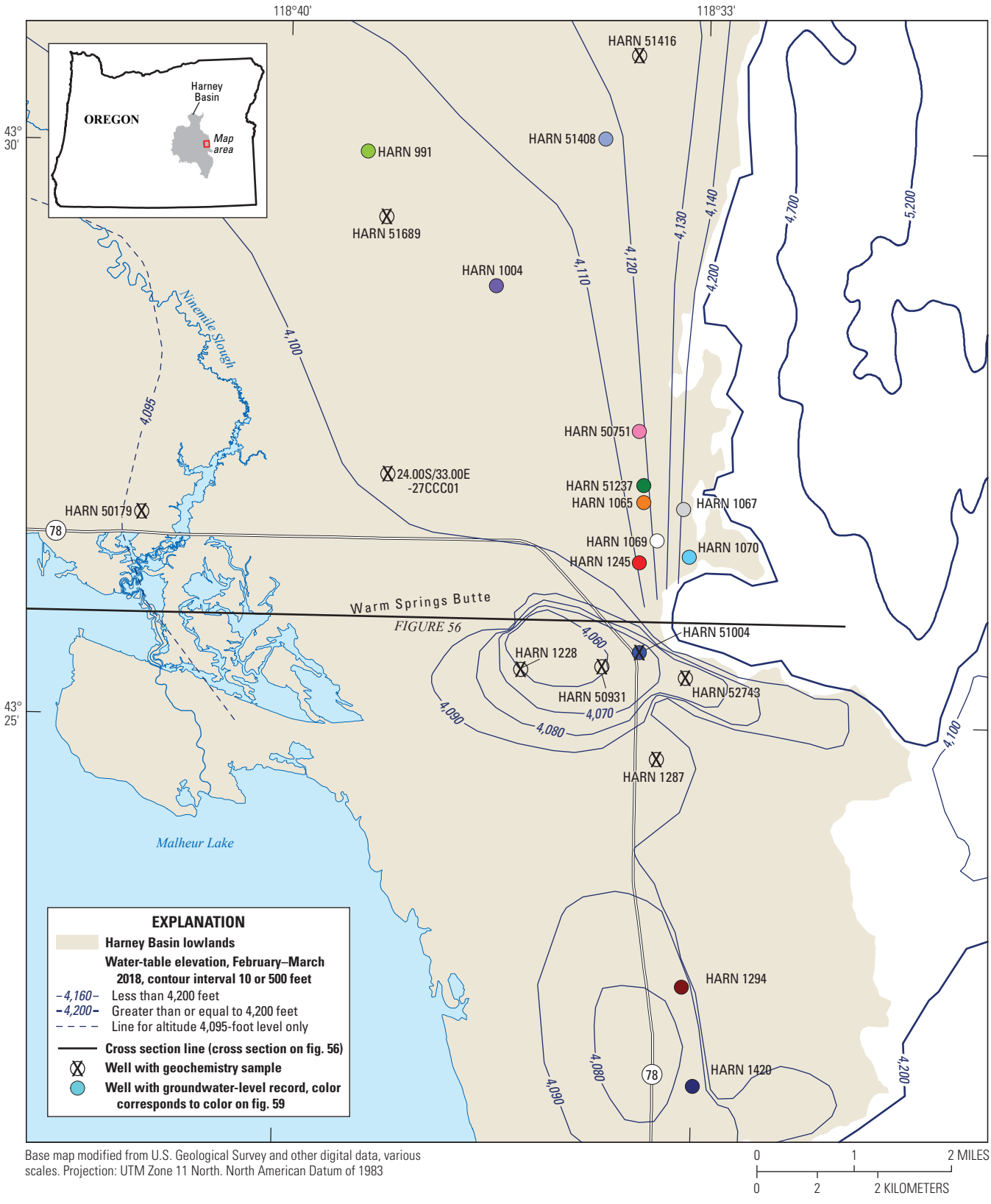

Figure 57. Locations of selected groundwater-level and geochemistry sites in the Crane area, Harney Basin, southeastern Oregon.

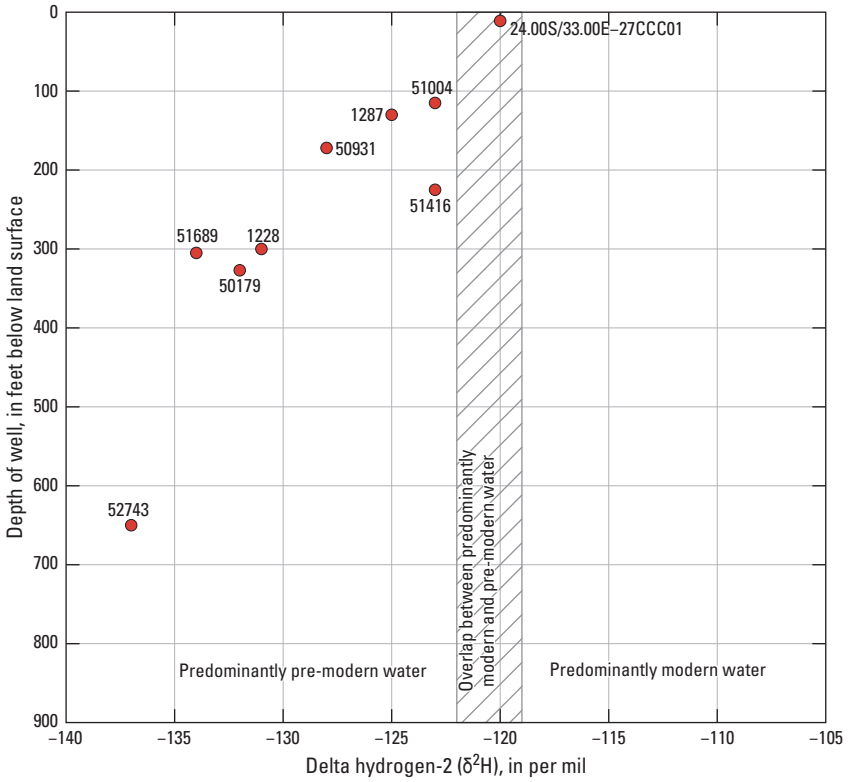

Figure 58. Relation between delta hydrogen-2 [δ^2H] and well depth in wells in the Crane area, Harney Basin, southeastern Oregon.

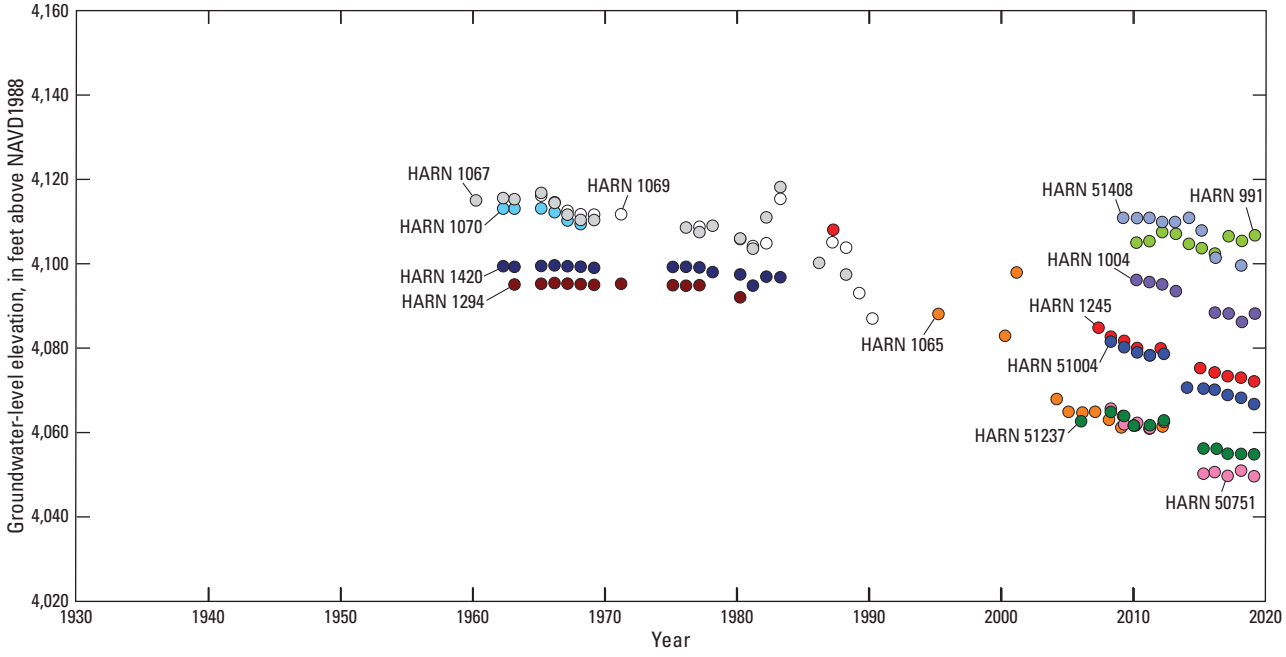

Figure 59. Groundwater levels during January–April at selected wells in the Crane area, Harney Basin, southeastern Oregon. Colored dots correspond to well locations shown on figure 57. NAVD1988, North American Vertical Datum of 1988.

Virginia Valley

The Younger basin fill HU and the underlying Voltage basalt HU are the principal sources of groundwater in the Virginia Valley area (figs. 9, 60); both are highly permeable, and transmissivity is relatively large across the area (fig. 7). Between about 2.5 and 1.5 Ma, surface water flowed through Virginia Valley and into the South Fork Malheur River near the location of Malheur Cave (plate 1). The channel through Virginia Valley was dammed by lava flows of the Voltage basalt about 1.5 million yrs ago, and subsequent volcanism and sedimentation has filled the old stream valley to the level of the Harney Basin lowlands (fig. 60). The Voltage basalt HU is at least 310 ft thick at HARN0052607 (fig. 60), but the maximum thickness of this valley-filling unit is unknown because no wells penetrate the entire thickness. Although now buried, the presence of the old stream channel is manifested in the elevation of the water table in Virginia Valley, which decreases to the east, indicating that groundwater flows eastward from the Harney Basin lowlands, through the valley, and toward the Malheur River (fig. 60; plate 2). Groundwater flow out of the Harney Basin into Malheur River Basin is relatively small owing to a constriction in the highly permeable Voltage basalt HU at Virginia Valley and is estimated to be about 3,000 acre-ft/yr (Garcia and others, 2022).

Converging flowpaths indicate that groundwater in the Virginia Valley area is recharged by inflows from the Harney Basin lowlands to the northwest, from the northeastern flanks of Steens Mountain, and from the southern Stinkingwater Mountains (plate 2). Evidence from the geochemical data indicates the groundwater in the part of Virginia Valley that is within the Harney Basin largely originates from the lowlands southeast of Malheur Lake. Contributions from Steens Mountain are more substantial in the groundwater underlying Anderson Valley and in the part of Virginia Valley outside the Harney Basin to the southeast. As was noted in the discussion for the Crane area, recharge from the Stinkingwater Mountains is expected to be a minor contribution owing to the limited extent of and low precipitation in the upland areas.

The seven wells (six of which penetrate or are completed in the Voltage basalt HU) in the Virginia Valley area that have geochemical data help constrain the source and travel time of groundwater recharging in this area. Some of these wells are in upland areas on the periphery of the Harney Basin lowlands; therefore, comparing elevations of the bottom of each well is more instructive than comparing depth below land surface, which has been used in other areas of predominantly low-relief. As was observed in the lower Silvies River/Poison Creek floodplain, a strong evaporative signal in the groundwater in the Virginia Valley area is indicated by the inverse relation between SC and deuterium excess (fig. 62). The four wells with highest SC and lowest deuterium excess–HARN0001494 (125 ft deep; bottom-hole elevation of 4,007 ft), HARN0052608 (145 ft deep; bottom-hole elevation of 3,979 ft), HARN0001495 (160 ft deep; bottom-hole elevation of 3,954 ft), and HARN0052607 (371 ft deep; bottom-hole elevation of 3,749 ft)–are drilled in a northwest-southeast trending trough of converging groundwater heads oriented toward the center of the Harney Basin (fig. 61; plate 2). Comparably high SC values and low values of deuterium excess were observed in other wells from central areas of the Harney Basin, including the Silvies River/Poison Creek floodplain area and the Crane area. The two samples that had the lowest SC and largest deuterium excess–HARN0001557 (128 ft deep; bottom-hole elevation of 4,057 ft) and HARN0001509 (291 ft deep; bottom-hole elevation of 4,078 ft)–are from wells situated on flowpaths primarily associated with Steens Mountain to the south (fig. 61), and their chemistry is consistent with their proximity to such a large recharge source. The last well with geochemical data–HARN0001517 (92 ft deep; bottom-hole elevation of 4,020 ft)–is in Virginia Valley 5.5 mi downgradient from HARN0052607 and HARN0052608 and is outside of the Harney Basin (fig. 61; plate 2). This well lies in the same main trough of converging heads as HARN0052607 and others upgradient in Virginia Valley, but likely receives a greater contribution of recharge from Steens Mountain as indicated by the surrounding hydraulic gradient and by its somewhat lower SC (fig. 62).

The stable isotope data are consistent with the conclusions reached from observations of flow direction, SC, and evaporation. As just discussed, the deuterium excess data indicate most of the stable isotope samples experienced a moderate to large amount of evaporation. An estimate of the original δ^2H value was made by adjusting them in the same manner as was done for the lower Silvies River/Poison Creek floodplain samples–all δ^2H values in the Virginia Valley area were adjusted along an evaporative slope of 4.7 to have a deuterium excess equal to +3.5 ‰, which corresponds to the median deuterium excess of the three largest values of deuterium excess observed in the upper Silvies River/Poison Creek floodplain. This value serves as an approximation of the deuterium excess in ancient recharge through groundwater flow from uplands into the Harney Basin lowlands. A similar value of deuterium excess (+4.1 ‰) was observed in a base-flow sample from Smyth Creek (plate 1), which drains the northeast flank of Steens Mountain about 20 mi south of Virginia Valley and reinforces the upper Silvies River value as a reasonable one to which to adjust. Without adjusting the δ^2H values, no relation between elevation of the bottom of wells and δ^2H is apparent; however, after adjustment, a clear separation in δ^2H between the two shallowest samples and the remaining samples is evident (fig. 63). Further, the two wells that have the largest adjusted δ^2H are the same two wells that were identified as being predominantly recharged from Steens Mountain. The adjusted δ^2H values in the five wells having the most negative values are larger than many of the oldest samples from the central Harney Basin, which tend to be less than -130 ‰. Adjusting them to a larger deuterium excess would shift them more negative, but no evidence is available to recommend doing so. Instead, these samples are more likely a mixture of less negative (and more recently recharged) groundwater from Steens Mountain and groundwater draining from central parts of the Harney Basin. A mixing of groundwaters also is supported by the head observations which indicate that groundwater flowpaths from the central parts of the Harney Basin and Steens Mountain are likely converging in the most northeastern parts of Virginia Valley (fig. 61; plate 2).

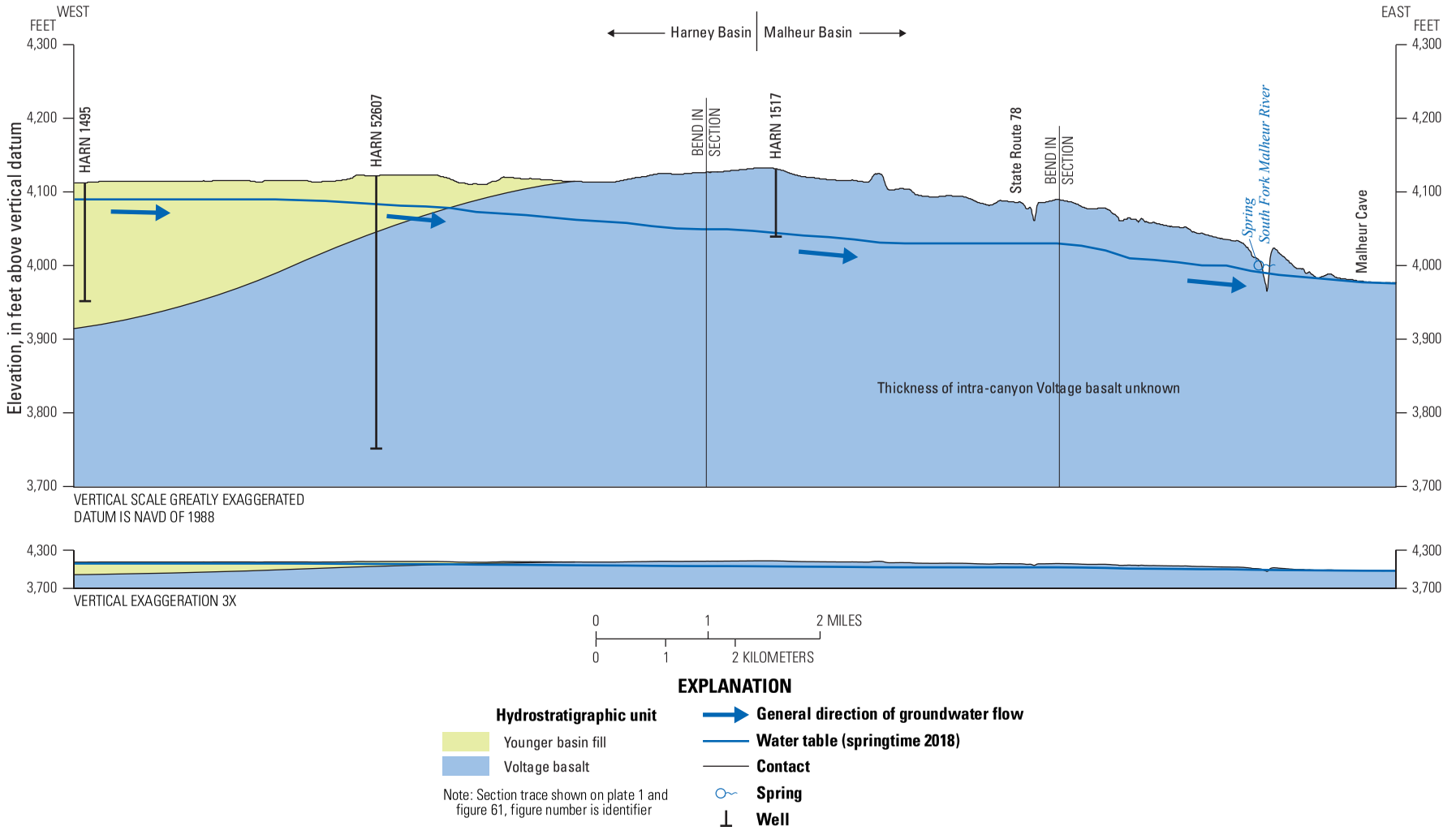

Figure 60. Schematic hydrogeologic cross section of Virginia Valley, Harney Basin, southeastern Oregon. Section trace shown on figure 61.

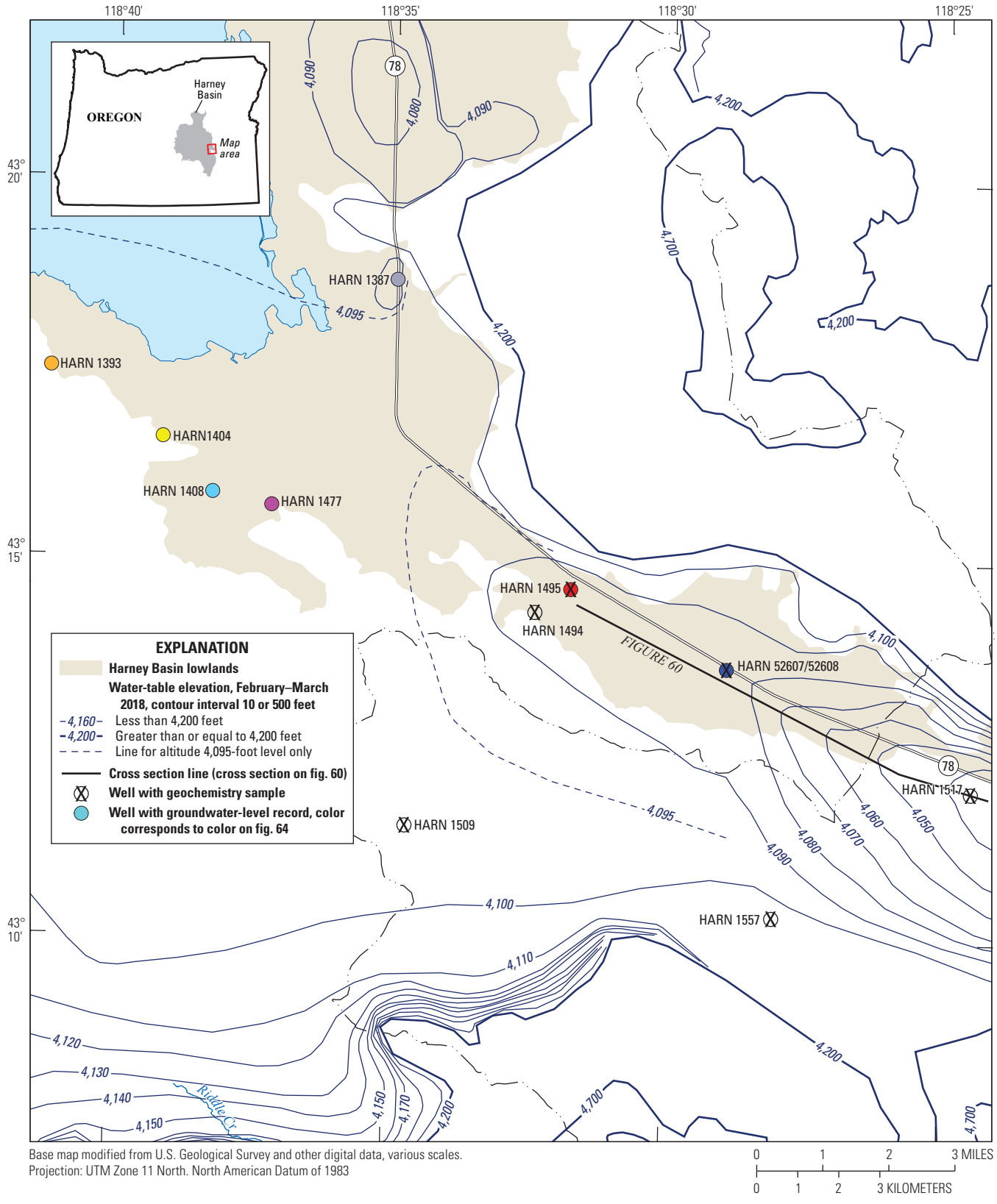

Figure 61. Locations of selected groundwater-level and geochemistry sites in the Virginia Valley area, Harney Basin, southeastern Oregon.

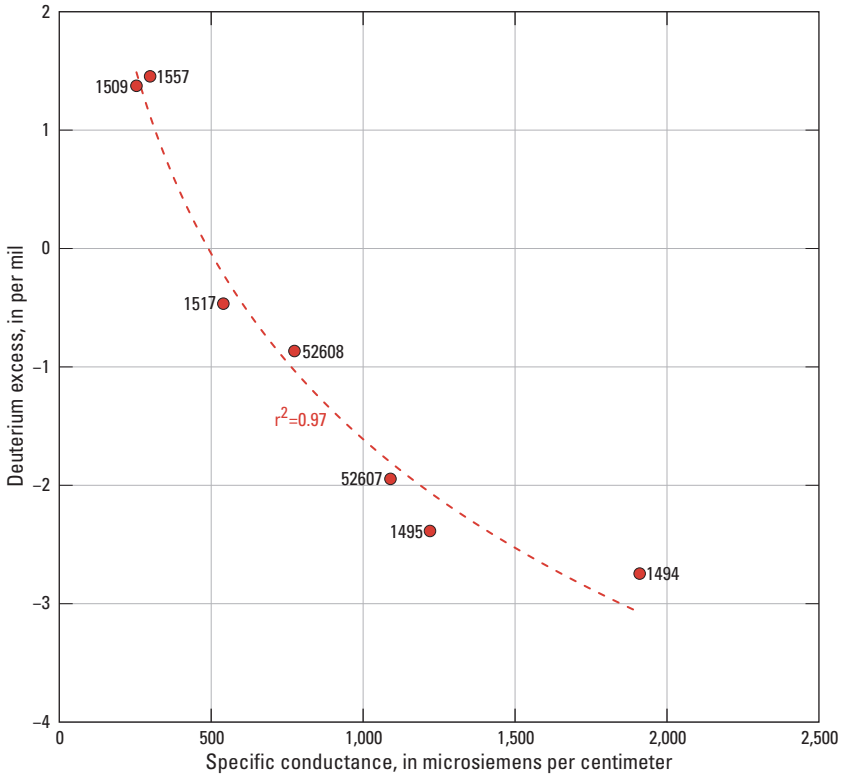

Figure 62. Relation between specific conductance and deuterium excess for wells in the Virginia Valley area, Harney Basin, southeastern Oregon.

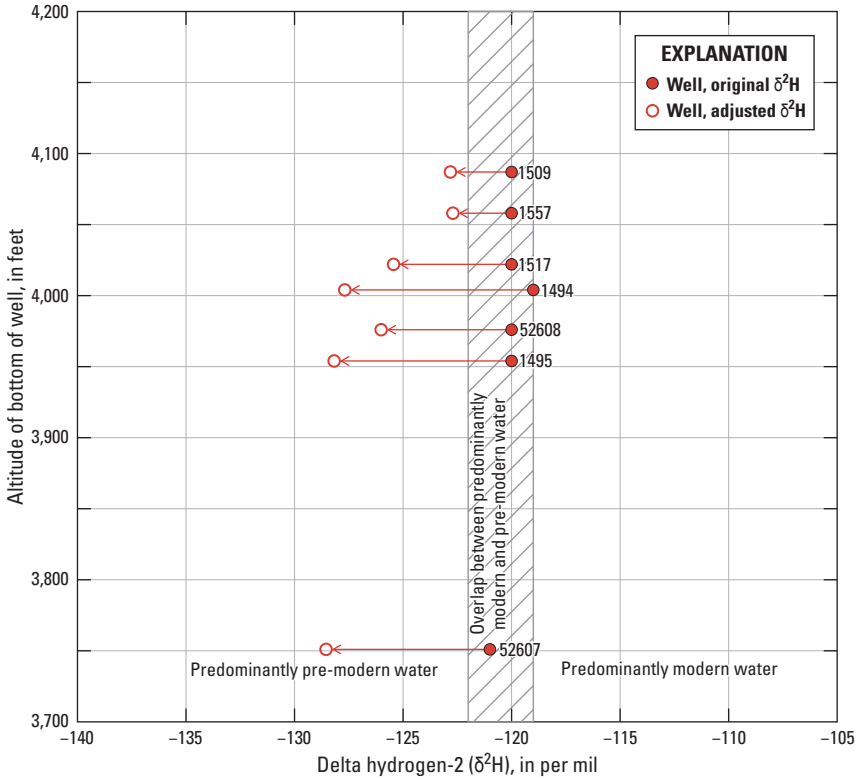

Figure 63. Relation between delta hydrogen-2 [δ^2H] and elevation of the bottom of the well for wells in the Virginia Valley area, Harney Basin, southeastern Oregon. The figure shows the measured δ^2H value (solid circles) and the δ^2H value adjusted to a deuterium excess of +3.52 ‰ (open circles).

The four ^{3}H samples collected from wells in this area were either tritium dead (HARN0052608 and HARN0001495) or had ^{3}H detected at 0.2 TU, which is at the detection limit (HARN0001494 and HARN0052607) and confirms that all or most of the water in these samples is pre-modern. The one ^{14}C sample from this area (HARN0052607) had a ^{14}C age of about 16,000 yrs and helped constrains the age of the pre-modern groundwater component in this area. Interestingly, it is younger than many of the ^{14}C ages obtained from wells in the central parts of the Harney Basin and further supports the idea of mixing between older groundwater from the basin center and somewhat younger groundwater with a source on or near Steens Mountain.

Seasonal groundwater-level fluctuations among wells in the Virginia Valley area during 2017–19 were about 5 ft, with highs in April–May and lows in September-October (for example, HARN0052607 in fig. 17*E*). Like other developed areas of the Harney Basin, peak groundwater levels occur in late winter prior to pumping for irrigation and lows occur at the end of the summer irrigation season. Groundwater elevations and seasonal groundwater-level fluctuations in the shallow and deep parts of the Voltage basalt HU filling Virginia Valley were nearly identical (HARN0052608, HARN0052607; fig. 17) and indicated little restriction to vertical movement of groundwater in this area, which is consistent with a hydrostratigraphic unit having a high vertical permeability. During 1960–90, groundwater levels in wells near Malheur Lake were weakly correlated with the water level in the lake and did not show any long-term increase or decline (fig. 64). Groundwater levels began declining in some areas sometime between 1990 and 2005–a more precise date cannot be determined due to a gap in groundwater-level monitoring during this period. During 2010–19, late winter groundwater levels declined 7–10 ft, or about 1 ft/yr, at HARN0001387 and HARN0001495 (fig. 64). Individual cones of depression are not observed around pumping centers in Virginia Valley, instead groundwater levels are declining more-or-less uniformly across the valley owing to the high permeability of the deposits.

Needs for Subsequent Monitoring and Research

This investigation was the first comprehensive hydrologic study of the entire Harney Basin. A large amount of data was collected and compiled from numerous sources, however the study was limited in duration and resources and was unable to address all temporal and spatial gaps in data. Effective management of groundwater in the Harney Basin will require ongoing monitoring of existing sites and establishing new sites to fill gaps that became apparent during this investigation.

Monitoring of groundwater levels and pumpage rates and volumes could be continued to track the response of the groundwater resources to further development, to guide and evaluate the effectiveness of management decisions, and to identify natural changes in recharge. Additional dedicated, multi-level clusters of monitoring wells, particularly in developed areas lacking sufficient dedicated observation-well data, would provide better information on connections between shallow and deep parts of the groundwater-flow system and practices implemented to stabilize groundwater levels. Areas where such well installations would be particularly useful include Bear Valley, Donner und Blitzen River floodplain, Sage Hen Valley, the upper and lower Silver Creek floodplains, and the flank of Steens Mountain (plate 1). An increase in the number of streamgages would help improve estimates of freshet volume and potential recharge in the Harney Basin lowlands. An improved understanding of the contribution of some of the larger intermittent streams (including Poison and Rattlesnake Creeks) to the freshet pulse would be extremely valuable. Only half of the surface water draining Steens Mountain is currently gaged. Flow measurements from springs, particularly the large springs in Warm Springs Valley, would be particularly helpful in understanding long-term system response to pumping and to climate fluctuations and trends. Collection of detailed geologic data (such as borehole geophysics, stratigraphy, and geochemistry) and hydrologic data (such as groundwater levels during the drilling operation, multi-well aquifer tests, and geochemistry) for each new well drilled would provide information to refine and improve the hydrostratigraphy and potentiometric-surface maps presented in this report. Surface geophysical surveys that better defined the extent of groundwater-level declines in shallow aquifers would improve understanding of current conditions within the groundwater-flow system. Continued geologic mapping of areas lacking detailed analysis would improve understanding of the region's permeability structure and probable groundwater flowpaths.

The response of the hydrologic system to changes in recharge induced by future changes in precipitation or land cover are not addressed in this study. Projections from global climate models for the Pacific Northwest indicate little change in annual mean rainfall, but bigger changes in 1) average annual temperatures, 2) in the timing of streamflow related to changing snowmelt and 3) altered forests due to increasing wildfire risk, insect and disease outbreaks, and longer-term shifts in forest types and species (Mote and others, 2014). The effects of these changes on future recharge estimates are unknown but potentially significant to future estimates of groundwater availability. The effects on the hydrologic system from these potential changes could be investigated with the aid of a numerical groundwater-flow model.

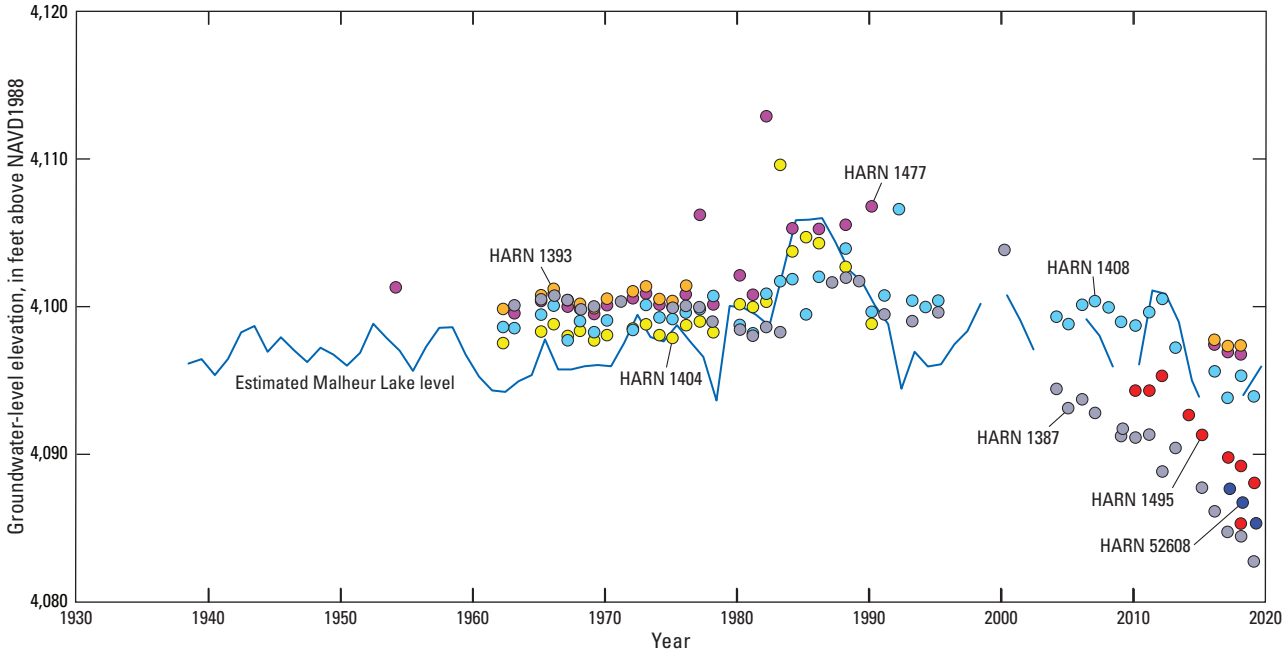

Figure 64. Groundwater levels during January–April at selected wells near Virginia Valley, Harney Basin, southeastern Oregon, 1930–2020. Estimated Malheur Lake level from U.S. Fish and Wildlife Service unpublished data. Colored dots correspond to well locations shown on figure 61. NAVD, North American Vertical Datum of 1988.

A numerical model can additionally address a variety of groundwater-management questions such as:

- How can the rates and distribution of pumpage be adjusted to provide maximum groundwater or economic benefit to the community while keeping undesired effects within acceptable limits?
- Will certain areas recover more quickly or more slowly after groundwater-management changes are implemented, and should they be managed differently?
- Where can short-term (seasonal) groundwater management strategies be implemented effectively to achieve short-term (seasonal) results?
- What is the lateral and vertical extent of the groundwater response to groundwater-management changes when implemented in different areas?
- Can artificial recharge be effectively directed to critical areas to help maintain groundwater levels?
- How are climate variability and trends likely to affect groundwater availability in the coming decades?

Summary

Groundwater in the 5,240 square mile Harney Basin occurs within a locally productive aquifer system that this investigation subdivided into three hydraulically connected regions for comparison and analyses. The regions are distinguished by geography and level of resource development, the hydraulic properties of the local geology, location in the interconnected basin-wide groundwater-flow system, and local rate and magnitude of recharge and discharge. The demand for groundwater in the Harney Basin has increased in recent years, leading to groundwater-level declines and prompting the Oregon Water Resources Department in 2016 to cease issuing groundwater permits for additional development. The ability of the resource to sustain existing uses and to accommodate additional development was not well known, and uncertainty existed regarding the extent to which groundwater development would affect nearby areas. Also, the degree of interconnectedness of the hydrologic system in the basin was not well understood. These concerns led the OWRD to enter into a cooperative agreement with the USGS to conduct a groundwater-availability study of the Harney Basin. The objectives of this 4.5-year study were to (1) develop a quantitative conceptual understanding of the groundwater-flow system of the Harney Basin, and provide the framework to (2) develop numerical hydrologic models to test the conceptualization of the groundwater-flow system, accurately simulate its response to current conditions and proposed groundwater development, and provide a tool for exploring management options. This report provides a summary of the framework of the groundwater-flow system and supports the data needs for the future development of a numerical groundwater-flow model. A companion report titled Hydrologic Budget of the Harney Basin Groundwater System, Oregon, provides a detailed description of the hydrologic budget for the Harney Basin (Garcia and others, 2022) and is summarized in this report.

Groundwater flow in the Harney Basin uplands is controlled by the topography and the distribution of recharge, geology, and the location and elevation of upland streams, springs, and other areas of discharge. Upland groundwater flow is controlled primarily by topography due to low-permeability rocks, which results in short, shallow flowpaths whereby upland recharge largely is balanced by discharge at nearby upland streams and springs.

Annual groundwater recharge to the Harney Basin lowlands is estimated as 173,000 acre-ft/yr, and the annual lowland groundwater discharge is estimated as 283,000 acre-feet per year (acre-ft/yr). Under current conditions, the annual groundwater discharge exceeds annual recharge by about 110,000 acre-ft/yr, indicating the lowland hydrologic budget is out of balance. The major perturbation to the groundwater budget relative to pre-development conditions is groundwater pumpage for irrigation, municipal, commercial-industrial, residential, and stock use. About 152,000 acre-ft/yr of groundwater was pumped in the lowlands for all purposes in 2017–18, and irrigation use accounts for about 95 percent of the annual volume pumped.

Recharge to the Harney Basin lowlands is supplied from infiltrating surface water as streams and rivers flow out of the uplands onto the sediments forming the relatively flat lowlands and through groundwater inflow from the surrounding uplands. Surface-water infiltration provided about 116,000 acre-ft/yr, and groundwater inflow from upland areas is estimated to have provided about 49,000 acre-ft/yr for 1982–2016. Additionally, lowland recharge from groundwater-supplied irrigation water and other pumped groundwater was about 8,000 acre-ft/yr.

On the Harney Basin lowlands, groundwater primarily discharges by pumpage and evapotranspiration (ET) from plants with roots that penetrate to the water table or capillary fringe. Pumpage has increased from about 51,000 acre-ft/yr in 1991 to about 152,000 acre-ft/yr during 2017–18. The mean annual estimated natural lowland groundwater discharge through ET is about 119,000 acre-ft/yr. An estimated 34,000 acre-ft/yr discharges at lowland springs, most of which is accounted for in estimates of groundwater discharge through ET. Minor amounts of groundwater discharge to lakes (about 730 acre-ft/yr) or flow eastward to the adjacent Malheur River Basin (about 3,100 acre-ft/yr).

In the uplands, groundwater flows from higher to lower elevations and the groundwater elevation is mainly controlled by the elevations of streams and springs. Beneath the Harney Basin lowlands, the influence of topography is subtler, but groundwater generally still flows toward the lowest areas of the basin occupied by Malheur and Harney Lakes. Groundwater pumpage has lowered groundwater levels and has changed groundwater-flow directions beneath the Harney Basin lowlands in some areas. The amount of groundwater-level decline depends on the amount of pumpage and the geology where the pumpage is withdrawn. Generally, groundwater levels in the Harney Basin peak in the late winter or early springtime due to (1) recovery from irrigation pumpage stress, (2) loading of freshet water on the surface and re-saturation of sediments, and (3) infiltration and recharge of precipitation and runoff. Groundwater levels decline during the summer months as groundwater leaves the system through ET and groundwater pumpage.

Groundwater in the Donner und Blitzen River floodplain is at shallow depths in the alluvial sediments. South of Diamond Lane where the floodplain is relatively narrow, groundwater is predominantly discharging upward to the river through the underlying sediments and at springs along the contact between the floodplain and surrounding uplands. Geochemical data indicate that recently recharged groundwater circulates to a depth of at least 100 ft below the Donner und Blitzen River floodplain south of Diamond Lane and likely originates as infiltration from the surrounding uplands rather than infiltration from the Donner und Blitzen River. North of Diamond Lane, the floodplain widens considerably, and the river transitions to a losing system where surface water

recharges the groundwater. Groundwater is recharged by the infiltration of water from the Donner und Blitzen River, within the main-stem channel and in the surrounding, seasonally flooded wetlands of the Malheur NWR. Annual groundwater-level fluctuations along the Donner und Blitzen River floodplain are about 2–5 feet per year (ft/yr). During 2015–19, wells in the northern part of the floodplain closer to areas with more deep irrigation wells declined 3–6 feet. Shallow wells in the southern part of the floodplain do not show a trend of declining groundwater levels.

In the upper floodplain of Silver Creek, low-permeability sedimentary deposits extend downward from the ground surface and overlie an extensive higher-permeability lithologic sequence that is penetrated by many of the wells in the area. Groundwater recharge in this area is primarily from infiltration of surface water from Silver Creek and the surrounding floodplain that is covered by seasonal flooding and groundwater inflow from the low-permeability uplands. In most years Silver Creek streamflow fully infiltrates upstream of Highway 20, and the streambed is dry the remaining distance to Moon Reservoir. The presence of tritium in shallow groundwater along the length of the upper Silver Creek floodplain attests to the importance of surface-water infiltration as a source of recharge. Groundwater levels in the deeper parts of the system show a smaller lateral hydraulic gradient, fluctuate similarly about 3–4 ft annually, and show declines of about 0.5 ft/yr during 2015–19. Overall, groundwater levels declined less than 10 ft since 1980. Deep groundwater flows to the south and east toward a broad trough beginning near the western end of Juniper Ridge and stretching downgradient toward Warm Springs Valley and Harney Lake. Groundwater pumpage in the upper and lower floodplains of Silver Creek will ultimately reduce groundwater discharge in the downgradient areas, including the Warm Springs Valley.

In the Weaver Spring/Dog Mountain area, the relatively high-permeability Proximal vent deposits HU is surrounded by the lower-permeability Younger and Older basin fill HUs. Shallow and deep groundwater levels in this productive area seasonally fluctuate about 15 ft/yr. Because the surrounding rocks are of much lower permeability and cannot supply groundwater at a rate sufficient to balance the current groundwater extraction rate, groundwater pumpage has removed groundwater from storage and led to large year-to-year declines in groundwater-level in this part of the basin. Since 2016, late winter groundwater levels have declined as much as 8 ft/yr, and the water table has been lowered in some areas to more than 100–140 ft below the ground surface. The geochemical data demonstrate that very little young water recharges the Weaver Spring/Dog Mountain area and indicate that the groundwater-level recovery during autumn and winter is due to movement of old groundwater from the plateau and surrounding low-permeability Younger and Older basin fill HUs rather than infiltration of local precipitation. Prior to groundwater development, the bed of Harney Lake was the lowest level in this part of the hydrologic system; however, the hydraulic head in the Weaver Spring/Dog Mountain decline area is now nearly 90 ft lower than the bed of Harney Lake and is inducing groundwater flow northward from the area beneath Harney Lake and Malheur Lake. During 2010–19, late winter groundwater levels declined as much as 60 ft, or about 6 ft/yr.

In the Silvies River/Poison Creek floodplain, groundwater flows in the Younger and Older basin fill HUs that underlie the Harney Basin lowlands. The permeability of these deposits is highly variable depending on location and depth. Along the main river course, coarser-grained, moderately permeable alluvial deposits grade laterally to finer-grained, less-permeable deposits on either side of the main river channels. The deposits also become increasingly less permeable downstream and away from the uplands as increasingly finer sediments are deposited as the river approaches Malheur Lake. Surface-water infiltration along the Silvies River/Poison Creek floodplain provides most of the recharge to this area of the Harney Basin lowlands; a smaller amount is contributed by groundwater inflow from the northern uplands. Despite the importance of surface-water infiltration to recharge, geochemical data indicate that the infiltration and circulation of modern recharge is limited and generally restricted to the upper 100 ft and most of the groundwater underlying the Silvies River/Poison Creek floodplain is thousands of years old. Late winter groundwater levels in shallow wells were commonly 4–5 ft below ground surface during 1960–75 but had increased to 7–12 ft below ground surface during 2015–19. Deeper groundwater levels were historically about the same as shallow levels, but they are now about 25 ft below ground surface owing to groundwater pumpage. Away from the immediate vicinity of the Silvies River channel, seasonal groundwater-level fluctuations are about 5 ft/yr.

Along the northern edge of the Harney Basin lowlands, stretching from the Prater Creek to the Mahon Creek floodplains, groundwater flows in the Younger and Older basin fill HUs that underlie the Harney Basin lowlands. Recharge to the groundwater in this area occurs primarily during the springtime freshet when the small, intermittent streams in the uplands flow onto the lowlands and lose water to the subsurface through relatively coarse deposits near the mountain front. Although infiltration of freshet water is the principal recharge source, geochemical data indicate that the volume of this recharge is limited and attest to the ancient age of the deep groundwater in this area. Some groundwater likely recharges the floodplain deposits as direct groundwater inflow from the low-permeability uplands to the north where groundwater levels are higher. The permeability of the basin fill is highly variable depending on location and depth. The deposits likely become increasingly less permeable downstream and away from where the streams first enter the lowlands. Groundwater levels in shallow wells throughout the area are generally 5–20 ft below the ground surface, and well yields are typically low. Seasonal groundwater-level fluctuations in the shallow wells are about 6–10 ft. Deeper wells near the mountain front commonly encounter higher-permeability deposits, and many have relatively high yields and transmissivities. Due to pumpage

at depth, late winter groundwater levels in the deeper wells drilled into the Older basin fill HU are 20 ft to more than 90 ft lower than groundwater levels in shallower wells. These pronounced depressions in hydraulic head of the deeper part of the system are muted at shallower depths near the water table due to low vertical permeability of deposits separating the shallow and deep parts of the groundwater-flow system in this area. Groundwater levels in deeper wells seasonally fluctuate as much as 110 ft north of Highway 20 and about 30–40 ft farther south with the greatest level of seasonal drawdown occurring in August. During 2008–18, late winter groundwater-levels in deep wells declined as much as 50 feet or nearly 5 feet per year.

In the Crane area, higher-permeability deposits along the eastern margin of the Harney Basin lowlands provide groundwater to many of the irrigation wells in the area, but the basin fill becomes increasingly finer-grained westward toward the center of the basin. This area is far from the major recharge sources in the Harney Basin and the large proportion of pre-modern water in well samples indicates that the amount of modern recharge is very small. The natural groundwater-flow direction is generally southwest toward Malheur Lake, with a minimal gradient; however, groundwater pumping has led to several areas of groundwater-level decline causing a much steeper gradient toward these pumping centers. In some places the depth to groundwater in late winter 2019 exceeded 60 ft, whereas prior to development it was only 10–20 ft deep. Seasonal groundwater-level fluctuations in the shallow wells are typically about 6–10 ft, but fluctuations at deeper wells are greater–as much as 40 ft. Long-term groundwater-level decline rates have been relatively consistent since 2010. During 2010–19, late winter groundwater levels declined 7–20 ft, or about 1–2 ft/yr.

Groundwater in the Virginia Valley area is flowing in the Younger basin fill HU and underlying lava flows of the Voltage basalt HU. Groundwater flow is to the east through the highly permeable Voltage basalt HU toward the Malheur River Basin. Geochemical data indicate that the groundwater in this area is a result of mixing between older groundwater from the Harney Basin center and somewhat younger groundwater with a source on or near Steens Mountain. The high regional permeability results in relatively small seasonal groundwater-level fluctuations, which were about 5 ft during 2017–19. Although the high-permeability deposits in this area minimize the development of large, deep drawdown cones, groundwater pumpage has affected groundwater levels across a broad area. During 2010–19, late winter groundwater levels in the Virginia Valley area declined 7–10 ft, or about 1 ft/yr.

A primary goal of this study was to greatly improve understanding of the regional groundwater-flow system in the Harney Basin to help resource managers and basin residents develop a strategy for managing the basin's groundwater. Developing such a strategy will require consideration of Oregon's water laws and characteristics of groundwater flow in general and for the Harney Basin in particular. Generally, increases in the annual volume of pumpage from the basin's groundwater-flow system will lead to groundwater-level declines and eventually be offset by diminished rates of natural discharge to springs and surface water. In some circumstances, the lowering of hydraulic head caused by pumpage could decrease the availability of groundwater for phreatophytes in riparian and wetland areas.

The timing and distribution of the effects of groundwater use are dictated to a large degree by the location and depth of pumpage. Pumpage is commonly greatest in the areas where higher-permeability geologic units allow for higher well yields. However, in the Harney Basin, many of these higher-permeability units are bounded by geologic units of much lower permeability through which groundwater can't flow rapidly enough to replenish the areas of greatest withdrawal, resulting in groundwater-level declines.

References Cited

Abatzoglou, J., 2012, Gridded meteorological datasets for the contiguous United States: U.S. Geological Survey data release, https://www.sciencebase.gov/catalog/item/520a6d2ae4b0026c2bc3d9f9.

Aquaveo, L.L.C., 2012, Harney Basin groundwater study: Aquaveo, LLC, 104 p.

Bauer, H.H., and Vaccaro, J.J., 1987, Documentation of a deep percolation model for estimating ground-water recharge: U.S. Geological Survey Open-File Report 86-536, 180 p. [Also available at https://doi.org/10.3133/ofr86536.]

Beamer, J.P., Huntington, J.L., Morton, C.G., and Pohll, G.M., 2013, Estimating annual groundwater evapotranspiration from phreatophytes in the Great Basin using Landsat and flux tower measurements: Journal of the American Water Resources Association, v. 49, no. 3, p. 518–533. [Also available at https://doi.org/10.1111/jawr.12058.]

Beamer, J.P., and Hoskinson, M.D., 2021, Historical irrigation water use and groundwater pumpage estimates in the Harney Basin, Oregon, 1991-2018: Oregon Water Resources Department Open File Report No. 2021-02, 53 p. [Also available at https://www.oregon.gov/owrd/wrdreports/OWRD_OFR_2021-02_Harney_Basin_METRIC_Irrigation_Use_Report.pdf.]

Bense, V., and van Balen, R., 2003, Hydrogeological aspects of fault zones on various scales in the Roer Valley Rift System: Journal of Geochemical Exploration, v. 78-79, p. 317–320. [Also available at https://doi.org/10.1016/S0375-6742(03)00031-1.]

Benson, L.V., 1981, Paleoclimatic significance of lake-level fluctuations in the Lahontan Basin: Quaternary Research, v. 16, no. 3, p. 390–403 [Also available at https://doi.org/10.1016/0033-5894(81)90018-1].

Benson, L.V., Currey, D.R., Dorn, R.I., Lajoie, K.R., Oviatt, C.G., Robinson, S.W., Smith, G.I., and Stine, S., 1990, Chronology of expansion and contraction of four great Basin lake systems during the past 35,000 years: Palaeogeography, Palaeoclimatology, Palaeoecology, v. 78, no. 3-4, p. 241–286. [Also available at https://doi.org/10.1016/0031-0182(90)90217-u.]

Biasi, J.A., 2019, Uplift history of Steens Mountain and onset of Basin and Range extension in eastern Oregon: Geological Society of America Abstracts with Programs, v. 51, no. 4.

Bondre, N.R., and Hart, W.K., 2008, Morphological and textural diversity of the Steens Basalt lava flows, Southeastern Oregon, USA—Implications for emplacement style and nature of eruptive episodes: Bulletin of Volcanology, v. 70, no. 8, p. 999–1019. [Also available at https://doi.org/10.1007/s00445-007-0182-x.]

Boschmann, D.E., 2021, Generalized geologic compilation map of the Harney Basin, Oregon: Oregon Water Resources Department Open File Report 2021-01, 57 p [Also available at https://www.oregon.gov/owrd/wrdreports/OFR_2021-01_report.pdf].

Bredehoeft, J.D., Belitz, K., and Sharp-Hansen, S., 1992, The hydrodynamics of the Big Horn Basin—A study of the role of faults: The American Association of Petroleum Geologists Bulletin, v. 76, no. 4, p. 530–546. [Also available at http://pubs.er.usgs.gov/publication/70017289.]

Brooks, H.C., 1979, Plate tectonics and the geologic history of the Blue Mountains: Oregon Geology, v. 41, no. 5, p. 71–80. [Also available at https://www.oregongeology.org/pubs/og/OGv41n05.pdf.]

Brooks, H.C., and Vallier, T.L., 1978, Mesozoic rocks and tectonic evolution of eastern Oregon and western Idaho, *in* Howell, D.G., and McDougal, K.A., eds., Mesozoic paleogeography of the western United States: Los Angeles, California, p. 133–146. [Also available at http://archives.datapages.com/data/pac_sepm/021/021001/pdfs/133.]

Brown, C.E., and Thayer, T.P., 1963, Low-grade mineral facies in Upper Triassic and Lower Jurassic rocks of the Aldrich Mountains, Oregon: Journal of Sedimentary Petrology, v. 33, no. 2, p. 411–425. [Also available at https://doi.org/10.1306/74D70E70-2B21-11D7-8648000102C1865D.]

Brown, C.E., and Thayer, T.P., 1966a, Geologic map of the Canyon City quadrangle, northeastern Oregon: U.S. Geological Survey IMAP 447, scale 1:250,000. [Also available at https://doi.org/10.3133/i447.]

Brown, C.E., and Thayer, T.P., 1966b, Geologic map of the Mount Vernon Quadrangle, Grant County, Oregon: U.S. Geological Survey Geologic Quadrangle Map GQ-548, scale 1:62,500. [Also available at https://doi.org/10.3133/gq548.]

Brown, C.E., and Thayer, T.P., 1977, Geologic map of the pre-Tertiary rocks in the eastern Aldrich Mountains and adjacent areas to the south, Grant County, Oregon: U.S. Geological Survey Miscellaneous Investigations Series Map I-1021, scale 1:62,500. [Also available at https://doi.org/10.3133/gq548.]

Brown, D.E., 1982, Map showing geology and geothermal resources of the southern half of the Burns 15 minute quadrangle, Oregon: Oregon Department of Geology and Mineral Industries Geologic Map Series GMS-20, scale 1:24,000. [Also available at https://www.oregongeology.org/pubs/gms/GMS-020.pdf.]

Brown, D.E., McLean, G.D., and Black, G.L., 1980a, Preliminary geology and geothermal resource potential of the northern Harney Basin, Oregon: Oregon Department of Geology and Mineral Industries Open File Report 0-80-6, 52 p. [Also available at https://www.oregongeology.org/pubs/ofr/O-80-06.pdf.]

Brown, D.E., McLean, G.D., and Black, G.L., 1980b, Preliminary geology and geothermal resource potential of the southern Harney Basin, Oregon: Oregon Department of Geology and Mineral Industries Open File Report 0-80-7, 90 p. [Also available at https://www.oregongeology.org/pubs/ofr/O-80-07.pdf.]

Camp, V.E., and Ross, M.E., 2004, Mantle dynamics and genesis of mafic magmatism in the intermontane Pacific Northwest: Journal of Geophysical Research. Solid Earth, v. 109, no. B8. [Also available at https://doi.org/10.1029/2003JB002838.]

Camp, V.E., Ross, M.E., Duncan, R.A., Jarboe, N.A., Coe, R.S., Hanan, B.B., and Johnson, J.A., 2013, The Steens basalt—Earliest lavas of the Columbia River Basalt Group, *in* Reidel, S.P., Camp, V.E., Ross, M.E., Wolff, J.A., Martin, B.S., Tolan, T.L., and Wells, R.E., eds., The Columbia River Flood Basalt Province: Geological Society of America Special Paper 497, p. 87–116. [Also available at https://doi.org/10.1130/SPE497.]

Cerling, T.E., and Quade, J., 1993, Stable carbon and oxygen isotopes in soil carbonates, *in* Swart, P.K., Lohmann, K.C., Mckenzie, J., and Savin, S., eds., Climate change in continental isotopic records. American Geophysical Union, p. 217–231 [Also available at https://doi.org/10.1029/GM078p0217].

Cerling, T.E., Solomon, D.K., Quade, J., and Bowman, J.R., 1991, On the isotopic composition of carbon in soil carbon dioxide: Geochimica et Cosmochimica Acta, v. 55, no. 11, p. 3403–3405. [Also available at https://doi.org/10.1016/0016-7037(91)90498-T.]

Claassen, H.C., and Downey, J.S., 1995, A model for deuterium and oxygen 18 isotope changes during evergreen interception of snowfall: Water Resources Research, v. 31, no. 3, p. 601–618. [Also available at https://doi.org/10.1029/94WR01995.]

Clark, I.D., and Fritz, P., 1997, Environmental isotopes in hydrogeology: Boca Raton, Florida, CRC Press, LLC, 328 p.

Clayton, R.N., and Degens, E.T., 1959, Use of carbon isotope analyses of carbonates for differentiating fresh-water and marine sediments: AAPG Bulletin, v. 43, no. 4, p. 890–897. [Also available at https://doi.org/10.1306/0BDA5CF6-16BD-11D7-8645000102C1865D.]

Cohen, A., Palacios-Fest, M., Negrini, R., Wigand, P., and Erbes, D., 2000, A paleoclimate record for the past 250,000 years from Summer Lake, Oregon, USA—II. Sedimentology, paleontology and geochemistry: Journal of Paleolimnology, v. 24, no. 2, p. 151–182. [Also available at https://doi.org/10.1023/A:1008165326401.]

Cooper, H.H., and Jacob, C.E., 1946, A generalized graphical method for evaluating formation constants and summarizing well field history: Washington, D.C., Eos (Washington, D.C.), v. 27, no. 4, p. 526–534. [Also available at https://doi.org/10.1029/TR027i004p00526.]

Cooper, L., 1998, Isotopic fractionation in snow cover, *in* Kendall, C., and MCDonnell, J.J., eds., Isotope tracers in catchment hydrology: Amsterdam, The Netherlands, Elsevier, p. 119–136. [Also available at https://doi.org/10.1016/B978-0-444-81546-0.50011-2.]

Corson-Dosch, N.T., and Garcia, C.A., 2022, Soil-water-balance (SWB) model archive used to simulate mean annual upland recharge from infiltration of precipitation and snowmelt in Harney Basin, Oregon, 1982–2016: U.S. Geological Survey data release, http://doi.org/10.5066/P94NH4D8.

Cox, C., Keller, G.R., and Harder, S.H., 2013, A controlled-source seismic and gravity study of the High Lava Plains (HLP) of Eastern Oregon: Geochemistry Geophysics Geosystems, v. 14, no. 12, p. 5208–5226. [Also available at https://doi.org/10.1002/2013gc004870.]

Cunningham, W.L., and Schalk, C.W., 2011, Groundwater technical procedures of the U.S. Geological Survey: U.S. Geological Survey Techniques and Methods 1–A1, 151 p. [Also available at https://pubs.usgs.gov/tm/1a1/.]

Davis, S.N., and DeWiest, R.J.M., 1966, Hydrogeology: New York, John Wiley & Sons, 463 p.

Dicken, S.N., 1950, Oregon geography—First preliminary edition: Ann Arbor, Michigan, Edwards Brothers, Inc., 104 p.

Dickinson, W.R., 1979, Mesozoic forearc basin in central Oregon: Geology, v. 7, no. 4, p. 166–170. [Also available at https://doi.org/10.1130/0091-7613(1979)7<166:MFBICO>2.0.CO;2.]

Dickinson, W.R., and Thayer, T.P., 1978, Paleogeographic and paleotectonic implications of Mesozoic stratigraphy and structure in the John Day inlier of central Oregon, *in* Howell, D.G., and McDougall, K.A., eds., Mesozoic paleogeography of the western United States: Los Angeles, p. 147–161. [Also available at https://archives.datapages.com/data/pac_sepm/021/021001/pdfs/147.htm.]

Dörr, H., and Münnich, K.O., 2016, Carbon-14 and carbon-13 in soil CO_2: Radiocarbon, v. 22, no. 3, p. 909–918. [Also available at https://doi.org/10.1017/s0033822200010316.]

Dugas, D.P., 1998, Late Quaternary variations in the level of paleo-Lake Malheur, eastern Oregon: Quaternary Research, v. 50, no. 3, p. 276–282. [Also available at https://doi.org/10.1006/qres.1998.2005.]

Eaton, G.P., 1982, The Basin and Range province—Origin and tectonic significance: Annual Review of Earth and Planetary Sciences, v. 10, no. 1, p. 409–440. [Also available at https://doi.org/10.1146/annurev.ea.10.050182.002205.]

Evans, J.G., and Geisler, T.M., 2001, Geologic field-trip guide to Steens Mountain Loop Road, Harney County, Oregon: U.S. Geological Survey Bulletin 2183, 15 p. [Also available at https://doi.org/10.3133/b2183.]

Feibelkorn, R.B., Walker, G.W., MacLeod, N.S., McKee, E.H., and Smith, J.G., 1982, Index to K-Ar age determinations for the state of Oregon: Isochron/West, v. 37, no. 3-60. [Also available at https://pubs.er.usgs.gov/publication/ofr82596.]

Fetter, C.W., 2001, Applied Hydrogeology 4th ed.: Upper Saddle River, New Jersey, Prentice-Hall, Inc., 598 p.

Ford, M.T., Grunder, A.L., and Duncan, R.A., 2013, Bimodal volcanism of the High Lava Plains and Northwestern Basin and Range of Oregon—Distribution and tectonic implications of age-progressive rhyolites: Geochemistry Geophysics Geosystems, v. 14, no. 8, p. 2836–2857. [Also available at https://doi.org/10.1002/ggge.20175.]

Freeze, R.A., and Cherry, J.A., 1979, Groundwater: Englewood Cliffs, New Jersey, Prentice-Hall, Inc., 604 p.

Friedman, I., Smith, G.I., Johnson, C.A., and Moscati, R.J., 2002, Stable isotope compositions of waters in the Great Basin, United States 2—Modern precipitation: Journal of Geophysical Research-Atmospheres, v. 107, no. D19, p. ACL 15-11-ACL 15-22. [Also available at https://doi.org/10.1029/2001jd000566.]

Fuller, R.E., 1931, The geomorphology and volcanic sequence of Steens Mountain in southeastern Oregon: University of Washington Publications in Geology, v. 3, p. 1–130. [Available at http://npshistory.com/publications/geology/state/wa/uw-1931-3-1/intro.htm.]

Garcia, C.A., Corson-Dosch, N.T., Beamer, J.P., Overstreet, B.T., Haynes, J.V., Grondin, G.H., Gingerich, S.B., and Hoskinson, M.D., 2022, Hydrologic budget of the Harney Basin groundwater system, Oregon: U.S. Geological Survey Scientific Investigations Report 2021-5128, 140 p. [Also available at https://doi.org/10.3133/sir20215128.]

Gardner, P.M., and Heilweil, V.M., 2014, A multiple-tracer approach to understanding regional groundwater flow in the Snake Valley area of the eastern Great Basin, USA: Applied Geochemistry, v. 45, p. 33–49. [Also available at https://doi.org/10.1016/j.apgeochem.2014.02.010.]

Gingerich, S.B., Johnson, H.M., Boschmann, D.E., Grondin, G.H., and Garcia, C.A., 2021, Contour dataset of the potentiometric surfaces of shallow and deep groundwater-level altitudes in Harney Basin, Oregon, February–March 2018: U.S. Geological Survey data release, https://doi.org/10.5066/P9ZJTZUV.

Gingerich, S.B., Johnson, H.M., Boschmann, D.E., Grondin, G.H., Garcia, C.A., and Schibel, H.J., 2022, Location information, discharge, and water-quality data for selected wells, springs, and streams in the Harney Basin, Oregon: U.S. Geological Survey. [Also available at http://doi.org/10.5066/P9J0FE5M.]

Gonthier, J.B., Collins, C.A., and Anderson, D.B., 1977, Ground-water data for the Drewsey Resource Area, Harney and Malheur Counties, Oregon: U.S. Geological Survey Open-File Report 77-741, 28 p. [Also available at https://doi.org/10.3133/ofr77741.]

Gonthier, J.B., 1985, A description of aquifer units in eastern Oregon: U.S. Geological Survey Water-Resources Investigations Report 84-4095, 39 p. [Also available at https://doi.org/10.3133/wri844095.]

Greene, R.C., 1972, Preliminary geologic map of the Burns and West Myrtle Butte 15-minute quadrangles, Oregon: U.S. Geological Survey Miscellaneous Field Studies Map MF-320, scale 1:62,500. [Also available at https://doi.org/10.3133/i680.]

Greene, R.C., 1973, Petrology of the welded tuff of Devine Canyon, southeastern Oregon: U.S. Geological Survey Professional Paper 797, 26 p. [Also available at https://doi.org/10.3133/pp797.]

Greene, R.C., Walker, G.W., and Corcoran, R.E., 1972, Geologic map of the Burns quadrangle, Oregon: U.S. Geological Survey Miscellaneous Geologic Investigations Map I-680, scale 1:250,000. [Also available at https://doi.org/10.3133/i680.]

Grondin, G.H., 2021, Methods and results for estimating groundwater pumped, returned, and consumed for non-irrigation uses in the Harney Basin, Oregon: Oregon Water Resources Department Open File Report 2021-03, 28 p. plus appendices [Also available at https://www.oregon.gov/owrd/wrdreports/OWRD_OFR_2021-003_Harney_Basin_non_irrigation_GW_use_report_stamped.pdf.]

Grondin, G.H., Boschmann, D.E., Schibel, H.J., and Scandella, B.P., 2021, Methods and results for estimating the hydraulic characteristics of the subsurface materials in the Harney Basin, Oregon: Oregon water Resources Department Open File Report 2021-04, 63 p. [Also available at https://www.oregon.gov/owrd/wrdreports/OFR_2021-04_Harney_Basin_subsurface_hydraulic_properties.pdf.]

Han, L.-F., Niel Plummer, L., and Aggarwal, P., 2014, The curved ^{14}C vs. $\delta^{13}C$ relationship in dissolved inorganic carbon—A useful tool for groundwater age- and geochemical interpretations: Chemical Geology, v. 387, p. 111–125. [Also available at https://doi.org/10.1016/j.chemgeo.2014.08.026.]

Heath, R.C., 1983, Basic ground-water hydrology: U.S. Geological Survey Water Supply Paper 2220, 86 p. [Also available at https://doi.org/10.3133/wsp2220.]

Hemphill-Haley, M.A., Page, W.D., Carver, G.A., and Burke, R.M., 2000, Paleoseismicity of the Alvord fault, Steens Mountain, southeastern Oregon: Quaternary Geochronology— Methods and Applications, v. 4, p. 537–540. [Also available at https://doi.org/10.1029/RF004p0537.]

Holmes, D.A., 1990, Pacific Northwest zeolite update, *in* Geitgey, R.P., and Vogt, B.V., eds., Industrial rocks and minerals of the Pacific Northwest—Oregon Department of Geology and Mineral Industries Special Paper 23 p. 79–88. [Also available at https://www.oregongeology.org/pubs/sp/SP-23.pdf.]

Houston, R.A., McClaughry, J.D., Duda, C.J.M., and Niewendorp, C.A., 2018, Geologic map of the Devine Ridge North 7.5' quadrangle, Harney County, Oregon: Oregon Department of Geology and Mineral Industries Geologic Map Series GMS-121, scale 1:24,000. [Also available at https://www.oregongeology.org/pubs/gms/p-GMS-121.htm.]

Hua, Q., Barbetti, M., and Rakowski, A.Z., 2013, 2013, Atmospheric radiocarbon for the period 1950–2010: Radiocarbon, v. 55, no. 4, p. 2059–2072. [Also available at https://doi.org/10.2458/azu_js_rc.v55i2.16177.]

Hubbard, L.L., 1975, Hydrology of Malheur Lake, Harney County, southeastern Oregon: U.S. Geological Survey Water-Resources Investigations Report 75-21, 40 p. [Also available at https://doi.org/10.3133/wri7521.]

Hudson, A.M., Quade, J., Ali, G., Boyle, D., Bassett, S., Huntington, K.W., De los Santos, M.G., Cohen, A.S., Lin, K., and Wang, X., 2017, Stable C, O and clumped isotope systematics and ^{14}C geochronology of carbonates from the Quaternary Chewaucan closed-basin lake system, Great Basin, USA—Implications for paleoenvironmental reconstructions using carbonates: Geochimica et Cosmochimica Acta, v. 212, p. 274–302. [Also available at https://doi.org/10.1016/j.gca.2017.06.024.]

Johnson, J.A., 1995, Geologic evolution of the Duck Creek Butte eruptive center, High Lava Plains, southeastern Oregon: Corvallis, Oregon, Oregon State University, Masters Thesis, 151 p. [Also available at https://ir.library.oregonstate.edu/concern/graduate_thesis_or_dissertations/bn999b569.]

Johnson, J.A., Hawkesworth, C.J., Hooper, P.R., and Binger, G.B., 1998, Major- and trace-element analyses of Steens Basalt, southeastern Oregon U.S. Geological Survey Open-File Report 98-482, 30 p. [Also available at https://doi.org/10.3133/ofr98482.]

Jordan, B.T., Grunder, A.L., Duncan, R.A., and Deino, A.L., 2004, Geochronology of age-progressive volcanism of the Oregon High Lava Plains—Implications for the plume interpretation of Yellowstone: Journal of Geophysical Research. Solid Earth, v. 109, no. B10. [Also available at https://doi.org/10.1029/2003jb002776.]

Jurgens, B.C., Böhlke, J.K., and Eberts, S.M., 2012, TracerLPM (Version 1)—An Excel® workbook for interpreting groundwater age distributions from environmental tracer data: U.S. Geological Survey Techniques and Methods 4-F3, 60 p. [Also available at https://doi.org/10.3133/tm4F3.]

Kohn, M.J., 2010, Carbon isotope compositions of terrestrial C3 plants as indicators of (paleo)ecology and (paleo)climate: Proceedings of the National Academy of Sciences of the United States of America, v. 107, no. 46, p. 19,691–19,695. [Also available at https://doi.org/10.1073/pnas.1004933107.]

Laczniak, R.J., Flint, A.L., Moreo, M.T., Knochenmus, L.A., Lundmark, K.W., Pohll, G., Carroll, R.W.H., Smith, J.L., Welborn, T.L., Heilweil, V.M., Pavelko, M.T., Hershey, R.L., Thomas, J.M., Earman, S., and Lyles, B.F., 2008, Ground-water budgets: U.S. Geological Survey Scientific Investigations Report 2007-5261, 43–68 p. [Also available at https://doi.org/10.3133/sir20075261.]

Lawrence, R.D., 1976, Strike-slip faulting terminates the Basin and Range province in Oregon: Geological Society of America Bulletin, v. 87, no. 6, p. 846–850. [Also available at https://doi.org/10.1130/0016-7606(1976)87<846:SFTTBA>2.0.CO;2.]

Leonard, A.R., 1970, Ground-water resources in Harney Valley, Harney County, Oregon: Oregon State Engineers Office Ground Water Report 16, 85 p.

Lohman, S.W., 1972, Ground-water hydraulics: U.S. Geological Survey Professional Paper 708, 70 p. [Also available at https://doi.org/10.3133/pp708.]

Lyle, M., Heusser, L., Ravelo, C., Yamamoto, M., Barron, J., Diffenbaugh, N.S., Herbert, T., and Andreasen, D., 2012, Out of the tropics—The Pacific, Great Basin lakes, and late Pleistocene water cycle in the western United States: Science, v. 337, no. 6102, p. 1629–1633. [Also available at https://doi.org/10.1126/science.1218390.]

MacLeod, N.S., Walker, G.W., and McKee, E.H., 1975, Geothermal significance of eastward increase in age of upper Cenozoic rhyolitic domes in southeastern Oregon: U.S. Geological Survey Open-File Report 75-348, 22 p.[Also available at https://doi.org/10.3133/ofr75348.]

Mayer, A., May, W., Lukkarila, C., and Diehl, J., 2007, Estimation of fault-zone conductance by calibration of a regional groundwater flow model—Desert Hot Springs, California: Hydrogeology Journal, v. 15, no. 6, p. 1093–1106. [Also available at https://doi.org/10.1007/s10040-007-0158-0.]

McClaughry, J.D., Duda, C.J., and Ferns, M.L., 2019, Geologic map of the Poison Creek and Burns 7.5' quadrangles, Harney County, Oregon: Oregon Department of Geology and Mineral Industries Geologic Map Series GMS-123, scale 1:24,000. [Also available at https://www.oregongeology.org/pubs/gms/p-GMS-123.htm.]

Meigs, A., Scarberry, K., Grunder, A., Carlson, R., Ford, M.T., Fouch, M., Grove, T., Hart, W.K., Iademarco, M., Jordan, B., and Milliard, J., 2009, Geological and geophysical perspectives on the magmatic and tectonic development, High Lava Plains and northwest Basin and Range, *in* O'Connor, J.E., Dorsey, R.J., and Madin, I.P., eds., Volcanoes to vineyards—Geologic field trips through the dynamic landscape of the Pacific Northwest—Geological Society of America Field Guide, p. 135–470. [Also available at https://doi.org/10.1130/2009.fld015(21).]

Minor, S.A., Rytuba, J.J., Grubensky, M.J., Vander Muelen, D.B., Goeldner, C.A., and Tegtmeyer, K.J., 1987, Geologic map of the High Steens and Little Blitzen Gorge Wilderness study areas, Harney County, Oregon: U.S. Geological Survey Miscellaneous Field Studies Map MF-1876, scale 1:24000. [Also available at https://doi.org/10.3133/mf1876.]

Moore, N.E., Grunder, A.L., and Bohrson, W.A., 2018, The three-stage petrochemical evolution of the Steens Basalt [southeast Oregon, USA] compared to large igneous provinces and layered mafic intrusions: Geosphere, v. 14, no. 6, p. 2505–2532. [Also available at https://doi.org/10.1130/Ges01665.1.]

Mote, P., Snover, A.K., Eigenbrode, S.D., Glick, P., Littell, J., Raymondi, R., and Reeder, S., 2014, Chapter 21—Northwest, *in* Melillo, J.M., Richmond, T.T.C., and Yohe, G.W., eds., Climate change impacts in the United States—The Third National Climate Assessment: U.S. Global Change Research Program, p. 487-513. [Also available at https://doi.org/10.7930/J04Q7RWX.]

Niewendorp, C.A., Duda, C.J.M., Houston, R.A., and McClaughry, J.D., 2018, Geologic map of the Devine Ridge South 7.5' quadrangle, Harney County, Oregon: Oregon Department of Geology and Mineral Industries Geologic Map Series GMS-120, scale 1:24,000. [Also available at https://www.oregongeology.org/pubs/gms/p-GMS-120.htm.]

Oldow, J.S., and Singleton, E.S., 2008, Application of terrestrial laser scanning in determining the pattern of late Pleistocene and Holocene fault displacement from the offset of pluvial lake shorelines in the Alvord extensional basin, northern Great Basin, USA: Geosphere, v. 4, no. 3, p. 536–563. [Also available at https://doi.org/10.1130/Ges00101.1.]

Oregon Biodiversity Information Center, 2010, Ecological systems map of Oregon: Oregon Biodiversity Information Center. [Also available at https://spatialdata.oregonexplorer.info/geoportal/details;id=776e6118422b429c8c3024f289f9f192.]

Oregon Department of Environmental Quality, 2021, AWQMS—Ambient water quality monitoring system: Oregon Department of Environmental Quality, accessed February 6, 2021 at https://www.oregon.gov/deq/wq/Pages/WQdata.aspx.

Oregon Water Resources Board, 1967, Sixth biennial report, various basin studies completed as of June 30 1967 including North Coast. Mid Coast, South Coast, Willamette, Umpqua, Rogue, Sandy, Hood, Deschutes, Goose, and Summer Lakes, John Day, Umatilla, Malheur Lake, Grande Ronde, and Powder, 40 p.

Oregon Water Resources Department, 2016, Rule 690-512-0020—Groundwater use in the Greater Harney Valley Groundwater Area of Concern: Oregon Secretary of State, accessed July 7, 2020, at https://secure.sos.state.or.us/oard/viewSingleRule.action?ruleVrsnRsn=180246.

Oregon Water Resources Department [OWRD], 2019, Groundwater information system: Oregon Water Resources Department, accessed August 28, 2019, at https://apps.wrd.state.or.us/apps/gw/gw_info/gw_info_report/Default.aspx.

Parker, D.J., and Armstrong, R.L., 1972, K-Ar dates and Sr isotope initial ratios for volcanic rocks in the Harney Basin, Oregon: Isochron-West, v. 5, p. 7–12.

Personius, S.F., Dart, R.L., Bradley, L.-A., and Haller, K.M., 2003, Map and data for Quaternary faults and folds in Oregon: U.S. Geological Survey Open File Report 03-095, 550 p. [Also available at https://doi.org/10.3133/ofr0395.]

Peterson, N.V., and Groh, E.A., 1964, Diamond Craters, Oregon: The Ore Bin, v. 26, no. 2, p. 17–34. [Also available at https://doi.org/10.1029/92TC02950.]

Pezzopane, S.K., and Weldon, R.J., II, 1993, Tectonic role of active faulting in central Oregon: Tectonics, v. 12, no. 5, p. 1140–1169. [Also available at https://doi.org/10.1029/92TC02950.]

Piper, A.M., Robinson, T.W., and Park, C.F., 1939, Geology and ground-water resources of the Harney Basin, Oregon, with a statement on precipitation and tree growth: U.S. Geological Survey Water Supply Paper 841, 189 p. [Also available at https://doi.org/10.3133/wsp841.]

Plummer, L.N., and Glynn, P.D., 2013, Radiocarbon dating in groundwater systems, Isotope Methods For Dating Old Groundwater: Vienna, Austria, International Atomic Energy Agency, p. 33–89.

PRISM Climate Group, 2019, Parameter-Elevation Regressions on Independent Slopes Model (PRISM) for 1981–2010: Oregon State University, accessed November 15, 2019, at http://prism.oregonstate.edu.

Reed, J.E., Bedinger, M.S., and Gonthier, J.B., 1984a, Maps showing ground-water levels, springs, and depth to ground water, Basin and Range Province: Oregon Water-Resources Investigations Report 83-4120B. [Also available at https://doi.org/10.3133/wri834120B.]

Reed, J.E., Bedinger, M.S., and Gonthier, J.B., 1984b, Maps showing ground-water units and number of large capacity wells, Basin and Range province: Oregon Water-Resources Investigations Report 83-4120A, 4 p. [Also available at https://doi.org/10.3133/wri834120A.]

Reimer, P.J., Bard, E., Bayliss, A., Beck, J.W., Blackwell, P.G., Ramsey, C.B., Buck, C.E., Cheng, H., Edwards, R.L., Friedrich, M., Grootes, P.M., Guilderson, T.P., Haflidason, H., Hajdas, I., Hatté, C., Heaton, T.J., Hoffmann, D.L., Hogg, A.G., Hughen, K.A., Kaiser, K.F., Kromer, B., Manning, S.W., Niu, M., Reimer, R.W., Richards, D.A., Scott, E.M., Southon, J.R., Staff, R.A., Turney, C.S.M., and van der Plicht, J., 2016, IntCal13 and Marine13 radiocarbon age Calibration curves 0–50,000 years cal BP: Radiocarbon, v. 55, no. 4, p. 1869–1887. [Also available at https://doi.org/10.2458/azu_js_rc.55.16947.]

Rinella, F.A., and Schuler, C.A., 1992, Reconnaissance investigation of water quality, bottom sediment, and biota associated with irrigation drainage in the Malheur National Wildlife Refuge, Harney County, Oregon, 1988-89: Water-Resources Investigations Report 91-4085. [Also available at https://doi.org/10.3133/wri914085.]

Robison, J.H., 1968, Estimated existing and potential ground-water storage in major drainage basins in Oregon: Open-File Report 68-232. [Also available at https://doi.org/10.3133/ofr68232.]

Robyn, T.L., and Hoover, J.D., 1982, Late Cenozoic deformation and volcanism in the Blue Mountains of Central Oregon—Microplate interactions?: Geology, v. 10, no. 11, p. 572–576. [Also available at https://doi.org/10.3133/b252.]

Russell, I.C., 1903, Preliminary report on artesian basins in southwestern Idaho and southeastern Oregon: U.S. Geological Survey Water Supply Paper 78, 53 p. [Also available at https://doi.org/10.3133/wsp78.]

Russell, I.C., 1905, Preliminary report on the geology and water resources of central Oregon: U.S. Geological Survey Bulletin, v. 252. 10.3133/b252. [Also available at https://doi.org/10.3133/b252.]

Russell, J.K., and Nicholls, J., 1987, Early crystallization history of alkali olivine basalts, Diamond Craters, Oregon: Geochimica et Cosmochimica Acta, v. 51, no. 1, p. 143–154. [Also available at https://doi.org/10.1016/0016-7037(87)90015-9.]

Rytuba, J.J., and McKee, E.H., 1984, Peralkaline ash flow tuffs and calderas of the McDermitt volcanic field, southeast Oregon and north central Nevada: Journal of Geophysical Research, v. 89, no. B10, no. B10, p. 8616–8628. [Also available at https://doi.org/10.1029/JB089iB10p08616.]

Sheppard, R.A., 1993, Geology and mineralogy of the Harney lake zeolite deposit, Harney County, Oregon, International Committee on Natural Zeolites, Zeo-Trip '93, an excursion to selected zeolite and clay deposits in southeastern Oregon and southwestern Idaho, June 26-28, 1993, p. 42-58. [Also available at https://doi.org/10.3133/b2108.]

Sheppard, R.A., 1994, Zeolitic diagenesis of tuffs in Miocene lacustrine rocks near Harney Lake, Harney County, Oregon: U.S. Geological Survey Bulletin 2108, 28 p. [Also available at https://doi.org/10.3133/b2108.]

Sherrod, D.R., Champion, D.E., and McGeehin, J.P., 2012, Age and duration of volcanic activity at Diamond Craters, southeastern Oregon: Journal of Volcanology and Geothermal Research, v. 247, p. 108–114. [Also available at https://doi.org/10.1016/j.jvolgeores.2012.08.008.]

Silberling, N.J., and Jones, D.L., 1984, Lithotectonic terrane maps of the North American Cordillera: U.S. Geological Survey Open File Report 84-523, 106 p. [Also available at https://doi.org/10.3133/ofr84523.]

Smith, G.I., Friedman, I., Veronda, G., and Johnson, C.A., 2002, Stable isotope compositions of waters in the Great Basin, United States 3—Comparison of groundwaters with modern precipitation: Journal of Geophysical Research-Atmospheres, v. 107, no. D19, p. ACL 16-11-ACL 16-15. [Also available at https://doi.org/10.1029/2001jd000567.]

Snyder, C.T., Hardman, G., and Zdenek, F.F., 1964, Pleistocene lakes in the Great Basin: U.S. Geological Survey Miscellaneous Geologic Investigations Map I-416, scale 1:1,000,000. [Also available at https://doi.org/10.3133/i416]

Soil Survey Staff, 2018, Soil Survey Geographic (SSURGO) database: Natural Resources Conservation Service, United States Department of Agriculture, accessed March 29, 2018, at https://sdmdataaccess.sc.egov.usda.gov.

Sokratov, S.A., and Golubev, V.N., 2009, Snow isotopic content change by sublimation: Journal of Glaciology, v. 55, no. 193, p. 823–828. [Also available at https://doi.org/10.3189/002214309790152456.]

Sommerfield, R.A., and Friedman, I., 1991, Isotopic changes during the formation of depth hoar in experimental snowpacks, in Taylor, H.P., J.R., O.N., and Kaplan, I.R., eds., Stable isotope geochemistry—A tribute to Samuel Epstein: The Geochemical Society, p. 205–209. [Also available at https://www.geochemsoc.org/files/1714/1269/7652/SP-3_205-210_Sommerfeld.pdf.]

Streck, M.J., 2002, Partial melting to produce high-silica rhyolites of a young bimodal suite—Compositional constraints among rhyolites, basalts, and metamorphic xenoliths from the Harney Basin, Oregon: International Journal of Earth Sciences, v. 91, no. 4, p. 583–593. [Also available at https://doi.org/10.1007/s00531-001-0246-7.]

Streck, M.J., and Grunder, A.L., 1995, Crystallization and welding variations in a widespread ignimbrite sheet; the Rattlesnake Tuff, eastern Oregon, USA: Bulletin of Volcanology, v. 57, no. 3, p. 151–169. [Also available at https://doi.org/10.1007/Bf00265035.]

Streck, M.J., and Grunder, A.L., 2012, Temporal and crustal effects on differentiation of tholeiite to calcalkaline and ferro-trachytic suites, High Lava Plains, Oregon, USA: Geochemistry Geophysics Geosystems, v. 13, no. 11, p. 23. [Also available at https://doi.org/10.1029/2012gc004237.]

Swanson, D.A., 1969, Reconnaissance geologic map of the east half of the Bend quadrangle, Crook, Wheeler, Jefferson, Wasco, and Deschutes Counties, Oregon: U.S. Geological Survey Open-File Report v, p. 68–266. [Also available at https://doi.org/10.3133/ofr68266.]

Swanson, D.A., and Robinson, P.T., 1968, Base of the John Day Formation in and near the Horse Heaven mining district, north-central Oregon, Professional Paper 600-D. U.S. Geological Survey, p. D154–D161. [Also available at https://doi.org/10.3133/pp600D.]

Talbot, M.R., 1990, A review of the palaeohydrological interpretation of carbon and oxygen isotopic ratios in primary lacustrine carbonates: Chemical Geology. Isotope Geoscience Section, v. 80, no. 4, p. 261–279. [Also available at https://doi.org/10.1016/0168-9622(90)90009-2.]

Thayer, T.P., 1957, Some relations of later Tertiary volcanology and structures in eastern Oregon, in Vulcanologia del Cenozoico—Section 1: American Geophysical Union, International Geological Congress, 20th, Report, Mexico City, 1956, no. 1, p. 231–245.

Thayer, T.P., and Brown, C.E., 1966, Geologic map of the Aldrich Mountain Quadrangle, Grant County, Oregon: U.S. Geological Survey Geologic Quadrangle Map GQ-438, scale 1:62,500. [Also available at https://doi.org/10.3133/gq438.]

Theis, C.V., 1935, The relation between the lowering of the piezometric surface and the rate and duration of discharge of a well using ground water storage: American Geophysical Union Transactions, v. 16, no. 2, p. 519–524. [Also available at https://doi.org/10.1029/TR016i002p00519.]

Thomas, J.M., Welch, A.H., and Dettinger, M.D., 1996, Geochemistry and isotope hydrology of representative aquifers in the Great Basin region of Nevada, Utah, and adjacent states: U.S. Geological Survey Professional Paper 1409-C, 100 p. [Also available at https://doi.org/10.3133/pp1409C.]

Tóth, J., 1963, A theoretical analysis of groundwater flow in small drainage basins: Journal of Geophysical Research, v. 68, no. 16, p. 4795–4812. [Also available at https://doi.org/10.1029/JZ068i016p04795.]

Townley, P.J., Soja, C.M., and Sidle, W.C., 1980, Groundwater data for the Riley and Andrews Resource Areas, southeastern Oregon: U.S. Geological Survey Open-File Report 80-419, 32 p. [Also available at https://doi.org/10.3133/ofr80419.]

U.S. Department of Agriculture Natural Resources Conservation Service, 2020, SNOwpack TELemetry Network (SNOTEL): U.S. Department of Agriculture Natural Resources Conservation Service, Ag Data Commons no. 1/6/2020, accessed March 22, 2020 at https://data.nal.usda.gov/dataset/snowpack-telemetry-network-snotel.

Vorhis, R.C., 1979, Transmissivity from pumped well data: Well Log, National Water Well Association Newsletter, v. 10, no. no. 11, p. 50–52.

Walker, G.W., 1963, Reconnaissance geologic map of the eastern half of the Klamath Falls (AMS) quadrangle, Lake and Klamath Counties, Oregon: U.S. Geological Survey Mineral Investigations Field Studies Map MF-260, scale 1:250,000. [Also available at https://doi.org/10.3133/mf260.]

Walker, G.W., 1969, Geology of the High Lava Plains Province, *in* Weissenborn, A.W., ed., Mineral and water resources of Oregon—Oregon Department of Geology and Mineral Industries Bulletin 64, p. 77–79. [Also available at https://www.oregongeology.org/pubs/B/B-064.pdf.]

Walker, G.W., 1974, Some implications of late Cenozoic volcanism to geothermal potential in the High Lava Plains of south-central Oregon: U.S. Geological Survey Open-File Report 74-1121, 14 p. [Also available at https://doi.org/10.3133/ofr741121.]

Walker, G.W., 1977, Geologic map of Oregon east of the 121st meridian: U.S. Geological Survey Miscellaneous Investigations Series Map I-902, scale 1:500,000. [Also available at https://doi.org/10.3133/i902.]

Walker, G.W., 1979, Revisions to the Cenozoic stratigraphy of Harney Basin, southeastern Oregon: U.S. Geological Survey Bulletin 1475, 35 p. [Also available at https://doi.org/10.3133/b1475.]

Walker, G.W., 1990, Overview of the Cenozoic geology of the Blue Mountains region, *in* Walker, G.W., ed., Geology of the Blue Mountains region of Oregon, Idaho, and Washington: U.S. Geological Survey Professional Paper 1437, p. 1–11. [Also available at https://doi.org/10.3133/pp1437.]

Walker, G.W., and Nolf, B., 1981, High Lava Plains, Brothers fault zone to Harney Basin, Oregon, *in* Johnston, D.A., and Donnelly-Nolan, J., eds., Guides to some volcanic terranes in Washington, Idaho, Oregon and northern California: U.S. Geological Survey Circular 838, p. 105–111. [Also available at https://doi.org/10.3133/cir838.]

Walker, G.W., Peterson, N.V., and Greene, R.C., 1967, Reconnaissance geologic map of the east half of the Crescent quadrangle, Lake, Deschutes, and Crook Counties, Oregon: U.S. Geological Survey Miscellaneous Investigations Series Map I-493, scale 1:125,000. [Also available at https://doi.org/10.3133/i493.]

Walker, G.W., and Repenning, C.A., 1965, Reconnaissance geologic map of the Adel quadrangle, Lake, Harney, and Malheur counties, Oregon: U.S. Geological Survey Miscellaneous Geologic Investigations Map I-446, scale 1:250000. [Also available at https://doi.org/10.3133/i446.]

Walker, G.W., and Swanson, D.A., 1968, Summary report on the geology and mineral resources of the Harney Lake and Malheur Lake areas of the Malheur National Wildlife Refuge, north-central Harney County, Oregon: U.S. Geological Survey Bulletin 1260-L, 17 p. [Also available at https://doi.org/10.3133/b1260L.]

Wallace, R.E., and Calkins, J.A., 1956, Reconnaissance geologic map of the Izee and Logdell quadrangles, Oregon: U.S. Geological Survey Mineral Investigations Field Studies Map MF-82, scale 1:62,500. [Also available at https://doi.org/10.3133/mf82.]

Waring, G.A., 1908, Geology and water resources of a portion of south-central Oregon: U.S. Geological Survey Water Supply Paper 220, 86 p. [Also available at https://doi.org/10.3133/wsp220.]

Waring, G.A., 1909, Geology and water resources of the Harney Basin region, Oregon: U.S. Geological Survey Water Supply Paper 231, 93 p. [Also available at https://doi.org/10.3133/wsp231.]

Weldon, R.J., Fletcher, D.K., Weldon, E.M., Scharer, K.M., and McCrory, P.A., 2003, An update of Quaternary faults of central and eastern Oregon: U.S. Geological Survey Open-File Report 02-301. [Also available at https://doi.org/10.3133/ofr02301.]

Wernicke, B., 1992, Cenozoic extensional tectonics of the U.S. Cordillera, *in* Burchfiel, B.C., Lipman, P.W., and Zoback, M.L., eds., The Cordillera Orogen—Conterminous U.S: Boulder, Colorado, Geological Society of America, p. 553–581. [Also available at https://doi.org/10.1130/DNAG-GNA-G3.553.]

Western Regional Climate Center, 2020, Cooperative climatological data summaries: Western Regional Climate Center. [Also available at http://wrcc.dri.edu/climatedata/climsum/.]

Winter, T.C., Harvey, J.W., Franke, O.L., and Alley, W.M., 1998, Ground water and surface water—A single resource: U.S. Geological Survey Circular 1139, 79 p. [Also available at https://doi.org/10.3133/cir1139.]

Zoback, M.L., 1989, State of stress and modern deformation of the northern Basin and Range province: Journal of Geophysical Research-Solid Earth and Planets, v. 94, no. B6, no. B6, p. 7105–7128. [Also available at https://doi.org/10.1029/JB094iB06p07105.]

Appendix 1. Geochemical Analytes and Sampling Methods

Geochemical tracers are useful for developing and refining understanding of groundwater-flow systems. They can help (1) identify sources of recharge, (2) confirm and refine groundwater flowpaths originally delineated using groundwater-level maps, and (3) quantify the rate of movement and age of groundwater. Carbon-14, tritium, and stable isotopes of water were used for these purposes in the Harney Basin and a brief overview of their use is provided below.

Oxygen-18 and Deuterium

A water molecule consists of two hydrogen (H) atoms and one oxygen (O) atom. Hydrogen has two stable isotopes (^{1}H and ^{2}H), and oxygen has three stable isotopes (^{16}O, ^{17}O, and ^{18}O). The superscript next to the element denotes the combined number of protons and neutrons in the element's nucleus. Elements with a larger number of protons and neutrons are heavier than those with fewer, thus ^{18}O is heavier than ^{16}O. The common isotopes, ^{1}H and ^{16}O, comprise more than 99 percent of those elements on Earth and combine to form most of the water in the planet's hydrosphere. However, a small percentage of water molecules contain one of the heavier stable isotopes: ^{2}H, ^{17}O, and/or ^{18}O. The relative abundance of the heavy stable isotopes in water varies according to well-understood physical processes and can be used to trace the movement of water in a watershed. The heavy stable isotopes used in this report are ^{2}H (deuterium) and ^{18}O.

Stable isotopes are analyzed by measuring the ratio of the heavier, less-abundant isotope to the lighter, more-abundant isotope and are reported as the difference relative to a known standard. The isotope ratios are reported as delta (δ) values expressed as parts per thousand (per mil; ‰). The δ value for an isotope ratio, R, is determined using:

$$\delta R = \left(\frac{R_{sample}}{R_{standard}} - 1 \right) \times 1{,}000 \qquad (2.1)$$

where

δR is the δ value for a specific isotope in the sample (^{2}H or ^{18}O),

R_{sample} is the ratio of the less-abundant isotope to the common isotope for a specific element in the sample, and

$R_{standard}$ is the ratio of the less-abundant isotope to the common isotope for the same element in the reference standard. The reference standard used in this report is Vienna Standard Mean Ocean Water (VSMOW) (Craig, 1961b; Coplen, 1994) and is defined as having a value of 0 for δ^{2}H and δ^{18}O.

A positive δR value indicates that the sample is enriched in the heavier isotope with respect to the standard. A negative δR value indicates that the sample is depleted in the heavier isotope with respect to the standard. Clark and Fritz (1997) summarized a discussion of isotope ratios as follows: differences in vapor pressure result in the preferential evaporation of water molecules containing the lighter isotopes, leaving the evaporating water body enriched in water molecules containing the heavier isotopes and the vapor mass depleted in water containing heavy isotopes. Similarly, rain or snow condensed from a vapor mass is enriched in heavy isotopes and the remaining vapor is further depleted. In this way vapor masses moving inland from the ocean become increasingly depleted resulting in precipitation that almost always has a negative δR value. Differences in the vapor pressure of $H_2{}^{18}O$ and ^{2}HHO mean the two molecules do not evaporate and condense in the same proportion; however, a predictable relation between the two δR values can be determined. Craig (1961a) first described the correlation between δ^{2}H and δ^{18}O for freshwaters across the globe. The relation is referred to as the Global Meteoric Water Line (GMWL; equation 2.2).

$$\delta^{2}H = 8 \times \delta^{18}O + 10 \qquad (2.2)$$

where

$\delta^{2}H$ is delta hydrogen-2, and

$\delta^{18}O$ is delta oxygen-18.

On a plot of δ^{2}H and δ^{18}O, the stable isotopes of water from a specific area typically plot along a line that differs somewhat from the GMWL (Clark and Fritz, 1997). The area-specific relation is referred to as the local meteoric water line (LMWL). In the Great Basin, moisture-source trajectory and history, temperature, relative humidity, and subcloud evaporation are important factors controlling the isotopic composition of precipitation (Friedman and others, 2002a, 2002b) and dictate the orientation of the LMWL on a δ^{2}H/δ^{18}O plot. The groundwater and surface water in an area may deviate from the LMWL due to post-depositional evaporation, differential sublimation, and mixing with geologically old water (paleowater) that fell as precipitation in a climate different from that prevailing in the area today. Samples of distinct types and sources of water from an area not only help define the LMWL, but their relation to one another and to the LMWL can be used to obtain insights into hydrologic processes and history of an area.

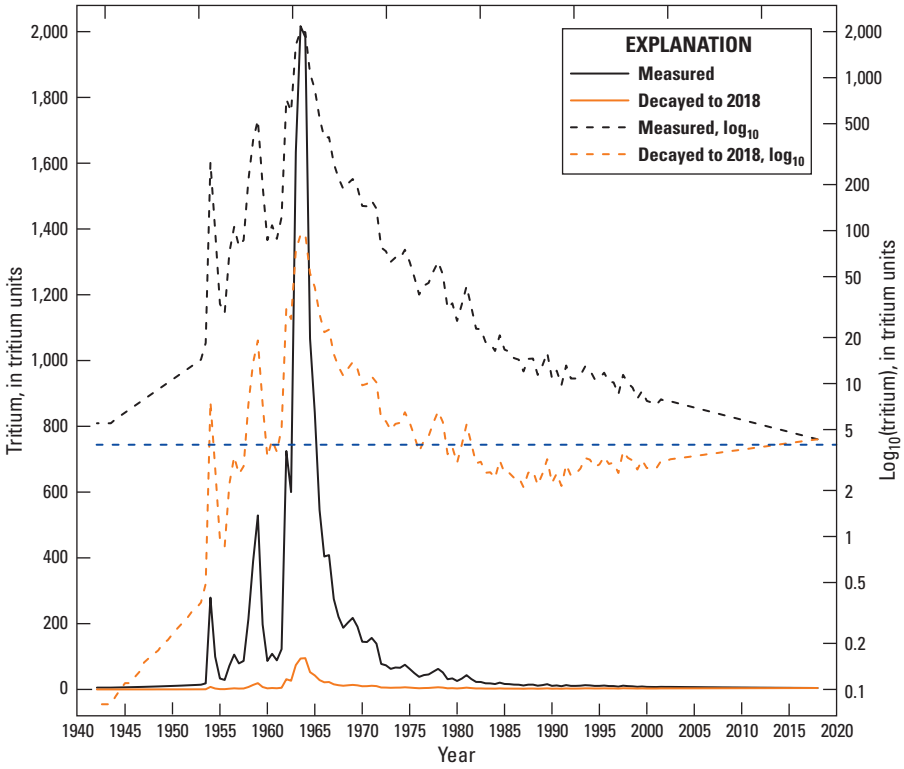

Figure 1.1. Time series of estimated tritium concentration in precipitation and time series of tritium concentration in precipitation decayed to 2018, the Harney Basin, southeastern Oregon, 1940–2020. Dashed blue line is drawn at 4.0 tritium units (TU) on the base 10 logarithm axis. Estimated tritium concentration taken from Michel and others (2018).

Carbon-14

Carbon-14 (^{14}C) is a naturally occurring radioactive isotope of carbon with a half-life of 5,730 years (yrs) that can be used to determine the apparent age of groundwater ranging from about 500 to more than about 40,000 yrs. Carbon-14 is produced in the upper atmosphere and is rapidly oxidized to carbon-14 dioxide ($^{14}CO_2$), which mixes into the lower atmosphere. Plants, water, and minerals that utilize or react with atmospheric carbon dioxide (CO_2) will have a ^{14}C activity similar to that in the atmosphere (Pearson and White, 1967). Atmospheric ^{14}C enters the groundwater-flow system through the infiltration of precipitation containing dissolved $^{14}CO_2$, plant respiration of $^{14}CO_2$ in the soil, oxidation of recent organic matter in the soil, and the dissolution of minerals containing geologically young carbon. Once isolated from the soil zone, the groundwater is isolated from new sources of atmospherically derived ^{14}C. Radioactive decay decreases the ^{14}C activity of the groundwater and the amount of decay can be used to estimate the time since the water sample was isolated from atmospheric ^{14}C inputs in the unsaturated zone. The time at which water becomes isolated from atmospheric ^{14}C is the recharge date and the time elapsed between that date and discharge is the residence time within the groundwater-flow system.

In addition to radioactive decay, the ^{14}C activity of groundwater in the unsaturated and saturated zone can be affected by additions of ^{14}C-free carbon (called "dead carbon"), including geogenic CO_2, methanogenic CO_2, oxidation of carbon-dead organic matter, and reactions involving minerals containing dead carbon, such as calcite (Clark and Fritz, 1997). The addition of dead carbon will increase the apparent age of a water sample by diluting the ^{14}C activity of recharge water, and therefore must be accounted for to obtain an accurate ^{14}C age. An evaluation of carbon-13 (^{13}C), a naturally occurring stable isotope of carbon, along with ^{14}C and the concentration of dissolved inorganic carbon (DIC), can help identify the presence and potential source of dead carbon introduced in the subsurface (Han and others, 2014).

In this study, unadjusted ^{14}C ages were calculated with the U.S. Geological Survey (USGS) software package TracerLPM (Jurgens and others, 2012) using a piston-flow model of the non-normalized ^{14}C activity of the DIC in a sample and the Cambridge half-life (5,730 yrs). Initial ^{14}C activity of DIC in recharge was determined iteratively and used the IntCal13 reconstruction of atmospheric ^{14}C (Reimer and others, 2016). The calculation of the mean ^{14}C age for samples collected for this study, including an analysis of potential dead carbon additions, is discussed in the main body of the report in the section "Geochemical Evaluation of Recharge, Flowpaths, and Residence Time."

Tritium

Tritium (^3H) is a naturally occurring radioactive isotope of hydrogen with a half-life of 12.32 yrs that can be used to determine the apparent age of groundwater recharged after about 1953. Less than 1 percent of atmospheric water molecules contain ^3H substituted for ^1H in their molecular structure. Water recharged before 1953 does not contain measurable amounts of ^3H due to radioactive decay. Prior to atmospheric testing of thermonuclear weapons in the 1950s and 1960s, the natural background concentration of ^3H in precipitation in Harney County was about 5.5 tritium units (TU; Michel and others [2018]). Atmospheric testing released a large amount of ^3H into the atmosphere and concentrations in precipitation peaked in 1964 at nearly 1,000 times higher than background concentrations. ^3H from the atmospheric testing of nuclear weapons has largely dissipated from the atmosphere due to sequestration and radioactive decay, and ^3H in modern precipitation is indistinguishable from natural background (fig. 1.1).

Comparing ^3H measured in a water sample from a spring or well with the atmospheric concentration history can help distinguish between water recharged before or after the beginning of weapons testing in the mid-1950s; 1953 is often used as the date when the influence of thermonuclear ^3H can be observed in precipitation records, and when the natural background ^3H in precipitation is surpassed and masked by thermonuclear ^3H (Nir and others, 1966; Lindsey and others, 2019). Due to radioactive decay, naturally occurring ^3H prior to the weapons testing period is no longer detectable. A water sample without detectable ^3H ("tritium dead") was wholly recharged prior to about 1953. Samples having detectable ^3H contain some water that was recharged between 1953 and the present.

In a single sample, ^3H cannot be used to precisely date groundwater recharged after 1953. Two factors contribute to this issue: (1) the increase and subsequent decrease of ^3H concentrations in the atmosphere due to atmospheric testing of nuclear weapons in the mid-20th century and (2) radioactive decay of ^3H. Both processes lead to non-unique recharge-year estimates for many measured ^3H concentrations. For example, a sample having a measured ^3H value of 4 TU (fig. 1.1) could have been recharged in 2014, sometime between 1975 and 1981, or sometime between 1954 and 1961. In addition to the limitations resulting from the atmospheric history and radioactivity of ^3H, the ^3H measured in a sample of groundwater represents a mean value of a mixture of groundwaters that were recharged at different times due to (1) dispersion in the unsaturated zone during recharge, (2) dispersion as the water traveled through the groundwater-flow system, (3) converging flowpaths in discharge areas, and (4) mixing of groundwater from different depths in wells having long open intervals.

Despite these limitations, ^3H is a useful semi-quantitative indicator of groundwater age. Groundwater in a tritium-dead sample can be definitively assigned a recharge age prior to 1953, and the presence of ^3H in a sample provides firm evidence that some fraction of the water in the sample was recharged after 1953.

Sampling and Analysis Methods

Water samples were collected following standard USGS protocols (U.S. Geological Survey, variously dated). Field parameters including pH, water temperature, and specific conductance were measured at each site just before the water sample was collected.

Samples for alkalinity and acid neutralizing capacity were collected in 250-mL or 500-mL high-density polyethylene (HDPE) bottles, filled with no headspace, capped, and sealed with electrical tape. Samples collected by USGS staff were filtered through a 0.45-micrometer (µm) capsule filter, and results are reported as alkalinity. Samples collected by Oregon Department of Environmental Quality (DEQ) were not filtered, and results are reported as acid neutralizing capacity. Little functional difference exists between the two values in groundwater and spring-water samples due to the low turbidity of most groundwater samples. Samples from both agencies were stored at 4 degrees Celsius (°C) until analysis. Samples collected by USGS staff were analyzed within 2 weeks of sample collection in the USGS Oregon Water Science Center Lab in Portland, Oregon, using an inflection-point method. Samples collected by DEQ staff were analyzed within 2 weeks of sample collection at the DEQ lab in Hillsboro, Oregon, using a fixed-end point method. Ideally, the alkalinity titrations would have been conducted on-site; however, sampling logistics precluded this approach. At the time of analysis by USGS, samples were visually inspected and no evidence of mineral precipitation or degassing in the samples was observed. Samples collected and analyzed by DEQ met the 14-day holding time of the DEQ lab.

Samples for stable isotopes of water ($\delta^{18}O$ and $\delta^{2}H$) were collected in 20-mL HDPE bottles, filled with no headspace, and capped with a polyseal-cone-lined cap. If the sampled water was turbid, the sample was filtered through a 0.45-µm capsule filter or 0.45-µm disc filter prior to filling the bottle. Samples were stored at ambient temperature, and the caps were periodically checked to ensure they remained tightly sealed. Analyses were conducted at the USGS Reston Stable Isotope Laboratory using mass spectrometry following methods by Révész and Coplen (2008a, b). The 2-sigma uncertainties are 0.2‰ for oxygen and 2‰ for hydrogen isotopic ratios reported relative to VSMOW.

Samples for ^3H were collected in 1,000-mL HDPE bottles, filled with no headspace, capped with a polyseal-cone lined cap, and sealed with electrical tape. Samples were stored at ambient temperature. Analyses were conducted at the USGS Tritium Laboratory in Menlo Park, California, or at the University of Miami Tritium Laboratory in Miami, Florida. Both labs use similar analytical methods in which samples are distilled, undergo electrolytic enrichment, and low-level counting. Methods used by the Menlo Park lab are described in Thatcher and others (1977) and McCurdy and others (2008), and those used by the Miami lab are described in Östlund and others (1969), Östlund and others (1974), and Östlund (1987).

Samples for carbon isotopes were collected in 1,000-mL glass bottles. Sample water was filtered through a 0.45-µm capsule filter, and the sample bottle was bottom filled with no headspace, capped with a polyseal-cone-lined cap, and sealed with electrical tape. Samples were stored at 4 °C until analysis. Analyses were conducted at the National Ocean Sciences Accelerator Mass Spectrometry facility at Woods Hole Oceanographic Institute. Accelerator mass spectrometry was used to measure the ratio of ^{14}C to ^{12}C and ^{13}C to ^{12}C in the samples. Methods and techniques used by the lab for reporting ^{14}C activity and the ^{13}C /^{12}C ratio are described by Olsson (1970), Stuiver and Polach (2016), and Stuiver (2016).

References Cited

Clark, I.D., and Fritz, P., 1997, Environmental isotopes in hydrogeology: Boca Raton, Florida, CRC Press, LLC, 328 p.

Coplen, T.B., 1994, Reporting of stable hydrogen, carbon, and oxygen isotopic abundances: Pure and Applied Chemistry, v. 66, no. 2, p. 273–276. [Also available at https://doi.org/10.1351/pac199466020273.]

Craig, H., 1961a, Isotopic variations in meteoric waters: Science, v. 133, no. 3465, p. 1702–1703. [Also available at https://doi.org/10.1126/science.133.3465.1702.]

Craig, H., 1961b, Standard for reporting concentrations of deuterium and oxygen-18 in natural waters: Science, v. 133, no. 3467, p. 1833–1834. [Also available at https://doi.org/10.1126/science.133.3467.1833.]

Friedman, I., Harris, J.M., Smith, G.I., and Johnson, C.A., 2002a, Stable isotope composition of waters in the Great Basin, United States 1—Air-mass trajectories: Journal of Geophysical Research-Atmospheres, v. 107, no. D19, p. ACL 14-11-ACL 14-14. [Also available at https://doi.org/10.1029/2001jd000565.]

Friedman, I., Smith, G.I., Johnson, C.A., and Moscati, R.J., 2002b, Stable isotope compositions of waters in the Great Basin, United States 2—Modern precipitation: Journal of Geophysical Research-Atmospheres, v. 107, no. D19, p. ACL 15-11-ACL 15-22. [Also available at https://doi.org/10.1029/2001JD000566.]

Han, L.F., Plummer, L.N., and Aggarwal, P., 2012, A graphical method to evaluate predominant geochemical processes occurring in groundwater systems for radiocarbon dating: Chemical Geology, v. 318, p. 88–112. [Also available at https://doi.org/10.1016/j.chemgeo.2012.05.004.]

Jurgens, B.C., Böhlke, J.K., and Eberts, S.M., 2012, TracerLPM (Version 1)—An Excel® workbook for interpreting groundwater age distributions from environmental tracer data: U.S. Geological Survey Techniques and Methods 4-F3, 60 p. [Also available at https://doi.org/10.3133/tm4F3.]

Lindsey, B.D., Jurgens, B.C., and Belitz, K., 2019, Tritium as an indicator of modern, mixed, and premodern groundwater age: U.S. Geological Survey Scientific Investigations Report 2019–5090, 18 p. [Also available at https://doi.org/10.3133/sir20195090.]

Michel, R.L., Jurgens, B.C., and Young, M.B., 2018, Tritium deposition in precipitation in the United States, 1953–2012: U.S. Geological Survey Scientific Investigations Report 2018-5086, 19 p. [Also available at https://doi.org/10.3133/sir20185086.]

McCurdy, D.E., Garbarino, J.R., and Mullin, A.H., 2008, Interpreting and reporting radiological water-quality data: U.S. Geological Survey Techniques and Methods 5-B6, 33 p. [Also available at https://doi.org/10.3133/tm5B6.]

Nir, A., Kruger, S.T., Lingenfelter, R.E., and Flamm, E.J., 1966, Natural tritium: Reviews of Geophysics, v. 4, no. 4, p. 441–456. [Also available at https://doi.org/10.1029/RG004i004p00441.]

Olsson, I.U., 1970, The use of oxalic acid as a standard, *in* Olsson, I.U., ed., Radiocarbon variations and absolute chronology: New York, New York, John Wiley & Sons, p. 17.

Östlund, H.G., 1987, Tritium, *in* Östlund, H.G., Craig, H., Broeker, W.S., and Spencer, D., eds., GEOSECS Atlantic, Pacific, and Indian Ocean expeditions Volume 7—Shorebased data and graphics: Washington, D.C., National Science Foundation, p. 7–10. [Also available at https://doi.org/10013/epic.43023.d001.]

Östlund, H.G., Dorsey, H.G., and Rooth, C.G., 1974, GEOSECS North Atlantic radiocarbon and tritium results: Earth and Planetary Science Letters, v. 23, no. 1, p. 69–86. [Also available at https://doi.org/10.1016/0012-821X(74)90033-8.]

Östlund, H.G., Rinkel, M.O., and Rooth, C., 1969, Tritium in the equatorial Atlantic Current System: Journal of Geophysical Research (1896-1977), v. 74, no. 18, p. 4535-4543. [Also available at https://doi.org/10.1029/JC074i018p04535.]

Pearson, F.J., Jr., and White, D.E., 1967, Carbon 14 ages and flow rates of water in Carrizo Sand, Atascosa County, Texas: Water Resources Research, v. 3, no. 1, p. 251–261. [Also available at https://doi.org/10.1029/WR003i001p00251.]

Reimer, P.J., Bard, E., Bayliss, A., Beck, J.W., Blackwell, P.G., Ramsey, C.B., Buck, C.E., Cheng, H., Edwards, R.L., Friedrich, M., Grootes, P.M., Guilderson, T.P., Haflidason, H., Hajdas, I., Hatté, C., Heaton, T.J., Hoffmann, D.L., Hogg, A.G., Hughen, K.A., Kaiser, K.F., Kromer, B., Manning, S.W., Niu, M., Reimer, R.W., Richards, D.A., Scott, E.M., Southon, J.R., Staff, R.A., Turney, C.S.M., and van der Plicht, J., 2016, IntCal13 and Marine13 radiocarbon age calibration curves 0–50,000 years cal BP: Radiocarbon, v. 55, no. 4, p. 1869–1887. [Also available at https://doi.org/10.2458/azu_js_rc.55.16947.]

Révész, K., and Coplen, T., 2008a, Determination of the delta(2H/1H)of Water—RSIL Lab Code 1574: U.S. Geological Survey Techniques and Methods 10-C1, 27 p. [Also available at https://doi.org/10.3133/tm10C1.]

Révész, K., and Coplen, T., 2008b, Determination of the delta(18O/16O)of Water—RSIL Lab Code 489: U.S. Geological Survey Techniques and Methods 10-C2, 28 p. [Aslo available at https://doi.org/10.3133/tm10C2.]

Stuiver, M., 2016, Workshop on ^{14}C data reporting: Radiocarbon, v. 22, no. 3, p. 964–966. [Also available at https://doi.org/10.1017/s0033822200010389.]

Stuiver, M., and Polach, H.A., 2016, Discussion reporting of ^{14}C Data: Radiocarbon, v. 19, no. 3, p. 355–363. [Also availabble at https://doi.org/10.1017/s0033822200003672.]

Thatcher, L.L., Janzer, V.J., and Edwards, K.W., 1977, Methods for determination of radioactive substances in water and fluvial sediments: U.S. Geological Survey Techniques of Water-Resources Investigations 05-A5, 95 p. [Also available at https://doi.org/10.3133/twri05A5.]

U.S. Geological Survey, variously dated, National field manual for the collection of water-quality data: U.S. Geological Survey Techniques and Methods, book 9, chap. A0, 4 p. [Also available at https://doi.org/10.3133/tm9A0.]

Publishing support provided by the U.S. Geological Survey
Science Publishing Network, Tacoma Publishing Service Center

For more information concerning the research in this report, contact the
Director, Oregon Water Science Center
U.S. Geological Survey
2130 SW 5th Avenue
Portland, Oregon 97201
https://www.usgs.gov/centers/or-water

USGS

Gingerich and others—**Groundwater Resources of the Harney Basin, Southeastern Oregon**—Scientific Investigations Report 2021-5103

ISSN 2328-0328 (online)
https://doi.org/10.3133/sir20215103